SCUOLA NORMALE SUPERIORE

Classe di Scienze

Corso di perfezionamento in

Metodi e Modelli per Le Scienze Molecolari

XXXIII ciclo

Improving the performances of the LIBS technique for the analysis of solid and liquid samples using noble metal nanoparticles

Settore Scientifico Disciplinare CHIM/01

Candidato
dr. Francesco Poggialini

Relatore	Supervisore interno
Dott. Stefano Legnaioli	Prof. Vincenzo Barone

Anno accademico 2021/2022

General Index

Chapter 2

Chapter 3

Chapter 4

Chapter 5

Chapter 6

List of abbreviations

AES – Atomic Emission Spectroscopy

AgNP – Silver Nanoparticle

AOTF – Acusto-Optic Tunable Filter

CCD – Charge-Coupled Device

CF-LIBS – Calibration Free LIBS

CNT – Carbon Nano Tubes

CRM – Certified Reference Material

DCP – Direct Current Plasma

DP-LIBS – Double Pulse LIBS

DSPME – Dispersive SPME

EF – Enhancement Factor

F-AAS – Flame Atomic Absorption Spectroscopy

FOC – Fiber Optic Cable

FWHM – Full Width at Half Maximum

GNS – Graphene Nano Sheets

GO – Graphene Oxide

iCCD – Intensified CCD

ICP – Inductively Coupled Plasma

LIBS – Laser Induced Breakdown Spectroscopy

LIPS – Laser Induced Plasma Spectroscopy

LOD – Limit of Detection

LSC – Laser Supported Combustion

LSD – Laser Supported Detonation

LSP – Localized Surface Plasmon

LSR – Laser Supported Radiation

LSS – Laser Spark Spectroscopy

LTE – Local Thermal Equilibrium

MCP – Microchannel Plate

MIP – Microwave Induced Plasma

Nd: YAG – Neodymium-Doped Yttrium Aluminum Garnet

NELIBS – Nanoparticle Enhanced LIBS

NP – Nanoparticle

OCT – Optical Coherence Tomography

OES – Optical Emission Spectroscopy

OPC-LIBS – One Point Calibration LIBS

PDA – Photodiode Array

PLAL – Pulsed Laser Ablation in Liquid

PMT – Photomultiplier Tube

POC – Photonic Crystal Core

ppm – Parts per Million (μg/Kg)

SEM – Scanning Electron Microscope

SEn-LIBS – Surface Enhanced LIBS

SERS – Surface-Enhanced Raman Spectroscopy

SO-DP-NELIBS – Spatially Offset DP-LIBS

SP-LIBS – Single Pulse LIBS

SPME – Solid Phase Micro Extraction

SPR – Surface Plasmon Resonance

SRM – Standard Reference Material

TEM – Transmission Electron Microscope

TFME – Thin Film Micro Extraction

UV-Vis – Ultraviolet and Visible Spectroscopy

Extended Abstract and Chapter Overview

Laser Induced Breakdown Spectroscopy (LIBS) is an optical emission atomic spectroscopy technique in which a highly energetic laser pulse of suitable duration and wavelength is used to generate a high-temperature plasma by focusing the beam on a small area on the sample surface. During the pulse, the laser energy is transferred to the sample which is vaporized and atomized. The vaporized sample is then heated and excited to the point where a laser-induced plasma is formed (Breakdown process). The excited species inside the plasma decay through the emission of photons of characteristic wavelengths. The observation and analysis of the light emitted by the decaying plasma yields information regarding the elemental composition of the sample. Both qualitative and quantitative information can be obtained by resolving the registered spectral signal. LIBS is theoretically capable analyzing, with almost real-time results, any sample without the need for a preparation step, independently from its components or state of aggregation.

Despite its many advantages, LIBS also present some limitations. First of all, its sensitivity is low when compared with other spectroscopic techniques, as LIBS LODs are in the range of ppm (µg/Kg). Moreover, the vast majority of LIBS applications are focused on the analysis of solids. In fact, the LIBS analysis of liquids is not routinely performed, and it is generally confined to research and fundamental studies. For liquids samples, a large fraction of the laser pulse energy is spent to vaporize the sample as well as to create the suitable conditions for the ignition and evolution of the plasma. The lifetime of the excited states of the emitting species is shortened significantly, making it more difficult to resolve the spectral signals.

Over the years, numerous authors developed new techniques and innovative methodologies aimed at improving the performances of LIBS. In order to improve the instrumental capabilities, the use of two consecutive laser pulses (Double Pulse LIBS, DP-LIBS) has proven to be one of the most successful and versatile modifications of conventional LIBS. In this configuration, the plasma plume expands inside the environment generated by the shockwave of the first laser pulse. The result is a drastic improvement in the emission intensity and spectra reproducibility, which can be exploited for the analysis of both solid and liquid samples.

Another recently proposed and very promising methodology is based on the plasmonic properties of noble metal nanoparticles (Nanoparticle Enhanced LIBS, NELIBS) to increase the intensity of the incident electromagnetic field on the sample surface. For solid samples, a thin layer of nanoparticles is deposited on its surface and then irradiated like in a standard LIBS measurement. For liquids, a drop of the sample solution can be deposited on a pre-prepared nanoparticle layer.

The intensity of the NELIBS spectra can be several orders of magnitude higher than standard LIBS spectra.

Another recent application proposes the coupling of LIBS and micro-extraction using carbon based substrates for the analysis of liquid samples. In this case, the elements of interest are extracted from the liquid matrix and pre-concentrated on a solid substrate, which can be readily and easily analyzed by LIBS.

The main goal of the research work described in this PhD thesis is the study, testing and implementations of innovative approaches aimed at improving the LIBS performances for the analysis of samples of various nature, using the advantages provided by the application of noble metal nanoparticles. Moreover, for the analysis of liquid samples, NELIBS was coupled to micro-extraction techniques.

In the first part of the research work, described in Chapter 2, it was studied how metal nanoparticles synthetized with “green” methodologies could be used for NELIBS applications. In light of the growing interest in green chemistry, as well as less environmentally impactful and less costly analytical methodologies, silver nanoparticles (AgNPs) were synthetized from silver nitrate solutions using coffee extract and tested for NELIBS applications. Copper standard reference materials (SRMs) were successfully analyzed using green NPs, and LODs for trace elements were estimated. The effectiveness of the green NPs was demonstrated by the construction of LIBS and NELIBS calibration curves. In addition, the analyses were performed using a portable instrument. The successful use for NELIBS with such instrumentation for the first time suggests the possibility of in-situ applications.

For continuous NELIBS testing, it was necessary to satisfy the requirement for the fast production of high-quality, pure and reproducible metal nanoparticles in relatively large quantities. Chapter 3 details the steps that were followed in order to develop a procedure for creating NPs suitable for NELIBS. This was achieved by re-configuring the available LIBS instrument to also allow for the Pulsed Laser Ablation in Liquid (PLAL) of noble metal targets. The procedure allowed for the extremely reproducible production of NP dispersion with tunable concentration and dimensions, with the addition of different surfactants, depending on the analytical requirements. The nanoparticles produced by PLAL during this phase of the research work were successfully used for NELIBS, but also for Surface-Enhanced Raman (SERS) applications, as briefly described in the Chapter. The same system was also used successfully for the production of graphene-based nanosheets that were used for micro-extraction applications. The same Chapter also gives an overview of the testing of various LIBS configurations, using different plasma light collection systems and setups.

As previously reported, the potential of DP-LIBS has been well documented in literature, and made it a very attractive technique for analytical applications. The possibility of combining the advantages of DP-LIBS and NELIBS was investigated, and the results of this study are reported in Chapter 4. The main problematic was the almost complete removal of the NPs after a single laser pulse, which would prevent the second pulse from interacting with the NP deposition. To solve this problem, a LIBS setup that used two parallel and non-collinear laser pulses was chosen, to ensure the activation of NPs during both pulses, while maintaining the low-density environment typical of DP-LIBS. The two laser beams are spatially separated so that the second beam is focused within the shock wave generated by the first one. Several tests on copper targets have been performed to determine the best set-up for the maximum magnitude of the signal enhancement by adjusting different parameters such as pulse energies and offset distances. Commercially available silver NPs and NPs prepared by PLAL have been tested and their performances compared with standard DP-LIBS.

Because of the previously mentioned restrictions linked to the specific nature of liquid matrixes, a novel strategy for the analysis of liquid samples, exploiting the signal-enhancing effects of NELIBS, was proposed and tested. Indeed, recent advances in the development of micro-extraction techniques for the analysis of heavy metals in water samples have demonstrated the feasibility of carbon-based thin films substrates for LIBS analysis. The analytes are adsorbed on a solid matrix that can be dried and analyzed by conventional LIBS, which solves many of the problematics arising from the LIBS analysis of liquids. Chapter 5 describes the research activity that was focused on improving the capabilities of graphene and graphene oxide thin film micro-extraction (TFME) substrates for LIBS analysis by the application of noble metal NPs. A methodology based on pulsed laser ablation for the preparation of a graphene/graphene oxide dispersion was adapted from literature. The procedure was optimized for the needs of the analysis and several techniques for the preparation of suitable substrates were tested. The optimal result was used for the subsequent measurements. At the same time, different strategies for the application of NPs were tested. The study focused on the extraction of chromium from aqueous solutions. The extraction parameters and conditions were optimized and calibration curves for LIBS and NELIBS were built, showing promising results.

Due to the presence of self-absorption phenomena in LIBS measurements, which were observed throughout this research work, a novel approach for spectral analysis and treatment was developed, called Time-Independent Extended C-Sigma, and the results are reported in Chapter 6. Indeed, having a method that allows for the determination of the extent of the effects of self-absorption on the spectral lines monitored in LIBS, using the experimental data obtained directly from a LIBS spectrum, would be a powerful tool for both quantitative analysis and spectral studies

of LIBS plasmas. The method developed in this research work is based on the recently introduced Extended C-sigma procedure and exploits the spectral information extracted from LIBS spectra acquired at different delay times after the laser pulse for building a time-independent Extended C-Sigma curve. The method intrinsically includes in the calculation the effects of self-absorption, which is one of the main sources of indetermination in LIBS applications. The method was successfully applied to the determination of the Stark broadening coefficient of several neutral and ionic emission lines of tantalum.

Chapter 1:

Introduction

Chapter 1 - Index

1 – Introduction

1. 1 – Principles and Characteristics of LIBS

Laser Induced Breakdown Spectroscopy (LIBS), also known as Laser Induced Plasma Spectroscopy (LIPS) or Laser Spark Spectroscopy (LSS), is an analytical technique that uses a high-power laser pulse to vaporize, atomize and excite a sample into a plasma (a collection of energized atoms, ions and electrons with overall neutral charge). In the simplest applications, the light emitted by the decaying plasma is then collected and analyzed, in order to discern the composition of the target sample. Since each element has a characteristic and unique set of emission wavelengths (generally in the Ultraviolet, Visible and Near-Infrared regions of the electromagnetic spectrum) it is possible to identify the presence of certain analytes in the investigated samples and to know their concentration.

Several papers and books already describe in detail the evolution of LIBS [1] [2] [3] [4] [5] [6] [7] [8] [9] [10] [11] [12], and a through description of this subject is not in the scope of this thesis. Similarly, a vast and comprehensive literature describes in detail the principles and mechanisms behind LIBS [1] [2] [3] [4] [5] [7] [8] [13] [14] [15], from the laser-matter interaction to the plasma evolution, evaluating the contributions of different electronic and optical components for the most commonly used instrumentations. Nevertheless, an overview of the fundamental aspects on the nature of laser-induced plasmas and the common characteristics of LIBS instrumentations will be given.

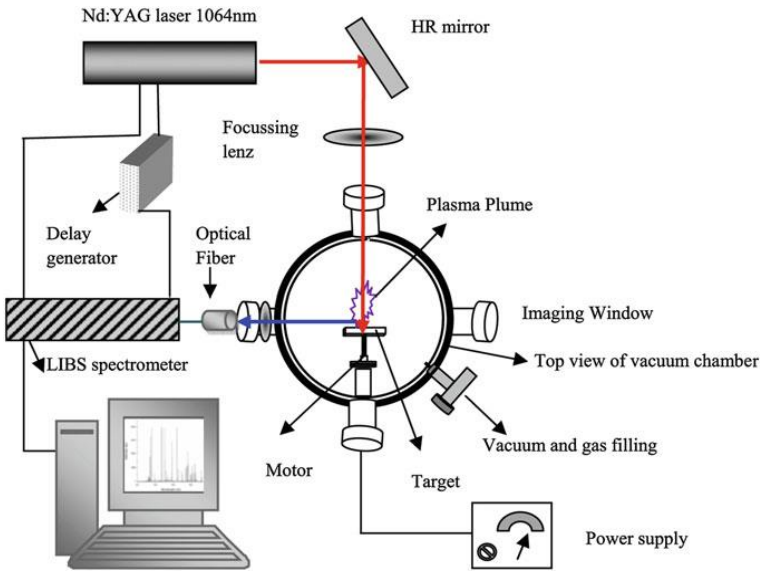

Figure 1 - Scheme of a LIBS system with a variable-atmosphere sample chamber [1]

The series of processes that are involved in a LIBS analysis can be generally summarized in four main phases:

1. A laser pulse of suitable duration (most commonly in the order of a few nanoseconds) and energy is focused on the surface of a sample.
2. A part of the pulse's energy is transferred to the sample, vaporizing a small fraction of material and forming a plasma plume (breakdown process). Depending on the pulse duration, the laser can interact with the vaporized species, further increasing the plasma temperature and energy.
3. An optical system (lenses, mirrors or optical fibers) gathers the light emitted from the decaying plasma species (atoms or, in some cases, ions) and directs it to a suitable analyzer/detector couple.
4. The emitted light is registered and analyzed to determine the elemental composition of the sample.

A lot of the principles behind LIBS are, as a matter of fact, the same that regulate the Optical Emission Spectroscopy (OES). As such, LIBS is closely related to other Atomic Emission Spectroscopies (AES) such as ICP, MIP-OES (Microwave Induced Plasma), DCP-OES (Direct-Current Plasma). The most obvious difference is that in LIBS the vaporized sample does not need to be transported to the plasma source. The plasma is, in fact, generated directly on the surface of the sample by the laser pulse. The processes of ablation and excitation happen at (almost) the same time and the samples don't usually need to be prepared or treated beforehand [1] [4].

1.1.1 – The LIBS Plasma

The laser ablation process is faster than a laser pulse that has a duration in the nanosecond range. This means that the laser can keep interacting with the produced vapor plume, further increasing its temperature, up to the point where a plasma starts to form. This whole process is generally called breakdown.

A plasma is matter aggregation state that is similar to the gaseous state, but that is characterized by the presence of a fraction of electrically charged, unbound species. The overall charge of a plasma is generally zero. While the species in a plasma are unbound, they are affected by the electromagnetic fields and currents generated by the other moving particles. As such, plasmas often act with a collective behavior [16]. Plasmas can be classified on the basis of their ionization degree, that is the fraction of free electrons with respect to the other species. A weakly ionized plasma is one where the fraction of free electrons is below 10%, while a highly ionized plasma can reach up to 100% (e.g. in stars or thermonuclear explosions). A LIBS plasma is generally classified as a weakly ionized plasma.

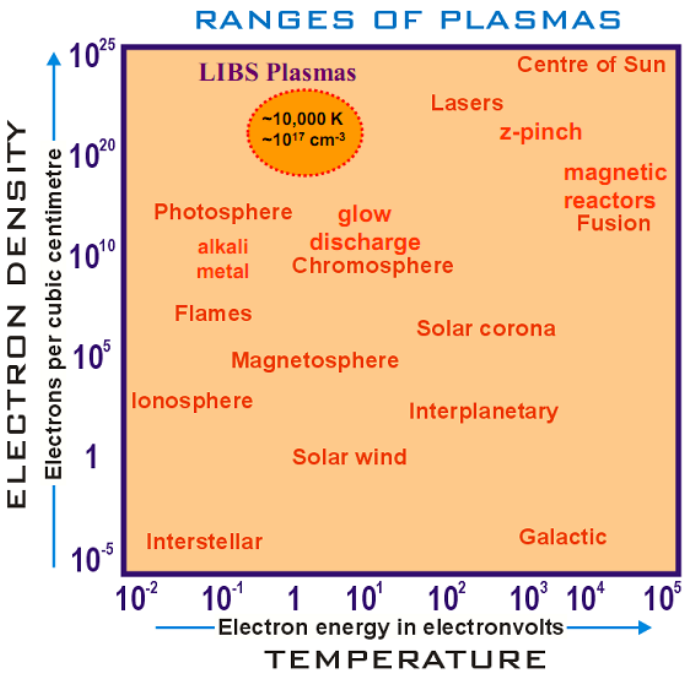

Figure 2 - Classification of various plasmas as a function of the electron density and temperature

In order for the plasma generation to start, some seed electrons need to first be present in the volume where the laser pulse is focused. These can be spontaneously generated by the natural earth radioactivity, by cosmic rays, by the first few photons of the pulse itself, by collisions with charged species (i.e. O_2^-) or by multiphoton ionization of molecules in the surrounding atmosphere. Secondly, it is necessary to reach an electron and ion density that is sufficiently high for the breakdown to occur. At laser irradiances commonly found in LIBS ($10^8 - 10^{10}$ W cm^{-2}) there are two main mechanisms that are responsible for the "ignition" of the plasma plume:

- Cascade Ionization
- Multiphoton Ionization

At low irradiance levels, the cascade ionization mechanism is prevalent [2]. The free electrons present in the focal volume of the pulse absorb the laser photons and are accelerated by the generated electric field. They come into collision with the neutral species in the vapor plume and quickly increase their temperature. A small fraction of these electrons gain sufficient energy to ionize a neutral species, according to the equation:

$$M + e^- \rightarrow M^+ + 2e^- \qquad \text{Equation 1.1}$$

This process generates new electrons that are accelerated by the electric field and cause further ionization. Another process that can increase the electron energy is the inverse bremsstrahlung, where an electron can absorb a photon while being inside the electric field of an atom or an ion. These processes contribute to an increase in the probability of collisions between the species, as

well as an increase in the ionized fraction within the plasma. As a consequence, the number of electrons in the plasma also increases and they too are accelerated by the laser pulse. This "chain reaction" continues until the breakdown occurs.

If the laser irradiance is high, the multiphoton ionization mechanism becomes prevalent instead. In this case the electrons are generated by the simultaneous absorption of several photons. This mechanism is non-linear, fast and does not require the presence of available seed electrons in the focal volume of the pulse. The multiphoton ionization can be represented using the equation:

$$M^0 + nhv \rightarrow M^+ + e^- \qquad \text{Equation 1.2}$$

Where n is the number of photons having hv energy and M a species in the vaporized plume in a neutral (^{0}) and ionized ($^+$) state.

As a general rule, both mechanisms contribute to the generation of the LIBS plasma but the proportion depends on several factors. As already mentioned, at low irradiances the prevalent mechanism is the cascade ionization. But the duration of the laser pulse, the laser's wavelength, the sample composition, the presence of impurities, etc. can also contribute differently to one mechanism or the other.

The inverse bremsstrahlung and multiphoton ionization mechanisms are also responsible for a phenomenon called "plasma shielding". This only happens when the laser pulse duration is longer than the time it takes for the plasma to ignite (a laser pulse lasting several ns is often subject to plasma shielding). In this case the plasma rapidly becomes optically thick and absorbs the remainder of the laser radiation. While this contributes to an increased plasma energy, ionization degree and temperature, it also prevents a fraction of the laser pulse from reaching the sample surface, effectively reducing the ablated mass. It should be noted that the extent of the plasma shielding effect also depends on the laser wavelength and irradiance [17].

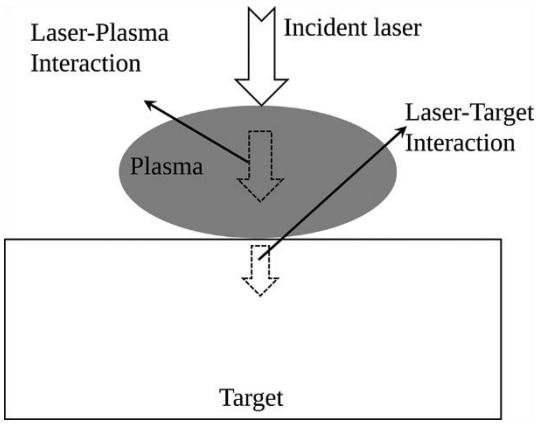

Figure 3 - Schematic representation of the plasma shielding effect [18]

The growing plasma expands outwards in all directions, but with a more pronounced fashion towards the direction of the laser beam where the photon absorption is higher than the rest of the plasma. This gives a slightly conical appearance to the plasma plume. This expansion happens with supersonic speed, compressing the surrounding atmosphere (if present) and generating a shockwave as well an audible sound.

The plasma evolution can then follow three different pathways, depending on the intensity of the incident radiation:

- Laser Supported Combustion (LSC)
- Laser Supported Detonation (LSD)
- Laser Supported Radiation (LSR)

In the conditions commonly encountered in LIBS, only the first two pathways are observed.

At low intensities (LSC regime) the shockwave precedes the absorption region (which coincides with the plasma front) and the energy used for the expansion towards the laser beam comes from the plasma radiation and the shockwave inertia itself. At higher intensities (LSD regime) the wavefront is strong enough to compress and heat up the surrounding atmosphere, so that the absorption zone comes just after the wavefront itself.

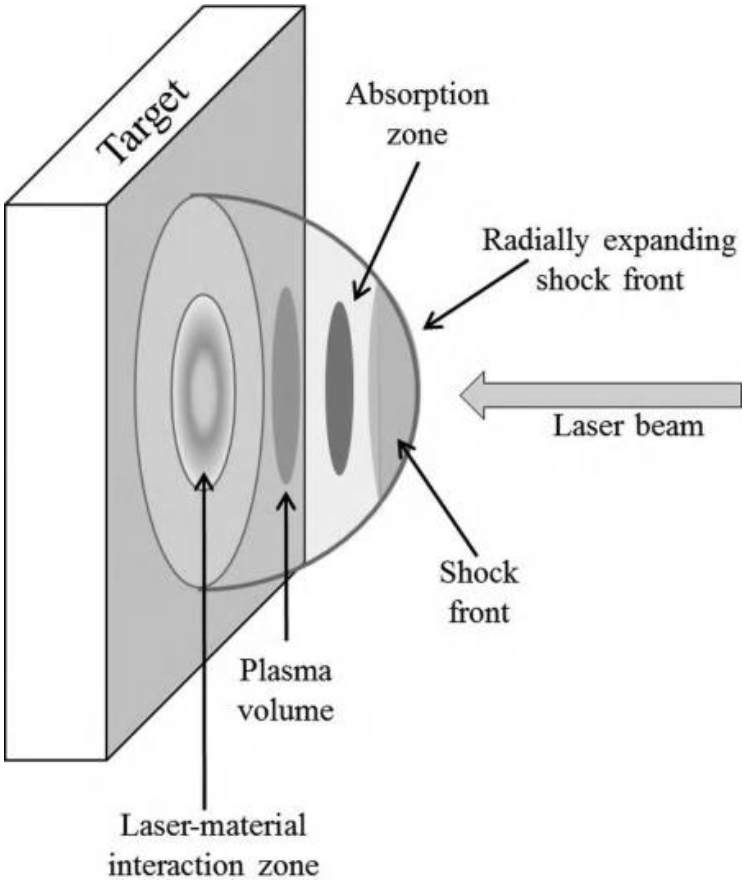

Figure 4 - Schematic representation of the evolution of a plasma generated on a solid surface [2]

As mentioned, the plasma becomes optically thick once the plasma absorption frequency coincides with the laser's own frequency. This condition arises when the electron density reaches a critical value:

$$n_e \approx \frac{(10^{21}\lambda^{-2})}{cm^3} \qquad \text{Equation 1.3}$$

Where λ is the laser wavelength in micrometers.

For example, for a conventional Nd:YAG laser that operates at the fundamental wavelength of 1064 nm, the value of n_e is roughly 10^{21} cm^{-3}. In this case the laser's energy will be absorbed, increasing the electron density and the plasma frequency until this becomes higher than the laser's frequency. At this point the laser radiation will be reflected, marking the end of the plasma formation process.

Once the laser pulse has ended (for pulses lasting from few fs to few ns), the plasma plume evolves with an inertial growth and expansion, followed by a cooling process [1] [2] [3] [5] [19] [20].

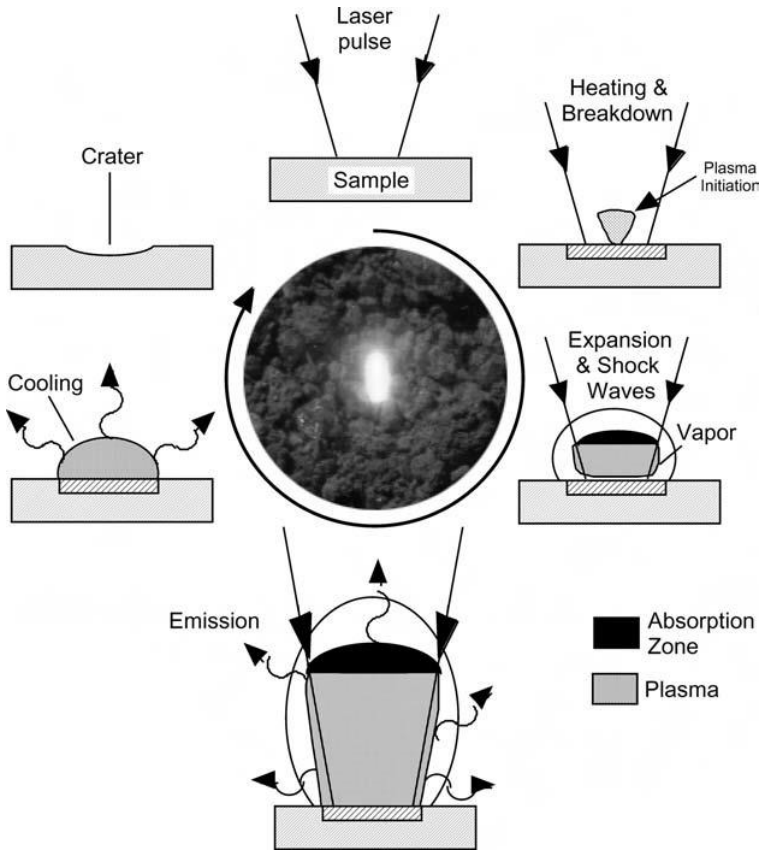

Figure 5 - Representation of the processes involved in a LIBS analysis [3]

The cooling process of the plasma plume is strongly influenced by the environmental and boundary conditions. If the plasma evolves in a vacuum, the plume expands adiabatically and the evolution of the ablated material follows Euler's hydrodynamic equations [21]. If the plasma is instead generated in a fluid (i.e. an atmosphere or a liquid), the plume compresses the surrounding

medium, transferring part of its energy by conduction, radiation and physically with the formation of a shockwave. In this case, the evolution of the shockwave can be described using Sedov's Theory [5] [22].

The emission signals of the species present in the plasma emerge during its cooling phase [1] [2] [3]. As previously mentioned, the emitted light contains information regarding the characteristic emission lines and, in turn, the nature of the atomized elements in the plasma. The intensity of these emissions depends on several physical parameters, such as the temperature of the plasma, matrix effects, the homogeneity of the plasma, etc., but also on spectroscopic parameters such as the probability of a transition, the energy difference between the excited and fundamental levels, etc.

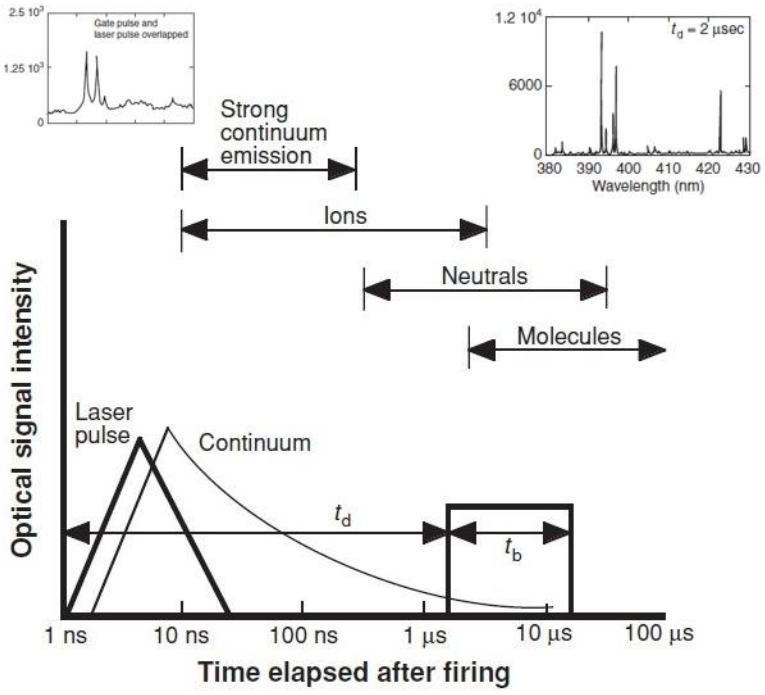

Figure 6 - Time scale of the emission processes in a LIBS plasma [3]

Figure 6 shows a schematic representation of the temporal scale of the evolution of the emission intensity of a LIBS plasma. The scale of the figure is generally valid for a ns pulse of a Nd:YAG laser operating at the fundamental wavelength of 1064 nm. If the pulses are longer (i.e. for a CO_2 laser) or shorter (i.e. for a Ti:Sapphire laser) the timescales expand or contract accordingly.

Right after the laser pulse, the emission intensity increases to a maximum and then decreases steadily. The acquisition of the LIBS spectrum is done during this decreasing phase. This can be justified by describing the various phenomena that are responsible for the emission of radiation by the cooling plasma.

There are two causes for the high intensity of emission during the first instants: the characteristic atomic emission and a continuous emission. The continuous emission is generated by the plasma as a result of free-free transitions (acceleration of electrons caused by the electrostatic interactions with ions and neutral species) and free-bound transitions.

The equations that represent free-free transitions in the electric field of an ion or a neutral atom are, respectively:

$$M^+ + e^-(mv_1^2/2) \rightarrow M^+ + e^-(mv_2^2/2) + hv \qquad \text{Equation 1.4}$$

$$M \quad + e^-(mv_1^2/2) \rightarrow M \quad + e^-(mv_2^2/2) + hv \qquad \text{Equation 1.5}$$

In the free-bound transition the electron is instead captured by an ion, releasing the accumulated kinetic energy as electromagnetic radiation (recombination energy), according to the following relation:

$$M^+ + e^- \rightarrow M \quad + hv \qquad \text{Equation 1.6}$$

The energy of the emitted photon (hv) is equal to the difference between the energy of the free electron and that of the energy level occupied after the recombination. Due to the fact that this difference can have any random value, the resulting emission is a continuous spectrum.

The transitions that are responsible for the characteristic emission of an element are those originating from bound-bound transitions. When an atom (or an ion) is in an excited state it will undergo a transition to a lower energetic state through a spontaneous or stimulated emission. The energy of the emitted photon is the difference between the energies of the levels involved in the transition. This process can be represented by the equations:

$$M^{+*} \rightarrow M^+ + hv \qquad \text{Equation 1.7}$$

$$M^* \rightarrow M \quad + hv \qquad \text{Equation 1.8}$$

The unspecific continuous emission decays faster than the atomic emission during the processes of plasma cooling. This means that after a certain time since the onset of the plasma, the characteristic signals of the plasma species become prevalent over the continuous background. This means that choosing the optimal time for the acquisition of the LIBS signal is a crucial step for the analysis. In fact, the preferred detection systems have the temporal resolution to investigate an interval in the plasma lifetime where the emission lines of interest are strong and not obscured by the background.

1.1.2 – Correlation Between Plasma Characteristics and Emission Intensity

In qualitative LIBS analyses, is sufficient to identify the spectral emission lines of the analytes of interest. On the other hand, in quantitative LIBS analyses, it is necessary to measure the intensity of such emission lines (either the absolute or relative intensity or, preferably, the integrated line intensity), which is correlated to the concentration of the analytes in the plasma.

There are two main factors that are responsible for the intensity of an emission line: the oscillator strength (a dimensionless quantity that describes the relative intensity of the emission) and the excitation conditions, namely the density of the emitting species inside the plasma. For example, in an optically thin plasma (i.e. with a low density of optically active species) the radiation emitted by an atom can more easily escape the plasma, without any significant absorption or scattering. In this condition the emission lines would be more intense and the results of the analysis would be qualitatively better. One of the main issues of quantitative LIBS analyses is, in fact, the self-absorption of some wavelengths by the plasma itself. This can lead, without suitable corrections or adjustments, to a result which is not representative of the composition of the analyzed sample.

To derive the analytical expression that describes the emission line intensity, it is necessary to first characterize the chemical and physical properties of the ensemble of atoms, ions, molecules and electrons present in the plasma. If a thermodynamic equilibrium exists, then the properties of the plasma can be described using the concept of temperature (T), using the Maxwell equation for the kinetic energy, the Boltzmann equation for the excitation energy, the Saha equation for the ionization energy and the Planck equation for the radiative energy.

In practice, such equilibrium conditions are rarely present in LIBS. To overcome this limitation, the concept of Local Thermodynamic Equilibrium (LTE) was introduced. LTE is an approximation that accepts the presence of a thermal equilibrium (with the exclusion of radiative phenomena) in small regions inside the plasma. This approximation can be accepted as true only after a certain time delay from the plasma ignition by the laser pulse, when a substantial number of collisions between the various species have already happened. In particular, in order for the population of the ionic and atomic states to be in equilibrium with the electron temperature (which is defined by the Maxwell distribution), it is necessary that the electron density is sufficiently high to ensure a high number of collisions. The McWhirter principle allows the determination of the lower limit for this condition to be verified:

$$n_e \geq 1.6 \cdot 10^{12} T^{1/2} (\Delta E)^3 \qquad \text{Equation 1.9}$$

The term ΔE, expressed in eV, is the highest transition energy necessary for the condition to be satisfied, while T is the plasma temperature. If the value of the electron density is higher than that

obtained by Equation 1.10, the electrons heat up rapidly and transfer their energy to the other species, determining the temperature of the entire plasma.

The most common method for the determination of the electron density in a LIBS plasma (provided the experiment is not performed in a near perfect vacuum or an inert atmosphere) is the observation of the Hydrogen emission line at the wavelength of 656.279 nm (H-α emission line from the Balmer Series). In a typical LIBS measurement, the Stark effect is the predominant contribution to line broadening. In brief: the presence of an electrical field inside the plasma plume, caused mainly by the electrons, perturbs the energy levels of the emitting species, thus producing a broadening of the emission lines. In the case of the H-α line, the electron density is proportional to the line broadening as expressed by the following equation:

$$n_e = C(n_e, T)\Delta\lambda_{FWHM}^{3/2} \qquad \text{Equation 1.10}$$

Where C is a constant that is found in tables in the literature [23].

The plasma temperature, when in LTE conditions, can be determined with various methods. Depending on the experimental conditions, some methods can be more viable or effective than others. T can be determined from the intensities (absolute or relative) of some emission lines (i.e. line couple ratio or Boltzmann plot), from the ratio of a line and the spectral background, etc.

For example, if two emission lines are considered, belonging to the same atomic species and having the same degree of ionization (in spectroscopic notation the symbol "I" refers to neutral species, while the symbol "II" refers to singly ionized species, and so on), but with upper transition levels of different energy, it is possible to use the Boltzmann equation (which allows the determination of the relative population of different energy levels) to determine the plasma temperature.

$$\frac{I_1}{I_2} = \frac{g_1 A_1 \lambda_2}{g_2 A_2 \lambda_1} exp\left[-\frac{E_2 - E_1}{K_B T}\right] \qquad \text{Equation 1.11}$$

A_1 and A_2 are the transition probabilities for the two transitions having wavelengths λ_1 and λ_2, g_1 and g_2 are the degenerations of the excited states, E_1 and E_2 are the energies of the excited states and T is the plasma temperature at the time of the observation.

Another method for the determination of the plasma temperature requires the construction of a Boltzmann plot. The intensity of a spectral line that corresponds to the transition between the two energy levels E_1 and E_2 of an atomic species s is given by:

$$I = n_s g_k A_{ki} \frac{e^{E_k/K_B T}}{U_S(T)} \qquad \text{Equation 1.12}$$

Where n_s is the density (expressed in particles/cm^3) of the species s, A_{ki} is the transition probability, g_k is the degeneration of the k-th level and $U_S(T)$ is the partition function of the emitting species at the plasma temperature T. Equation 1.14 can be rearranged to give:

$$ln\left(\frac{I}{g_k A_{ki}}\right) = \frac{-E_k}{K_B T} + C \qquad \text{Equation 1.13}$$

Which can be viewed as the equation for a linear plot (y = mx + c). By plotting the line intensities as a function of the energy of the excited state and applying a linear regression, the slope of the resulting line will be (-1/K_BT), from which the temperature can be readily obtained.

If the LIBS spectra shows both the ionic and neutral emission lines of a same atomic species, it is possible to use a combination of the Saha and Boltzmann equations for the determination of the plasma temperature:

$$ln\left(\frac{I_{ij}^{II} A_{mn}^{I} g_m^{I}}{I_{mn}^{I} A_{ij}^{II} g_{ij}^{II}}\right) = ln\left(\frac{2(2\pi m_c kT)^{3/2}}{n_e\, h^3}\right) - \frac{E_{ion} - \Delta E_{ion} + E_i^{II} - E_m^{I}}{kT} \qquad \text{Equation 1.14}$$

Where h is the Planck constant, E_{ion} is the first ionization potential, ΔE_{ion} is a correction constant and n_e is the electron density.

More recently, in order to solve the problems related to the scarcity of calibration standards for LIBS, an algorithm called Calibration Free LIBS (CF-LIBS) [24] [25] [26] [27] has been developed.

Proposed first by Ciucci et al [24], it is meant to compensate for the matrix effects by applying the equations derived from the LTE assumption. The spectral data is analyzed in order to make each LIBS measurement self-consistent and avoid the need for calibration curves. This way, the relative concentrations of the elements present in the plasma can be determined directly. It must be stressed out that the method rests on the assumptions that the abundance of the emitting species in the plasma reflects the chemical composition of the sample (stoichiometric ablation), that the plasma is optically thin and is in LTE conditions.

Once the electron density and the plasma temperature are known, the Boltzmann plots can be constructed. For CF-LIBS, a separate plot is generated for (ideally) each of the species in the plasma. In practice, only the major components of the plasma and the minor elements of interest are selected. Considering the graphical representation of each species in the Boltzmann plot as points on lines with equations *y = mx + q*, the cumulative plot will consist of parallel lines (one for each species) having the same slope but different intercept. The intercept of each species, q^s, is expressed by the equation:

$$q^s = \log\left(\frac{F n_s}{U_s(T)}\right) \qquad \text{Equation 1.15}$$

Where n_s is the number density of the species s in the plasma, $U_s(T)$ is the partition function of the species s at the temperature T, and F is an experimental efficiency parameter. The number density of each species can be thus derived from Equation 1.18, provided all the other parameters are known. The total number density of the element of interest is obtained by the sum of the neutral and the ionized species in the plasma (typically, this includes neutral and singly ionized species). The relative abundance c_a of an element a is obtained as:

$$c_a^m = \frac{(n_a^I + n_a^{II})M_a}{\sum_{a'} n_{a'} M_{a'}} \qquad \text{Equation 1.16}$$

Where M_a is the atomic mass. Since a closure condition is assumed ($\sum n_{a'} = 100\%$), the trace elements that have not been considered will be included in the fraction of the most abundant element, which will be slightly overestimated.

While the algorithm is very powerful, CF-LIBS is not without limitations. First of all, the correct application of the procedure requires the knowledge of the intensity of the spectral lines emitted by all the elements of interest and of the plasma temperature. Similarly, while it can be theoretically applied to all elements of the periodic table, relevant spectral information must be available regarding the elements and the emission lines to be measured. This includes first ionization energy and atomic mass for each element, upper and lower level energy and statistical weight, transition probability for each spectral line to be measured, partition function value in the range of temperature of interest for each neutral and firstly ionized species. These values can be obtained from spectral databases [28]. Even though LIBS is generally able to detect most elements with ppm sensitivity, it is also often characterized by a shot-to-shot variability of about 5%, and transition probability values are often known only to within 10%-20%. Therefore, the uncertainties associated with CF-LIBS method are usually greater than the theoretical minimum.

A variation of CF-LIBS, first elaborated by Gaudiuso et al [29] and then finalized by Cavalcanti et al [30] is based on the use of a single, matrix-matched calibration standard (easier to acquire than the several required for a full calibration curve) for the determination of some experimental parameters. This approach, called One Point Calibration LIBS (OPC-LIBS) relies on the determination of a corrective parameter $P(\lambda) = F(\lambda)g_iA_{ki}$ in the measured line intensity (according to the Boltzmann equation):

$$I_m = C_S P(\lambda) \frac{e^{-E_k/K_B T}}{U_S(T)} \qquad \text{Equation 1.17}$$

The experimental values are adjusted in order to reproduce the concentrations of the known sample (by CF-LIBS), and then the obtained P(λ) values are used for the usual CF-LIBS analysis of the unknown samples. The authors demonstrated how the OPC method is fairly robust, as it can

generally account for variations in the plasma temperature and electron density between samples, but it requires that the same emission lines are used in the analysis of both the SRM and the unknown samples.

1.1.3 – LIBS Analysis of Solid Samples

Since the first scientific publication on LIBS [31], which involved the analysis of metallic samples, LIBS has been widely used to investigate solid samples such as metals and alloys, but also geological materials and biological samples (usually dried). In this section, an overview of the processes that occur during a LIBS analysis of a solid sample will be given.

The series of chemical and physical processes that lead to the ablation of a sample can be summarized in three main events, schematized in Figure 7:

1. Laser-Matter interaction, which comprises the heating, the evaporation and the breaking of chemical bonds (this kind of processes have been detailed extensively in many papers on laser-heating of various materials [32] [33] [34]) and plasma generation.
2. Plasma expansion and cooling.
3. Particle ejection and condensation.

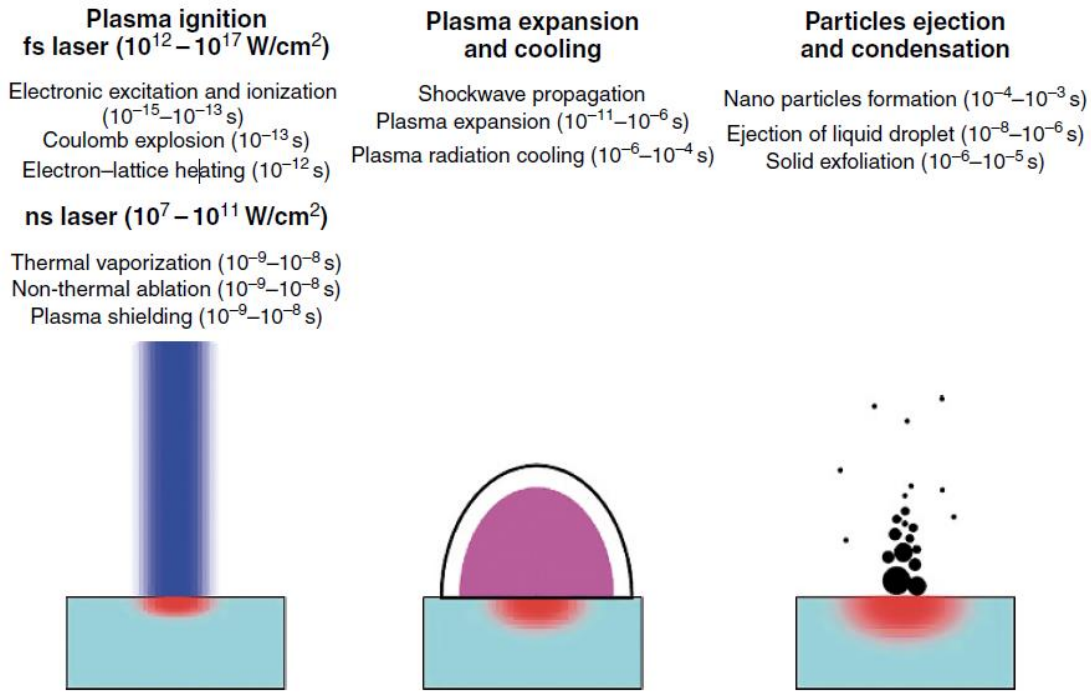

Figure 7 - Summary of the processes involved in a LIBS analysis

Initially, a laser pulse of sufficiently high energy is focused on the surface of a sample. The dimensions, position and depth of the sampling area should also be chosen suitably, depending on the requirements of each application. During this first phase, the mechanisms and plasma

properties strongly depend on the laser parameters, namely the pulse duration and the pulse energy (or irradiance).

For nanosecond lasers (irradiance ≤10^8 W/cm^2), which are the most common laser sources in LIBS, the main mechanism is thermal vaporization, with distinct phase transitions from solid to liquid to vapor and finally to plasma. In this case, the laser energy is absorbed by the sample and partially converted into heat. The sample's temperature increases rapidly up to a critical point (the melting and vaporization temperatures of the sample's material), when a rapidly expanding jet of high-pressure vaporized material (ablation) is observed.

In the case of femtosecond lasers (irradiance 10^{12} - 10^{17} W/cm^2), several distinct electronic phenomena are observed, depending on the nature of the sample. In the case of metals and conductive samples, the electron in the conduction bands can directly absorb the laser energy and readily ignite a high energy plasma. In the case of semi-conductors and dielectric materials, the plasma can be ignited by non-linear processes such as cascade ionization and multiphoton ionization (as described in the previous sections). The highly energetic species generated by a fs pulse usually lead to a process called Coulomb explosion or non-thermal fusion [5].

Lastly, picosecond lasers (which can reach irradiances of about 10^{10} - 10^{13} W/cm^2) can give rise to both thermal and non-thermal phenomena, depending on the laser parameter and the sample's nature.

The different mechanisms responsible for a sample ablation are also responsible for the different shapes of laser-generated craters on the sample surface, as shown in Figure 8.

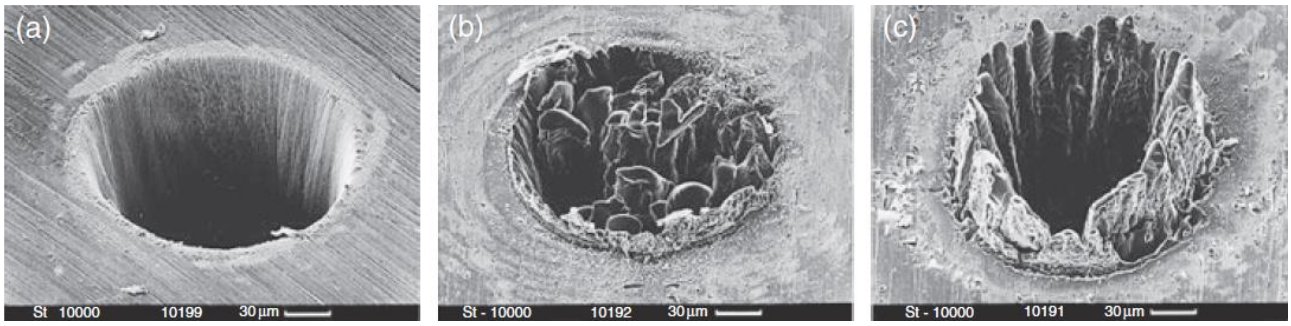

Figure 8 – Different shapes of the ablation craters on a 100 µm thick steel sample, generated by (a) 200 fs laser pulse, (b) 80 ps laser pulse and (c) 3.3 ns laser pulse. Figure from [5]

The amount of ablated material is dependent on may factors (i.e. energy and duration of the laser pulse, sample's material, etc.) but can be estimated using the equation:

$$M = \frac{E(1-R)}{C_p(T_b-T_0)+L_v} \qquad \text{Equation 1.18}$$

Where R is the surface reflectivity, C_p is the specific heat capacity, T_b is the boiling temperature (°K), T_0 is the ambient temperature, E is the energy of the laser pulse and L_v is the latent heat of vaporization [2].

If the sample is subject to large thermal stress gradients, such as in the case of a rapid heating process, large particles can break off from the surface and be ejected into the growing vapor plume. As the vapor plume evolves from the molten sample, the high pressure can eject liquid particles into the plume itself. These particles can further interact with the laser pulse to be ablated, or can fall away from the laser beam and solidify around the ablation spot. Once the plasma starts to dissipate and cool down, the formation of solid and liquid particles is observed. Nanometer-sized particles are formed when the plasma plume cools below the boiling point of the sample's material (≈3000°K), and the process continues until the temperature reaches the condensation point (≤2000°K).

1.1.4 – LIBS Analysis of Liquid Samples

While most considerations made for LIBS plasmas that are generated and evolve in an atmosphere are still valid for LIBS plasma created in a liquid, the higher density of the surrounding environment strongly influences the plasma dynamics, its lifetime and the emitted radiation.

As with the generation of a plasma on the surface of a solid sample, the irradiance that is necessary to initiate the breakdown is strongly dependent on the properties of the surrounding environment such as its ionization energy, the presence of impurities and, less significantly, the temperature of the liquid (which is related to its density). It should be noted that the efficiency of laser generation of plasmas inside a liquid is greatly reduced if compared with a similar plasma generated in a gaseous atmosphere or in vacuum. This is due to a higher dispersion of the laser light by the presence of suspended solids, by a higher absorption of laser energy before the focal point, the formation of bubbles (and consequently the loss of energy needed for the vaporization of the matrix). Nevertheless, for any given liquid matrix the laser energy that is required for the breakdown depends on the characteristics of the laser pulse and the laser itself. Parameters such as wavelength, pulse duration, beam diameter and focal length are crucial and generally need to be optimized for each application.

The ignition of the plasma follows the same processes that have been discussed previously, for plasmas generated in a gaseous atmosphere on solid samples. Cascade and multiphoton ionization processes can occur in liquid samples as well, albeit with slight differences. In the case of a liquid environment, the seed electrons needed for the cascade ionization mechanism are generally supplied by traces of impurities that are present in the focal point of the laser pulse.

Once the plasma is ignited inside the liquid environment it expands supersonically, compressing the liquid and generating a high-pressure shockwave. However, the plasma expansion is strongly inhibited by the confinement caused by the surrounding medium. In these conditions, the internal temperature and pressure are higher than those registered in a plasma that evolves in a gas. On the other hand, a large fraction of the plasma energy is converted into mechanical energy.

Along with the shockwave, a layer of vapor is produced and it surrounds the expanding plasma. This layer expands adiabatically, creating a distinct cavitation bubble. The dimension of the cavitation bubble increases with the laser pulse energy and duration [35] [36]. During the first instants the pressure inside the bubble is higher than the hydrostatic pressure of the surrounding liquid, and a rapid expansion is observed. As the bubble expands and the vapor layer condenses, the internal pressure drops below the one exerted by the liquid medium, causing the bubble to stop expanding, shrink and eventually collapse. The rapid collapse causes a sharp increase in the local temperature and internal gases which, in turn, give rise to a second shockwave as the cavitation bubble "rebounds". Depending on the maximum size of the bubble, this phenomenon can happen multiple times in a cyclic fashion, lasting several milliseconds [37] [38]. The collapse of the cavitation bubble is so energetic that emits energy in the form of acoustic waves as well as visible (and infrared) light [39]. The emitted radiation, however, is short-lived and characterized by a continuous spectrum that, in some cases, can hinder LIBS analyses.

These phenomena all contribute negatively to the plasma lifetime and expansion, and cause it to more rapidly cool down and dissipate. As such, the resulting light emission (and in turn the LIBS signal intensity) is greatly reduced when compared to plasmas that evolve in a gas.

An estimation of the energy balance for the generation of a plasma in water was first proposed by Vogel and co-workers [40]. The absorbed laser energy is dissipated according to the relation:

$$\delta E_{in} = E_s + E_b + E_v + E_r + E_x \qquad \text{Equation 1.19}$$

Where E_s is the energy of the shockwave, E_b is the energy of the cavitation bubble, E_r is the radiative energy of the plasma, E_v is the energy of evaporation and E_x is a corrective factor for unknown energy losses. For example, a nanosecond laser pulse at the fundamental Nd:YAG wavelength of 1064 nm can expend more than 90% of its energy to ignite the underwater plasma.

Due to all the aforementioned factors, as a general rule the LIBS signals registered from the emission of a plasma generated in a liquid are less intense and less defined than a conventional LIBS plasma in a gas or on a solid sample. In particular it is observed that the plasma emission lasts only a few microseconds or less [2] [5], the spectra are dominated by a continuous emission that decays in the same time interval as the strongest elemental emissions and, finally, the emission

lines are significantly broadened due to a higher plasma density (i.e. by self-absorption or Stark broadening).

1.2 – LIBS Instrumentation

The basic components of a LIBS instrument are generally similar between standard setups. Each research group or company then uses variations on the geometry or the components, depending on the required performances and on the particular application. Figure 9 offers a schematic representation of the various parts that can be found in a generic LIBS system.

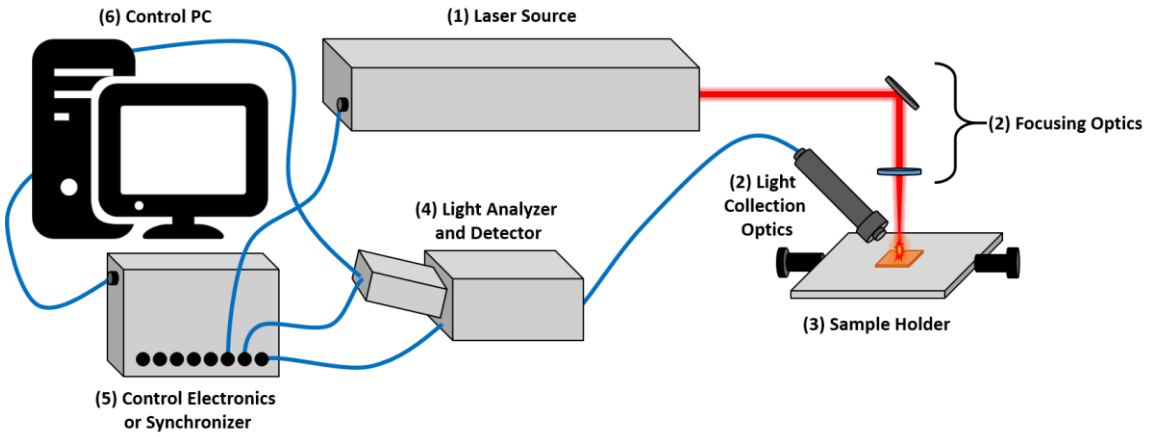

Figure 9 - Schematic representation of a generic LIBS setup

1. The laser source.
2. The optical system:
    - Mirrors and lenses are commonly used to direct the laser beam from the laser source output to the sampling area and to focus the pulse on the sample. In some applications, fiber optics can be used.
    - The light collection system can have numerous configurations. From a lens that directly focuses the plasma light into the analyzer, to a probe-and-fiber configuration for remote analysis.
3. Sample support: usually not strictly necessary, it can be useful for irregular samples or to fine-tune the sampling position. In some cases, this can be swapped out for a controlled atmosphere chamber with temperature, pressure and composition regulators.
4. Light analyzer and detector: this part of the LIBS instrument is responsible for dispersing the incoming light into its spectral components and it registers the intensity corresponding to each wavelength.
5. Control electronics and synchronizer: since the precise timing between the laser pulse and the spectral acquisition is critical in LIBS, a separate system to control and synchronize the

various components can be used (e.g. a pulse generator module). In most modern systems, this operation is often performed directly by the control PC.

6. Control PC: can be used to control the laser and detector triggers, and is used to store and analyze the registered spectra.

1.2.1 – Laser Sources

The main component of a LIBS instrument is the laser. It is used to ablate and vaporize solid samples, to excite the atomized material and generate the light-emitting plasma. As mentioned in the previous sections, the first laser was introduced in 1960 for a paper by Maiman [41]. A detailed description of the working principles and theory of lasers is beyond the scope of this thesis, and is thoroughly presented in several books [33] [34].

It should be noted that only high-energy pulsed lasers are used in LIBS, due to their capability of generating plasmas on almost any material. Moreover, the laser characteristics and performances can have strong repercussions on the quality of LIBS measurements. Because of that, the choice of the laser source is one of the most critical aspects for the construction of an analytical instrument. The main properties of each laser beam are: intensity, directionality, monochromaticity and coherence.

The intensity (also known as irradiance or power density, expressed in W cm^{-2}) represents the maximum laser power divided by the cross-section of the output beam. Modern lasers can generate very brief pulses, allowing powers in excess of billions (in some cases even trillions) of Watts per surface unit to be reached. Still, what is crucial in LIBS is the actual amount of power delivered on the sample, which is also a function of the system used to direct and focus the laser beam.

The directionality of the beam is associated with the possibility of focusing it on very small areas. The coherence is also related to the beam divergence, but it is of little importance in LIBS. Similarly, monochromaticity is not critical in LIBS, since the plasma generation and evolution are almost completely dependent on the amount of power delivered on the sample. Nevertheless, the choice of the laser wavelength as well as the pulse duration are crucial in LIBS, as the laser-matter interaction phase is strongly dependent on these parameters.

Several studies have demonstrated how laser sources emitting in the UV region tend to have high ablation efficiency, high reproducibility, high spatial resolution and lower continuous background emission (i.e. higher Signal/Noise ratio) because a larger fraction of the pulse's energy is absorbed by the target material [42] [43] [44] [45] [32] [46] [47]. However, using wavelengths in the near-infrared allows to lower the energy required for the ablation of the sample. In other words, the breakdown threshold is lower [47] [48].

The pulse length, defined as the full width at half maximum (FWHM) of the energy/time profile of the laser pulse, mainly influences the fraction of energy that is transferred to the sample and the fraction of the laser pulse that interacts with the formed plasma. It is also crucial in the plasma evolution processes, discussed in the previous sections.

In LIBS applications are frequently required laser powers in the order of MWs, that can fairly easily generate a plasma on the sample. These power levels can be achieved by applying short laser pulses (in the order of few ns) by an operation called Q-Switching. The Q-Switch device is located in the path of the laser photons and blocks them from traveling outside the cavity. By forcing the photons inside the resonant cavity, the pumping of the laser medium continues and the electrons are accumulated on the excited energy level, guaranteeing the population inversion. After this accumulation, the Q-Switch is rapidly activated and the photons can escape the cavity for a brief moment, generating an intense and short pulse. The simplest system is the Passive Q-Switch, realized by an optically absorbent and saturable material which becomes optically transparent once it has absorbed enough photons. While cost effective and of simple construction, these systems do not offer the levels of control required in most LIBS applications. Active Q-Switch systems are almost always implemented in LIBS instruments. In these systems, a KDP electro-optical crystal (KH_2PO_4) is used to block the path of the laser photons. By applying a suitable electric signal, the crystal is "switched open" (i.e. the refraction index changes) by the Pockel's effect (these types of Q-Switches are also called Pockel's cells) and photons can escape the resonant cavity. Active Q-Switches offer much higher control over the pulse repetition rate and the timing between the lamp activation and the laser discharge.

Several kinds of laser sources have been used in LIBS, depending on the requirements for each specific application, but the most common systems are based on a Q-Switched Solid State Nd:YAG (Neodymium-doped Yttrium Aluminum Garnet, Nd:$Y_3Al_5O_{12}$) laser source. As of today, numerous Nd:YAG lasers are available in the commercial market. From the larger, liquid cooled, tabletop systems (with output powers in excess of 3 J over few ns and a repetition rate of 10-15 Hz) to the smaller, air cooled portable systems (with output powers around 20 mJ or lower, longer pulse durations and low repetition rates).

Another very versatile laser system that has been used in LIBS applications is the Ti:Sapphire laser. In this case, the active medium is a crystalline matrix (sapphire or corundum) doped with Titanium atoms, with the chemical formula Ti^{3+}:Al_3O_3. Unlike Nd:YAG lasers, the emission of a Ti:Sapphire laser is generated by both electronic and vibrational transitions in the crystal lattice, and the pumping is achieved by the use of a secondary laser that emits in the absorption frequencies of the active medium (i.e. around 500 nm).

One of the most interesting characteristics of Ti:Sapphire lasers is that they can emit along a broad range of wavelengths (from 660 nm to 1180 nm). With the addition of frequency-doubling crystals, these lasers can easily cover the entire visible and near-IR spectrum, making them particularly attractive for those applications that require a very specific wavelength or wavelength range. In addition, Ti:Sapphire lasers can deliver extremely short pulses, in the order of tens of femtoseconds [49] [50]. Despite these advantages, Ti:Sapphire lasers are complicated systems, difficult to operate and maintain and are generally very expensive. Because of this, they are generally used for fundamental research or extremely specific applications.

Recently, the scientific community has shown a growing interest in fiber lasers. These systems use an optical fiber doped with rare earth elements (Erbium, Ytterbium, Neodymium) as the active medium. Fiber lasers are generally based on double-clad fibers, in which the active medium is contained in the fiber core (where the laser light also propagates), while the pumping light propagates in the inner cladding layer. The main advantage of fiber lasers is that the medium is inherently flexible, meaning that it can easily deliver the laser light to the target and can be more easily focused. This can be advantageous in those LIBS applications that require the laser source, analyzer and control systems to be far away from the sample itself (e.g. monitoring of nuclear wastes, industrial manufacture monitoring, etc.) [51] [52]. Moreover, some fiber lasers can deliver pulses of duration comparable to those from Ti:Sapphire lasers (i.e. a few fs).

1.2.2 – Optical Systems

The optical system comprises all those components that are needed to direct and focus the laser beam from the laser output to the sample, as well as all those components that are used to collect the light emitted by the plasma during the LIBS measurement. In the case of stand-off LIBS, it is not uncommon to find laser focusing and light collection configurations based around a mirror telescope system (Cassegrain reflectors) [53], although the laser power required for such applications is significantly higher than most LIBS applications. While most components are shared between the laser optics and the light collection system (e.g. lenses, mirrors, telescopes, etc.), some observations should be made.

The choice of mirrors with the correct specifications for a LIBS application is critical. For example, plane mirrors are generally used to direct the laser beam through the desired optical path, while mirrors with other geometries (e.g. elliptic mirrors) can be used to project the plasma light into an analyzer's input slit.

The first characteristic of a mirror that should be considered is the substrate. Borosilicate glass is the cheapest substrate and it is generally used for non-transmitting mirrors, while more specialized substrates (ceramic, fused silica) can be used for more extreme environmental conditions or with

high-power lasers. A reflective layer (or more layers) is then applied to the substrate by various means (i.e. evaporative deposition, plasma sputtering, atomic layer deposition, vacuum deposition). The efficiency of the coating is strongly dependent not only on the nature of the coating itself, but also on the thickness of the layer and the combination of different layer materials. Generally, the reflective coating is made of a thin metal deposition, followed by a dielectric transparent layer that protects the metal from oxidation and increases the mirror's resistance to damage. The most commonly used metals are aluminum (overall good reflective medium, with the lowest cost), gold or platinum.

A lens or a combination of lenses can be used to focus the laser pulse on the sample as well as to create an adjustable focus system that allows for the analysis of samples of variable geometry, or to reduce the measurement spot dimensions. Similarly, a lens-based system can be used to focus the plasma light into the analyzer even with long focal lengths (provided the optical path between the plasma and the lenses is unobstructed). It should be noted that longer focal lengths also come at the expense of a smaller field of view and, in turn, are more sensitive to vibrations and collimation errors. In addition, the geometry of the lens should also be considered as it influences the focal length and dispersion of the transmitted laser beam.

The typical focal length for *in-situ* measurements is in the range of 50 to 150 mm, with lenses of 25-50 mm in diameter. The diameter of a pulsed Nd:YAG laser is generally 6-8 mm, which allows the use of smaller lenses if necessary. The most common lens materials are BK7 (borosilicate glass), quartz and NaCl. The material should be chosen in order to have the maximum transmission at the laser wavelength. If used to collect the plasma light, they should efficiently transmit the spectral bands of interest. In general, BK7 can be used for the visible and near IR ranges. The anti-reflective coatings minimize back reflections and maximize the energy transmitted to the target. An uncoated lens will generally reflect about 4% of the incident light at each surface, meaning that for an entire optical system made from uncoated lenses, the energy losses could be significant.

1.2.2.1 – Fiber Optics

Fiber optics (Fiber Optic Cables, FOCs) are extensively used in LIBS as they significantly simplify the collection of the plasma light. In fact, FOCs are particularly useful where the detection system cannot be placed near the target. In addition, the use of FOCs can aid in delivering the laser light onto the target without the need of sophisticated optical systems [54]. However, laser damage to the fiber itself or its external components (junctions, cladding, outer skin, etc.) is one of the main limitations in the use of FOCs to transmit laser pulses.

Figure 10 - A technician positions the FOC probe on the target [54]

On the other hand, the use of FOCs as a means to collect the plasma emission is very widespread [5] [55] [56] [57] [58] [59]. In this case the fiber can be directly focused on the plasma, although the presence of a lens (or lenses) is not uncommon. Nevertheless, both approaches present some limitations that must be taken into consideration when building a LIBS setup.

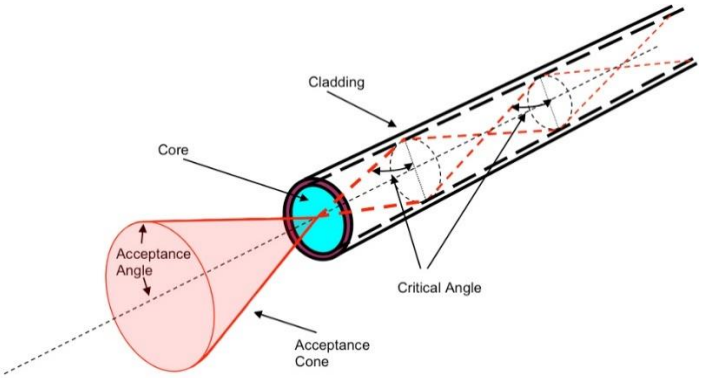

Figure 11 - Schematic representation of an optical fiber. Adapted from [60]

Since the LIBS plasma is not homogeneous, using a lens to focus the emitted light into the fiber means that small changes in the plasma morphology can alter the registered spectra. On the other hand, the total amount of light that can be collected with this approach is higher. If the fiber is placed near the plasma without a focusing system, the light that can be collected is given by the fraction of photons that enter the fiber with the correct angle. The range of angles that allows light propagation inside the fiber gives the acceptance angle (or acceptance cone), as described in Figure 11. Because of this, the optimal distance of the fiber head from the plasma plume is usually a few centimeters.

Once the light has entered the fiber core, it is transmitted through the FOC length by a total internal reflection phenomenon that is the result of the different refractive indexes of the core and the cladding elements. Depending on the application, different materials can be used to fabricate optical fibers. In the same way the lenses must be chosen to allow the wavelengths of interest to pass through without interference, similarly one should choose a FOC that is specifically optimized for the requirements of the analysis. While most fiber cores are made of fused silica, their content of OH groups can vary depending on the application requirements. FOCs working in the UV and Visible range have a high content of OH groups, while FOCs working in the IR range have OH contents in the order of 1-2 ppm or less (since OH groups strongly absorb IR radiation). Several other fiber cores are available, depending on the specific application, like low cost polymeric cores or IR-dedicated glass cores (Selenide, Sulfide, Telluride glasses). Photonic crystal core (POC) fibers have been successfully used to deliver ps laser pulses to generate a spark [61].

The second outermost layer, generally called buffer, determines the operating environment of the FOC. Typically made of Polyamide, they allow temperature ranges of -100 to 400°C as well as protection against solvents. The outermost layer is generally made of PVC, Kevlar or metal interlocking segments. It is manufactured to offer protection against scratching, chemical contamination and, in some cases, to prevent excessive bending of the FOC which could break the inner core.

1.2.3 – Light Analyzers and Detectors

In this section, an overview of the most commonly used analyzers and detectors for LIBS applications will be given. Due to the high complexity of LIBS spectra (large number of emission lines over a wide region of the electromagnetic spectrum) an ideal light analyzer system should meet some critical requirements:

- The analyzer should cover a wide spectral range and, at the same time, have a sufficiently high resolution to resolve spectral lines that are close together.
- The detector should have a high dynamic range (i.e. the registered line intensity should change with the concentration of the emitting species without saturating the detector) and a high quantum efficiency (i.e. the conversion of photons into electrical signals) over the entire registered spectrum.
- The system should be able to register the spectra and visualize the data rapidly (ideally, in real-time).

A vast number of options are available for the detection and analysis of LIBS signals, depending on the required application.

If there is only a single wavelength (or a narrow enough band) to be monitored, the simplest solution is the implementation of a spectral filter or a monochromator, coupled with a simple detector (e.g. a photomultiplier tube). This option, employed for imaging techniques or for single-line monitoring, is simple to realize and has low setup costs. Acusto-Optic tunable filters (AOTF) are an improved version of pass-band filters that can be fine-tuned to allow narrow wavelength bands through. These devices maintain the robustness and reliability of filters (there are no moving parts) but allow the monitoring of multiple wavelengths for a more versatile application.

As of today, however, the most commonly used devices in LIBS applications are the spectrographs (or analyzers) due to their much higher performances and versatility with respect to spectral filters. Numerous types of analyzers are commercially available, each one with its unique configuration of mirrors, diffraction reticles and prisms. While the basic principle is the same for all configurations (the incoming light is spatially resolved and each component is registered separately), each system presents different advantages and limitations. The most commonly used analyzers for LIBS applications are based on the Czerny-Turner and Echelle configurations.

Once the plasma radiation has been spatially resolved, it is directed towards a suitable detector. As a general rule, a light detector is any device that is capable of converting the incoming photon into a measurable signal (generally, a current or an electric potential difference). The most common detectors are photomultiplier tubes (PMTs), photodiode arrays (PDAs) or charge-coupled devices (CCDs). The latter class, commonly found as image sensors for digital cameras, is widely used in LIBS applications, often coupled with an image intensifier system (and classified as iCCDs). Beside increasing the amount of photons that arrive on the detector surface, image intensifiers can act as pseudo-shutters, electrically preventing the passage of photons and allowing to fine-tune the signal acquisition gates and duration. In fact, the use of iCCDs allows time-resolved measurement of LIBS plasmas, which is a requirement in numerous LIBS experiments [3].

Analyzers and detectors are almost often found integrated as a single system (sometimes called spectrometer) which is set up by its manufacturer to best satisfy the needs of a particular application. Recent advances in electronics and miniaturization allowed the construction of small, portable spectrometers that still offer a wide range of capabilities. They can analyze the entire visible spectrum (as well as the near IR and UV, in some cases) with high spectral and temporal resolution. While the integration of input slits, focusing lenses, analyzer (reticle or prism), collimating optics and detectors into a single instrument prevents the users from adjusting the system to particular needs, it also improves its robustness by reducing (or eliminating) misalignment issues.

1.2.3.1 – Czerny-Turner Analyzers

The Czerny-Turner analyzer configuration is the most common not only in LIBS applications, but in almost all of the commercial instruments available. The Czerny-Turner analyzer is among the simplest systems for spectral analysis. A schematic representation is given in Figure 12.

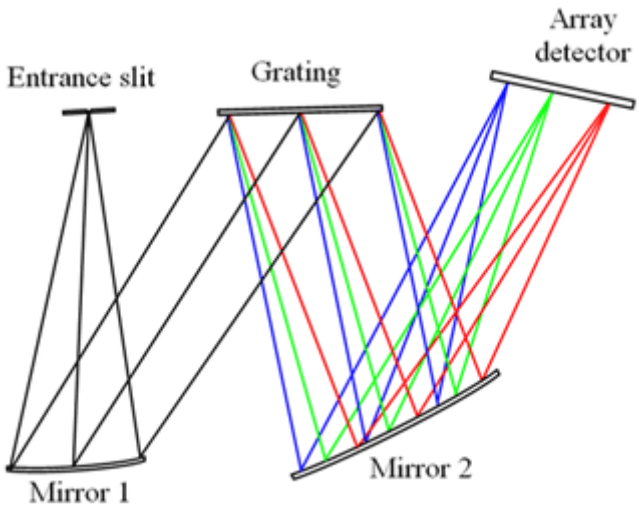

Figure 12 - Scheme of a Czerny-Turner analyzer [BWTek]

The light enters the instrument through a slit (either of fixed width or adjustable) and is collimated by a mirror onto a diffraction grating. The light is then split in its components and reflected into a detector (for a detailed description on the working principles of diffraction gratings, see References [62] [63] [64]). While the first Czerny-Turner systems required either a moving reticle or multiple, single wavelength detectors (PMTs), most modern instruments use a digital detector (PDAs or CCDs) which can register the entire spectrum that has been resolved spatially along the detector plane. This has allowed the realization of instruments without moving parts, increasing the reliability while lowering costs, dimensions and energy consumptions. Some modern instruments make extensive use of miniaturized components and integrated electronics, and can reach the dimension of a common deck of cards (see Figure 13). Such devices find extensive use in portable and handheld LIBS instruments.

Figure 13 – Comparison (not to scale) of an old Czerny-Turner spectrometer (Jarrell-Ash 78-466, 122×71 cm, 114 kg) and a modern compact, USB powered spectrometer (AvaSpec-Mini4096CL, 9.5x6.8x2 cm, 175 g, [65])

One of the limitations of Czerny-Turner analyzers is the relatively limited spectral range, even though the resolution is good enough for most LIBS applications (0.1-0.3 nm). Most spectrometers have a spectral range of about 900 nm (200-1100 nm), which is dictated by the type of detector array that is used in the system. In fact, in order to register wavelengths in the IR region, InGaAs (Indium Gallium Arsenide) detectors are needed [66], but such detectors have poor performances in the visible range. Some companies offer modular spectrometers, where each module can be configured for a specific wavelength region.

Figure 14 - Avantes AvaSpec Multi-Channel modular spectrometer [67]

However, these kinds of spectrometers present the issue of needing multiple inputs of the same plasma emission if each window needs to be measured at a given time. While this could be solved using fiber optic bundles or split fiber optics, the inhomogeneity of the LIBS plasma (as well issues connected with split FOCs and FOCs bundles) could pose a problem as not all the spectrometer inputs could contain the same analytical information.

1.2.3.2 – Echelle Spectrograph

The elevated complexity of LIBS spectra demands, as mentioned, the analysis with a wide spectral range. One possible solution is the sequential analysis of spectral regions, but this would require performing multiple measurements on a sample. As most samples are inhomogeneous, this is generally not feasible. Moreover, variations and fluctuations in the plasma plume (or in the laser source) would render each spectrum not perfectly equivalent to the others. Simultaneous measurements of the complete spectrum are required for getting optimal analytical information from the analysis.

Echelle spectrometers have been used in LIBS experiments since the late 1990s [68] [69], and have been detailed in a review by Detalle and coworkers [70]. They offer excellent resolution ($\lambda/\Delta\lambda \geq 10000$) and are capable of covering a wide spectral range (generally from 190 nm to 1000 nm). Often coupled with an iCCD detector, they represent the "workhorse" of LIBS research and analysis.

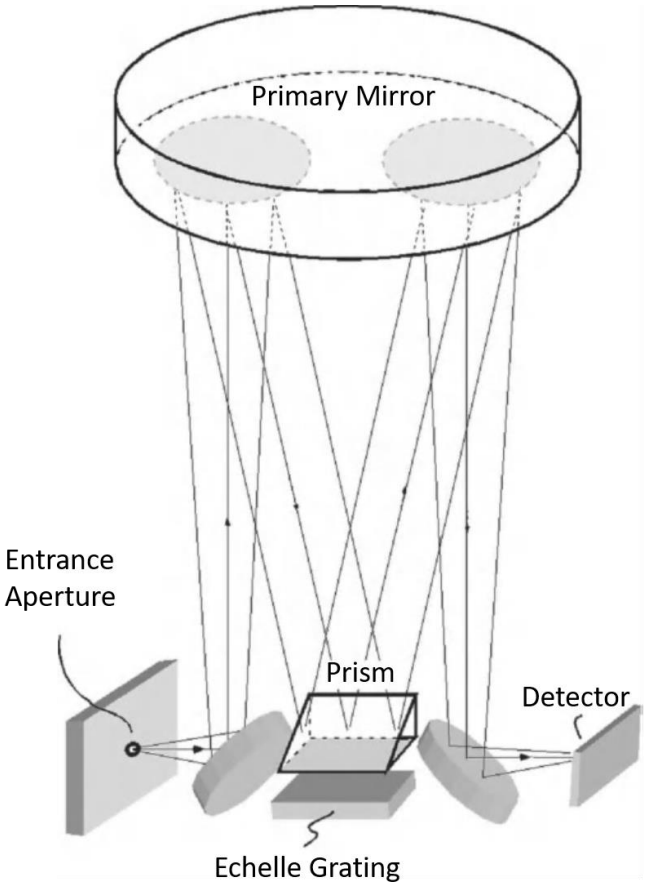

Figure 15 - Diagram of an Echelle spectrometer. Adapted from [2]

Echelle spectrometers use two separate resolving elements, suitably arranged, to generate a spatially resolved two-dimensional image of the input light. The first dispersing element is a grating (called Echelle grating) with a blaze angle greater than those found in conventional spectrometers.

To avoid overlapping images of high-wavelength lines with shorter ones (a consequence of the high blazing angle), a second dispersing element is used. A secondary grating or a prism is positioned orthogonally to the Echelle grating, dispersing the various orders in a perpendicular direction with respect to the orders resolved by the primary element. The result is a high-resolution, 2D "plot" of the spectral lines as a function of their dispersion order. The resolved image can be captured whole by a 2D detector such as a CCD or an iCCD. The lack of moving parts makes Echelle spectrometers highly robust and reliable, as well as allowing the construction of compact instruments. In fact, most of the times the largest component of an Echelle spectrometer is the detector assembly (i.e. iCCD, cooling system and power supply).

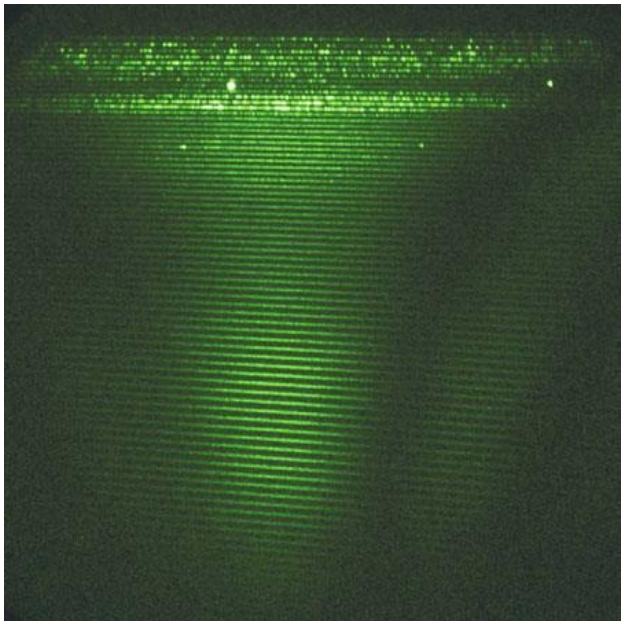

Figure 16 - Echellogram of a Deuterium-Tungsten lamp. Adapted from [1]

Despite their exceptional potentialities, Echelle spectrometers have several limitations that need to be taken into account:

- The resolution is not uniform throughout the entire spectrum due to the dispersion method and the spectral sensitivity decreases with increasing wavelengths. Spectra recorded with Echelle spectrometers are less intense and resolved for wavelengths over 600 nm.
- Spectral regions that fall between the dispersion orders are not detected by the system.
- High intensities can cause "blooming" effects, where excess electrons are transferred from a saturated CCD pixel to the neighboring ones.
- The internal optics are heat-sensitive and can deform, leading to wavelength shifts that require several calibrations during the day.

- Depending on the detector, Echelle spectrometers can have slow acquisition times. As such, they are not suitable for fast sampling applications.
- Their cost is several times higher than a Czerny-Turner spectrometer.
- The control software is generally more complex, and relies on mathematical algorithms to transform the Echellogram into a readable spectrum.

Figure 17 - A compact, portable Echelle spectrometer with an iCCD detector (Aryelle 200, 260x160x185 mm) [71]

1.2.4 – Detector Devices

Detectors utilized in LIBS applications are devices that can convert the incoming photons coming from the analyzer into an electric signal that can be recorded, analyzed and subsequently converted into a readable spectrum. Depending on the selected analyzer and the requirement of the LIBS application, a specific detector can be used. As previously mentioned, the most common examples are photomultiplier tubes (PMTs) and photodiode arrays (PDAs, CCDs).

1.2.4.1 – Photomultiplier Tube

The simplest photoelectric detector, the PMT is compact, robust, reliable and is relatively inexpensive for its performances. PMTs come in different sizes and construction materials, depending on the required performances. A schematic representation of a PMT is given in Figure 18.

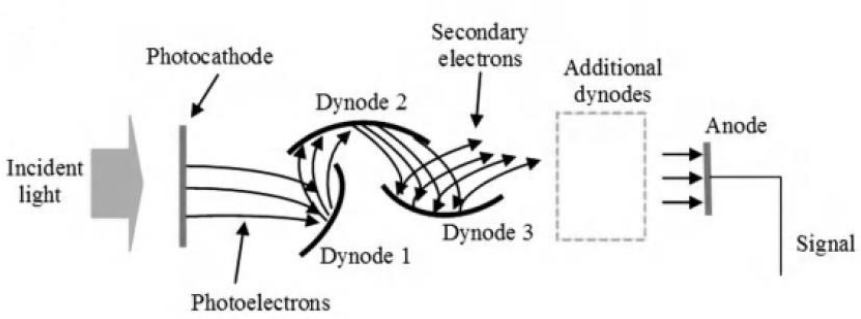

Figure 18 - Scheme of a PMT. Adapted from [2]

The components of a PMT are contained in a vacuum tube to minimize interferences. The incoming light hits a photo-emissive cathode and emits electrons. The electrons are accelerated towards dynodes (electrodes covered in a secondary emitting material) by an increasingly positive potential. Each electron that hits a dynode generates additional electrons, in a cascade process that can produce up to 10^8 electrons for each single photon. Once the electrons reach the anode they generate a measurable, and amplified, electrical current that can be translated into a spectral signal.

PMTs have extremely fast response rates (less than 1 ns), but their construction makes them suitable for monitoring single wavelengths and not large spectral ranges. As such, they are primarily used to analyze single emission lines or to monitor the evolution of an elemental emission over time.

1.2.4.2 – Photodiode Array, CCD and Intensifiers

In LIBS, photodiode arrays (PDA) are usually employed because of their capability of providing simultaneous acquisition of emission lines along a wide range of wavelengths quickly and with high sensitivity. A PDA is a linear matrix of photodiodes (semiconductor diodes) that is arranged in such a way that the light resolved in a line by an analyzer hits the PDA chip more or less perfectly. When a photon of sufficient energy hits a diode, a photocurrent is generated that is proportional to the number of photons that hit the detector over the selected integration time. The circuit then "reads" the charge of each diode sequentially, and then discharges them. The control software is calibrated so that each diode (pixel) corresponds to a determined wavelength, and so the LIBS spectrum can be generated. Commercially available PDAs can be found with up to 4,096 elements, each element being about 25 µm wide and 1–2 mm tall [1] [2].

CCDs are devices similar to PDAs, but the pixels are arranged in a two-dimensional matrix. To accommodate a larger number of photoactive elements (and in turn a higher resolution with less dead zones), each element is generally smaller than those found on a PDA (13x13 µm). Some CCD detectors have square shapes, while others might be rectangular. The exact configuration is

dictated by the requirements of the application or by the light dispersion pattern of the analyzer. A generic representation of a CCD is given in Figure 19.

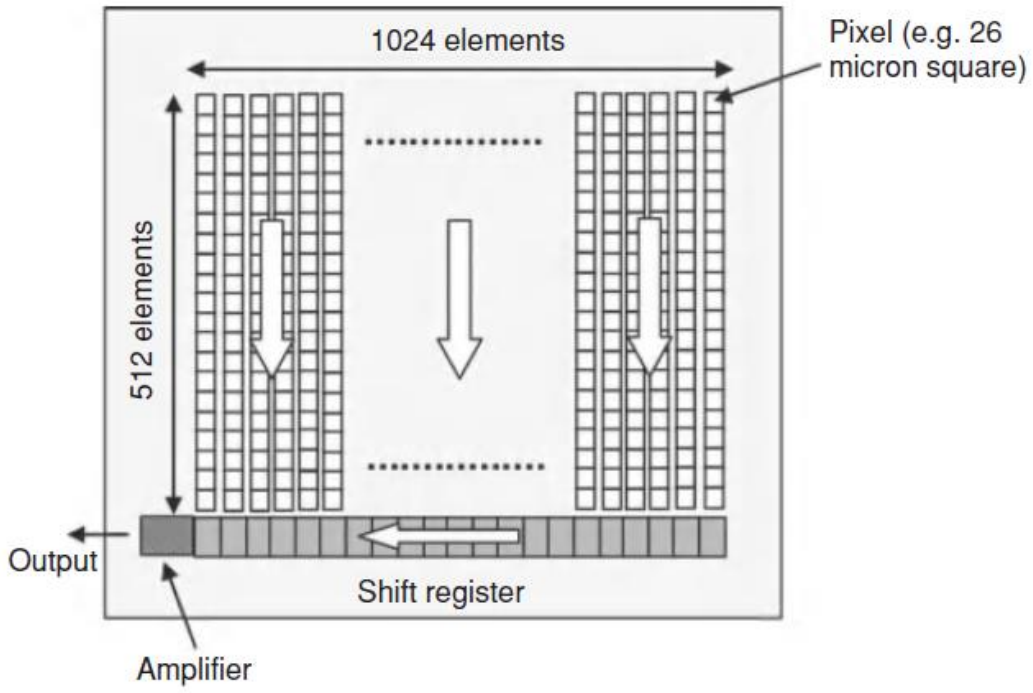

Figure 19 - Scheme of a rectangular CCD detector. Adapted from [2]

Like in a PDA, the CCD is read out by shifting all the pixel rows vertically downward into the shift register (another diode row), which is then read out sequentially. After the pixel information (1024 separate pixels) in the shift register is read out, all rows are shifted down again, and the new data in the shift register are read out. For a 512-pixel vertical array, 512 cycles are required to completely read the sensor. Both the PDA and the CCD can be used to record a spectrum presented at the focal plane of the spectrograph. Using the CCD, however, a two dimensional spectral distribution can be read simultaneously, as in the case of Echelle spectrometers. On the other hand, the PDA is best for single-shot measurements in which the signal levels are near the saturation level of the detector.

As mentioned, both PDA and CCD register the accumulated signal over a selected time frame (i.e. they are time-integrated detectors). Typical readout times of CCD arrays are in the order of a millisecond, while the LIBS signal decays in the microsecond time scale (for ns laser pulses). In order to obtain a time-resolved spectra, a shutter system must be implemented. While mechanical shutters are too slow for the timescales involved, electronic shutters can easily work at the speeds required.

The most common electronic shutters used with array detectors are microchannel plates (MCPs). These are two-dimensional devices which can be switched on and off on the order of a few

microseconds to few ns, to permit or prohibit the passage of light. A scheme of a MCP is given in Figure 20.

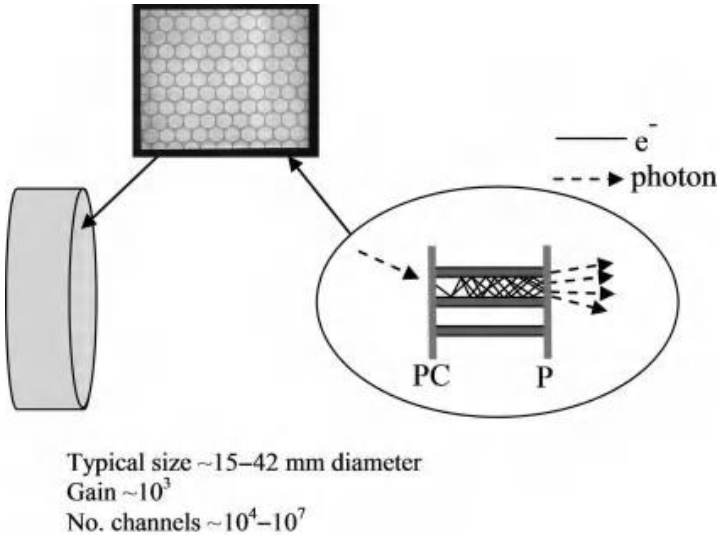

Figure 20 - Scheme of a MCP. Adapted from [2]

MCPs consist of an array of glass tubes (~10 to 100 µm diameter) with length to diameter ratios of 40–100. The size of the MCP determines the number of tubes and arrays range from 10^4 to 10^7 individual tubes. Gating is provided by applying a high voltage (~1.5 kV) between the front and back sides of the plate. When a photon strikes the PC side (when the voltage is applied), an electron is expelled and travels down the tube in the MCP. The insides of the tubes are coated with a material that produces the secondary electron yield. In effect, each tube is a continuous dynode structure resembling a PMT. Because the electron is accelerated by the applied voltage, it acquires kinetic energy and frees other electrons as it travels down the channel. A single electron can give rise to as many as 10^3 electrons at the back end of the MCP. Lastly, the electrons strike the luminescent phosphor screen (P) at the back of the MCP and produce many more photons than the single one that initiated the cascade process. By adjusting the voltage, the gain of the MCP can be controlled. It should be noted that MCPs do not store or record the incident light as they act only as gates.

MCPs coupled with CCDs are often referred to as a single device called iCCD (intensified CCD). iCCDs are among the most widely used in LIBS research, thanks to their imaging capabilities, the high temporal resolution, high sensitivity and, if coupled with an Echelle spectrometer, high spectral resolution [68] [69] [72] [73].

1.2.5 – Control Electronics

In LIBS analysis, triggered-gated detection (i.e. the control of both the exposure time and the time delay between the laser pulse and the beginning of the signal detection) is very common. This kind of approach allows:

- To control the delay time, so to remove the high intensity background continuum.
- To control the integration time.
- To average over multiple spectra so to compensate for pulse intensity fluctuations.

Both the delay and the gate time can be controlled either by the electronics associated with the detection system or by a separate delay-gate generator. In both cases the trigger pulse can be generated directly by the laser (e.g. when the Q-switch unit has an available output signal) or by a fast photodiode detecting the laser output. In alternative, the laser itself can be externally triggered by means of a very precise pulse generator that, at the same time, has to provide the trigger signal for the detector readout system. Most commercially available LIBS systems rely on an external PC to send the timed signals to the laser and the detector unit.

1.3 – LIBS Applications

Recent advances in technology, manufacturing industry, biomedical applications, etc. have created several new applications and requirements for analytical techniques. The request for fast, reliable, low cost instrumentation has risen significantly, especially for those systems that allow for in-situ measurements. The request for portable instruments has also risen, with many different producers offering commercial solutions tailored for specific needs [74] [75] [76]. Conventional atomic spectroscopy techniques (e.g. ICP, AAS, OES, etc.) generally cannot offer such requirements. In fact, most of the instrumentation is large, expensive and built to be housed in a laboratory, with the suitable supporting infrastructure and systems. The flexibility and versatility of LIBS makes it particularly attractive for many applications in a vast number of fields. LIBS analyses are fast, micro-destructive, multi-elemental and can generally cover most of the Near UV/Vis/Near IR spectrum. The measurements can be performed on almost any sample material, in most environmental conditions (from a vacuum to molten metal pools), remotely or in a stand-off configuration. The instrumentation is (generally) cheaper than other spectroscopic instruments and can be optimized and adjusted for many applications [3].

A rapid literature search using the keywords “Laser Induced Breakdown Spectroscopy” shows the constant growth in scientific publications regarding LIBS in the last 20 years. This continuing trend shows just how popular the technique has become, and how many new applications and methods are being explored at the present day.

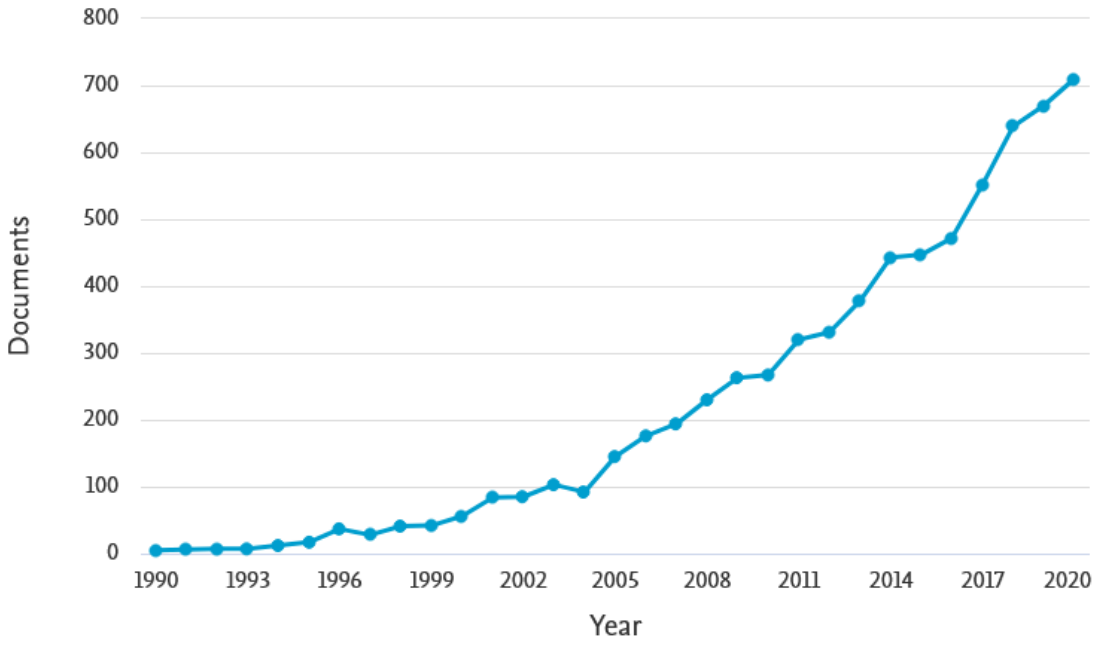

Figure 21 - Scientific publications on LIBS per year. Source: Scopus (Keywords: Laser Induced Breakdown Spectroscopy)

Thanks to the rapidity of the analyses and the possibility of remote monitoring, LIBS has always found widespread use in the industry. A project funded by the European Commission (LaCoMoRe) demonstrated the capability of LIBS in monitoring continuous steel casting, aiding in reducing steel waste when changes in the steel grade are required and an intermediate composition region is formed in the products [77] [78]. Moreover, LIBS was successfully used to directly analyze molten metals to assess the composition of the material and the presence of impurities [79] [80], and several companies offer off-the-shelf solutions for LIBS analysis in the metalwork industry [81] [82]. A prototype combining LIBS and IR spectroscopy was tested to investigate the possibility of applying LIBS to recycling plants for real-time identification of different materials [83].

The capability of LIBS of performing remote analyses or in a completely stand-off configuration makes it particularly attractive for those applications where hazardous conditions do not allow the presence of an operator near the target of interest. One of such applications is the investigation of radioactive samples or structures in the vicinity of nuclear reactors [54]. The first of such applications dates back to 1995 with a monitoring campaign of a Magnox reactor control rods [84]. Since then, dedicated LIBS instruments have been developed and fielded [85]. LIBS has been also used for the detection of explosives with stand-off configurations that employ mirror telescopes (Cassegrain configuration) to focus the laser pulse and register the plasma light [53] [86].

Recently, LIBS was used as a fast and simple multi-elemental technique for the analysis of biological samples. LIBS also allows for high spatial resolution, as well as depth profiling measurements. It also represents a much easier method to generate elemental distribution maps when compared

to other atomic analytical techniques. For example, LIBS was successfully used in the analysis of biological fluids [87] and plant material [88] [89]. However, biological samples are often inhomogeneous and the analytes of interest (e.g. heavy metals) are present in concentrations that are below the common LODs of LIBS techniques. Moreover, the literature on biological samples focuses almost exclusively on solid samples. While some of the limitations of the LIBS analysis of liquids were explained in the previous sections, a more detailed description of the such limitations will be given in this paragraph.

One of the fields where LIBS has become popular in recent years is cultural heritage [90]. Samples with archeological, artistic and cultural value are generally difficult to analyze or sample and transport into a dedicated laboratory. However, one of the most valuable pieces of information that should be available to restorers, curators or historians is the detailed chemical characterization of an artifact. LIBS can offer a solution to these limitations thanks to its micro-destructive character, the possibility of performing in-situ measurements and (if needed) 2D elemental mapping of the samples and a depth profiling analysis. LIBS has been used to analyze pigments from painted artworks and frescos [91] [92] [93] [94] as well as to characterize metal artifacts [95] [96](e.g. statues, coins, etc.). LIBS was also used in combination with other techniques for detailed characterizations of artworks and artifacts [97]. Recently, LIBS was coupled with OCT to perform a stratigraphic characterization of ancient bowed instruments [98].

One of the more exotic and recent applications of LIBS is its implementation on space exploration missions, in particular for the geological study of celestial bodies. Due to the reduced dimensions and the high performances of miniaturized LIBS systems, there have been proposals for instruments for the study of Europa (one of Jupiter's moons) [99] and for the exploration of bodies without an atmosphere [100]. However, the two most noteworthy LIBS applications in space exploration are the ChemCam [101] [102] and SuperCam [103] instruments installed in the martial exploration rovers Curiosity (landed in 2012) and Perseverance (landed in 2021). The two systems feature similar configurations, using a 1064 nm laser wavelength and telescopic focusing and acquisition optics which allow the analysis of samples at a distance of 7 m (and more in the case of SuperCam).

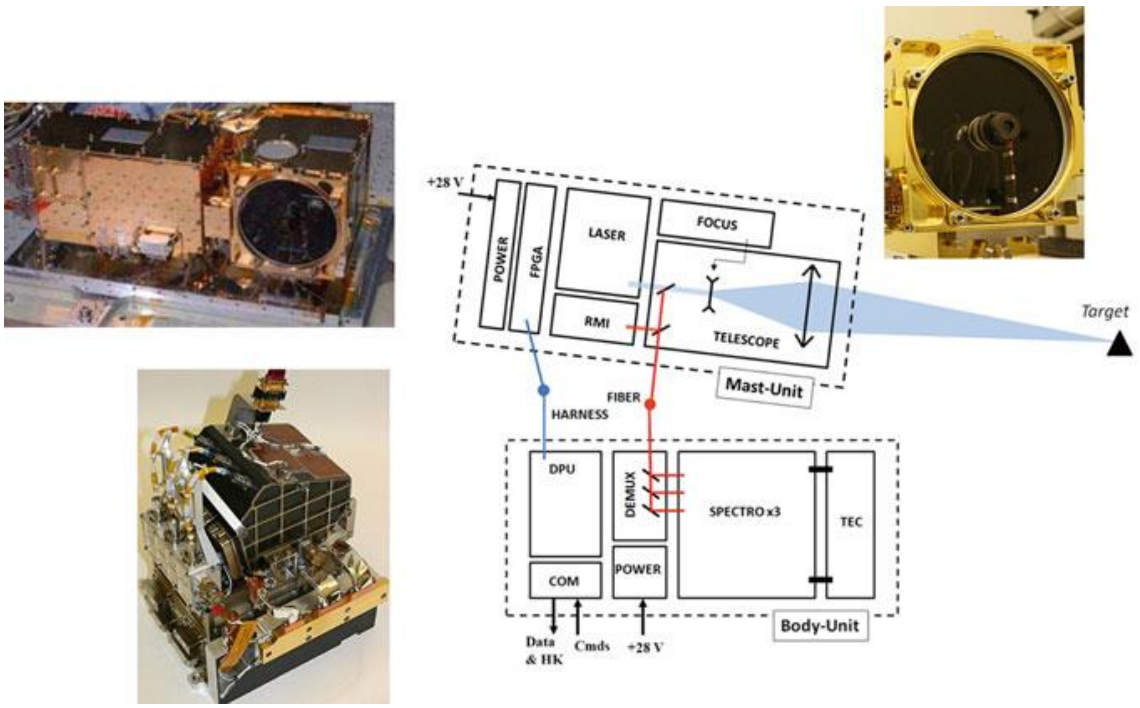

Figure 22 - Diagram and pictures of the ChemCam instrument [1] [102]

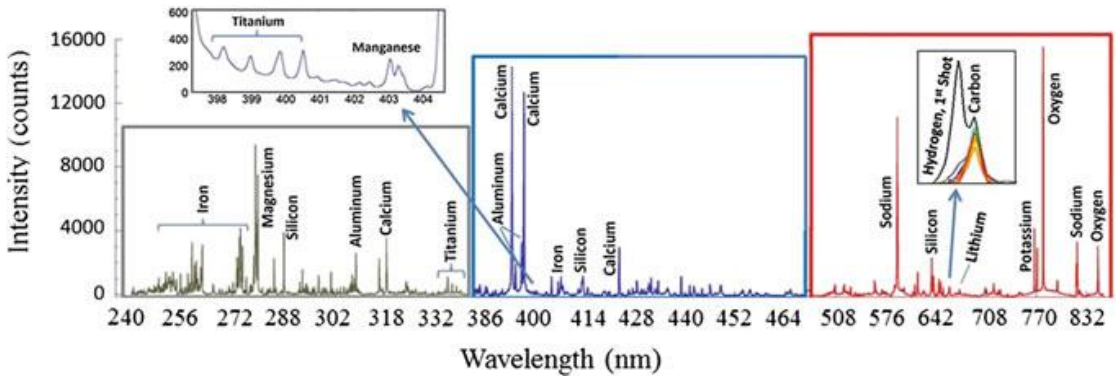

Figure 23 - Example of a LIBS spectum registered by ChemCam of a Martian soil sample [1]

1.4 – Analytical characteristics of LIBS

Many of the strengths of LIBS were presented in the previous sections, while less words were spent on some of its limitations. Being based on the same principle of other atomic emission spectroscopies, LIBS has some of the main advantages of these techniques, namely being able to perform multi-elemental analyses in a single measurement. Moreover, the method of generating the emitting plasma using a laser pulse allows several advantages that are absent in the more conventional techniques. Nevertheless, LIBS presents some shortcomings when the direct analysis of some types of samples is needed, for example the analysis of liquids and samples with an organic matrix.

Over the years, many publications and books have been published in which the several advantages of LIBS, as well as its limitations, are thoroughly detailed [1] [2] [3] [104] [105] [106] [107]. The

scope of this section is to give an overview on the main advantages of LIBS as well as on its main drawbacks on the analysis of solid and liquid samples. In addition, some of the strategies that have been developed and proposed to overcome such limitations will be presented.

1.4.1 – Advantages and Limitations of LIBS

As mentioned previously, the main advantage of LIBS is probably its capability of generating an emission spectrum for all the species in a sample simultaneously. This instantaneous, multi-elemental capacity can be exploited through the use of high-resolution (both spectral and temporal) spectrometers, making LIBS one of the few techniques with such a wide operating range. LIBS is extremely competitive for the rapidity of its analyses (a spectrum can generally be acquired in a few micro- or milliseconds), which can be generally considered real-time. In addition, the costs for the instrumentation and the operation are much lower than the other conventional atomic spectroscopy techniques.

The peculiar method of plasma generation of LIBS allows, in theory, to analyze any substance (gas, liquid, solid) without the need for a preliminary sample preparation step. When the sample needs to be treated before the analysis, this step can be generally fairly simple (e.g. there is no need for a complete digestion of the sample using acids, microwaves, high temperature and pressures, etc.). Most lasers employed in LIBS instruments can generate a plasma in a wide range of conditions, from an almost perfect vacuum, to high-pressure and high-temperature environments without the need for sophisticated installations. Moreover, LIBS allows the analysis of otherwise difficult materials to digest and treat, like in the case of ceramics, superconductors or glass. With specific instrumental configuration, LIBS presents acceptable sensitivity towards some elements that are otherwise difficult to monitor with conventional spectroscopic techniques (e.g. F, Cl).

LIBS is one of the few techniques that allow for actual stand-off analyses, using dedicated instrumental configurations. With the only requirement being having “optical” access to the target, LIBS allows the investigation and monitoring of samples in hazardous environments or that are hard to reach for conventional techniques. If required, LIBS can also be set up for remote operation, where only the laser and the plasma light collection optics are placed near the sample, with the operators, the spectrometer and the control systems at a safe distance.

By combining these properties of LIBS, it is evident how a completely automatic and portable (in some cases, even hand-held) system can be set up. Indeed, advances in computing power, miniaturization of electronics and optical systems as well as advances in software engineering, allowed LIBS to become one of the options for on-line monitoring in several industrial manufacturing processes.

While LIBS is particularly well suited for industrial applications, a more sophisticated use of its capabilities can be exploited when the optical system allows for a high spatial resolution. By reducing the sampling area to a micrometer scale, it is possible to generate accurate and high resolution maps (elemental imaging) of the target surface or investigate its stratigraphic composition (depth profiling), which makes LIBS particularly useful for geological and geochemical applications. Moreover, the reduced dimension of such craters allow the use of technique for the analysis of valuable and historical objects in the cultural heritage field (e.g. statues, paintings, metallic artifacts, textiles, etc.).

One of the main shortcomings of LIBS is that the achievable LODs are relatively high when compared to other spectroscopic techniques. The LOD (Limit of Detection) has been defined by IUPAC (1997) as follows:

"The limit of detection […] is derived from the smallest measure, x_L, that can be detected with reasonable certainty for a given analytical procedure. The value of x_L is given by the equation $x_L = x_b + ks_b$ where x_b is the mean of the blank measures, s_b is the standard deviation of the blank measures and k is a numerical factor chosen accordingly to the confidence level desired."

In LIBS, the LOD values are influenced by a large number of factors, such as the laser pulse energy, the measurement integration time and delay and the sample's characteristics. Nevertheless, LIBS LODs are generally in the order of ppm [3]. A wide variety of approaches and techniques have been tested and proposed to improve the performances of LIBS [108] and a brief overview of some of these methods will be given in this section.

Improving the instrumentation with more powerful lasers or high-resolution spectrometers has been, up until recently, the preferred strategy. In fact, one of the most common techniques for improving LIBS performances is the use of two sequential laser pulses instead of a single one, in what is called Double Pulse LIBS (DP-LIBS). This methodology, useful for both solid and liquid samples, will be detailed in Section 1.5. Nevertheless, this creates the issue of increasing significantly the cost and complexity of the instrumentation, as well as that of the analytical procedures, often requiring specialized operators. Moreover, these costs (in money and time) should be compared to the possibility of employing other analytical techniques, even those that might require sample treatment, that allow for lower LODs.

A novel approach for improving LIBS performances, called Nanoparticle Enhanced LIBS (NELIBS) will be discussed in detail in Section 1.6.

1.4.2 – Quantitative LIBS Analysis of Solid Samples

The areas (and in turn, the volumes) analyzed with LIBS are generally very small. It is also possible that the analyzed samples do not possess a homogeneous distribution of their elemental components (for example, in the case of a rock sample) [109]. Another issue arises when the surface layers of a sample do not have the same chemical composition as the underlying bulk. This can happen when analyzing metals and alloys where, due to oxidation, fusion and manufacturing processes and environmental contamination, a layer several micrometers thick can form on the surface of the sample. Since the ablation rate (i.e. the depth of the material ablated by each laser pulse) can range from a few nanometers to 10-20 μm, the first measurements (or more) would give incorrect analytical results [1].

The sampling geometry must be also carefully considered. If the samples have surface irregularities or irregular shapes, the distance between the sampling spot and the focusing lens changes with each measurement. Even though the plasma can still form (if there is enough energy deposited on the sample surface), the ablated mass, plasma temperature and electron density can change, altering the registered emission signal [110].

One of the main disadvantages of LIBS is the low sensitivity when compared with other spectroscopic techniques. Generally, LIBS LODs are in the range of ppm (parts per million, μg/Kg), with an average uncertainty of 5-15% [3] [111]. Additionally, the experimental conditions can heavily influence the quality of a LIBS measurement, especially in its reproducibility. The calibration curves can suffer from changes in the environmental conditions such as fluctuations in the surrounding atmosphere or in the optical path [112] [113].

LIBS is also particularly susceptible to matrix effects. These phenomena occur when the physical properties and the composition of a sample influence the emission signal related to the concentration of the analyte, even if its concentration is constant. For example, variations in the heat capacity, reflectivity, vaporization temperature, etc. of a sample can influence the amount of material that is ablated with each laser pulse. On the other hand, easily ionized elements can increase the electron density in the plasma and reduce the emission intensity of elements with higher ionization energy. This can lead, if not corrected, to serious issues in the calibration steps and the quantitative analysis of unknown samples.

Another major issue is that certified or standard reference materials (CRMs, SRMs) for LIBS are hard to obtain, as very few commercially available options exist (on the other hand SRMs for alloys and metals are generally available). In fact, due to the extreme versatility of the technique and the tendency of performing measurements on the samples as-is (i.e. without digestion or preparation), it is impossible to obtain SRMs with every combination of matrix-concentration required in LIBS.

Generally, the treatment and manipulation of solid samples aims to eliminate or reduce matrix effects. Mechanical separation techniques allow for the separation of various sample fractions with the use of sieves, by exploiting different physical properties (density, magnetic properties) or by chemical treatment (salt separation, acid dissolution). If the sample is inhomogeneous it can be treated by digestion, crushing and milling or fusion to create a uniform dispersion of the analytes.

However, the core advantage of LIBS is the ability of performing analyses without the need of sample manipulation. To compensate for matrix effects, the ideal solution would be to build calibration curves using standard samples with a similar matrix as the unknown sample and with a concentration range within the scope of the analysis. However, as previously mentioned, SRMs that are suitable for LIBS are not easy to obtain. It is possible, in the case of relatively simple matrices (e.g. soil, water) to produce various spiked samples with known concentrations of the analyte, starting from a suitable blank (e.g. uncontaminated soil, tap or mineral water). This might not be possible for increasingly complex matrices, and the method still requires a large number of calibration samples to be effective [20].

Another widely used approach is based on the internal calibration technique. In brief, an analyte whose concentration remains constant (or can be assumed constant) in the samples is chosen, and the variation of its analytical signal is used to correct for the fluctuations of the other analytes. If no such analyte is present in the sample, it can be added before the measurement in a known concentration to each sample. Ideally, such an analyte should respond in the same way to the matrix effects as the analyte of interest [114].

The emission spectra can be corrected indirectly by normalizing the line intensities to a physical quantity that can be obtained from each LIBS measurement. Such quantities can include the total emission intensity [115], the plasma temperature [73], the electron density, the ablated mass [116] or the energy of the pulse's shockwave [117]. Some, more sophisticated correction methods implement algorithms that take into account other phenomena such as self-absorption [118]. This method allows for the correction of the emission spectrum by taking into account fluctuations in the plasma properties or in the ablation process.

One of the most versatile and attractive algorithms for the analysis of LIBS spectra and spectroscopic data is the Calibration Free LIBS (CF-LIBS), which was described in detail in the previous sections.

1.4.3 – Limitations on the Analysis of Liquid Samples and Proposed Solutions

As described in Section 1.1.4, a LIBS plasma generated in a liquid shows a low emission intensity and duration due to the confining effect of the surrounding medium. A large fraction of the laser pulse energy is spent to vaporize the sample as well as to create the suitable conditions for the

ignition and evolution of the plasma in the liquid sample (i.e. the expanding shockwave and the subsequent cavitation bubble), meaning that the resulting plasma plume will be less energetic. The lifetime of the excited states of the emitting species is shortened significantly (a few microseconds or less) when compared to a plasma generated on a solid sample, making it more difficult to separate the emission lines of the analytes from the continuous background. Because of this, LIBS is less sensitive and precise for the analysis of liquid samples and, comparatively, less attention has been paid to the analysis of liquids. Moreover, the existence of already well established and developed techniques for high-performance analysis of liquids (e.g. ET- and F-AAS, ICP-OES, ICP-MS, etc.) further discourages the implementation of LIBS as a new approach for the analysis of such samples, aside from some proof-of-concept studies [119] [120] [121].

Some of the problems of LIBS analysis of liquids are not directly related to the plasma dynamics [5]. Depending on the instrumental configuration, frequent cleaning of the optical components might be required to remove the deposits splashed and ejected from the liquid sample after the laser pulses. The shockwave can create an aerosol above the liquid surface that can disrupt both the laser beam and the plasma emission, reducing the fraction of radiation that is transferred to the sample or the amount light that is able to reach the spectrometer. Moreover, waves and sloshing of the liquid surface are created by laser pulse, which can reduce the reproducibility of subsequent measurements and the precision of the analyses. The presence of induced bubbles (that might be transparent to the laser wavelength) can also alter the characteristics of the laser-induced plasma, as well as the laser-liquid interaction by altering the sample surface unpredictably.

The strategies proposed to improve the performances of LIBS towards the analysis of liquid samples are generally more complex than those implemented for the analysis of solids. Many approaches require a heavy manipulation of the samples in order to convert them into matrices more suitable for LIBS analysis.

As mentioned previously, one of the most common strategies to improve LIBS capabilities towards the analysis of liquids without any sample treatment is the use of DP-LIBS. A detailed overview of this method will be given in Section 1.5.

The simplest approach is the generation of the LIBS plasma immediately on the surface of the sample. While it can be challenging to fine tune the optical system, the results can allow LODs of few ppm [122] [123] [124]. The sample is allowed to evaporate slightly and the plasma (ignited just above the liquid surface) evolves in the surrounding air, with mechanisms and characteristics comparable to those encountered in LIBS plasmas generated over solid samples. However, the generated shockwave produces waves and splashing from the liquid that can alter the laser-surface

interaction, as well as a partial shielding of the sample by the ejected droplets. Moreover, if the focusing lenses are near the sample, they can be contaminated by the generated spray of liquid.

Other strategies require a minimal treatment of the sample, while still necessitating dedicated instrumental configurations. For example, liquid samples can be fed into a droplet generator to produce single (or a sequence of) droplets of known size, each with a volume of a few µL. The droplets are then "fed" into the laser pulse, which vaporizes them and generates a plasma [125] [126] [127] [128] [129]. A similar technique uses various methods (e.g. ultrasounds, electrospray, pressure nebulizers, etc.) to nebulize the liquid sample and create an aerosol plume. The LIBS probe is suitably aligned and used to create a plasma inside the small cloud of sample droplets [108] [130] [131] [132]. Alternatively, the liquid sample can be forced to flow in a continuous and thin stream. The laser pulse is focused onto the surface of the stream so that only a small quantity of sample is vaporized, reducing the effects of spraying and increasing the shot-to-shot precision. A sheath gas (N_2, Ar He or compressed air) stream can be fed around the liquid column, in order to eliminate completely the risk of splashing and contamination of the optical components [133] [134].

While these methods allow to solve the issues related to the presence of large liquid surfaces, they generally do not offer much higher performances while still requiring large volumes of sample.

If adapting the instrumental configuration does not sufficiently increase the performances of the technique, the alternative is to treat the samples in order to convert them in a form that is more suitable for LIBS. Indeed, in some cases sample preparation is unavoidable to obtain a sensitivity comparable to that of LIBS analyses on solid and gaseous samples.

In the case of suspended solids in a liquid matrix, a simple filtration, followed by the analysis of the dried residue [135] can be implemented. Other approaches focus on the separation of the analytes from the liquid matrix by using chelating agents and a microfiltration step. Indeed, LODs in the order of ppb were successfully obtained for the analysis of heavy metals in liquid samples using a mixed cellulose ester membrane [136].

Another possibility is to convert the liquid sample into a solid. Depending on the chosen procedure, this operation can be very simple or rather complicated. It has been demonstrated that freezing liquid samples using liquid nitrogen, and then performing the LIBS measurement on the surface of the frozen samples can increase the sensitivity, the emission intensity and overall signal quality [137]. Liquid samples can also be mixed with polymer dispersions (such as PVA) in order to convert them into solids thanks to the curing process of the polymer itself [138].

The simplest approach is the deposition of a sample droplet onto a suitable substrate, and to evaporate the solvent. The dried residue is then analyzed by LIBS as a conventional solid sample.

Most of the time, the substrates are metal or semiconductor foils, and the technique is known as Surface Enhanced LIBS (SEn-LIBS). In this case, the substrate acts as a "booster" for the plasma generation, providing an excess of electrons and ionizable species that would be lacking in the breakdown of just the dried sample residue. This enhanced plasma allows for much higher emissions when compared to the analysis of dried droplets on insulating substrates (i.e. glass, polymers, etc.) [139]. It was demonstrated that a higher sensitivity can be achieved for the analysis of liquid samples dried on aluminum substrates, when compared to a direct LIBS analysis on suspended droplets [140]. In a similar fashion, the liquid sample can be adsorbed on a porous substrate and dried. In this case the role of the substrate is not to enhance the LIBS plasma, but to immobilize the analytes contained into the liquid sample and, effectively, transfer them in a solid matrix. Several substrates have been tested for this application: graphite, filter paper, membranes, polymer fibers, etc. [141] [142] [143] [144].

Lastly, a widely employed methodology is based on the micro-extraction technique. Micro-extraction is commonly used in analytical chemistry as a means to pre-concentrate the analytes, or to selectively separate them from the matrix to avoid interferences and contaminations, and as such it has been thoroughly described in literature [114].

The first application of solid-phase micro-extraction (SPME) for LIBS was investigated by Wang et al in 2014 [145]. The authors used a Dispersive SPME approach, preceded by the complexation of the metal ions by diethylditiocarbamate (DDTC). When the extracting material (nanostructured graphite) was added to the solution, the chelated metals were adsorbed. The graphite powder was then separated by centrifugation, mixed with a commercial adhesive to form a solid pellet and analyzed by LIBS. The authors reported LODs in the order of a few ppb.

In recent years, the use of carbon-based SPME methods has attracted some interest for LIBS applications. Indeed, many papers were published, proposing novel strategies to create simple, reliable and effective substrates to extract the analytes from a liquid sample and make them readily available for LIBS analysis. A more detailed overview of this approach will be given in Section 1.7.

1.5 – Double Pulse LIBS (DP-LIBS)

As mentioned in the previous sections, the pursuit of lower LODs and growing interest for LIBS as a substitute for more complex and costly instrumentations, sparked a renewed interest in ways to improve the capabilities of the technique. Piepmeier and Malmstadt studied the effect of multiple laser pulses on the signal enhancement of an Aluminum target in 1982 [146]. It was the first time that a single laser source was used to deliver multiple pulses for LIBS applications, and possibly the first introduction of the modern concept of DP-LIBS. With the advancements in laser and detector technology, the DP technique resurfaced at the start of the 1990s. In 1991, the group of Uebbing

and Niemax investigated the possibility of an orthogonal configuration for DP-LIBS, where the second laser pulse was used to reheat the plasma produced by the first pulse [147]. In the same years, the group of Pershin explored DP-LIBS and proposed an explanation for the observed decrease of the atmospheric emission in the application of multiple pulses, as well as a possible mechanism for the increase in the signal to noise ratio observed during DP-LIBS measurements [5] [6]. Right at the start of the new millennium, many research groups started to investigate the fundamentals and the principles behind DP-LIBS, both from a theoretical point of view and with a systematic investigation of the influence of several experimental parameters on the signal enhancement and the plasma characteristics [148] [149] [150] [151].

It is worth noting that a fundamental difference between SP and DP-LIBS is the geometry of the plasma plume that is generated. This is a critical aspect that has to be taken into account, as a non-optimized light optical collection system can lead to a decrease in the spectral quality. This issue has been highlighted in the work of Palleschi et al [152] where different light acquisition geometries have been tested. Another criticality is evidenced in the work of De Giacomo et al [153], where it is demonstrated that the temporal evolution of such plasmas is not the same as their SP analogues, and so a different range of acquisition delays and integration windows might be necessary.

1.5.1 – DP-LIBS Configurations

1.5.1.1 – Collinear DP Geometry

Generally, a collinear DP-LIBS configuration allows for a higher ablated mass, when compared to a SP experiment of comparable energy. In addition, if the DP experiment is performed in air, at atmospheric pressure, the emission related to the gases present in the atmosphere (eg. N, O) is greatly reduced.

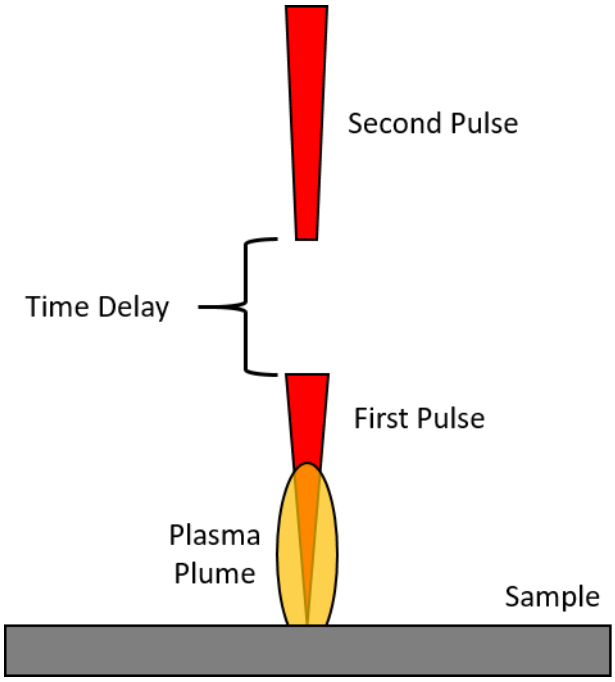

Figure 24 - Collinear DP-LIBS configuration

Figure 24 shows the simple collinear geometry setup. The two laser pulses follow the same optical path and are focused onto the sample surface, separated by a suitable time delay. However, the simplicity of this kind of approach presents a few drawbacks.

Obtaining two laser pulses having comparable and stable energies as well as beam quality is a particularly delicate operation. Over the years, this issue has been almost completely solved by the advancement in laser technologies. Nowadays it is possible to find on the market numerous systems capable of delivering two or more laser pulses, within a single pumping cycle, with tunable energies and surprising beam stability. Another limitation to consider in the case of a single laser source is that both laser pulses will necessarily be of the same wavelength and, in general, duration.

The collinear DP configuration, however, remains simple enough even if two separate laser sources are used. In this case, the added complexity is found in the synchronization setup, usually relying on an external electronic delay generator. On the other hand, the study and modeling of the effects of the two laser pulses becomes more complicated when multiple wavelength and different pulse duration are involved

1.5.1.2 – Orthogonal DP Geometry

One of the most crucial advantages of a two-laser arrangement is that it enables the use of non-collinear geometries for DP-LIBS studies. The most common configuration, in such cases, is the so-called orthogonal DP-LIBS. In this setting, one laser pulse is focused on the sample, following a

perpendicular path with respect to its surface. Another pulse, instead, is parallel to the sample's surface and orthogonal to the other pulse's path.

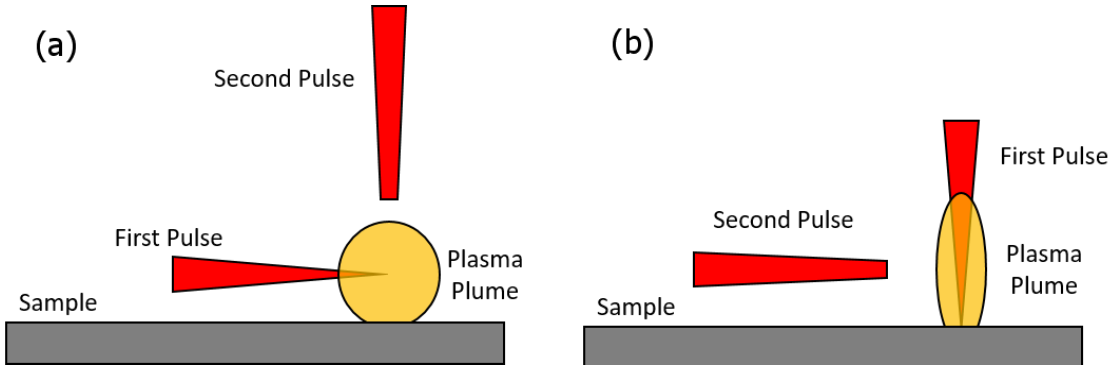

Figure 25 - Orthogonal DP-LIBS configuration in (a) Pre-Ablation and (b) Re-Heating mode

The various orthogonal DP-LIBS configurations can be summarized in the two categories, shown in Figure 25.

In the Pre-Ablation configuration, the first laser pulse travels parallel to the sample's surface, and it's focused just above the desired sampling spot. This generates a plasma plume in the atmosphere above the target, without any considerable interaction with the sample surface, that "prepares" the environment for the second laser pulse, that follows a perpendicular path. In the Re-Heating configuration, instead, the first laser pulse is focused onto the sample, in a similar fashion of a standard SP-LIBS experiment. The second laser pulse then travels parallel to the sample's surface and interacts with the plasma generated by the first pulse, "re-heating" it.

The group of Sanginés investigated the mechanisms behind the signal enhancement obtained from both configurations [154]. They found that, in the case of the Pre-Ablation mode, the signal enhancement is mainly due to the generation of a low-density environment around the sampling spot, by the spark of the first laser pulse. This leads to a longer lasting plasma from the second pulse and, in turn, a higher Signal-to-Noise ratio. In the case of the Re-Heating mode, instead, the enhancement is due to the absorption of the second pulse's energy by the plasma generated by the first pulse.

Overall, the increased complexity of the orthogonal configuration is not usually offset by a signal enhancement large enough to justify its application for analytical purposes. However, the lower power intensities required in the Pre-Ablation configuration can be interesting for those applications where damaging the sample must be avoided or contained (i.e. archeology, cultural heritage). An exception to this statement must be done in the case of a very peculiar application of the orthogonal Re-Heating configuration, named Resonance Enhanced Laser Induced Plasma Spectroscopy (RELIPS), that was investigated by the group of Cheung [155] [156]. In brief, this

approach uses a tunable laser source for the generation of the second pulse, that is adjusted so that its wavelength is the same of a resonant emission line of the sample's matrix, maximizing the absorption effects and, in turn, the re-heating and exciting effects on the plasma. In particular, the authors demonstrated the possibility of reaching Limits of Detection of about 100 attomoles for minor elements and suggested the application of this technique for high resolution depth profiling, due to the low damage and ablation rate observed.

1.5.1.3 – Parallel DP-LIBS Geometry

In this configuration, the two laser pulses follow a path that is orthogonal to the sample's surface, but are focused on two nearby, but separate spots. This configuration is particularly interesting in the case of fundamental studies, however, in some cases it has been successfully applied for specific applications.

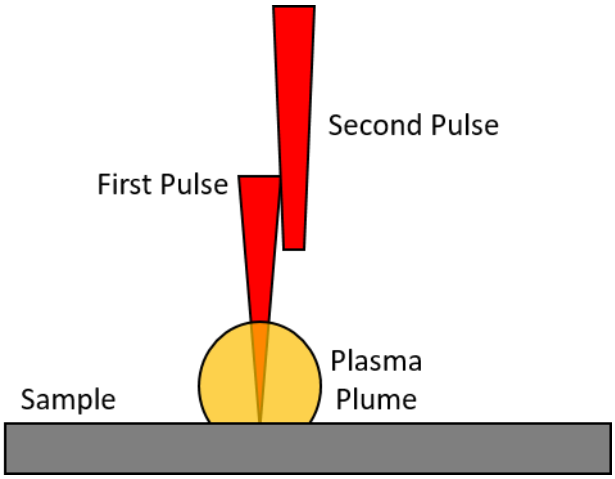

Figure 26 - Parallel DP-LIBS configuration

The group of Nishijima used a parallel DP-LIBS configuration for the analysis of thin layers [157]. The authors found the classic collinear DP configuration unsuitable for the analysis of thin deposited layers, as the thickness of such deposition is of the same order of the first pulse's ablation rate. The use of two lasers, delivering pulses with an offset of a few millimeters on the target's surface demonstrated the potential of this configuration, named Spatially Offset Double-Pulse LIBS (SODP-LIBS), as both pulses were able to interact with an undamaged analyte layer. Moreover, the second pulse, when suitably delayed, interacted with the residual plasma of the first pulse, inducing a partial re-heating of the atomized material.

1.5.1.4 – Variable Pulse Duration in DP-LIBS

It is known from literature that a laser pulse of a duration in the order of the femtoseconds yields a plasma that is more reproducible and a more regular ablation crater, when compared to the more conventional laser pulses, in the order of nanoseconds [156].

The group of Angel was among the first to investigate the possible application of a fs/ns DP orthogonal configuration [158] [159]. They discovered that the best performances were associated to a fs laser pulse for the ablation of the target, while a ns pulse was used for the re-heating of the generated plasma. However, the magnitude of the signal enhancement generated by this configuration when compared to SP-LIBS (approximately 80 times for aluminum and 30 times for copper) does not justify the increased complexity of the instrumentation for analytical purposes.

Worth mentioning is the work of the group of Deguchi [160], where a peculiar application of a DP-LIBS having different pulse duration is realized. A configuration where the first laser pulse is longer (35 μs) than the second (6-7 ns) is used to analyze metal samples underwater. Where SP experiments of such samples show a continuous background and substantial noise, the application of the Long-Short DP (LS-DP) allows for the acquisition of much clearer spectra. This is mainly due to the generation of a cavitation bubble near the sample's surface by the first microsecond-long laser pulse, that allows the second shorter pulse to reach the target and ignite a plasma, mostly unhindered by the surrounding liquid.

1.5.1.5 – Variable Wavelength in DP-LIBS

The first reported study of DP-LIBS using pulses of different wavelengths is by the group of Niemax, who investigated this approach in an orthogonal Re-Heating configuration [161].

In principle, a pulse with a wavelength shorter than the fundamental 1064 nm Nd:YAG emission can be more tightly focused on the sample surface and a higher fraction of its energy can be transferred to the sample. This is due to the lower absorption of the laser's light by the generated plasma by inverse Bremsstrahlung, the so-called plasma shielding. Since the inverse Bremsstrahlung absorption is proportional to λ^3, it is clear that a laser with a shorter wavelength is capable of a more substantial ablation, at the cost of a lower plasma temperature if compared to an infrared laser pulse [162]. These observations suggest that a DP setup that uses pulses of different wavelengths, each one optimized for either ablation or plasma re-heating, could be worth investigating.

The group of Sabsabi conducted a thorough investigation of DP-LIBS using a combination of fourth harmonic (266 nm) and fundamental (1064 nm) pulses from an Nd:YAG laser [149]. It was demonstrated that this configuration yielded an ablation crater that was larger than one obtained for a DP experiment using only IR pulses, with no major difference in the case of positive or negative pulse delays. In addition, with a 0 delay (where both pulses arrive on the sample's surface at the same time), the ablation crater was smaller than the ones obtained in DP configuration. The authors also determined the values for the plasma temperature and found that, for positive delays, there was almost no difference between IR-IR and UV-IR configuration. In the case of negative

delays, however, the IR-IR configuration yielded a higher temperature than the IR-UV configuration. As for the LIBS signal, it was found that the difference between the IR-IR configuration and the UV-IR configuration was minimal, while still showing a significant increase in intensity when compared to SP-LIBS spectra.

In the end, while these results are very interesting from a theoretical and fundamental point of view, the marginal boost in analytical performances does not justify the instrumental setup complexity.

1.5.1.6 – Multiple Pulse LIBS

Given the significant signal enhancement obtained from DP-LIBS configurations, some research groups investigated the possibility of exploiting a higher number of pulses, with the aim of obtaining an even higher boost in analytical performances of the technique.

The first approaches were described by the group of Noll [163]who investigated the effects of up to 4 laser pulses on a steel sample, reporting an increase in the signal intensity with respect to the SP configuration.

Recently, the group of Galbács [164] [165] presented an approach where 7 consecutive pulses from a Q-Switched Nd:GGG (Neodymium-Doped Gadolinium Gallium Garnet) laser were used to obtain a substantial signal enhancement. However, it should be noted that the authors used a time-integrating spectrometer, which accumulated the signal generated by each pulse. While the presented signal enhancement mechanism is not interesting from an analytical point of view, it is undoubtedly reasonable that using a high number of laser pulses for each measurement would increase the reproducibility of the spectra.

A particularly interesting approach has been proposed recently by the group of Prochazka [166]. The authors used an orthogonal configuration, triple-pulse system, in order to combine the advantages of the Pre-Ablation and the Re-Heating approaches. The authors used two second-harmonic (532 nm) Nd:YAG lasers for both the Pre-Ablation and the main (middle) pulse, while an IR Nd:YAG laser (1064 nm) was used to generate the third pulse, in order to increase the energy absorption by the plasma.

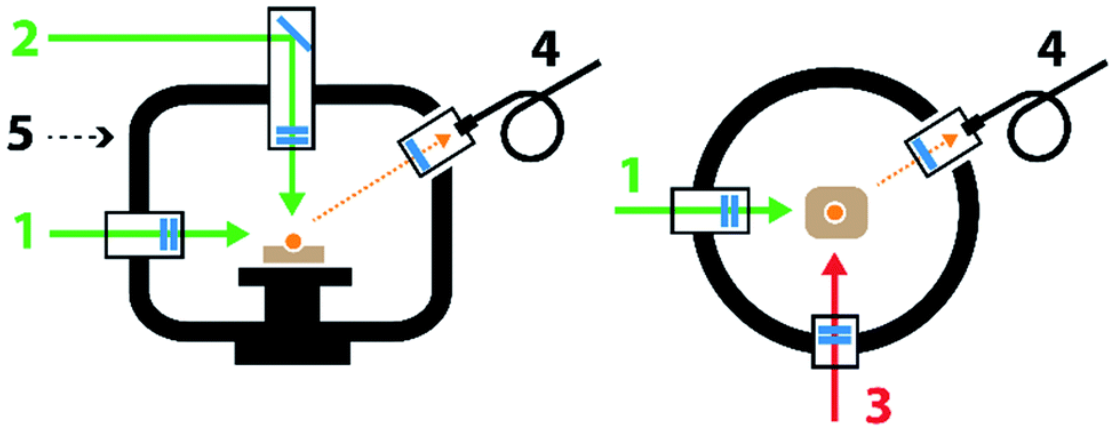

Figure 27 - Front view (left) and top view (right) schematic pictures of the interaction chamber with laser pulses and collection optics. All laser pulses are perpendicular to each other. Ablation pulse (2) is directed from the top of the chamber (5), perpendicular to the sample surface, pre-ablation pulse (1) came from the left side of the chamber (5) collinear to the sample surface and re-heating pulse (3) is directed from the front of the chamber (5) collinear to the sample surface. The collection optics (4) is placed on the right side of the chamber *[166]*

While the magnitude of the signal enhancement was found to be heavily dependent on the investigated emission line, the results showed how the triple-pulse configuration yields a higher signal not only when compared to SP-LIBS, but also with respect to both orthogonal DP-LIBS configurations.

1.5.2 – Signal Enhancement in DP-LIBS: Principles and Theory

The combination of two (or more) laser pulses for LIBS experiments makes studying the processes that occur on the samples and in the plasma much more complicated than in the SP case. In fact, we observe a number of interactions between the second laser pulse and the environment generated by the first, and modeling such a system is extremely difficult. Moreover, despite the large number of papers published on the subject and of experiments performed, the exact mechanisms behind DP-LIBS are still being discussed and explored today [153] [167] [168].

What emerges from the various works on DP-LIBS is that there is a substantial difference in the environment where the plasma evolution occurs and because of that, the different behavior of the plasma over time and space can explain the signal enhancement effects.

During a SP experiment conducted in air, as was mentioned in the previous sections, a large part of the plasma energy is spent to compress the surrounding atmosphere, generating a shockwave. The air also exerts a confining action on the plasma plume's expansion. At the same time, the evolving plasma heats the air molecules, giving rise to emission lines of both atomic species and molecular adducts between the sample and air.

In the case of DP-LIBS, the plasma plume expands inside the environment behind the shockwave of the first pulse. The expansion, in the first moments, is faster than in the SP case, due to a lower

gas density and, since the environment has a higher temperature, less energy is dissipated. Once the expanding plume reaches the edge of the shockwave, it can be reflected back and contract towards the point of origin. Usually, it is observed that the plasma plume generated by the second pulse has a longer life time than the one generated by a single laser pulse.

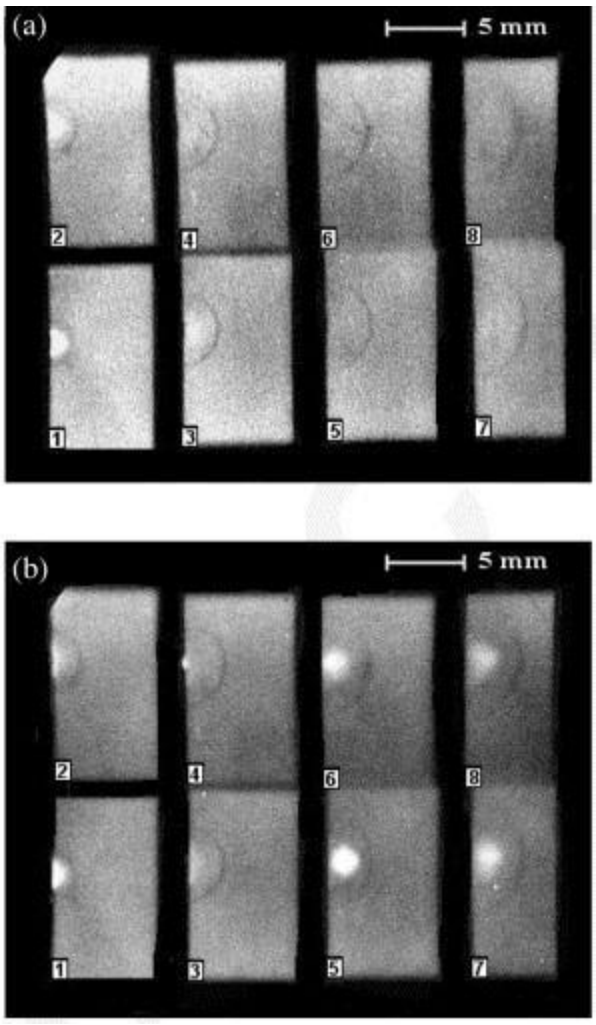

Figure 28 - Shadowgrams of the laser produced plasma in (a) single pulse (b) double pulse configuration. In both sequences, the first photograph (left bottom) has been taken at a delay time of ~500 ns with respect to the first laser pulse, while the temporal delay between photographs is 500 ns [151]]

It has been observed that the environment behind the first pulse's shockwave, in typical DP-LIBS conditions, is equivalent to an atmospheric pressure of about 50 torr, which is very close to the pressure that yields a maximum LIBS signal [113]. It is interesting to note that this interpretation can be applied not only to a collinear configuration, but also to the orthogonal Pre-Ablation configuration.

There are, however, other factors that can contribute to the signal enhancement in DP-LIBS.

It is known that the intensity of a LIBS spectra is proportional to the ablated mass, and it was observed that the ablation crater in DP-LIBS is generally greater (2-5 times) than the one in SP-LIBS, although the crater volume is not linearly dependent on the changes caused by the first laser pulse.

Another factor that influences the LIBS signal is the plasma temperature, and it is particularly important for long detection times. In these conditions, the SP plasma is either already decayed or of low intensity, while the DP plasma is still evolving. However, the signal enhancement caused by the temperature is meaningful only if the detection system has a high spatial resolution as the distribution of the SP and DP plasmas are quite different. Indeed, if the signal is averaged along the entire plasma plume, the values of temperature for both SP-LIBS and DP-LIBS will be comparable, as a result of the averaging of the cold outer shell (which is larger in the case of DP) and the hot core.

1.5.3 – DP-LIBS Applications

1.5.3.1 – DP-LIBS of Solid Samples

In recent years, DP-LIBS has been used successfully for the investigation of historical, archeological and Cultural Heritage artifacts. The group of Grupce used DP-LIBS in the orthogonal re-heating configuration for the determination of the materials used in the manufacturing of an ancient roman marble bust, discovering a gold-mercury amalgam [169]. Recently, the group of Columbu employed DP-LIBS to study limestone statues from the 9th-8th century BC [170]. Palleschi et al published several works where collinear DP-LIBS was applied in the analysis of ancient artifacts, thanks to a transportable, integrated instrument called Modì [171]. Studies were conducted for the characterization of bronze statues [96] and coins [172]. More recently, DP-LIBS analyses were coupled with Optical Coherence Tomography (OCT) for the stratigraphic characterization of the paint and coating of ancient bowed instruments [98].

Among the various applications of DP-LIBS, one of the most interesting and diverse is the detection and analysis of dangerous materials in a stand-off configuration, where the operators and the instrumentation are relatively far away from the sample. One of such applications was developed by the Army Research Laboratory (USA) in collaboration with Applied Photonics Ltd. (UK) for the stand-off detection of explosives using a DP setup [53], and a review on the subject has been published by Gottifried and her group [173]. It was found that DP-LIBS was able to reveal spectral characteristics that were not distinguishable with conventional SP-LIBS. In this case it has been noted that the main advantage of a DP-LIBS setup was the reduction of the emission coming from the atmosphere.

While the application of DP-LIBS in the biology and medical field is not as widespread as in other fields, it is worth mentioning the work by the group of Galiová [174]. The orthogonal re-heating

DP-LIBS configuration allowed the authors to obtain satisfactory spectra from the samples, while maintaining the size of the ablation craters small, and minimizing the damage on the sample's surface. The authors were able to obtain high-resolution maps of the composition of fossil snake bones, allowing for the discrimination of healthy specimens from others, showing bone diseases such as *Osteitis Deformans*.

1.5.3.2 – DP-LIBS of Liquid Samples

The first applications of DP-LIBS to liquid samples date back to 1984, when Cremers et al demonstrated the capabilities of this configuration for the improvement of the LODs for several elements in water [175]. Since then, and especially in recent years, many research groups investigated the properties of DP-LIBS for the analysis of liquids [124].

In general, the mechanisms of DP-LIBS in a liquid matrix are similar to those already described in the previous sections for the analysis of solid samples in that atmosphere. In this case, the first pulse is used to generate a cavitation bubble inside of which, the second pulse can generate a plasma. Effectively, this generates a plasma that is no longer confined by the liquid, but can evolve in a low-density environment.

Rifai et al quantified traces of Fe, Pb and Au in water using a DP setup in Re-Heating configuration with two wavelengths (the plasma was generated by a UV 266 nm laser and re-heated by an IR 1064 nm pulse) [176]. Koch et al employed a DP laser source operating at a wavelength of 532 nm and an optical fiber probe to measure dissolved Mg in water samples, reaching LODs of 80 ppm [177]. The group of Lazic investigated the instrumental parameters for an optimal generation of the LIBS plasma and the cavitation bubble in water, demonstrating an improvement in the LOD for Mg [178]. Similarly, a systematic study of the instrumental parameters for identifying the optimal measurement conditions of DP-LIBS for liquid samples was performed by Cristoforetti et al [179].

1.6 – Nanoparticle Enhanced LIBS (NELIBS)

One of the simplest ways to enhance the performances of LIBS (and in turn its sensitivity) is to increase the efficiency of the energy transfer between the laser pulse and the sample. This can be done, up to a certain degree, by changing the laser parameters [180] or by altering the background environment [181]. However, when the laser source and experimental parameters cannot be changed, the only way to improve the efficiency of the laser-sample interaction is manipulating the sample itself. This manipulation should not change the chemical composition nor be time-consuming, in order not to lose typical LIBS advantages such as fast and straightforward analysis.

Impurities and superficial defects are known to generally lower the breakdown threshold due to their low thermal conductivity and the reduced size [14] [182], which leads to an increase of the

local laser energy density. In particular, if two adjacent solids are hit by a laser radiation, the solid with the lower breakdown threshold generates electrons that increase the local temperature at the interface zone.

For this reasons, the application of metallic nanoparticles appears as an ideal solution:

- Nanoparticles can be easily deposited onto a sample in the form of a colloidal solution
- The contamination of the sample is minimal
- Their effect on the sample under laser irradiation is significant due to their peculiar properties
- They are almost completely removed during laser irradiation

This novel methodology, named Nanoparticle-Enhanced LIBS (NELIBS) has been introduced and explored by De Giacomo and coworkers [183] [184] [185] [186] [187] [188], and applied to the study of gemstones, liquids and molecular bands [189] [190] [191]. Although the methodology is still relatively new and unexplored, NELIBS has already shown great potential for enhancing the performances of traditional LIBS in laboratory applications.

1.6.1 – Principles of NELIBS

When metallic nanoparticles (NPs) are applied on the surface of a target, an incident laser pulse will interact mainly with the nanoparticles themselves. The laser radiation induces a coherent and collective oscillation of the conduction electrons on the NPs surface and which amplifies the incident electromagnetic field. This, in turn, enhances the local electric field near the NPs surface and in the gaps between the NPs, and increases the intensity of the incident laser beam. This phenomenon can greatly increase the amount of electrons that are extracted from a conductive material and can decrease the time required for the breakdown.

A different phenomenon occurs if the laser pulse is resonant with the surface plasmon of the NPs. A plasmon is defined as the electron density displacement caused by a collective oscillation of the surface electrons of the NPs when they interact with the laser radiation. If the NPs average diameters are smaller than the incident wavelength, this oscillation is localized on the particles themselves and it is called Localized Surface Plasmon (LSP). When a laser pulse with the same frequency of the LSP irradiates the NPs, a strong oscillation of conduction electrons is induced and consequently an accumulation of charge density at the border of the NPs is formed. Since the oscillation is in phase with the incident electromagnetic field, the instantaneous electrostatic field of the generated dipole produces a huge near field electromagnetic enhancement that is confined on the surface of NPs and in the surrounding region. When the distance between adjacent NPs is

smaller than a certain value (which is proportional to the NP size), the LSP from nearby particles couples, forming a new electromagnetic "hot-spot" between the particles (see Figure 29).

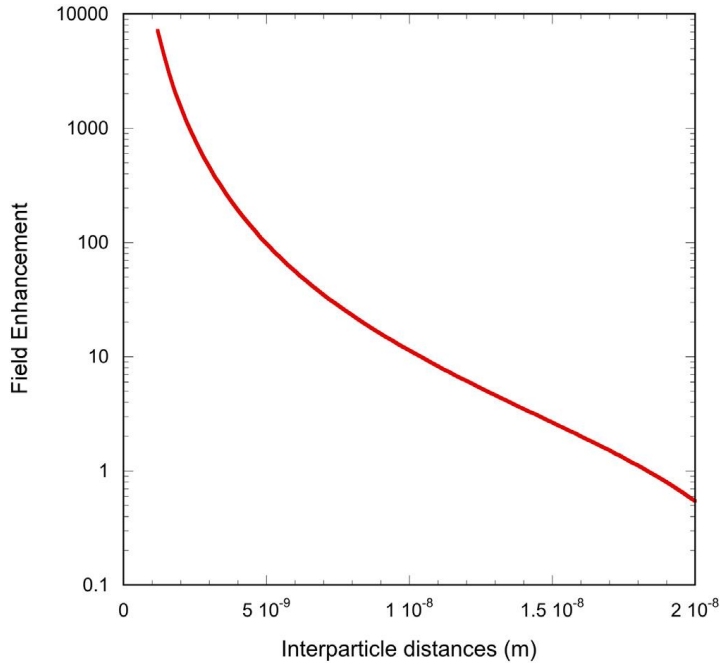

Figure 29 - Field enhancement as function of interparticle distance for spherical NPs [186]

A particle irradiated by an intense laser pulse at resonance wavelength can experience different phenomena. For low energies, the only effect is the photons absorption by NPs and a moderate heating due to the LSP resonance. At higher energies, surface evaporation occurs, reducing the size of the NPs. At laser irradiance comparable or higher than GW/cm^2, violent evaporation and boiling of the melted NPs leads to particle fragmentation or to the electron ejection, inducing the breakdown of the NPs.

When NPs are deposited on a conducting sample's surface, the electromagnetic field of the incident radiation is strongly increased. This phenomenon changes the way the ablation and the plasma induction occur, because the photons of the laser pulse do not couple directly with the sample. If the deposition is optimal, the laser field enhancement can switch the production of seed electrons from the typical multiphoton ionization to field emission. This allows an instantaneous emission of electrons, even before the NPs are destroyed by the effects of the laser pulse. Moreover, the electrons accelerate upon laser irradiation in the opposite and parallel direction to the incoming laser, further increasing the electron flow due to the Schottky effect, inducing an efficient breakdown and an efficient plasma excitation.

As mentioned, since the field enhancement is localized along the "hot-spots" between the NPs, several points of electron extraction are available in the laser spot, leading to the creation of several ignition points for the plasma. SEM images of the surface of metallic samples after a NELIBS

measurement clearly show the presence of many burst cavities with dimensions for a few hundred nanometers [184].

In the case of insulating samples, the field enhancement is not sufficient to remove electrons from the bulk substrate and two different phenomena can occur, depending on the laser irradiance and excitation wavelength. If the laser wavelength is in resonance with the LSP, a strong local heating is produced. Moreover, if the irradiance is high enough (> 1 GW/cm^2), the NPs can be subjected to the breakdown process, with consequent ignition of the plasma. In this case, the sample in contact with the NPs can be transferred in the plasma phase as well. Otherwise, if the laser pulse is not resonant with the LSP and the distance between NPs is short, then breakdown can occur by electron transfer between NPs by tunneling effect. Indeed, these phenomena can be exploited to perform surface analysis of samples or to limit the damage induced by the laser pulse [190]. Moreover, NPs deposited on an insulated target can be exploited as a substrate for liquid analysis [189]. After drying the liquid sample on a NPs deposition, the NELIBS advantages can be exploited (i.e. coupling of the laser electromagnetic field with the LSP, adsorption of the analytes on the NPs, increase in the emitting species "fed" into the plasma).

Semiconductor are samples that fall in between the two cases discussed above. Depending on the energy gap between the valence band and the conduction band, NELIBS can work like with metallic or dielectric samples.

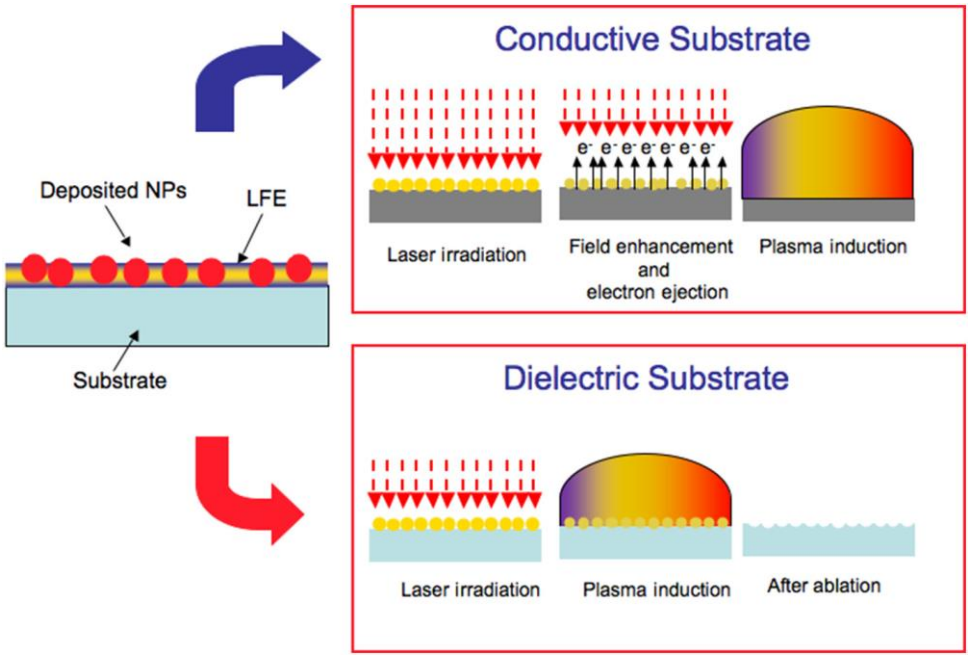

Figure 30 - Diagram of the sample ablation and plasma generation in NELIBS [186]

The main differences between LIBS and NELIBS can be found in the ablation and excitation processes that affect the plasma characteristics. Since the electrons are immediately ejected, the

initial plasma temperature and ionization degree are higher in NELIBS than in LIBS. The ablated material is reflected back from the shockwave wall and it is concentrated closer to the sample surface. This effect allows a greater number density of emitting species near the target and a faster drop of temperature at later stages of the plasma evolution. This suggests that a different configuration of optical detection system is required to optimize the acquired signal from NELIBS analyses.

1.6.2 – Sample Preparation for NELIBS

While NELIBS can seem fairly easy and immediate to implement, there are some steps that need to be taken into account during the sample preparation in order to obtain good results. It was already mentioned how the distance between the NPs (which is related to their dimensions) is crucial for the "hot-spot" field enhancement to occur. In this section, an overview on the critical aspects involved in preparing a sample for NELIBS is proposed.

The main step of a NELIBS analysis is the deposition of the metallic NPs on the sample surface. The simplest way to accomplish this is to dry one (or more) drop of a colloidal solution on the selected measurement area. Such solutions can be either commercially available dispersions (Merck-Sigma) or prepared ad-hoc. Generally, the presence of a coffee ring effect is observed (i.e. a larger concentration of NPs is deposited on the outer ring of the dried droplet) which can hinder the measurement reproducibility and quality. To avoid this, the laser spot should be focused inside the deposited NPs circle (generally in the center), where the concentration is more homogeneous. In addition, the dimensions of the laser spot should be adjusted in order to irradiate a sufficiently high number of NPs. Ideally, the laser spot should be as large as the NPs deposition (if not larger). If the laser spot is in the order of tens of µm, smaller NPs should be used to guarantee that the critical number of NPs irradiated by the pulse is reached. For example, if the laser beam spot is 100 µm in diameter, 5 nm size NPs give an enhancement of one order of magnitude on metallic alloys, while 50 nm size NPs do not show any reproducible signal enhancement.

Another crucial requirement is the purity and quality of the colloidal NPs solution. While this might seem obvious, it should be stressed that any foreign element in the solution can be absorbed onto the NPs, resulting in a strong emission signal due to the NELIBS enhancement. For example, many commercial dispersions of noble metal NPs are obtained by chemical reduction of metal salts, and can contain residual counter-ions such as alkali metals. This can severely hinder the analysis of such elements using commercially available NPs solutions. The NPs solution should also be characterized by small distribution of particle sizes. Although this might not set back the generation of a NELIBS enhancement, it could affect the reproducibility of the measurements.

Once the optimal NPs are chosen, they should be deposited on the sample surface at an optimal inter-particle distance, so that their aggregation during the drying process is prevented. In the case of colloidal solutions, this distance can be tuned by changing the NPs concentration (so that the deposited volume and the deposition size remain constant between measurements).

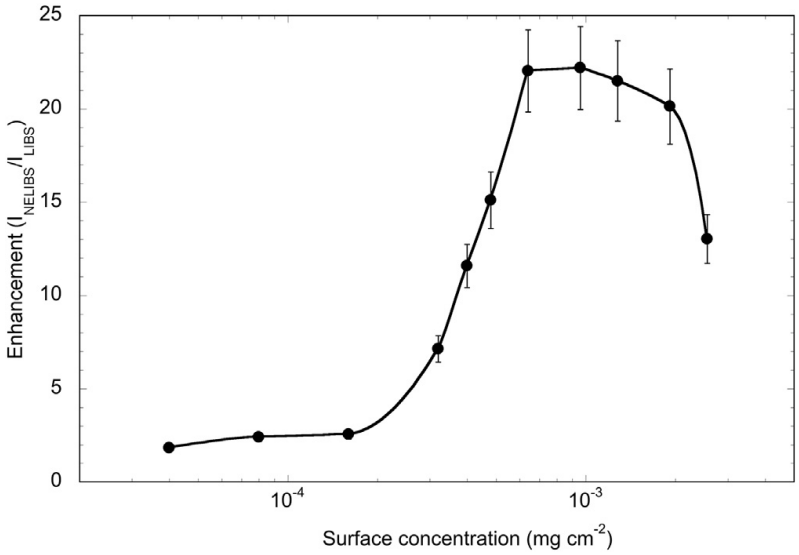

Figure 31 - NELIBS enhancement as a function of NPs concentration [183]

Generally, for low surface concentrations, where the inter-particle distance is much larger than particle diameter, NPs act like insulated defects on the sample surface decreasing the breakdown threshold. In these conditions, the enhancement grows linearly with the number of NPs deposited on the surface, as shown in Figure 31. When the concentration of NPs reaches a certain critical concentration, the inter-particle distance becomes effective for inducing the collective oscillation of the surface electrons of adjacent NPs. There is an optimum value of the packing density, namely the ratio between the diameter of the NPs (2r) and the inter-particle distance (D), which provides the maximum field enhancement and this, in turn, corresponds to the maximum emission signal of the laser induced plasma.

In practice, finding a balance between the optimal NPs surface concentration and an inter-particle distance sufficient to avoid NPs aggregation is crucial for NELIBS. The aggregation rate is connected to surface energy, concentration and mobility of the deposited NPs. Their mobility on the sample surface depends on the electrostatic interaction between the NPs surface electrons and the surface charge distribution of the substrate. In the case of metals, the charges are delocalized, inducing a propagating surface plasmon that propagates across the surface, dragging the NPs with a mutual interaction between the LSP and the surface charges of the metal substrate. In the case of dielectric, since the charges are fixed in specific points on the substrate, when the NPs are deposited, they interact with the localized charge of the dielectric. In this case only a mechanical force or an external perturbation to the charge distribution can move the NPs. Because of this, the

preparation of a metal sample for NELIBS is not an easy task. In order to avoid NPs aggregation, two main options are available:

- Use a lower NPs concentration than the optimal one.
- Add a stabilizing substance to the NPs solution, generally a salt (e.g. KCl) or an organic substance (e.g. citrate or phosphate ions, polymers), to reduce the surface reactivity of the NPs themselves.

1.6.3 – Applications of NELIBS

1.6.3.1 – Analysis of Solid Samples

As mentioned briefly in the previous sections, the first applications of NELIBS involved the analysis of metallic targets. De Giacomo and co-workers used titanium, copper, iron, steel and brass targets as a benchmark for fundamental studies on NELIBS, as well as insulating materials such as Teflon [183]. Nevertheless, Ti was frequently used due to its metallic nature, high purity of the sample and its strong and relatively isolated spectral emission lines [184] [185]. Silver and gold nanoparticles, both commercially available dispersion and ad-hoc prepared solutions, were deposited on the samples and dried by blowing hot air on the droplets. This assured a rapid evaporation of the solvent and reduced the formation of a coffee-ring.

In a similar fashion, Kiris and co-workers investigated nanocomposites and alloyed nanoparticles for the analysis of aluminum samples [192]. The authors fabricated the Ni-C composited through an electrical discharge between Ni electrodes in ethanol, while the Ag-Cu nanoparticles were produced using the PLAL approach and a Ag-Cu alloy target. It was demonstrated how both compounds gave rise to a signal enhancement when deposited on an aluminum foil and it was found that the entity of the enhancement of the Ag-Cu nanoparticles was twice that of the Ni-C composite.

In a recent work by Niu and co-workers, commercially available silver nanoparticles were used to improve the detection of Cd in rice flour [193]. The authors investigated two different approaches, namely the deposition of the NPs on a flour pellet and the preparation of a film by mixing the flour with the nanoparticle dispersion and drying it on a glass substrate. While the signal enhancement for the film deposition was found to be significant (i.e. 20-fold), the NP deposition on the pellet did not yield significant enhancement, due to the aggregation of the NPs on the sample surface which acts, effectively, as a shield for the sample itself.

An innovative use of NELIBS is the analysis of transparent and delicate samples, such as gemstones [190]. The application of NPs on the surface of such samples has several advantages. For example, it is much easier to focus the laser beam on the samples. Moreover, the NPs significantly lower the

breakdown threshold, which allows the use of lower laser pulse energy that does not damage the samples but still yields a relatively good spectrum. Because of this, NELIBS shows potential for the analysis of precious gemstones or delicate glass artifacts (such are those found in the field of cultural heritage) with LIBS.

Lastly, the longer-lasting plasma emission generated in NELIBS measurements was exploited to study the molecular AlO bands in the emission spectrum of an Al plasma. Koral and co-workers [191] demonstrated how the NELIBS emission corresponding to molecular bands lasts much longer and intensely than that registered in normal LIBS experiments.

1.6.3.2 – Analysis of Liquid Samples

NELIBS has also been used successfully for the analysis of liquid samples. In particular, for the detection of analytes at ppm and sub-ppm concentrations. In this case, the sample preparation procedure differs from conventional NELIBS in that the nanoparticles are deposited onto a dielectric substrate (i.e. glass) and then a portion of the liquid sample is dried on top of the NPs. As the solvent evaporates, the analytes are deposited on the substrate and on the nanoparticles, so that when the laser pulse is triggered, the resulting plasma is enhanced by the plasmonic effects and it is also enriched in excited species deriving from vaporization of the NPs themselves. De Giacomo and co-workers [189] demonstrated the feasibility of such an approach by preparing NELIBS substrates using gold NPs and studying both standard aqueous solutions of Pb, as well as biological samples (e.g. human blood serum) spiked with Pb. The authors obtained good enhancement for the standard solutions, while the NELIBS effects on the serum samples were less pronounced.

Another approach was proposed [194], using amyloid fibrils coated with gold NPs as a substrate for liquid sample analysis. The fibrils aid in immobilizing the nanoparticles, ensuring that the optimal distance is maintained for the plasmonic enhancement to take place, despite further substrate manipulation. Using this approach, the authors obtained LODs in the order of a few ppb for Cr, Pb, Tl and Cd.

1.7 – Carbon-Mediated Micro-Extraction for LIBS Analysis of Liquid Samples

As previously mentioned, there are several strategies to improve LIBS performances for the analysis of liquid samples. However, many of them require either a dedicated instrumental setup, or a time-consuming and radical sample treatment. Ideally, to fully exploit the advantages of LIBS, a sample preparation method should be simple and rapid (so that it does not impact significantly on the overall procedure), cost-effective, easily down-scalable and should be suitable to be integrated in an automated process.

The most promising option are based on the solid phase micro-extraction technique [114] [195] [196] [197], in particular the use of thin absorbent films of a suitable material that can be used to extract and pre-concentrate the analytes on a solid matrix that can then be analyzed by LIBS. This technique is generally called Thin Film Micro-Extraction (TFME). In brief, an inert substrate (e.g. glass, ceramic, Teflon) is covered with a thin film of an extracting medium and inserted in the desired sample. While it is immersed (with or without agitation), the analytes migrate from the solution to the adsorbent and are retained. After a certain time, the substrate is removed, dried and analyzed with LIBS as a conventional solid sample. It has been shown, as it will be detailed in the following sections, that some of the best absorbent materials are based on carbon structures such as graphite, activated carbon, graphene and graphene oxide.

1.7.1 – Principles of Solid Phase Micro-Extraction

The micro-extraction process can be defined as an extraction technique where the extractant (either a liquid or a solid) has a much lower volume than the sample that is being extracted. For example, common SPME extractants have volumes lower than 100 mg for samples of 1 mL or higher. As such, the extraction is not quantitative, but only a small fraction of the analyte is absorbed and removed from the sample. However, given the small volumes, the concentration of the analyte in the extractant will be much higher.

The basic mechanism of SPME is the partition of the analytes between the sample and the solid extractant (which can be a fiber, a thin film, dispersed particles, etc.). When the extractant comes in contact with the liquid sample, the analytes diffuse into the former (called acceptor phase) until the concentrations are in equilibrium. The relation between the equilibrium concentrations of an analyte can be expressed by the equation:

$$n^{eq} = \frac{K_p V_e C_s^0 V_s}{K_p V_e + V_s} \qquad \text{Equation 1.20}$$

Where n^{eq} are the moles that are absorbed by the solid phase at the equilibrium, C_s^0 is the analyte starting concentration in the sample, V_e and V_s are the volumes of the extractant and the sample, respectively. K_p is the partition coefficient of the analyte between the solid phase and the sample, and it can be expressed as the ratio between the equilibrium concentrations of the analyte:

$$K_p = \frac{C_e^{eq}}{C_s^{eq}} \qquad \text{Equation 1.21}$$

Normally, in SPME applications, the volume of the sample is much larger than the volume of the extractant. In this case, we can assume that $V_s >> K_p V_e$ and Equation 1.20 can be simplified as:

$$n^{eq} = K_p V_e C_s^0 \qquad \text{Equation 1.22}$$

We can see that the extracted analyte at the equilibrium is directly proportional to the starting concentration of the analyte in the sample, but it does not depend on the volume of the sample itself. However, this condition is true only for large sample volumes or for K_p values that are not too great.

To quantify the efficiency of the extraction, two additional parameters are defined, namely the recovery R (%) and the enrichment E factors. R can be defined as the amount of analyte that can be extracted from the sample:

$$R = \frac{K_p}{K_p + {V_s}/{V_e}} \cdot 100 \qquad \text{Equation 1.23}$$

As expected, the recovery does not depend only on the partition coefficient K_p, but also on the ratio between the sample volume and the extractant phase volume. As such, if the K_p is not great, a micro-extraction process will almost always have very low recovery values. On the other hand, the enrichment factor E is defined as the amount of analyte that is deposited on the extractant:

$$E = \frac{R}{{V_e}/{V_s}} \qquad \text{Equation 1.24}$$

Even if the absolute amount of analyte recovered is small, if there is a large difference in the volumes of the sample and the extractant phase (as is the case for micro-extraction applications), the enrichment factor E will be high. Because of this, the final objective of micro-extraction is not to obtain high R fractions (as is the case for exhaustive extractions used in separation techniques), but rather to maximize the E values.

Another factor that should be considered is the kinetic aspect of the extraction procedure [195] [196] [197]. While a detailed description of the processes involved in SPME is not in the scope of this work, it should be pointed out that an efficient diffusion of the analytes in the sample over the acceptor phase is necessary for good extraction results. As such, it is generally advisable to implement stirring or mixing of the liquid samples when they come in contact with the extractant.

1.7.2 – Thin Film Micro-Extraction TFME

There are many different configurations for solid phase micro-extraction, as shown in Figure 32.

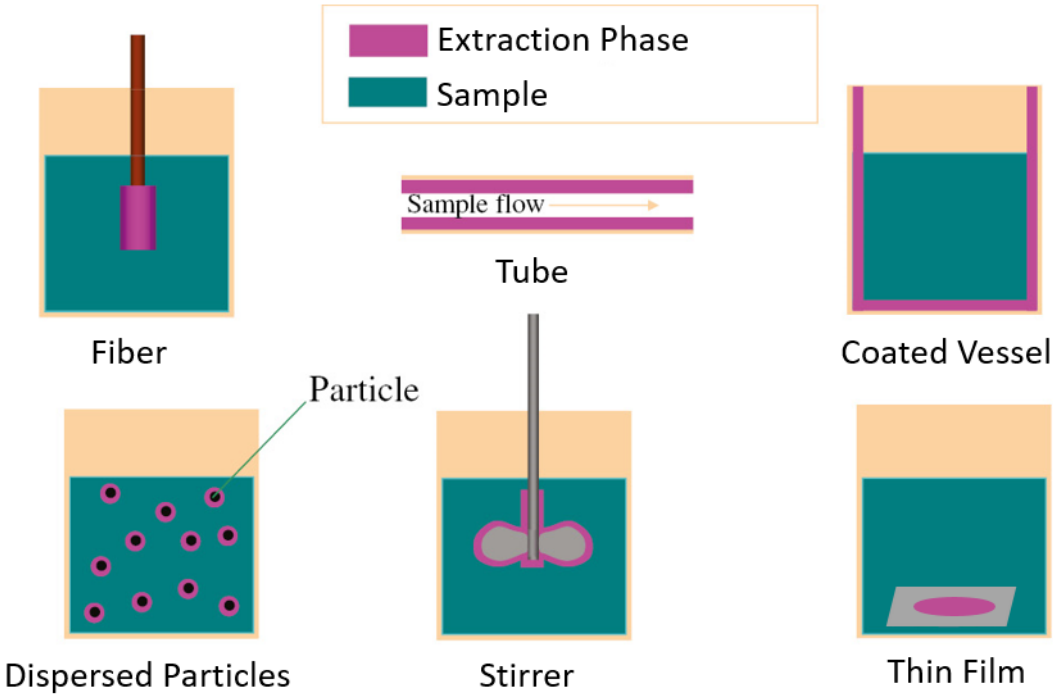

Figure 32 - Different configurations of SPME. Adapted from [198]

Thin-Film micro-extraction, developed by Bruheim et al in 2003 [199], is the most suitable for LIBS applications. Dispersive SPME (DSPME, where the extractant is composed of solid particles dispersed in the liquid sample) could also be applied, and has indeed been used successfully in recent applications [200]. However, the solid phase needs to be first separated from the sample, then dried and then treated to produce a suitable target for LIBS. Moreover, the peculiar planar geometry of TFME substrates allows for higher surface/volume ratios than those found in SPME that relies on spherical geometries (i.e. DSPME).

In TFME the extractant is deposited and fixed to a (generally) rigid support as a thin film. This guarantees that the surface area available to the analyte is large, as well as allowing an easier manipulation of the extractant-support system. The main steps involved in a TFME procedure are schematized in Figure 33. If necessary, the sample is pre-treated to adjust its pH, to derivatize the analytes, to form metal complexes. The TFME substrates are then introduced into the liquid samples for a certain time (determined beforehand) to extract the analytes of interest. If deemed necessary, an agitation system can be added to the sample holder. In some cases, the agitation can be produced directly by mounting the extraction substrates to a moving arm that allows them to spin inside the liquid. Generally, after the analyte has been adsorbed onto the substrate, a desorption step would be required to free the analytes and introduce them into the analytical instrumentation (this step is commonly performed via a thermal desorption procedure) [201]. However, the use of LIBS allows skipping this step as the measurement would be performed

directly on the substrates. Indeed, a drying step is still crucial to ensure the maximum reliability of the analysis.

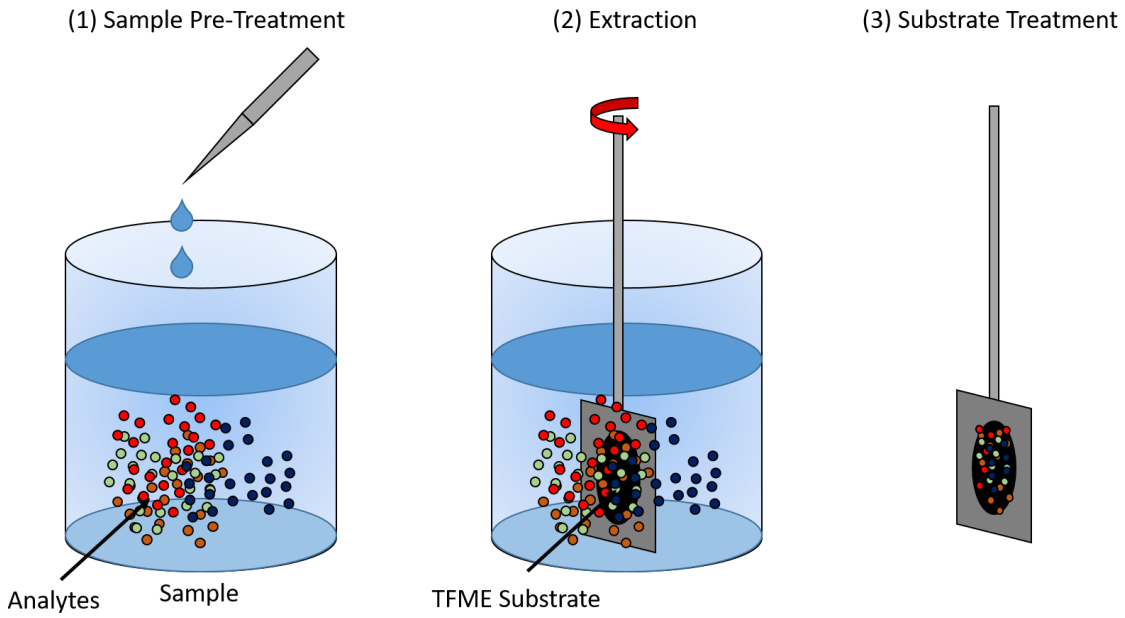

Figure 33 - Main steps of TFME

As previously mentioned, the amount of analyte that is extracted depends on its initial concentration in the sample, the partition coefficient K_p and the volume of extractant. Because of this, the optimization of an extraction procedure generally focuses on maximizing the affinity of the analyte towards the extractant, as well as the volume of solid phase that can be used. The coefficient K_p can be generally optimized by altering physical and chemical parameters such as temperature, agitation intensity, ionic strength of the sample. In addition, the chemical composition of the extractant itself must be taken into account as it strongly influences the extraction efficiency as well as its affinity towards certain analytes. At the same time, increasing the volume of extractant directly increases the amount of analyte that can be extracted from the sample. However, this can lead to an increase in the time required to reach the same extraction efficiency (as the time required to reach an equilibrium between the sample and the extractant increases), which might be undesirable for some applications.

1.7.3 – Carbon-Based Extractants

In SPME, the nature of the extractant defines the range of applicability of the technique itself. The affinity towards an analyte or the presence of complex matrices generally determines which solid phase is to be used. Many SPME tools, already primed with different extractants are commercially available. The most common are Polymethyldisiloxane (PDMS), Divinylbenzene (DVB),

Carboxane/PDMS, long-chain hydrocarbons C8 and C18 and so on. However, the typical extractants present some limitations such as a limited range of operating temperatures, limited selectivity and unsuitability for certain solvents. Because of this, many researchers focused on identifying alternatives for SPME extractants.

Recent advances in material chemistry allowed the introduction of various absorbent materials having their morphology, physical and chemical characteristics fine-tuned for SPME applications. In some cases, these materials offer a high available surface area, specific functional groups and adjustable active site dimensions. As such, these materials offer better analyte transfer kinetics and higher enrichment factors than the classic SPME extractants.

Since LIBS is an atomic spectroscopy technique, in this section only the solid phases dedicated to the extraction of metals from liquid samples will be described. Indeed, these extractants are the ones that are generally used in LIBS analyses. However, there is a wide variety of materials that have been synthetized and used for the extraction of metals from liquid matrices. For example, Ionic Polymers (IP), carbon nanotubes (CNTs), graphene and graphene oxide (G and GO), activated carbon (AC), metallic and metal oxide nanostructures, polymeric resins. Carbon based materials, in particular graphite, graphene and graphene oxide, show the most promise for TFME coupled with LIBS applications. This is due to their high surface area and a large number of active sites which lead to an increased extraction efficiency and a high enrichment factor. In addition, they show a high extracting capacity, high conductivity and are easily modifiable to add ad-hoc functional groups [202] [203] [204].

1.7.3.1 – Graphene

Graphene [205] is a carbon-based material made of a single sheet of carbon atoms with sp^2 hybridization. Two different approaches can be used to obtain pure graphene, a top-down (in which nanostructures are produced from bulk materials) and a bottom-up (in which the starting material consists of atoms or small molecules) procedure.

In the top-down approach, graphene is prepared from bulk graphite, either by mechanical or chemical exfoliation or by chemical synthesis. This allows the graphene layers, stacked in the graphite and held together by weak van der Waals forces, to be separated. Mechanical exfoliation is one of the simplest methods in which a simple direct contact with an adhesive tape can take off the graphene layers from the surface of a graphite piece. However, it has only been implemented on a small scale and is highly susceptible to contamination. In the same way, organic solvents can be used to separate the graphite layers. Other exfoliation methods include the use of electric fields or sonication [206]. Chemical reduction of graphene oxide (GO) is the most popular method to obtain graphene. In this case, the final product is reduced GO (r-GO), which has properties similar

to graphene but its structure is slightly different. A wide variety of chemical reduction agents can be employed, even though some of them are highly toxic. As an alternative, greener reduction agents and thermally-mediated or electrochemical reduction are also employed.

Conversely, the bottom-up approaches are another alternative to synthesize high-quality graphene layers. The leading methods used include pyrolysis, chemical vapor deposition (CVD), plasma synthesis, and epitaxial growth. Graphene sheets are prepared from small building blocks and precisely assembled, usually employing molecular modeling to build the layers. The main advantage of bottom-up methods is the production of high-quality graphene sheets. However, these methods are not used for large-scale production.

Unlike other carbon structures, like CNTs and fullerenes, in graphene both the sides of its structure are available for the capture of analytes. It is generally used for the capture of those compounds that have aromatic rings like pesticides, polycyclic aromatic hydrocarbons (PAHs) or polychlorobyphenyls (PCBs), thanks to the interaction between the π-electrons of the rings of these compounds and the sp^2 orbitals on the graphene sheets. It has also been used for the extraction of metals as-is or with the addition of specific chelating agents. These substances bind themselves to the metals in the sample and then are absorbed on the graphene thanks to the presence of π-bond electrons in their structure. Graphene has also been used in conjunction with magnetic nanoparticles (generally iron oxides) that aid in dispersing and recovering the graphene sheets (for DSPME) as well as increasing the efficiency of the extraction [207] [208] [209] [210].

1.7.3.2 – Graphene Oxide

Graphene oxide [209] [210] is a material based on graphene which is widely used thanks to its great versatility. GO sheets are functionalized with a large number of oxygen-containing groups (hydroxyl –OH, carboxyl –CO, epoxide -O-, carbonyl –COOH). The addition of such groups imposes a hydrophilic character to GO, as well a weaker interaction between layers. As a consequence, GO is much easier to exfoliate than graphene. Moreover, the presence of charged and electron-rich groups allows GO to establish ionic interactions with metal ions and hydrogen bonds with organic analytes [211] [212]. Additional functionalization of GO is also easier due to the presence of such oxygen-containing groups which can be substituted.

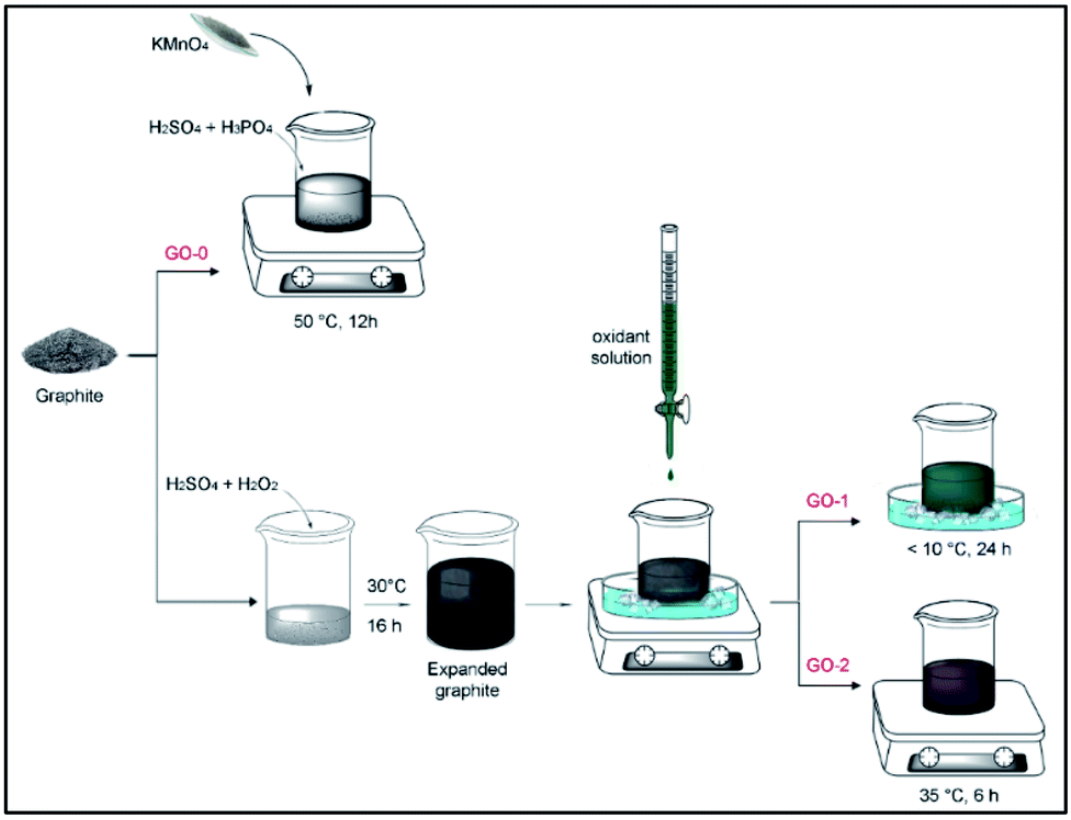

Figure 34 - Different synthetic pathways for the preparation of GO. Adapted from [213]

There are several methods for the production of GO, although the vast majority of them start with the chemical treatment of graphite bulk. The most popular is the so-called Hummers' Method [214] which has, during the years, been subjected to numerous improvements and modifications [215] [216]. In general, an oxidizing agent (usually $KMnO_4$ in H_2SO_4) at a controlled temperature (<10°C) is used. The oxidation degree of the final product (that is, the amount of oxygen containing groups) depends largely on the synthetic process and the quality of the starting material. The final step is the exfoliation (either mechanical or chemical) of the various oxidized layers (graphite oxide).

1.7.4 – Coupling of TFME and LIBS

It is well reported in literature how solid phase micro-extraction techniques are a powerful and versatile tool for chemical analysis. The various SPME procedures and tools allow for the treatment of a vast array of samples with different matrices, and for the determination of numerous analytes (being them organic compounds or metals). Several works have proposed the use of SPME for environmental and biomedical applications, as well as for the analysis of foodstuff, drugs and biological samples. With the growing interest in SPME applications and the use of LIBS for routine, in-situ analysis and as a robust and reliable analytical tool, it appears that a combination of the two techniques would be most advantageous.

Indeed, the benefits of a possible combination of LIBS and SPME are numerous:

- The analytes are retained in a solid matrix, which is the ideal substrate for LIBS analysis.
- The enrichment of the analytes by SPME can overcome the low sensitivity of LIBS, as well as increase the reproducibility when compared to the analysis of liquids.
- The desorption step is not necessary since LIBS can perform the measurement directly onto the SPME substrate.

As previously mentioned, LIBS has been successfully coupled with a DSPME technique using graphene oxide as the extractant [200]. While the potential of such an application were demonstrated, there is still the issue of recovering the extractant from the liquid sample, drying it and treating it to produce a suitable matrix for LIBS. Because of this, it appears that the ideal SPME approach for coupling with LIBS is the use of thin films of extractant, fixed onto rigid substrates (TFME).

TFME methodologies allow for much simpler analytical procedures, as well as an easier automation of the measurements. Moreover, the integration with LIBS is much simpler due to the nature of the substrates themselves. The use of (relatively) low cost materials for the production of TFME substrates (e.g. glass supports and carbon-based extractant) is ideal for the creation of single-use, serially-made, commercially available extraction “tags” that could be dipped in a sample (or even in a contaminated water source), dried and readily analyzed using a LIBS instrument (e.g. a handheld instrument).

Two recent papers by Ripoll and co-workers [217] [218] investigate the implementation of TFME-LIBS for the determination of metals in water samples. The authors evaluated two different kinds of procedures for depositing GO on different substrates (glass and ceramic), namely electrospray deposition (ESD), mould deposition (MD) and drop casting (DC). It was demonstrated how the experimental procedure for the preparation of the substrates has a strong influence on the subsequent LIBS analyses, with ESD being the most reproducible. In fact, this can affect the homogeneity of the generated adsorbent layer and, in turn, the distribution of the extracted analytes over the adsorbent material and the precision of the obtained LIBS signal. Moreover, the nature of the support can influence the LIBS analysis of the analyte-enriched adsorbent, due to possible spectral interferences from the substrate material. Nevertheless, the authors were able to obtain LODs in the order of a few tens of ppm (µg/L) for several metals (e.g. Ni, Pb, Cr).

Bibliography

[1] S. Musazzi and U. Perini, Laser Induced Breakdown Spectroscopy: THeory and Application, Springer, 2014.

[2] D. A. Cremers and L. J. Radziemski, Handbook of Laser-Induced Breakdown Spectroscopy, John Wiley and Sons Ltd., 2006.

[3] A. W. Miziolek, V. Palleschi and I. Schechter, Laser-Induced Breakdown Spectroscopy (LIBS): Fundamentals and Applications, Cambridge: Cambridge University Press, 2006.

[4] Y. I. Lee, K. Song and J. Sneddon, Laser Induced Breakdown Spectrometry, Huntington: Nova Science Publishers, 2000.

[5] J. P. Singh and S. N. Thakur, Laser-Induced Breakdown Spectroscopy, Amsterdam: Elsevier, 2007.

[6] R. W. Bogue, "Boom time for LIBS technology," *Sensor Review,* vol. 24, p. 353, 2004.

[7] Y. I. Lee, Y. J. Yoo and J. Sneddon, "Recent advances in laser-induced breakdown spectrometry," *Spectroscopy,* vol. 13, no. 7, p. 14, 1998.

[8] V. Majidi and M. R. Joseph, "Spectroscopic applications of laser-induced plasmas," *Critical Reviews in Analytical Chemistry,* vol. 23, no. 3, pp. 143-162, 1992.

[9] L. J. Radziemski, "From laser to LIBS, the path of technology development," *Spectrochimica Acta Part B: Atomic Spectroscopy,* vol. 57, no. 7, pp. 1109-1113, 2002.

[10] R. H. Scott and A. Strasheim, "Laser induced plasmas for analytical spectroscopy," *Spectrochimica Acta Part B: Atomic Spectroscopy,* vol. 25, no. 7, pp. 311-316, 1970.

[11] J. Sneddon and Y. I. Lee, "Laser Induced Breakdown Spectrometry," *The Chemical Educator,* vol. 3, no. 6, pp. 1-7, 1998.

[12] D. A. Rusak, B. C. Castle, B. W. Smith and J. D. Winefodner, "Fundamentals and applications of laser-induced breakdown spectroscopy," *Critical Reviews in Analytical Chemistrly,* vol. 27, no. 4, pp. 257-290, 1997.

[13] C. Aragon and J. A. Aguilera, "Characterization of laser induced plasmas by optical emission spectroscopy: A review of experiments and methods," *Spectrochimica Acta Part B: Atomic Spectroscopy,* vol. 63, no. 9, pp. 893-916, 2008.

[14] L. J. Radziemsky and D. A. Cremers, Laser Induced Plasmas and Applications, Marcel Dekker Inc., 1989.

[15] A. De Giacomo, M. Dell'Aglio, R. Gaudiuso and O. De Pascale, "Plasma processes and emission spectra in laser induced plasmas: A point of view," *Spectrochimica Acta Part B: Atomic Spectroscopy,* vol. 100, pp. 180-188, 2014.

[16] P. A. Sturrock, Plasma Physics: An Introduction to the Theory of Astrophysical, Geophysical and Laboratory Plasmas, Cambridge: Cambridge University Press, 1994.

[17] J. Aguilera, C. Aragon and F. Penalba, "Plasma shielding effect in laser ablation of metallic samples and its influence on LIBS analysis," *Applied Surface Science,* vol. 127, pp. 309-314, 1998.

[18] M. Deepak, U. V. Bhandarkar and S. S. Joshi, "Transient Analysis of Laser Ablation Process With Plasma Shielding: One-Dimensional Model Using Finite Volume Method," *Journal of Micro and Nano Manufacturing,* vol. 1, no. 1, pp. 11007-11009, 2013.

[19] R. Noll, Laser-Induced Breakdown Spectroscopy: Fundamentals and Applications, Berlin: Springer Berlin Heidelberg, 2012.

[20] F. Anabitarte, A. Cobo and J. Lopez-Higuera, "Laser-induced breakdown spectroscopy: Fundamentals, applications and challenges," *ISRN Spectroscopy,* vol. 2012, p. 12, 2012.

[21] Y. Zeldovich and Y. Raizer, Physics of Shock Waves and High-Temperature Hydrodinamic Phenomena, Dover: Dover Publications, 2012.

[22] L. Sedov, Similarity and Dimensional Methods in Mechanics, Elsevier Science, 2014.

[23] H. R. Griem, Plasma Spectroscopy, New York: McGraw-Hill, 1964.

[24] A. Ciucci, M. Corsi, V. Palleschi, S. Rastelli, A. Salvetti and E. Tognoni, "New procedure for quantitative elemental analyisis by laser induced breakdown spectroscopy," *Journal of Applied Spectrsoscopy,* vol. 53, no. 8, pp. 960-964, 1999.

[25] M. Corsi, G. Cristoforetti, M. Hidalgo, S. Legnaioli, V. Palleschi, A. Salvetti, E. Tognoni and C. Vallebona, "Double pulse, calibration-free laser-induced breakdown spectroscopy: A new technique for in situ standard-less analysis of polluted soils," *Applied Geochemistry,* vol. 21, pp. 748-755, 2006.

[26] E. Tognoni, G. Cristoforetti, S. Legnaioli, V. Palleschi, A. Salvetti, M. Mueller, U. Panne and I. Gornushkin, "A numerical study of expected accuracy and precision in Calibration-Free Laser-Induced Breakdown Spectroscopy in the assumption of ideal analytical plasma," *Spectrochimica Acta Part B: Atomic Spectroscopy,* vol. 62, pp. 1287-1302, 2007.

[27] E. Tognini, G. Cristoforetti, S. Legnaioli and V. Palleschi, "Calibration-Free Laser-Induced Breakdown Spectroscopy: State of the art," *Spectrochimica Acta Part B: Atomic Spectroscopy,* vol. 65, pp. 1-14, 2010.

[28] N. I. o. S. a. Technology, "NIST Atomic Spectra Database (version 5.8)," [Online]. Available: https://www.nist.gov/pml/atomic-spectra-database. [Accessed 2021].

[29] R. Gaudiuso, M. Dell'Aglio, O. De Pascale, A. Santagata and A. De Giacomo, "Laser-induced plasma analysis of copper alloys based on Local Thermodynamic Equilibrium: An alternative approach to plasma temperature determination and archeometric applications," *Spectrochimica Acta Part B: Atomic Spectroscopy,* Vols. 74-75, pp. 38-45, 2012.

[30] G. H. Cavalcanti, D. V. Teixera, S. Legnaioli, G. Lorenzetti, L. Pardini and V. Palleschi, "One-point calibration for calibration-free laser-induced breakdown spectroscopy quantitative analysis," *Spectrochimica Acta Part B: Atomic Spectroscopy,* vol. 87, pp. 51-56, 2013.

[31] F. Brech and L. Cross, "Optical microemission stimulated by a ruby laser," *Applied Spectroscopy,* vol. 16, p. 59, 1962.

[32] L. Fornarini, V. Spizzichino, F. Colao, R. Fantoni and V. Lazic, "Influence of laser wavelength on LIBS diagnostics applied to the analysis of ancient bronzes," *Analytical and Bioanalytical Chemistry,* vol. 385, pp. 272-280, 2006.

[33] O. Svelto, Principles of Lasers, New York: Springer, 2010.

[34] A. E. Siegman, Lasers, Sansalito: University Science Book, 1986.

[35] C. E. Brennen, Cavitation and bubble dynamics, Cambridge: Cambridge University Press, 2014.

[36] M. Cui, Y. Deguchi, Z. Wang, C. Yao, L. Tan and D. Zang, "Study of signal enhancement in collinear femtosecond-nanosecond double-pulse laser-induced breakdown spectroscopy," *Optics and Laser Technology,* vol. 122, 2020.

[37] I. Akhatov, O. Lindau, A. Topolnikov, R. Mettub, N. Vakhitova and W. Lauterborn, "Collapse and rebound of a laser induced cavitation bubble," *Physics of Fluids,* vol. 13, pp. 2805-2819, 2001.

[38] V. Lazic, J. Laserna and S. Jovicevic, "Insights in the laser-induced breakdown spectroscopy signal generation underwater using double pulse excitation - Part I: Vapor bubble, shockwaves and plasma," *Spectrochimica Acta Part B: Atomic Spectroscopy,* vol. 82, p. 42, 2013.

[39] M. P. Brenner, S. Hilgenfeldt and D. Lohse, "Single bubble sonoluminescence," *Reviews of Modern Physics,* vol. 74, no. 2, p. 425, 2002.

[40] A. Vogel, J. Noack, K. Nahen, D. Theisen, U. P. Busch, D. Hammer, G. Noojin, B. Rockwell and R. Birngruber, "Energy balance of optical breakdown in water at nanosecond to femtosecond time scales," *Applied Physics B,* vol. 68, pp. 271-280, 1999.

[41] T. H. Maiman, "Stimulated optical radiation in ruby," *Nature,* vol. 187, pp. 493-494, 1960.

[42] R. E. Russo, X. Mao, H. Liu, J. Gonzalez and S. S. Mao, "Laser ablation in analytical chemistry—a review," *Talanta,* vol. 57, no. 3, pp. 425-451, 2002.

[43] S. Shuttleworth, "Optimisation of laser wavelength in the ablation sampling of glass materials," *Applied Surface Science,* vol. 96, pp. 513-517, 1996.

[44] M. Ducreux-Zappa and J. M. Mermet, "Analysis of glass by UV laser ablation inductively coupled plasma atomic emission spectrometry. Part 2. Analytical figures of merit," *Spectrochimica Acta Part B: Atomic Spectroscopy,* vol. 51, no. 3, pp. 333-341, 1996.

[45] S. F. Durrant, "Laser ablation inductively coupled plasma mass spectrometry: achievements, problems, prospects," *Journal of Analytical Atomic Spectroscopy,* vol. 14, no. 9, pp. 1385-1403, 1999.

[46] L. M. Cabalin and J. J. Laserna, "Experimental determination of laser induced breakdown thresholds of metals under nanosecond Q-switched laser operation," *Spectrochimica Acta Part B: Atomic Spectroscopy,* vol. 53, no. 5, p. 723, 1998.

[47] L. Cabalin, D. Romero, C. C. Garcia, J. Baena and J. J. Laserna, "Time-resolved laser-induced plasma spectrometry for determination of minor elements in steelmaking process samples," *Analytical and Bioanalytical Chemistry,* vol. 372, no. 2, pp. 352-359, 2002.

[48] D. Menut, P. Fichet, J.-L. Lacour, A. Rivoallan and P. Mauchien, "Micro-laser-induced breakdown spectroscopy technique: a powerful method for performing quantitative surface mapping on conductive and nonconductive samples," *Applied Optics,* vol. 42, no. 30, pp. 6063-6071, 2003.

[49] D. E. Spence, P. N. Kean and W. Sibbet, "60-fsec pulse generation from a self-mode-locked Ti:sapphire laser," *Optical Letters,* vol. 16, no. 1, pp. 42-44, 1991.

[50] K. Yamakawa and C. P. Barty, "Ultrafast, ultrahigh-peak, and high-average power Ti:sapphire laser system and its applications," *IEEE Journal of Selected Topics in Quantum Electronics,* vol. 6, no. 4, pp. 658-675, 2000.

[51] "Evaluation of a compact high power pulsed fiber laser source for laser-induced breakdown spectroscopy," *Journal of Atomic Analytical Spectrometry,* vol. 26, no. 7, pp. 1354-1361, 2011.

[52] F. He, J. H. Price, K. T. Vu, A. Malinowski, J. K. Sahu and D. J. Richardson, "Optimisation of cascaded Yb fiber amplifier chains using numerical-modelling," *Optics Express,* vol. 14, no. 26, pp. 12846-12858, 2006.

[53] F. C. De Lucia and J. L. Gottifried, "Classification of explosive residues on organic substrates using laser induced breakdown spectroscopy," *Applied Optics,* vol. 51, no. 7, p. B83, 2012.

[54] A. I. Witehouse, J. Young and I. M. Botheroyd, "Remote material analysis of nuclear power station steam generator tubes by laser-induced breakdown spectroscopy," *Spectrochimica Acta Part B: Atomic Spectroscopy,* vol. 56, pp. 821-830, 2001.

[55] J. P. Singh, A. K. Rai, H. Zhang, F. Y. Yueh and A. Weisberg, "Parametric study of a fiber optic laser induced breakdown spectroscopy probe for analysis of aluminum alloys," *Spectrochimica Acta Part B: Atomic Spectroscopy,* vol. 56, no. 12, pp. 2371-2383, 2001.

[56] D. A. Cremers, I. J. Barefield and A. C. Koskelo, "Remote elemental analysis by laser induced breakdown spectroscopy using a fiber optic cable," *Applied Spectroscopy,* vol. 49, no. 6, pp. 857-860, 1995.

[57] S. M. Angel, S. R. Goode and B. J. Marquardt, "In situ determination of lead in paint by laser-induced breakdown spectroscopy using a fiber optic probe," *Analytical Chemistry,* vol. 68, pp. 977-981, 1996.

[58] H. Zhang, F.-Y. Yueh and J. P. Singh, "Laser-induced breakdown spectrometry as a multimetal continuous-emission monitor," *Applied Optics,* vol. 38, no. 9, pp. 1459-1466, 1999.

[59] K. Y. Yamamoto, D. A. Cremers, M. J. Ferris and L. E. Foster, "Detection of Metals in the Environment Using a Portable Laser-Induced Breakdown Spectroscopy Instrument," *Applied Spectroscopy,* vol. 50, no. 2, pp. 222-233, 1996.

[60] M. Lowe, N. Donaldson, A. Spiro, C. Gosselin and M. Nadeau, "Fiber Optics in Medicine," *MedEdPORTAL,* 4 12 2015.

[61] S. Konorov, O. A. Kolevatova, A. B. Fedotov and E. E. Serebryannikov, "Waveguide modes of electromagnetic radiation in hollow-core microstructure and photonic-crystal fibers," *Journal of Experimental and Theoretical Physics,* vol. 96, no. 5, pp. 857-869, 2003.

[62] E. G. Loewen and E. Popov, Diffraction Gratings and Applications, CRC Press, 1997.

[63] M. C. Hutley, Diffraction Gratings, Academic Press, 1982.

[64] C. Palmer, Diffraction Grating Handbook, Newport: MKS, 2020.

[65] "AvaSpec-Mini4096CL," Avantes, 2020. [Online]. Available: https://www.avantes.com/products/spectrometers/compactline/avaspec-mini4096cl/. [Accessed 19 08 2020].

[66] T. P. Pearsall and M. A. Pollack, "Photodiodes for Optical Fiber Communication," *Semiconductors and Semimetals,* vol. 17, pp. 174-246, 1985.

[67] "Multi-Channel Spectrometers," Avantes, 2020. [Online]. Available: https://www.avantes.com/products/spectrometers/starline/multi-channel-spectrometers/. [Accessed 19 08 2020].

[68] H. E. Bauer, F. Leis and K. Niemax, "Laser induced breakdown spectrometry with an échelle spectrometer and intensified charge coupled device detection," *Spectrochimica Acta Part B: Atomic Spectroscopy,* vol. 53, no. 13, pp. 1815-1825, 1998.

[69] C. Haisch, U. Panne and R. Niessner, "Combination of an intensified charge coupled device with an echelle spectrograph for analysis of colloidal material by laser–induced plasma spectroscopy," *Spectrochimica Acta Part B: Atomic Spectroscopy,* vol. 53, no. 12, pp. 1657-1667, 1998.

[70] V. Detalle, R. Heon, M. Sabsabi and L. St-Onge, "An evaluation of a commercial Échelle spectrometer with intensified charge-coupled device detector for materials analysis by laser-induced plasma spectroscopy," *Spectrochimica Acta Part B: Atomic Spectroscopy,* vol. 56, no. 6, pp. 1011-1025, 2001.

[71] "ARYELLE 200," LTB - Lasertechnik Berlin, 2020. [Online]. Available: http://www.ltb-berlin.de/en/products/spectrometers/aryelle-200/. [Accessed 19 8 2020].

[72] J. E. Carranza, E. Gibb, B. W. Smith, D. W. Hahn and J. D. Winerforder, "Comparison of nonintensified and intensified CCD detectors for laser-induced breakdown spectroscopy," *Applied Optics,* vol. 42, no. 30, pp. 6016-6021, 2003.

[73] U. Panne, M. Clara, C. Haisch and R. Niessner, "Analysis of glass and glass melts during the vitrification of fly and bottom ashes by laser-induced breakdown spectroscopy. Part II. Process analysis," *Spectrochimica Acta Part B: Atomic Spectroscopy,* vol. 53, no. 14, pp. 1969-1981, 1998.

[74] B. Vysetti, "Current advances in the miniaturization of analytical instruments. Applications in cosmochemistry, geochemistry, exploration and environmental sciences," *Journal of Applied Geochemistry,* vol. 31, pp. 40-44, 2016.

[75] E. H. Evans, J. Pisonero, C. M. Smith and R. N. Taylor, "Atomic spectrometry update: Review of advances in atomic spectrometry and related techniques," *Journal of Analytical Atomic Spectrometry,* vol. 36, no. 5, pp. 868-891, 2021.

[76] J. R. Bacon, O. T. Butler, W. R. Cairns, O. Cavoura, J. M. Cook, C. M. Davidson and R. Merz-Kraus, "Atomic spectrometry update-a review of advances in environmental analysis," *Journal of Analytical Atomic Spectrometry,* vol. 36, no. 1, pp. 10-5, 2021.

[77] G. Lorenzetti, S. Legnaioli, E. Grifoni, S. Pagnotta and V. Palleschi, "Laser-based continuous monitoring and resolution of steel grades in sequence casting machines," *Spectrochimica Acta Part B: Atomic Spectroscopy,* vol. 112, pp. 1-5, 2015.

[78] D. Mier, P. Nazim Jalali, P. Ramirez Lopez, J. Gurel, A. Strondl, L. M. Cabalin, T. Delgado, J. Ruiz, J. J. Laserna, B. Campanella, S. Legnaioli, G. Lorenzetti, S. Pagnotta, F. Poggialini and V. Palleschi, "A stochastic model of the process of sequence casting of steel, taking into account imperfect mixing," *Applied Physics B,* vol. 125, 2019.

[79] S. W. Hudson, J. Craparo, R. De Saro and D. Apelian, "Applications of laser induced breakdown spectroscopy (LIBS) in molten metal processing," *Metallurgical and Materials Transactions B,* vol. 48, pp. 2731-2742, 2017.

[80] A. K. Rai, F. Y. Yueh and J. P. Singh, "Laser induced breakdown spectroscopy of molten aluminum alloy," *Applied Optics,* vol. 42, p. 2078, 2003.

[81] "DTE EA-2500 Real TIme Elemental Analyzer," DT Equipment ehf, [Online]. Available: http://www.dtequipment.com/ea-2500. [Accessed 2021].

[82] "Online Chemistry Analyser," Tecnar, [Online]. Available: https://tecnar.com/online-chemistry-analyser/. [Accessed 2020].

[83] Brite Euram III Project, *Sure-Plast. Development of multipurpose industrial units for recycling of plastic wastes by on-line pattern recognition of polymer features.*

[84] A. Duckworth, "Remote metal analysis by laser induced breakdown spectroscopy," *British Nuclear Engineering Society (BNES) Conference Proceedings,* pp. 259-263, 1995.

[85] A. P. Ltd., "Laser spectroscopic remote detection of surface contamination". International Patent Application Patent PCT/GB01/00866.

[86] R. Gonzalez, P. Lucena, L. M. Tobaria and J. J. Laserna, "Standoff LIBS detection of explosive residues behind a barrier," *Journal of Analytical Atomic Spectroscopy,* vol. 24, pp. 1123-1126, 2009.

[87] X. Y. Liu and W. J. Zhang, "Recent developments in biomedicine fields for laser induced breakdown spectroscopy," *Journal of Biomedical Science and Engineering,* vol. 1, pp. 147-151, 2008.

[88] L. C. Trevizan, D. Santos Jr, R. E. Samad, N. D. Vieira, L. C. Nunes, I. A. Rufini and F. J. Krug, "Evaluation of laser induced breakdown spectroscopy for the determination of micronutrients in plant materials," *Spectrochimica Acta Part B: Atomic Spectroscopy,* vol. 64, no. 5, pp. 369-377, 2009.

[89] Q. Sun, M. Tran, W. Smith and J. D. Winefordner, "Direct determination of P, Al, Ca, Cu, Mn, Zn, Mg and Fe in plant materials by laser induced breakdown spectroscopy," *Canadian Journal of Analytical Sciences and Spectroscopy,* vol. 44, pp. 164-170, 1999.

[90] A. Botto, B. Campanella, S. Legnaioli, M. Lezzerini, G. Lorenzetti, S. Pagnotta, F. Poggialini and V. Palleschi, "Applications of laser induced breakdown spectroscopy in cultural heritage and archaeology: a critical review," *Journal of Analytical Atomic Spectroscopy,* vol. 34, pp. 81-103, 2019.

[91] L. Burgio, R. J. Clark, T. Stratoudaki, M. Doulgeridis and D. Anglos, "Pigment Identification in Painted Artworks: A Dual Analytical Approach Employing Laser-Induced Breakdown Spectroscopy and Raman Microscopy," *Applied Spectroscopy,* vol. 54, no. 4, pp. 463-469, 2000.

[92] L. Burgio, K. Melessanaki, M. Doulgeridis, R. J. Clark and D. Anglos, "Pigment identification in paintings employing laser induced breakdown spectroscopy and Raman microscopy," *Spectrochimica Acta Part B: Atomic Spectroscopy,* vol. 56, no. 6, pp. 905-913, 2001.

[93] L. Caneve, A. Diamanti, F. Grimaldi, G. Palleschi, V. Spizzichino and F. Valentini, "Analysis of fresco by laser induced breakdown spectrscopy," *Spectrochimica Acta Part B: Atomic Spectroscopy,* vol. 65, no. 8, pp. 702-706, 2010.

[94] I. Borgia, L. M. Burgio, M. Corsi, R. Fantoni, V. Palleschi, A. Salvetti, M. C. Squarcialupi and E. Tognoni, "Self-calibrated quantitative elemental analysis by laser induced plasma spectroscopy: Application to pigment analysis," *Journal of Cultural Heritage,* vol. 1, 2000.

[95] M. Corsi, G. Cristoforetti, M. Giuffrida, M. Hidalgo, S. Legnaioli, L. Masotti, V. Palleschi, A. Salvetti, E. Tognoni, C. Vallebona and A. Zanini, "Archaeometric analysis of ancient copper artifacts by laser induced breakdown spectroscopy," *Microchimica Acta,* vol. 152, pp. 105-111, 2005.

[96] M. Ferretti, G. Cristoforetti, S. Legnaioli, V. Palleschi, A. Salvetti, E. Tognoni, E. Console and P. Palaia, "In situ study of the Porticello Bronzes by portable X-Ray fluorescence and laser induced breakdown spectroscopy," *Spectrochimica Acta Part B: Atomic Spectroscopy,* vol. 62, no. 12, pp. 1512-1518, 2007.

[97] I. Osticioli, N. F. Mendes, S. Porcinai, A. Cagnini and E. Castellucci, "Spectroscopic analysis of works of art using a single LIBS and pulsed Raman setup," *Analytical and Bioanalytical Chemistry,* vol. 394, pp. 1033-1041, 2009.

[98] F. Poggialini, G. Fiocco, B. Campanella, S. Legnaioli, V. Palleschi, M. Iwanicka, P. Targowski, M. Sylwestrzak, C. Invernizzi, T. Rovetta, M. Albano and M. Malagodi, "Stratigraphic analysis of historical wooden samples from ancient bowed string instruments by laser

induced breakdown spectroscopy," *Journal of Cultural Heritage,* vol. 44, pp. 275-284, 2020.

[99] S. G. Pavlov, E. K. Jessberger, H. W. Hubers, S. Schroder, I. Rauschenbach, S. Florek, J. Neumann, H. Henkel and S. Klinkner, "Miniaturized laser-induced plasma spectrometry for planetary in situ analysis – The case for Jupiter's moon Europa," *Advances in Space Research,* vol. 47, no. 4, pp. 764-778, 2011.

[100] S. G. Pavlov, S. Schroder, I. Rauschenbach, E. K. Jessberger and H. W. Hubers, "Low-energy laser induced breakdown spectroscopy for in-situ space missions to solar system bodies without atmospheres," *Planetary and Space Science,* vol. 71, no. 1, pp. 57-63, 2012.

[101] S. e. a. Maurice, "The ChemCam Instrument Suite on the Mars Science Laboratory (MSL) Rover: Science Objectives and Mast Unit Description," *Space Science Reviews,* vol. 170, pp. 95-166, 2012.

[102] R. e. a. Wiens, "The ChemCam Instrument Suite on the Mars Science Laboratory (MSL) Rover: Body Unit and Combined System Tests," *Space Science Reviews,* vol. 170, pp. 167-227, 2012.

[103] R. C. Wiens, S. Maurice and F. Rull Perez, "The SuperCam Remote Sensing Instrument Suite for the Mars 2020 Rover: A Preview," *Spectroscopy,* vol. 35, no. 5, pp. 50-55, 2017.

[104] J. J. Laserna, J. M. Vadillo and P. Purohit, "Laser induced breakdown spectroscopy (LIBS): fast, effective and agile leading edge analytical technology," *Applied Spectroscopy,* vol. 72, no. 51, pp. 35-50, 2018.

[105] N. Omenetto and D. W. Hahn, "Laser-Induced Breakdown Spectroscopy (LIBS), Part II: Review of Instrumental and Methodological Approaches to Material Analysis and Applications to Different Fields," *Applied Spectrosocopy,* vol. 66, no. 4, pp. 347-419, 2012.

[106] D. A. Cremers and R. C. Chinni, "Laser induced breakdown specrtroscopy - capabilities and limitations," *Applied Spectroscopy Reviews,* vol. 44, no. 6, pp. 457-506, 2009.

[107] N. Omenetto, B. W. Smith, E. Gibb, T. Correll, I. B. Gornushkin and J. D. Winerfordner, "Comparing several atomic spectroscopy methods to the super stars: special emphasis on laser induced breakdown spectroscopy, LIBS, a future super star," *Journal of Analytical Atomic Spectroscopy,* vol. 19, pp. 1061-1083, 2004.

[108] S. C. Jantzi, V. Motto-Ross, F. Trichard, Y. Markushin, N. Melikechi and A. De Giacomo, "Sample treatment and preparation for laser induced brekdown spectroscopy," *Spectrochimica Acta Part B: Atomic Spectroscopy,* vol. 115, pp. 53-63, 2016.

[109] D. A. Cremers, A. S. Eppler, D. D. Hickmott, M. J. Feris and A. C. Koskelo, "Matrix effects in the detection of Pb and Ba in soils using laser induced breakdown spectroscopy," *Applied Spectroscopy,* vol. 50, pp. 1175-1181, 1996.

[110] R. Multari, L. E. Foster, D. A. Cremers and M. J. Ferris, "Effect of Sampling Geometry on Elemental Emissions in Laser-Induced Breakdown Spectroscopy," *Applied Spectroscopy,* vol. 50, no. 12, pp. 1483-1499, 1996.

[111] W. Lee, J. Wu, Y. Lee and J. Sneddon, "Recent applications of laser induced breakdown spectrometry: a review of material approaches," *Applied Spectroscopy Reviews,* vol. 39, no. 1, pp. 27-97, 2004.

[112] D. A. Cremers, B. Salle, S. Maurice and R. C. Wiens, "Laser induced breakdown spectroscopy for space exploration applications: influence of the ambient pressure on the calibration curves prepared from soil and clay samples," *Spectrochimica Acta Part B: Atomic Spectroscopy,* vol. 60, no. 4, pp. 479-490, 2005.

[113] G. Cristoforetti, S. Legnaioli, V. Palleschi, A. Salvetti and E. Tognoni, "Influence of ambient gas pressure on laser-induced breakdown spectroscopy technique in the parallel double-pulse configuration," *Spectrochimica Acta Part B: Atomic Spectroscopy,* vol. 59, no. 12, pp. 1907-1917, 2004.

[114] D. A. Skoog, D. M. West, F. J. Holler and S. R. Crouch, Fundamentals of Analytical Chemistry, Cengage Learning Inc, 2014.

[115] D. Body and B. L. Chadwick, "Optimization of the spectral data processing in a LIBS simultaneous elemental analysis system," *Spectrochimica Acta Part B: Atomic Spectroscopy,* vol. 56, no. 6, pp. 725-736, 2001.

[116] S. I. Gornushkin, I. B. Gornushkin, J. M. Anzano, W. B. Smith and J. D. Winerfordner, "Effective Normalization Technique for Correction of Matrix Effects in Laser-Induced Breakdown Spectroscopy Detection of Magnesium in Powdered Samples," *Applied Spectroscopy,* vol. 56, no. 4, pp. 433-436, 2002.

[117] C. Chalead, P. Mauchien, N. Aandre, J. Uebbing, J. L. Lacour and C. Geertsen, "Correction of matrix effects in quantitative elemental analysis with laser ablation optical emission spectroscopy," *Journal of Analytical Atomic Spectroscopy,* vol. 12, pp. 183-188, 1997.

[118] V. Lazic, R. Barbini, F. Colao, R. Fantoni and A. Palucci, "Self-absorption model in quantitative laser induced breakdown spectroscopy measurements on soils and sediments," *Spectrochimica Acta Part B: Atomic Spectroscopy,* vol. 56, no. 6, pp. 807-820, 2001.

[119] L. Nollet and L. De Gelder, Handbook of Water Analysis, CRC Press, 2007.

[120] E. H. Evans, J. Pisonero, C. M. Smith and R. N. Taylor, "Atomic spectrometry update: review of advances in atomic spectrometry and related techniques," *Journal of Analytical Atomic Spectroscopy,* vol. 35, no. 5, pp. 830-851, 2020.

[121] J. R. Bacon, O. T. Butler, W. R. Cairns, J. M. Cook, C. M. Davidson, O. Cavoura and R. Mertz-Kraus, "Atomic spectrometry update – a review of advances in environmental analysis," *Journal of Analytical Atomic Spectroscopy,* vol. 35, no. 1, pp. 9-53, 2020.

[122] G. Arca, A. Ciuccu, V. Palleschi, S. Rastelli and E. Tognoni, "Trace element analysis in water by the laser induced breakdown spectroscopy technique," *Applied Spectroscopy,* vol. 51, no. 8, pp. 1102-1105, 1997.

[123] P. Fichet, P. Mauchien, J. F. Wagner and C. Moulin, "Quantitative elemental determination in water and oil by laser induced breakdown spectroscopy," *Analitica Chimica Acta,* vol. 429, no. 2, pp. 269-278, 2001.

[124] B. Charfi and M. A. Harith, "Panoramic laser induced breakdown spectrometry of water," *Spectrochimica Acta Part B: Atomic Spectroscopy,* vol. 57, no. 7, pp. 1141-1153, 2002.

[125] Y. Ito, O. Ueki and S. Nakamura, "Determination of colloidal iron in water by laser induced breakdown spectroscopy," *Analtica Chimica Acta,* vol. 299, no. 3, pp. 401-405, 1995.

[126] E. M. Cahoon and J. R. Almirall, "Quantitative analysis of liquids from aerosols and microdrops using laser induced breakdown spectroscopy," *Analytical Chemistry,* vol. 84, no. 5, pp. 2239-2244, 2012.

[127] M. S. Cheri and S. H. Tavassoli, "Quantitative analysis of toxic metals lead and cadmium in water jet by laser induced breakdown spectroscopy," *Applied Optics,* vol. 50, no. 9, pp. 1227-1233, 2011.

[128] M. A. Meneses-Nava, I. Rosas-Roman, O. Barbosa-Garcia, M. Rodriguez and J. L. Maldonado, "Stability evaluation of water droplets levitated by a TinyLev acoustic levitator for laser induced breakdown spectroscopy," *Spectrochimica Acta Part B: Atomic Spectroscopy,* vol. 168, 2020.

[129] S. T. Jarvinen, S. Saari, J. Keskinen and J. Toivonen, "Detection of Ni, Pb and Zn in water using electrodynamic single-particle levitation and laser-induced breakdown spectroscopy," *Spectrochimica Acta Part B: Atomic Spectroscopy,* vol. 99, pp. 9-14, 2014.

[130] S. Zhong, R. Zheng, Y. Lu, K. Cheng and J. Xiu, "Ultrasonic nebulizer assisted LIBS: A promising metal elements detection method for aqueous sample analysis," *Plasma Science and Technology,* vol. 17, no. 11, pp. 979-984, 2015.

[131] S. S. Golik, A. Y. Mayor, V. V. Lisitsa, Y. S. Tolstonogova, A. A. Ilyin, A. V. Borovskiy and O. A. Bukin, "Limits of Detection of Chemical Elements in an Aqueous Aerosol in Filament-Induced Breakdown Spectroscopy," *Journal of Applied Spectroscopy,* vol. 88, no. 2, pp. 337-342, 2021.

[132] L. A. Alvarez-Trujillo, V. Lazic, J. Moros and J. J. Laserna, "Standoff monitoring of aqueous aerosols using nanosecond laser-induced breakdown spectroscopy: Droplet size and matrix effects," *Applied Optics,* vol. 53, no. 13, pp. 3773-3782, 2017.

[133] A. Kumar, F. Y. Yueh and J. P. Singh, "Double pulse laser induced breakdonw spectroscopy with liquid jets of different thickness," *Applied Optics,* vol. 42, no. 30, pp. 6047-6051, 2003.

[134] Y. Feng, J. Yang, J. Fan, G. Yao, X. Ji, X. Zhang, X. Zheng and Z. Cui, "Investigation of laser induced breakdown spectroscopy of a liquid jet," *Applied Optics,* vol. 49, no. 13, pp. C70-C74, 2010.

[135] M. Gondal and T. Hussain, "Determination of poisonous metals in wastewater collected from paint manufacturing plant using laser induced breakdown spectrscopy," *Talanta,* vol. 71, no. 1, pp. 73-80, 2007.

[136] X. Wang, Y. Wei, Q. Lin, J. Zhang and Y. Duan, "Simple, fast matrix conversion and membrane separation for ultrasensitive metal detection in aqueous samples by laser induced breakdown spectroscopy," *Analytical Chemistry,* vol. 87, no. 11, pp. 5577-583, 2015.

[137] H. Sobral, R. Sangines and A. Trujillo-Vasquez, "Detection of trace elements in ice and water by laser induced breakdown spectroscopy," *Spectrochimica Acta Part B: Atomic Spectroscopy,* vol. 78, pp. 62-66, 2012.

[138] Q. Lin, X. Han, J. Wang, Z. Wei, K. Liu and Y. Duan, "Ultra trace metallic element detection in liquid samples using laser induced breakdown spectroscopy based on matrix conversion and crosslinked PVA polymer membrane," *Journal of Analytical Atomic Spectroscopy,* vol. 31, pp. 1622-1630, 2016.

[139] B. Campanella, I. Degano, E. Grifoni, S. Legnaioli, G. Lorenzetti, S. Pagnotta, F. Poggialini and V. Palleschi, "Identification of inorganic dyeing mordant in textiles by surface-enhanced laser-induced breakdown spectroscopy," *Microchemical Journal,* vol. 139, pp. 230-235, 2018.

[140] M. Aguirre, S. Legnaioli, F. Almodovar, M. Hidalgo, V. Palleschi and A. Canals, "Elemental analysis by surface enhanced laser induced breakdown spectroscopy combined with liquid liquid microextraction," *Spectrochimica Acta Part B: Atomic Spectroscopy,* vol. 79, pp. 88-93, 2013.

[141] P. Yaroshchyk, R. J. Morrison, D. Body and B. L. Chadwick, "Quantitative determination of wear metals in engine oils using LIBS: the use of paper substrates and a comparison between single and double pulse LIBS," *Spectrochimica Acta Part B: Atomic Spectroscopy,* vol. 60, no. 11, pp. 1482-1485, 2005.

[142] D. Alamelu, A. Sarkar and S. Aggarwal, "Laser induced breakdown spectroscopy for simultaneous determination of Sm, Eu and Gd in acqueous solutions," *Talanta,* vol. 77, no. 1, pp. 256-261, 2008.

[143] Z. Chen, Y. Godwal, Y. Y. Tsui and R. Fedosejevs, "Sensitive detection of metals in water using laser induced breakdown spectroscopy on wood sample substrates," *Analytical Methods,* vol. 49, no. 13, pp. C87-C94, 2010.

[144] A. Sarkar, D. Alamelu and S. K. Aggarwal, "Determination of thorium and uranium in solution by laser-induced breakdown spectrometry," *Applied Optics,* vol. 47, no. 31, pp. G58-G64, 2008.

[145] X. Wang, L. Shi, Q. Lin, X. Zhu and Y. Duan, "Simultaneous and sensitive analysis of Ag (I), Mn (II) and Cr (III) in aqueous solutions by LIBS combined with dispersive solid phase micro-extraction using nano-graphite as an adsorbent," *Journal of Analytical Atomic Spectroscopy,* vol. 29, pp. 1098-1104, 2014.

[146] E. H. Piepmeier and H. V. Malmstadt, "Q-Switched Laser Energy Absorption in the Plume of an Aluminum Alloy," *Analytical Chemistry,* vol. 41, no. 6, pp. 700-707, 1982.

[147] K. Niemax, F. Leis, W. Sdorra, J. Brust and J. Uebbing, "Reheating of a Laser-Produced Plasma by a Second Pulse Laser," *Applied Spectroscopy,* vol. 45, no. 9, 1991.

[148] L. St-Onge, M. Sabsabi and P. Cielo, "Analysis of solids using laser-induced plasma spectroscopy in double-pulse mode," *Spectrochimica Acta Part B: Atomic Spectroscopy,* vol. 53, no. 3, p. 407, 1998.

[149] L. St-Onge, V. Detalle and M. Sabsabi, "Enhanced laser-induced breakdown spectroscopy using the combination of fourth-harmonic and fundamental Nd:YAG laser pulses," *Spectrochimica Acta Part B: Atomic Spectroscopy,* vol. 57, no. 1, p. 121, 2002.

[150] D. N. Stratis, K. L. Eland and M. S. Angel, "Dual-pulse LIBS using a pre-ablation spark for enhanced ablation and emission," *Applied Spectroscopy,* vol. 54, no. 9, p. 1270, 2000.

[151] M. Corsi, G. Cristoforetti, M. Giuffrida, M. Hidalgo, S. Legnaioli, V. Palleschi, A. Salvetti, E. Tognoni and C. Vallebona, "Three-dimensional analysis of laser induced plasmas in single and double pulse configuration," *Spectrochimica Acta Part B: Atomic Spectroscopy,* vol. 57, pp. 723-735, 2004.

[152] G. Cristoforetti, S. Legnaioli, V. Palleschi, A. Salvetti and E. Tognoni, "Characterization of a collinear double pulse laser-induced plasma at several ambient gas pressures by spectrally- and time-resolved imaging," *Applied Physics B,,* vol. 80, no. 4-5, pp. 559-568, 2005.

[153] A. De Giacomo, M. Dell'Aglio, D. Bruno, R. Gaudiuso and O. De Pascale, "Experimental and theoretical comparison of single-pulse and double-pulse Laser Induced Breakdown Spectroscopy on metallic samples," *Spectrochimica Acta Part B: Atomic Spectroscopy,* vol. 63, p. 805, 2008.

[154] R. Sangines, V. Contreras, H. Sobral and A. Robledo-Martinez, "Optimal emission enhancement in orthogonal double-pulse laser-induced breakdown spectroscopy," *Spectrochimica Acta Part B: Atomic Spectroscopy,* vol. 110, pp. 139-145, 2015.

[155] S. L. Lui and N. H. Cheung, "Resonance-enhanced laser-induced plasma spectroscopy: ambient gas effects," *Spectrochimica Acta Part B:: Atomic Spectroscopy,* vol. 58, no. 9, pp. 1613-1623, 2003.

[156] W. L. Yip and N. H. Cheung, "Analysis of aluminum alloys by resonance-enhanced laser-induced breakdown spectroscopy: How the beam profile of the ablation laser and the energy of the dye laser affect analytical performance," *Spectrochimica Acta Part B: Atomic Spectroscopy,* vol. 64, no. 4, pp. 315-322, 2009.

[157] D. Nishijima, E. M. Hollmann and R. P. Doerner, "Spatially-offset double-pulse laser-induced breakdown spectroscopy: A novel technique for analysis of thin deposited layers," *Spectrochimica Acta Part B: Atomic Spectroscopy,* vol. 124, pp. 82-86, 2016.

[158] J. Scaffidi, J. Pender, W. Pearman, S. R. Goode, B. W. Colston, J. C. Carter and S. M. Angel, "Dual-pulse laser-induced breakdown spectroscopy with combinations of femtosecond and nanosecond laser pulses," *Applied Optics,* vol. 45, no. 30, pp. 6099-6109, 2003.

[159] J. Scaffidi, W. Pearman, J. C. Carter and S. M. Angel, "Observations in Collinear Femtosecond–Nanosecond Dual-Pulse Laser-Induced Breakdown Spectroscopy," *Applied Spectroscopy,* vol. 60, no. 1, pp. 65-71, 2006.

[160] M. Cui, Y. Deguchi, Z. Wang, C. Yao, L. Tan and D. Zang, "Signal Improvement for Underwater Measurement of Metal Samples Using Collinear Long-Short Double-Pulse Laser Induced Breakdown Spectroscopy," *Frontiers in Physics,* vol. 8, 2020.

[161] W. Sdorra, J. Brust and K. Niemax, "Basic investigations for laser microanalysis: IV. The dependence on the laser wavelength in laser ablation," *Microchimica Acta,* vol. 108, no. 1, pp. 1-10, 1992.

[162] G. Cristoforetti, G. Lorenzetti, P. A. Benedetti, S. Legnaioli, E. Tognoni and V. Palleschi, "Effect of laser parameters on plasma shielding in single and double pulse configurations during the ablation of an aluminium target," *Journal of Physics D: Applied Physics,* vol. 42, no. 22, 2009.

[163] R. Sattmann, V. Sturm and R. Noll, "Laser-induced breakdown spectroscopy of steel samples using multiple Q-switch Nd:YAG laser pulses," *Journal of Physics D: Applied Physics,* vol. 28, no. 10, p. 2181, 1995.

[164] G. Galbacs, V. Budavari and Z. Geretovszky, "Multi-pulse laser-induced plasma spectroscopy using a single laser source and a compact spectrometer," *Journal of Analytical Atomic Spectrometry,* vol. 20, no. 9, pp. 974-980, 2005.

[165] G. Galbacs, N. Jedlinszki, G. Cseh, Z. Galbacs and L. Turi, "Accurate quantitative analysis of gold alloys using multi-pulse laser induced breakdown spectroscopy and a correlation-based calibration method," *Spectrochimica Acta Part B: Atomic Spectroscopy,* vol. 63, no. 5, pp. 591-597, 2008.

[166] D. Prochazka, P. Porizka, J. Novotny, A. Hrdlicka, K. Novotny, P. Sperka and J. Kaiser, "Triple-pulse LIBS: laser-induced breakdown spectroscopy signal enhancement by combination of pre-ablation and re-heating laser pulses," *Journal of Analytical Atomic Spectrometry,* vol. 35, pp. 293-300, 2020.

[167] S. M. Pershin and A. Y. Bukharov, "«Enhancement of the contrast of laser plasma emission spectra accompanying two-pulse irradiation of a surface by neodymium laser radiation," *Soviet Journal of Quantum Electronics,* vol. 22, p. 405, 1992.

[168] G. Cristoforetti and E. Tognoni, "Basic mechanisms of signal enhancement in ns double-pulse laser-induced breakdown spectroscopy in a gas environment," *Journal of Analytical Atomic Spectrometry,* vol. 29, pp. 1318-1338, 2014.

[169] O. Grupce, M. Simileanu, A. Raskovska, L. J. Dzidrova, B. Minceva-Sukarova, R. Radvan, M. Surbanovska and J. Striber, "Characterization of roman marble bust using LIBS and μ-Raman spectroscopy. A case study," *PONTICA,* vol. 43, p. 563, 2010.

[170] S. Columbu, S. Carboni, S. Pagnotta, S. Legnaioli, M. Lezzerini, S. Raneri, V. Palleschi and A. Usai, "Laser-Induced Breakdown Spectroscopy analysis of the limestone Nuragic statues from Mont'e Prama site (Sardinia, Italy)," *Spectrochimica Acta Part B: Atomic Spectroscopy,* vol. 149, p. 62, 2018.

[171] A. Bertolini, G. Carelli, F. Francesconi, M. Francesconi, L. Marchesini, P. Marsili, F. Sorrentino, G. Cristoforetti, S. Legnaioli, V. Palleschi, L. Pardini and A. Salvetti, "Modì: a

new mobile instrument for in situ double-pulse LIBS analysis," *Analytical and Bioanalytical Chemistry,* vol. 385, no. 2, p. 240, 2006.

[172] L. Pardini, A. El Hassan, M. Ferretti, A. Foresta, S. Legnaioli, G. Lorenzetti, E. Nebbia, F. Catalli, M. A. Harit, D. Diaz Pace, F. Anabitarte Garcia, M. Scuotto and V. Palleschi, "X-Ray Fluorescence and Laser-Induced Breakdown Spectroscopy analysis of Roman silver denarii," *Spectrochimica Acta Part B: Atomic Spectroscopy,* Vols. 74-75, p. 159, 2012.

[173] J. L. Gottifried, F. C. De Lucia Jr., C. A. Munson and A. W. Miziolek, "Laser-induced breakdown spectroscopy for detection of explosives residues: a review of recent advances, challenges, and future prospects," *Analytical and Bioanalytical Chemistry,* vol. 395, p. 283, 2009.

[174] M. Galiová, J. Kaiser, K. Novotny, M. Ivanov, M. Nývltová Fišáková, L. Mancini, G. Tromba, T. Vaculovič, M. Liska and V. Kanický, "Investigation of the osteitis deformans phases in snake vertebrae by double-pulse laser-induced breakdown spectroscopy," *Analytical and Bioanalytical Chemistry,* vol. 398, no. 2, p. 1095, 2010.

[175] D. A. Cremers, L. J. Radziemski and T. R. Loree, "Spectrochemical analysis of liquids using the laser spark," *Applied Spectroscopy,* vol. 38, pp. 721-729, 1984.

[176] K. Rifai, S. Laville, F. Vidal, M. Sabsabi and M. Chaker, "Quantitative analysis of metallic traces in water-based liquids by UV-IR double-pulse laser-induced breakdown spectroscopy," *Journal of Analytical Atomic Spectroscopy,* vol. 27, no. 2, pp. 276-283, 2012.

[177] S. Koch, R. Court, W. Garen, W. Neu and R. Reuter, "Detection of manganese in solution in cavitation bubbles using laser induced breakdown spectroscopy," *Spectrochimica Acta Part B: Atomic Spectroscopy,* vol. 60, no. 7-8, pp. 1230-1235, 2005.

[178] V. Lazic, S. Jovicevic, R. Fantoni and F. Colao, "Efficient plasma and bubble generation underwater by an optimized laser excitation and its application for liquid analyses by laser-induced breakdown spectroscopy," *Spectrochimica Acta Part B: Atomic Spectroscopy,* vol. 62, no. 12, pp. 1433-1442, 2007.

[179] G. Cristoforetti, M. Tiberi, A. Simonelli, P. Marsili and F. Giammanco, "Towards the optimization of double pulse LIBS underwater: effects of experimental parameters on the reproducibility and dynamics of laser induced cavitation bubble," *Applied Optics,* vol. 51, no. 7, pp. B30-B41, 2012.

[180] A. Bogaerts and Z. Chen, "Effect of laser parameters on laser ablation and laser-induced plasma formation: a numerical modeling investigation," *Spectrochimica Acta Part B: Atomic Spectroscopy,* vol. 60, pp. 1280-1307, 2005.

[181] A. De Giacomo, M. Dell'Aglio, R. Gaudiuso, S. Amoruso and O. De Pascale, "Effects of the background environment on formation, evolution and emission spectra of laser-induced plasmas," *Spectrochimica Acta Part B: Atomic Spectroscopy,* vol. 78, pp. 1-19, 2012.

[182] C. T. Walters, R. H. Barnes and R. E. Beverly III, "Initiation of laser-supported-detonation (LSD) waves," *Journal of Applied Physics,* vol. 49, no. 5, p. 2937, 1978.

[183] A. De Giacomo, R. Gaudiuso, C. Koral, M. Dell'Aglio and O. De Pascale, "Nanoparticle-Enhanced Laser-Induced Breakdown Spectroscopy of Metallic Samples," *Journal of Analytical Chemistry,* vol. 85, pp. 10180-10187, 2013.

[184] A. De Giacomo, R. Gaudiuso, C. Koral, M. Dell'Aglio and O. De Pascale, "Nanoparticle Enhanced Laser Induced Breakdown Spectroscopy: Effect of nanoparticles deposited on sample surface on laser ablation and plasma emission," *Spectrochimica Acta Part B: Atomic Spectroscopy,* vol. 98, pp. 19-27, 2014.

[185] A. De Giacomo, M. Dell'Aglio, R. Gaudiuso, C. Koral and G. Valenza, "Perspective on the use of nanoparticles to improve LIBS analytical performance: nanoparticle enhanced laser induced breakdown spectroscopy (NELIBS)," *Journal of Analytical Atomic Spectrometry,* vol. 31, p. 1566, 2016.

[186] M. Dell'Aglio, R. Alrifai and A. De Giacomo, "Nanoparticle Enhanced Laser Induced Breakdown Spectroscopy (NELIBS), a first review," *Spectrochimica Acta Part B: Atomic Spectroscopy,* vol. 148, pp. 105-112, 2018.

[187] Z. Salajkova, V. Gardette, J. Kaizer, M. Dell'Aglio and A. De Giacomo, "Effect of spherical gold nanoparticles size on nanoparticle enhanced Laser Induced Breakdown Spectroscopy," *Spectrochimica Acta Part B: Atomic Spectroscopy,* vol. 179, p. 106105, 2021.

[188] A. De Giacomo, R. Alrifai, V. Gardette, Z. Salajkova and M. Dell'Aglio, "Nanoparticle enhanced laser ablation and consequent effects on laser induced plasma optical emission," *Spectrochimica Acta Part B: Atomic Spectroscopy,* vol. 166, p. 105794, 2020.

[189] A. De Giacomo, C. Koral, G. Valenza, R. Gaudiuso and M. Dell'Aglio, "Nanoparticle Enhanced Laser-Induced Breakdown Spectroscopy for Microdrop Analysis at subppm Level," *Analytical Chemistry,* vol. 88, pp. 5251-5257, 2016.

[190] C. Koral, M. Dell'Aglio, R. Gaudiuso, R. Alrifai, M. Torelli and A. De Giacomo, "Nanoparticle-Enhanced Laser Induced Breakdown Spectroscopy for the noninvasive analysis of transparent samples and gemstones," *Talanta,* vol. 182, pp. 253-258, 2018.

[191] C. Koral, A. De Giacomo, X. Mao, V. Zorba and R. E. Russo, "Nanoparticle Enhanced Laser Induced Breakdown Spectroscopy for Improving the Detection of Molecular Bands," *Spectrochimica Acta Part B: Atomic Spectroscopy,* vol. 125, pp. 11-17, 2016.

[192] V. V. Kiris, A. V. Butsen, E. A. Ershov-Pavlov, M. I. Nedelko and A. A. Nevar, "Nanoparticle enhanced laser induced breakdown spectroscopy using copper-silver and nickel-carbon nanocomposites on aluminium," *International Journal of Nanoscience,* vol. 18, no. 03n04, 2019.

[193] J. Niu, J. Lu and F. Xu, "Determination of cadmium in rice using nanoparticle-enhanced laser-induced breakdown spectroscopy combined with film preparation," *Journal of Analytical Atomic Spectroscopy,* vol. 35, p. 2990, 2020.

[194] M. Dell'Aglio, Z. Salajková, A. Mallardi, R. Mezzenga, L. van't Hag, N. Cioffi, G. Palazzo and A. De Giacomo, "Application of gold nanoparticles embedded in the amyloids fibrils asenhancers in the laser induced breakdown spectroscopy for the metalquantification in

microdroplets," *Spectrochimica Acta Part B: Atomic Spectroscopy,* vol. 155, pp. 115-122, 2019.

[195] J. Pawliszyn, Solid Phase Microextraction: Theory and Practice, Wiley, 1997.

[196] J. Pawliszyn, Handbook of Solid Phase Microextraction, Elsevier, 2012.

[197] C. K. Zacharis and P. D. Tzanavaras, Solid-Phase Microextraction, MDPI, 2020.

[198] C. Poole, Z. Mester, M. Miro, S. Pedersen-Bjergaard and J. Pawliszyn, "Extraction for analytical scale sample preparation (IUPAC Technical Report)," *Pure and Applied Chemistry,* vol. 88, no. 7, pp. 649-687, 2016.

[199] L. Bruheim, X. Liu and J. Pawliszyn, "Thin-Film microextraction," *Analytical Chemistry,* vol. 75, no. 4, pp. 1002-1010, 203.

[200] F. J. Ruiz, L. Ripoll, M. Hidalgo and A. Canals, "Dispersive micro solid-phase extraction with graphene oxide as adsorbent for sensitive elemental analysis of aqueous samples by laser induced breakdown spectroscopy (LIBS)," *Talanta,* vol. 191, pp. 162-170, 2019.

[201] R. Jiang and J. Pawliszyn, "Thin-film microextraction offers another geometry for solid-phase microextraction," *Trends in Analytical Chemistry,* vol. 113, pp. 93-101, 2019.

[202] A. L. de Toffoli, V. S. Maciel, B. G. Fumes and F. M. Lancas, "The role of graphene-based sorbents in modern sample preparation techniques," *Journal of Separation Science,* vol. 41, no. 1, pp. 288-302, 2018.

[203] B. Hashemi and S. Rezania, "Carbon-based sorbents and their nanocomposites for the enrichment of heavy metal ions: a review," *Microchimica Acta,* vol. 186, pp. 1-20, 2019.

[204] A. Gul, N. G. Khaligh and N. M. Julkapli, "Surface modification of Carbon-Based Nanoadsorbents for the Advanced Wastewater Treatment," *Journal of Molecular Structure,* vol. 1235, 2021.

[205] N. Nouri, P. Khorran and H. Sereshti, "Applications of three dimensional graphenes for preconcentration, extraction and sorption of chemical species: a review," *Microchimica Acta,* vol. 186, no. 4, p. 232, 2019.

[206] P. Solis-Fernandez, M. Biset and H. Ago, "Synthesis, structure and applications of graphene-based 2D heterostructures," *Chemical Society Reviews,* vol. 15, 2017.

[207] R. Kumar, P. Rauwel and E. Rauwel, "Nanoadsorbants for the removal of heavy metals from contaminated water: Current scenario and future directions," *Processes,* vol. 9, no. 8, 2021.

[208] O. E. Plastiras, E. Deliyanni and V. Samanidou, "Applications of graphene-based nanomaterials in environmental analysis," *Applied Sciences,* vol. 11, no. 7, 2021.

[209] H. Grajek, J. Jonik, Z. Witkiewicz, T. Wawer and M. Purchala, "Applications of Graphene and Its Derivatives in Chemical Analysis," *Critical Reviews in Analytical Chemistry,* vol. 50, pp. 445-471, 2020.

[210] E. V. Soares-Maciel, K. Mejia-Carmon, M. Jordan-Sinisterra, L. F. da Silva, D. A. Vargas Medina and F. M. Lancas, "The Current Role of Graphene-Based Nanomaterials in the Sample Preparation Arena," *Frontiers in Chemistry,* vol. 8, 2020.

[211] I. Duru, D. Ege and A. R. Kamali, "Graphene oxides for removal of heavy and precious metals from wastewater," *Journal of Material Science,* vol. 51, no. 13, pp. 6097-6116, 2016.

[212] F. Perreault, A. F. De Faria and M. Elimelech, "Environmental applications of graphene-based nanomaterials," *Chemical Society Reviews,* vol. 44, no. 16, pp. 5861-5896, 2015.

[213] Z. Benzait, P. Chen and L. Trabson, "Enhanced synthesis method of graphene oxide," *Nanoscale Advances,* vol. 3, pp. 223-230, 2021.

[214] W. S. Hummers and R. E. Offeman, "Preparation of Graphitic Oxide," *Journal of American Chemical Society,* vol. 80, no. 6, p. 1339, 1958.

[215] S. Shamaila, A. K. Sajjad and A. Iqbal, "Modifications in development of graphene oxide synthetic routes," *Chemical Engineering Journal,* vol. 294, pp. 458-477, 2016.

[216] J. Y. Lim, N. M. Mubarak, E. C. Abdullah, S. Nizamuddin and M. Khalid, "Recent trends in the synthesis of graphene and graphene oxide based nanomaterials for removal of heavy metals — A review," *Journal of Industrial and Engineering Chemistry,* vol. 66, pp. 29-44, 2018.

[217] L. Ripoll, J. Navarro-Gonzalez, S. Legnaioli, V. Palleschi and M. Hidalgo, "Evaluation of Thin Film Microextraction for trace elemental analysis of liquid samples using LIBS detection," *Talanta,* vol. 223, 2021.

[218] L. Ripoll, S. Legnaioli, V. Palleschi and M. Hidalgo, "Evaluation of electrosprayed graphene oxide coatings for elemental analysis by thin film microextraction followed by LIBS detection (TFME-LIBS)," *Spectrochimica Acta - Part B Atomic Spectroscopy,* vol. 183, 2021.

[219] L. Moenke-Blankeburg, Laser Micro Analyisis, John Wiley and Sons Ltd., 1989.

[220] E. Cerrai and R. Trucco, "On the matrix effect in laser sampled spectrochemical analysis," *Energia Nucleare,* vol. 15, pp. 581-585, 1968.

[221] K. W. Marich, P. W. Carr, W. J. Tretyl and D. Glick, "Effect of matrix material on laser-induced elemental spectral emission," *Analytical Chemistry,* vol. 42, pp. 1775-1779, 1970.

[222] L. J. Radziemsky and T. R. Loree, "Laser-induced breakdown spectroscopy: time-resolved spectrochemical applications," *Plasma Chemistry and Plasma Processes,* vol. 1, pp. 281-293, 1981.

[223] D. A. Cremers, "The analysis of metals at a distance using laser-induced breakdown spectroscopy," *Applied Spectroscopy,* vol. 41, pp. 572-578, 1987.

[224] D. A. Cremers and L. J. Radziemsky, "Direct detection of beryllium on filters using the laser spark," *Applied Spectroscopy,* vol. 39, pp. 57-60, 1985.

[225] N. G. Basov, V. A. Danilychev and Y. M. Popov, "Soviet Journal of Quantum Electronics," *Stimulated emission in the vacuum ultraviolet region,* vol. 1, no. 1, pp. 18-22, 1971.

[226] K. C. Patel, "Continuous-wave laser action on vibrational-rotational transitions of CO2," *Physical Revieww,* vol. 134, no. 5A, pp. A1187-A1193, 1964.

[227] G. Lorenzetti, S. Legnaioli, E. Grifoni, S. Pagnotta and V. Palleschi, "Laser-based continuous monitoring and resolution of steel grades in sequence casting machines," *Spectrochimica Acta Part B: Atomic Spectroscopy,* vol. 112, pp. 1-5, 2015.

[228] L. M. Cabalin, T. Delgado, J. Ruiz, D. Mier and J. J. Laserna, "Stand-off laser-induced breakdown spectroscopy for steel-grade intermix detection in sequence casting operations. At-line monitoring of temporal evolution versus predicted mathematical model," *Spectrochimica Acta Part B: Atomic Spectroscopy,* vol. 146, pp. 93-100, 2018.

[229] T. Delgato, J. Ruiz, L. M. Cabalin and J. J. Laserna, "Distinction strategies based on discriminant function analysis for particular steel grades at elevated temperature using stand-off LIBS," *Journal of Analytical Atomic Spectrometry,* vol. 31, p. 2242–2252, 2016.

[230] D. Mier, P. Nazim Jalali, P. Ramirez Lopez, J. Gurel, A. Strondl, L. M. Cabalin, T. Delgado, J. Ruiz, J. J. Laserna, B. Campanella, S. Legnaioli, G. Lorenzetti, S. Pagnotta, F. Poggialini and V. Palleschi, "A stochastic model of the process of sequence casting of steel, taking into account imperfect mixing," *Applied Physics B,* vol. 125, 2019.

[231] M. Galiová, J. Kaiser, K. Novotny, M. Ivanov, M. Nývltová Fišáková, L. Mancini, G. Tromba, T. Vaculovič, M. Liska and V. Kanický, "Investigation of the osteitis deformans phases in snake vertebrae by double-pulse laser-induced breakdown spectroscopy," *Analytical and Bioanalytical Chemistry,* vol. 398, no. 2, p. 1095, 2010.

Chapter 2:

Green-Synthetized Silver Nanoparticles for Nanoparticle-Enhanced Laser Induced Breakdown Spectroscopy (NELIBS) using a Mobile Instrument

Chapter 2 - Index

2 - Green-Synthetized Silver Nanoparticles for Nanoparticle-Enhanced Laser Induced Breakdown Spectroscopy (NELIBS) using a Mobile Instrument

2.1 – Introduction

The advantages and limitations of LIBS have been illustrated in Chapter 1. The technique has many of the main advantages of the atomic spectroscopy techniques, such as the fast and simultaneous determination of almost all elements. In addition, it is relatively easy to operate and can be used to analyze virtually any sample with little to no preparation required. On the other hand, quantitative analysis with LIBS is not easy to perform, due to the need of matrix-matched standards and the relatively low precision of the technique. The sensitivity is also low when compared with more complex atomic spectroscopy techniques such as ICP-OES. In fact, sensitivity in LIBS is affected by the laser pulse energy, the beam focalization setup, the type of spectrometer used and the light collection parameters.

It has been mentioned that, traditionally, the preferred method for improving LIBS performances has been the implementation of more effective ablation procedures (e.g. multiple laser pulses, controlled atmosphere, vacuum conditions, etc.) or the use of more powerful lasers and high resolution spectrometers [1] [2] [3]. However, this approach significantly increases the costs and the complexity of the instrumental setup. Moreover, the optimization of the experimental parameters requires in-depth knowledge of the instrumentation, the principles of Laser-Induced Plasmas (LIPs) and of laser-matter interaction.

In recent years, several studies have explored the possibility of treating the samples in order to enhance the LIBS signal. A review by De Giacomo et. al. presents the most common methods for in-situ treatment and the preparation of LIBS samples of different nature [4]. This approach could be applied in those cases where the instrumental setup cannot be modified (i.e. a portable LIBS system) or is not convenient to do it.

One of most interesting methods proposed by De Giacomo et al., and discussed in Chapter 1, is the Nanoparticle-Enhanced LIBS (NELIBS) technique [5] [6] [7] [8] [9] [10] [11] [12] [13]. This method seems ideal for in-situ applications, as well as for a simple and fast improvement of LIBS capabilities. It could also be applied in those cases where the instrumental setup cannot be modified, or is not convenient to do it, for example in the case of a commercial LIBS setup. These instruments usually have a set of parameters that are fixed by the manufacturer due to the intrinsic limits that guarantee their portability. In addition, these products are usually intended for

applications (e.g. cultural heritage, geology, industry, etc.) where the operators do not necessarily possess the knowledge to optimize the instruments' parameters.

Nevertheless, NP solutions that are suitable for NELIBS are usually expensive and sometimes not readily available. Thanks to the growing interest in Green Chemistry, the literature is rich in methods for the "green synthesis" of silver NPs (AgNPs), using plant extracts for the reaction with silver nitrate solutions. In brief, the phytochemical compounds extracted from the plant material act as reducing agents when they come in contact with the silver ions in a solution, producing silver nuclei which act as seeds for the growth of NPs. Moreover, these substances also act as capping agents, increasing the stability of the NPs and preventing further aggregation when the reaction is completed. The relative simplicity of these methods makes them a potential way to obtain nanoparticles which could be used for NELIBS applications.

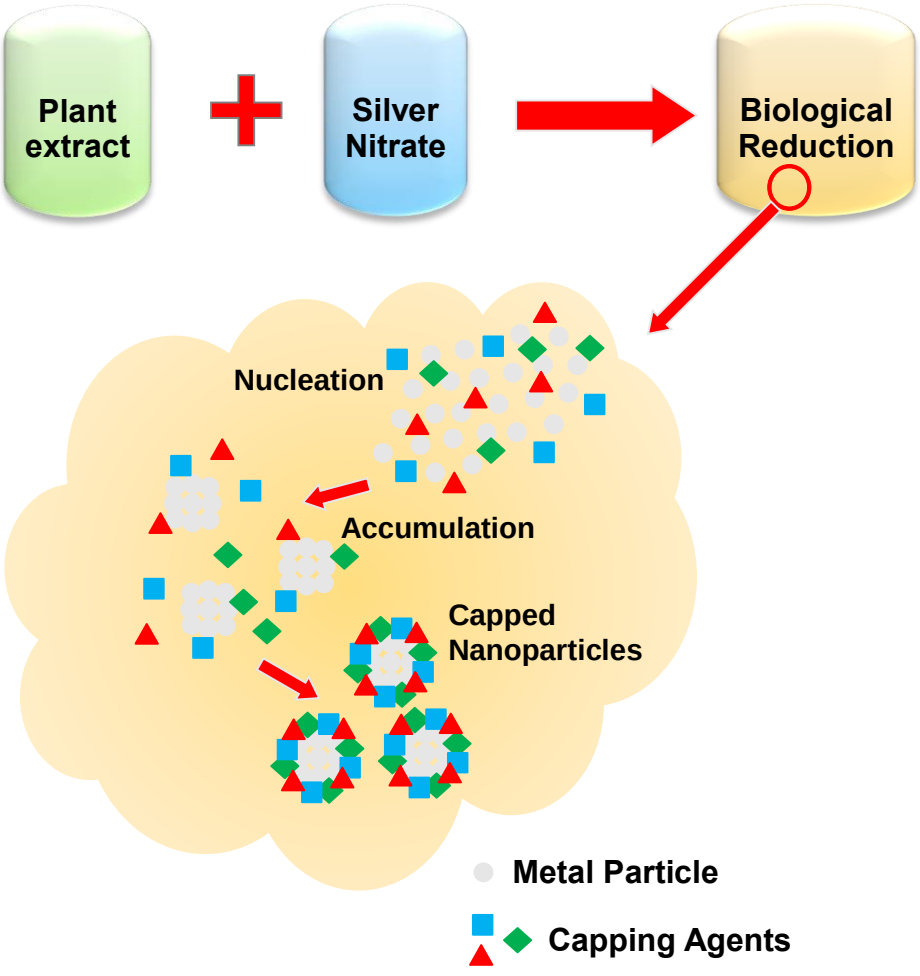

Figure 1 - Nanoparticle formation using plant extracts

In this work, a procedure for the synthesis of a solution of AgNPs was developed. The obtained NPs are suitable for NELIBS, "green", low cost, quick to prepare and the synthesis can be realized with basic laboratory equipment. The performances of the synthesized NPs were tested for NELIBS analysis with a mobile LIBS system and compared them with the signal enhancement observed

using commercially available AgNPs. The enhancement of the Limits of Detection (LODs) for Zn and Cr and Mn was also investigated using NIST Standard Reference Materials (SRMs).

2.2 – Materials and Methods

2.2.1 – Materials

Commercially available ground coffee (100% Arabica) was obtained at the local supermarket. HPLC grade ethanol (Honeywell, Chromasolv, grade ≥99.8%) was used for the preparation of the coffee extract. Silver nitrate (AgNO3 solid, for analysis) from Merck was used as the AgNPs precursor.

A commercially available silver nanoparticle solution (Silver dispersion, aqueous buffer, sodium citrate stabilizer from Sigma-Aldrich) with an average NP diameter of 20 nm was used as a reference for the observation of the NELIBS signal enhancement effect.

Copper samples were used in this study as their metallic and highly conductive nature is ideal for the application of the NELIBS technique. Preliminary measurements and the optimization of the experimental procedure were carried out using commercially available copper sheets. Standard reference materials (SRM 394 Unalloyed Copper I, SRM 395 Unalloyed Copper II, SRM 398 Unalloyed Copper V, SRM 399 Unalloyed Copper VI, National Bureau of Standards) were used for building the calibration curves and for the estimation of LODs improvements in NELIBS. In preparation for the analyses, the copper sheets were cut into small (approximately 1,5x3 cm) pieces, thoroughly cleaned and treated with a solution of HCl 1M (Titolchimica S.p.A.) in an ultrasonic bath in order to remove the superficial oxide layer. After drying at 90°C for 30 minutes, the samples were prepared for NELIBS analyses. The SRMs were similarly treated and air-dried before the analyses.

Deionized water from an Elga Purelab Option DV 35 water filtration system was used throughout the study. All the glassware was thoroughly washed with deionized water and acetone.

2.2.2 – Instrumentation

UV-Vis measurements were performed using a Perkin Elmer Lambda 25 double beam spectrophotometer. Scans were performed from 300 nm to 600 nm (scan rate 240 nm/min, 1 nm slits).

A Zeiss Libra 120 Transmission Electron Microscope (courtesy of NEST Institute, Pisa, Italy), equipped with an OMEGA in-column filter and operating at an accelerating voltage of 120 kV, was used for investigating the dimensions of the synthetized nanoparticles. The solutions were deposited on carbon-coated copper grids (Mesh 300).

LIBS and NELIBS analyses were performed using the Modì instrument [14]. Modì is equipped with a Nd:YAG laser (LS2134-D, Lotis Lasers) operating at the fundamental wavelength (1064 nm) and delivering two laser pulses of up to 110 mJ per pulse in 15 ns FWHM. The delay between the pulses can be adjusted from 0 to 100 µs, with a maximum repetition rate of 10 Hz. The laser beams are focused into an experimental chamber using a plano-convex lens and the plasma emission is collected by an optical fiber placed at a distance of 1 cm from the sample and at an angle of 45° with respect to the laser beam. The ablation spot has a fixed diameter of approximately 300 µm. The spectrum is resolved using a double spectrometer (AvaSpec-2048-2, Avantes) which operates in the range of 180 nm to 450 nm with a resolution of 0,1 nm and from 450 nm to 900 nm with a resolution of 0,3 nm. The acquisition delay can be varied from 1,26 µs up to several seconds. The acquisition gate is fixed at 2 ms. In this work, it was chosen to use the system in single pulse mode in order to follow the established NELIBS procedure. The acquisition delay was set at 300 ns from the end of the laser pulse. The measurements were carried out with a pulse energy of up to 105 mJ.

2.2.3 – Synthesis and recovery of the silver nanoparticles

The method that was chosen for the preparation of the silver nanoparticle solution was based on the one proposed by Dhand et. al. [15], and suitably modified to fit the requirements of this study.

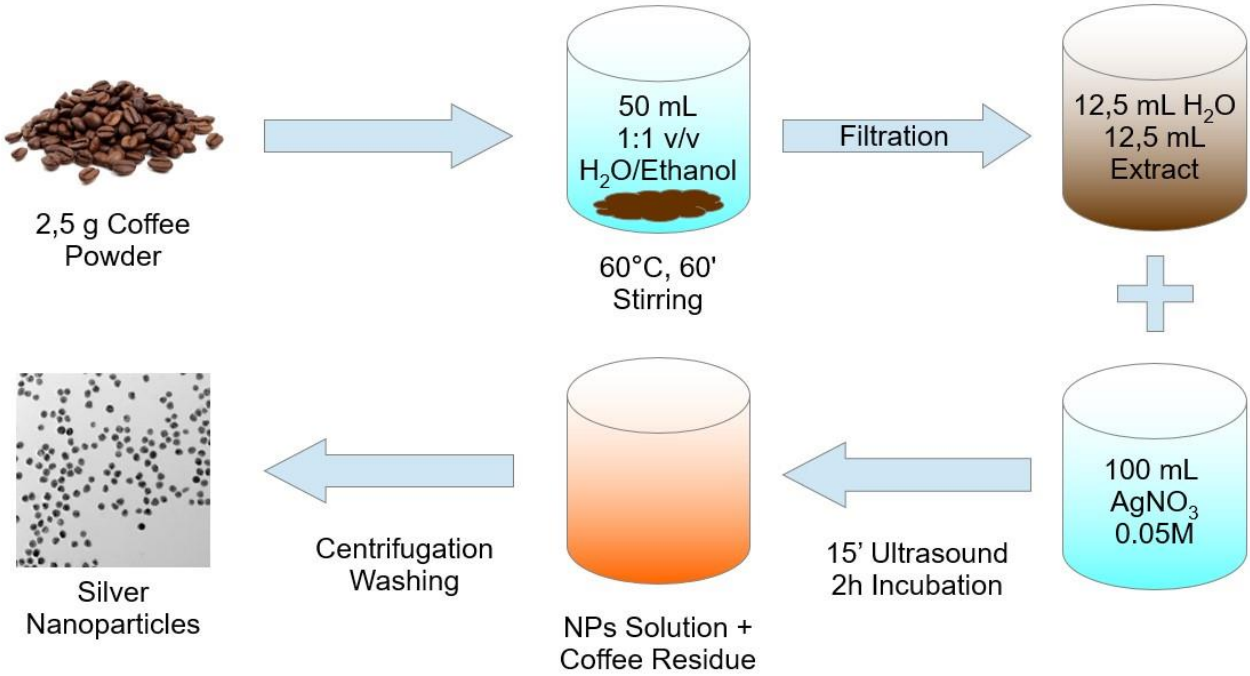

Figure 2 - Synthesis of the silver nanoparticles using coffee extract as the reducing agent

A hydro-alcoholic coffee extract was prepared by mixing 2,5 g of ground coffee with 50 mL of a solution 1:1 v/v of ethanol and water. The solution was kept under vigorous stirring at 60°C on a heated plate for one hour. Subsequently, the agitation was turned off and the solution was allowed

to cool down to room temperature. Finally, the solid residue was removed by two consecutive filtration steps with Whatman No.1 filter paper. The extract was stored in the dark at 4°C.

For the NPs synthesis, 12,5 mL of coffee extract were diluted to 25 mL with deionized water and added to 100 mL of a 0,05 M solution of $AgNO_3$ in an Erlenmeyer flask. The mixture was placed in an ultrasonic bath and the agitation was maintained for 15 minutes at room temperature. The observed color change in the solution, from pale brown to orange, is the indication that the silver nitrate has been successfully reduced to elemental silver and NPs have formed. The flask was then removed from the bath and wrapped in aluminum foil in order to prevent light from interacting with unreacted silver nitrate. After an incubation period of two hours at room temperature, the solution was centrifuged at 5600 g and the solid residue was washed two times with deionized water. It was then dispersed in 10 mL of deionized water and transferred in screw-cap PET vials which were stored in the dark at 4°C.

To prepare the AgNP dispersions for NELIBS analysis, the synthetized NP solutions were then freeze-dried and 20 mg of the solid residue were dispersed in 10 ml of deionized water using an ultrasonic bath for 30 min. The obtained solution was stored in glass screw-cap vials at 4°C in the dark.

Figure 3 - "Green" silver nanoparticles dispersion after the preparation procedure

2.3 – Results and Discussion

2.3.1 – Characterization of the silver nanoparticles

In order to verify the success of the reaction and the presence of AgNPs in the solution, UV-Vis absorbance analyses were conducted of the $AgNO_3$ solution, the coffee extract and the yellow-orange solution obtained at the end of the reaction. Samples were suitably diluted with deionized water in order to avoid signal saturation.

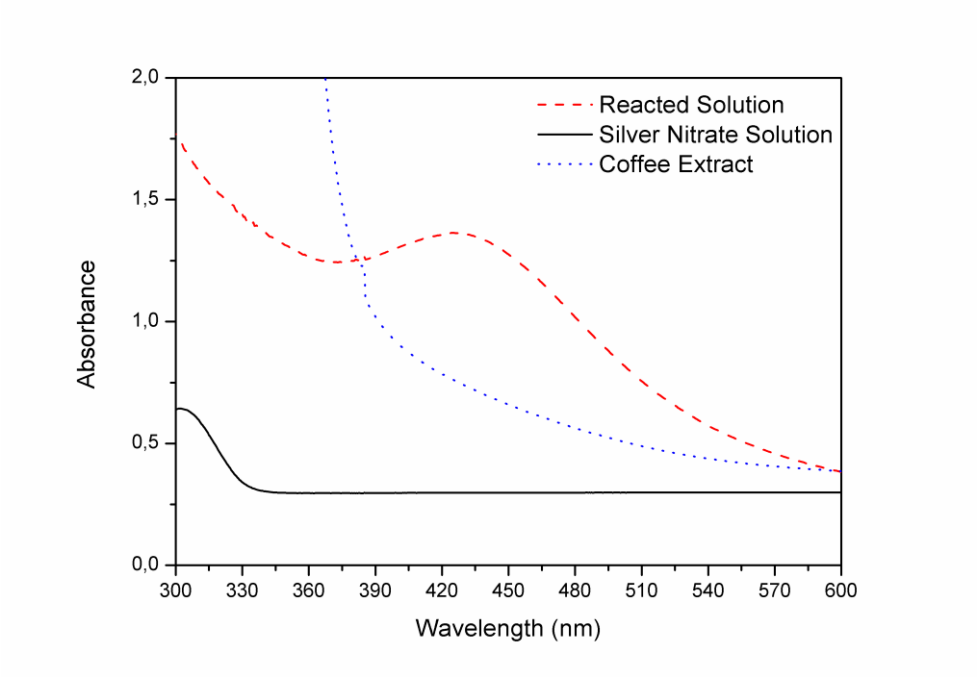

Figure 4 - UV-Vis spectra of silver nitrate solution (black continuous line), coffee extract (blue dotted line) and the AgNP solution (red dashed line)

In Figure 4 are reported the UV-Vis spectra of the silver nitrate solution, the coffee extract and the reacted solution of AgNPs. A clear absorbance band can be observed around 435 nm in the spectrum relative to the AgNP solution. This is an indication of the presence of silver nanostructures as the band is caused by their surface plasmon resonance (SPR) phenomena, which is characteristic of nanostructures dispersed in liquid solutions. The wavelength value corresponding to the maximum absorbance value in the UV-Vis spectrum could be used to estimate the size of the NPs, even though it is a method prone to errors and interferences [16].

TEM images show the presence of spherical and spheroidal nanoparticles, grouped in clusters. The presence of seeds and areas where nanostructures are still forming could also be observed. This suggests that the reaction could be prolonged, even though it could lead to the formation of larger NPs and non-spherical nanostructures, which are unsuitable for NELIBS analyses.

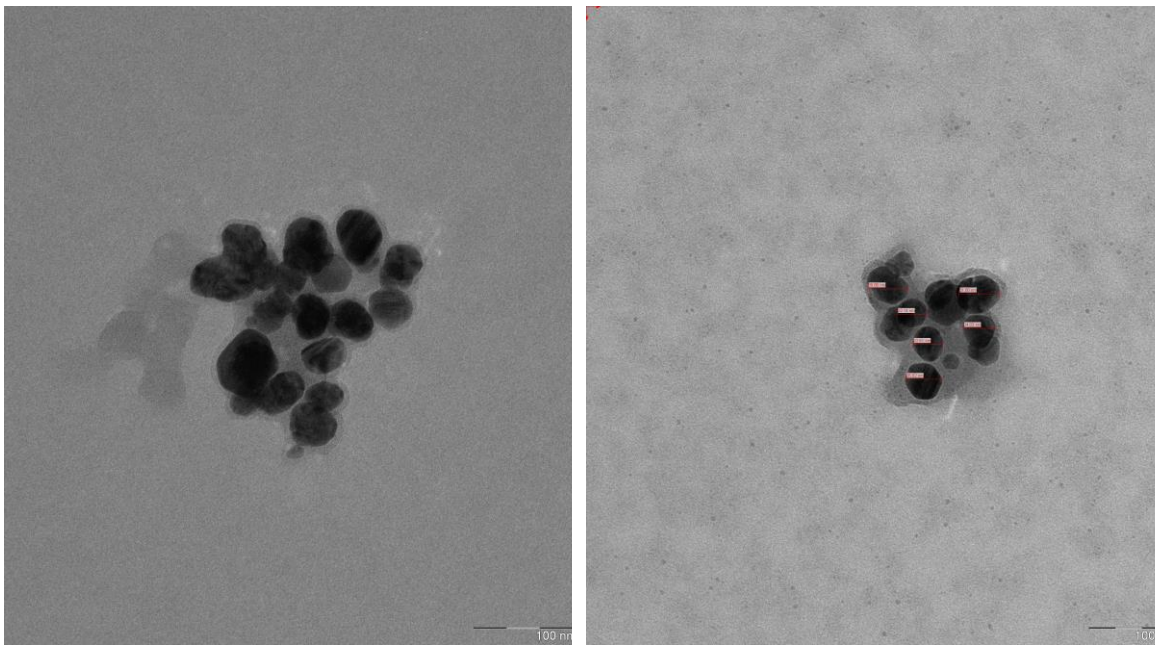

Figure 5 - TEM images of the "green"-synthetized nanoparticles. (100nm scale)

The average diameter of the AgNPs was estimated from the TEM images to be between 20 and 30 nm. As the solutions appear to be relatively diluted, a concentrated nanoparticle solution was prepared to test the NELIBS performances at various NP concentrations. The detailed results are reported in the following sections.

It is important to point out, however, some of the disadvantages related to the “green” synthesis of silver nanoparticles. These methods are mostly used to produce NPs for antimicrobial applications, where precise control of the geometry and the size of the nanostructures is not required and this could be a problem in NELIBS. The NP dimensions can be optimized, but only after a series of tests using various concentrations of coffee extract or $AgNO_3$, as well as variations in the reaction times, temperatures, etc.

Moreover, the NPs obtained with the use of a “green” synthesis are generally coated with the same phytochemicals that act as reductants for the $AgNO_3$ solution. These organic substances can hinder the laser-nanoparticle interaction and negatively affect the enhancement of the LIBS signal. There is also a risk of sample contamination if the NPs are not thoroughly and carefully washed.

Despite these limitations, this kind of approach has several advantages over the more conventional methods of NPs production (i.e. chemical reduction, laser ablation in vacuum, etc.). It is in line with the trends of Green Chemistry and it is a relatively inexpensive method that can yield a large quantity of NPs in a short time. It doesn’t require aggressive or toxic reagents and its low complexity means that it can be performed by personnel with limited laboratory experience. This, coupled with the possibility of using a portable LIBS instrument, makes this method potentially ideal for in-situ applications.

2.3.2 – LIBS and sample treatment parameter optimization

Finding the optimal instrumental parameters as well as experimental procedure is critical in NELIBS, in order to obtain the highest enhancement possible. In this study, the effect of the laser pulse energy and the air-drying time on the signal enhancement were investigated, expressed as the ratio between NELIBS and LIBS integrated emission line intensities (Enhancement Factor, EF).

Five 5 µL droplets of a commercially available 20 nm silver nanoparticles dispersion were deposited onto a copper sheet for each different measure. Each droplet was analyzed with a single laser pulse and the obtained spectra were averaged. The non-resonant copper emission lines at 521,8 nm (Cu I) and at 578,1 nm (Cu I) were observed due to their relatively high intensity and position in the emission spectrum (i.e. far from possible interferences).

Figure 6 - Nanoparticles deposited on a copper sheet. Each droplet had a diameter of approximately 4 mm. The small dot near the center of each droplet is the LIBS crater

The effect of the laser pulse energy on the signal enhancement is illustrated in Figure 6. The lower limit at about 40 mJ is the lowest energy at which a measurable plasma could be reliably obtained, while the upper limit at about 105 mJ is the highest safe energy output of the laser.

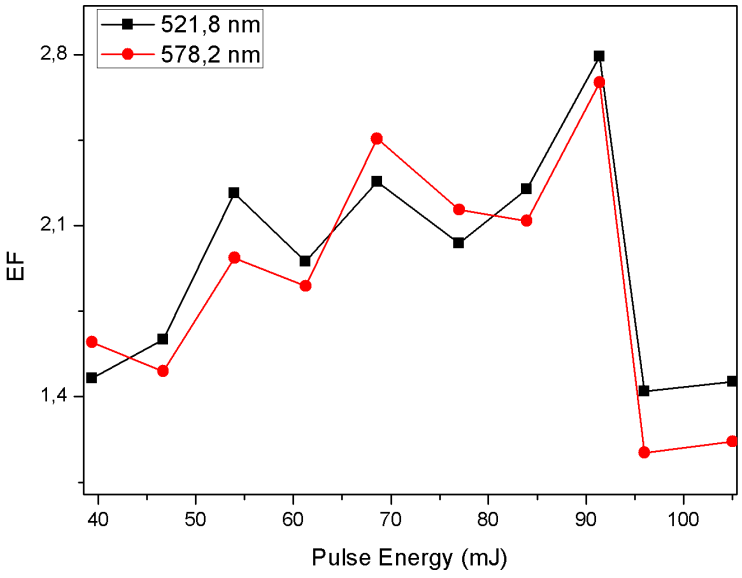

Figure 7 – EF registered for 20 nm AgNPs as a function of the laser pulse energy

It can be seen that the EF gradually increases with the pulse energy. The highest enhancement was obtained for a pulse energy of about 90 mJ and a sharp EF decrease was observed when using higher energies. This is consistent with the results presented in the works of De Giacomo [7]. In fact, if the pulse energy is increased over a threshold value, the NELIBS enhancing effects can no longer be achieved, and the AgNPs act simply as thermally conductive surface defects.

As LIBS performances are greatly affected by the sample surface characteristics, the dryness of the NP deposition in NELIBS is even more crucial for achieving a good signal enhancement. From a series of preliminary tests, it was found that a quick drying of the copper sheets at 90°C or with hot air did not yield any appreciable signal enhancement. The depositions were then analyzed after different drying times at ambient temperature (25°C) in air. The results are shown in Figure 8.

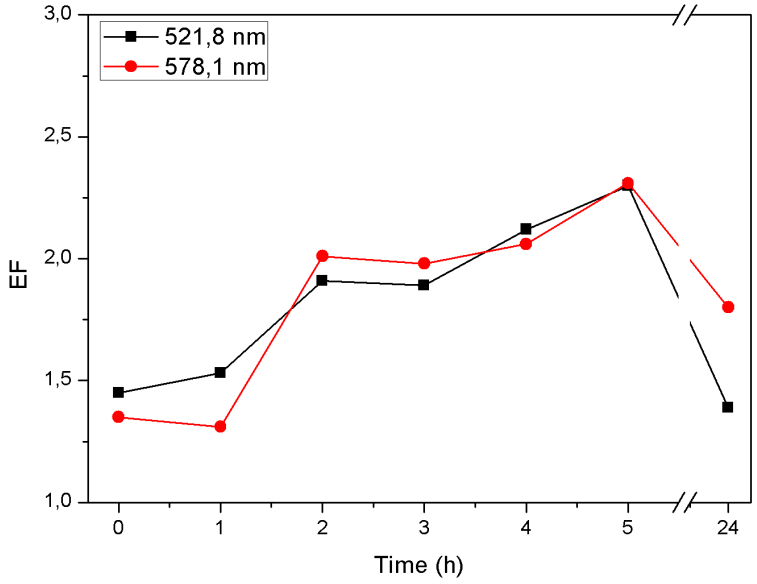

Figure 8 - EF registered for 20 nm AgNPs as a function of air-drying time

In a similar trend to the one observed for the pulse energy, the EF tends to increase with the drying time, up to a maximum at about 5 hours. After that, the EF decreases due to the oxidation of the samples, which is particularly noticeable in the near proximity of the nanoparticle deposition.

Based on these results, it was decided to use a 90 mJ pulse energy, corresponding to an irradiance of approximately $8{,}5 \times 10^{13}$ W/m^2 and 4-5 hours of air-drying for the subsequent NELIBS analyses.

2.3.3 – Green nanoparticles NELIBS

Another critical parameter in NELIBS is the surface concentration of the NP deposition on the sample and, consequently, the NPs concentration in the deposited solution. De Giacomo et al [7] described the presence of a critical concentration value for a defined NP diameter, above which a

sharp decrease in NELIBS performances occurs. This is due to the change in the inter-particle distance, which is crucial for the plasmon oscillation to take place and, in turn, for the local field enhancement that is correlated to the NELIBS signal enhancement.

In this study, a dispersion of 2,0 mg/mL NPs was prepared by suspending 20 mg of freeze-dried NPs in 10 mL of deionized water. From this solution, diluted batches of NP dispersion were prepared, namely 1:5, 1:10, 1:50 and 1:100 v/v. These dispersions had a NP concentration of 0,4 mg/mL, 0,2 mg/mL, 0,04 mg/mL and 0,02 mg/mL respectively. The samples were then prepared and analyzed with the same procedure used for the optimization step and the results are illustrated in Figure 9.

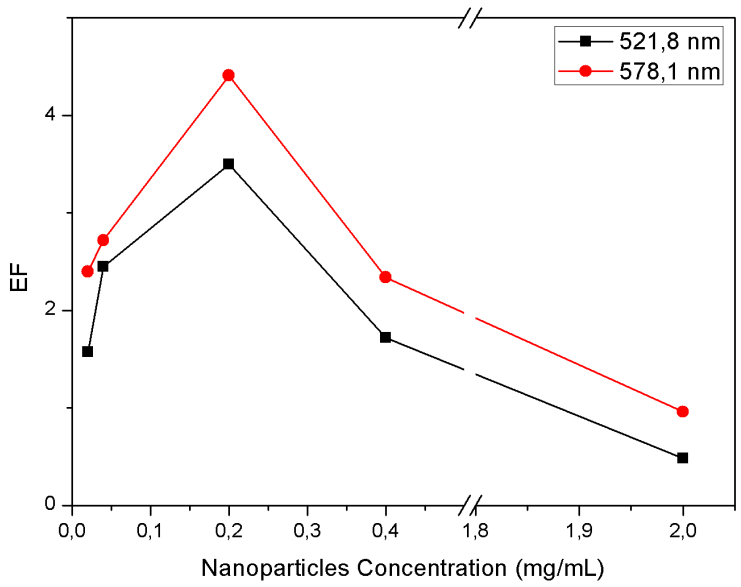

Figure 9 - "Green" nanoparticles EF as a function of the NP concentration

The highest EF was obtained with the NPs solution at 0,2 mg/mL, resulting in a calculated surface concentration of approximately 1,4 mg/cm^2. Using NP dispersions with higher concentrations resulted in much lower values of EF.

It is interesting to note how the EF registered when using the synthesized nanoparticles (with the optimal procedure and instrumental parameters) is almost two times higher than the one registered when using commercially available AgNPs.

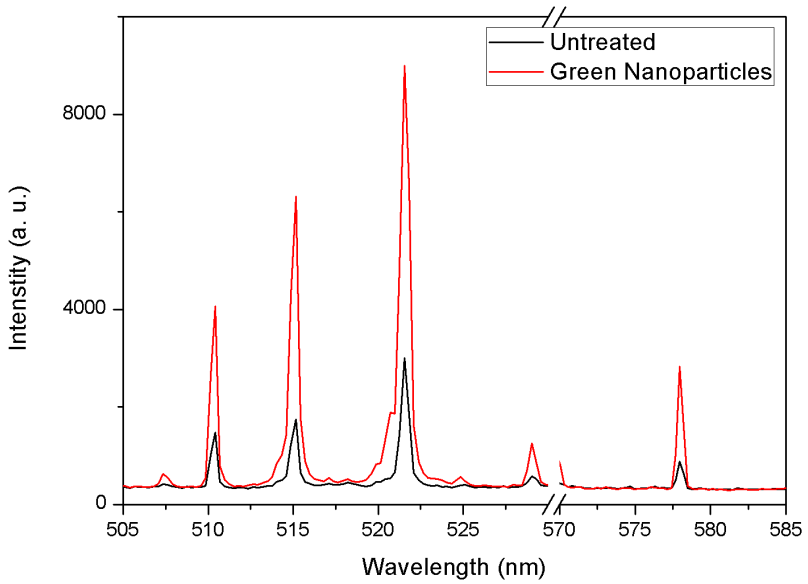

Figure 10 – Comparison between LIBS (black) and NELIBS spectra (red) obtained using 0,2 mg/mL "green" NPs, in the range showing the signal enhancement for the copper emission lines

2.3.4 – Calibration curves and LOD enhancement

In order to quantify and compare the performances of the synthesized NPs with commercially available ones, a calibration of the LIBS system was performed using copper alloy SRMs. Based on preliminary tests, it was decided to investigate the emission lines for Zn I (334,5 nm) and Cr I (359,4 nm). The concentration values for these elements are reported in Table 1.

	Zn	**Cr**
SRM 394	405 ± 15	2,0 ± 0,1
SRM 395	12,2 ± 0,7	6,0 ± 0,5
SRM 398	24 ± 1	0,30 ± 0,08
SRM 399	45 ± 3	0,5 ± 0,1

Table 1 - Concentrations (in ppm) for the investigated elements in the SRMs

Five 5 µL droplets of both 20 nm commercially available NPs and “green” NPs (0,2 mg/mL solution) were deposited on the SRM surface and allowed to dry before the analysis. Five individual spectra were recorded for each SRM and the averages of the integrated line intensities were used to build the curves in Figures 11.

NELIBS analyses show that the EF is not the same for copper and the trace elements. This is to be expected as the signal enhancement is related to the upper level energy of the observed transition [5].

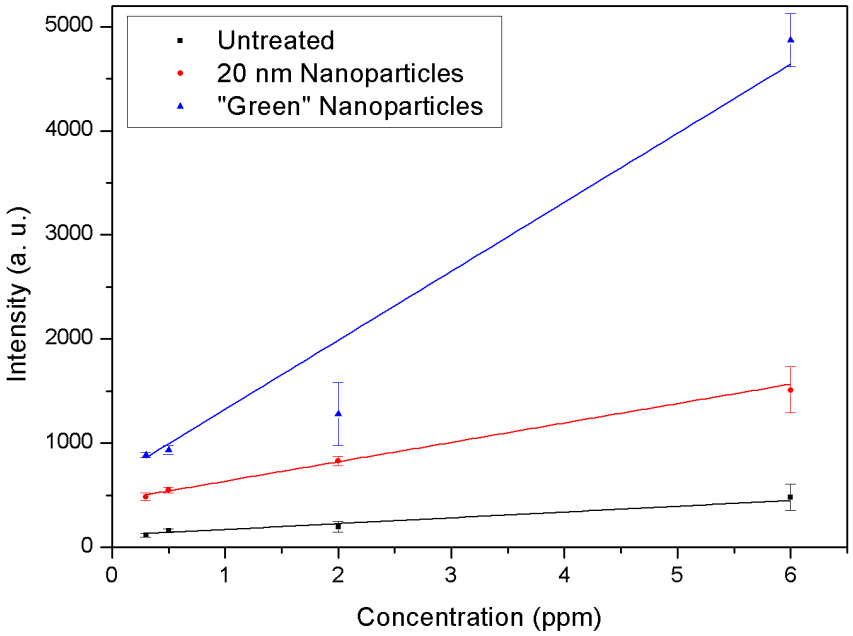

Figure 11 - Calibration curves for Cr

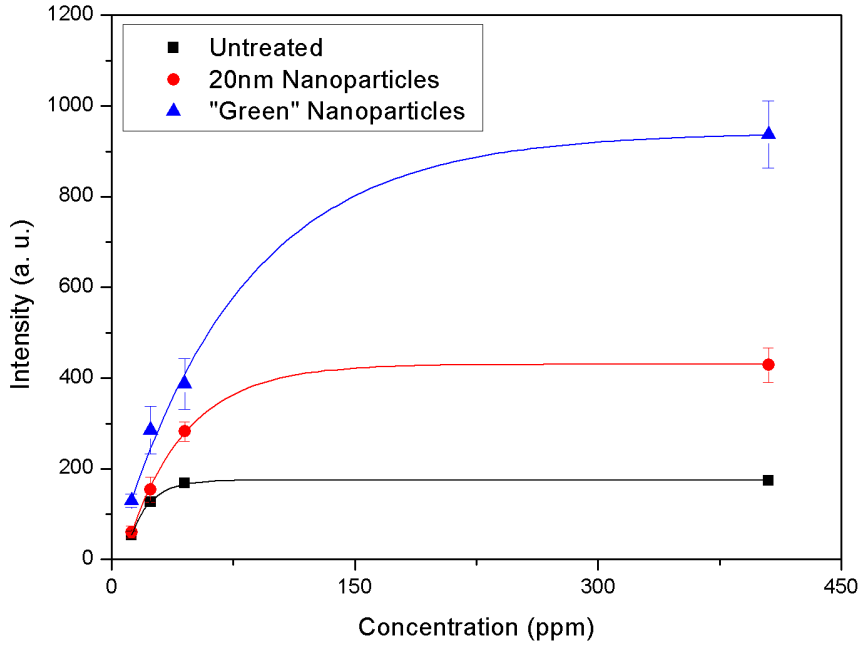

Figure 12 - Calibration curves for Zn

In Table 2 are reported the values of R^2 for each curve.

	R^2		
	Untreated	**20 nm NPs**	**Green NPs**
Zn	0,998	0,998	0,989
Cr	0,76	0,997	0,925

Table 2 - Values of R^2 for the calibration curves

It was observed how, in the case of Chromium, the use of NELIBS increased the quality of the calibration curves. Indeed, this is due to the increased signal intensity, which allows for a better signal to noise ratio and integration of the line intensity. In the case of Zinc, it was observed a marked non-linear behavior of the emission intensity for the selected line and it was decided to adopt an exponential function for the data fitting, with satisfactory results. It is necessary to point out, however, that the standard deviation values, reported in Figures 11-12, are in some cases relatively high (i.e. ≈25%). This is due in part to the surface dependent nature of LIBS and of the used instrumental setup, and in part to the not ideal nature of the SRMs which are supplied in small metal chippings. This greatly hindered the NP deposition and the focalization of the laser onto the sample's surface.

From the calibration curves, the limits of detection (LODs) that are obtainable with NELIBS were estimated. The values reported in Table 3 are obtained by using the relation $LOD \approx 3\sigma/Slope$.

	Untreated	**20 nm NPs**	**Green NPs**
Cr (ppm)	1,0	0,6	0,1

Table 3 - LODs for Cr

As expected, the LODs are lower in the case of NELIBS analyses. These values also show how, generally, the performances of the "green" NPs are comparable with those of commercially available NP solutions.

The use of an exponential fitting for Zinc meant that this kind of LOD estimation could not be applied. Even if only 3 points are not enough for an accurate estimation of the LOD, a linear fitting was implemented for the low-concentration zone of the calibration curve. The results are summarized in Table 4.

	Untreated	**20 nm NPs**	**Green NPs**
LOD (ppm)	6,4	5,9	5,3
R^2	0,64	0,998	0,91

Table 4 - LODs and R2 values for the linear fitting of Zn

2.4 – Conclusions

In this work, a simple and low-cost method for the “green synthesis” of silver nanoparticles was successfully adapted. The method allowed for the preparation of NPs of comparable morphology with commercially available ones, which were suitable for NELIBS applications.

The parameters for NELIBS analyses were also optimized and a procedure for the preparation of nanoparticle depositions on the investigated samples was established.

A signal enhancement was registered using green-synthetized NPs. Such enhancement was higher than the one obtained with commercially available NP solutions. The LODs obtainable with NELIBS were also investigated and estimated using the “green” nanoparticles. Values of ≈6 ppm for Zn and ≈0,1 ppm for Cr were found. These LODs were found to be comparable with those obtained when using commercially available AgNPs.

These results are encouraging and further studies should be carried out in order to improve the quality of the synthesized nanoparticles and obtain a more intense NELIBS signal. It is known from the literature that, in order to obtain the best enhancements in NELIBS (up to 2 orders of magnitude), the use of a laser capable of investigating a much larger area while maintaining a sufficiently high power density is necessary, as the entire NP deposition should be ablated during the laser pulse [8]. Nevertheless, the successful application of NELIBS to a mobile, relatively low-power LIBS system is an interesting result as it demonstrates the versatility of the NELIBS method, and could be a starting point for further optimization towards in-situ NELIBS applications.

Bibliography

[1] S. Musazzi e U. Perini, Laser Induced Breakdown Spectroscopy: Theory and Application, Heidelberg: Springer, 2014.

[2] D. A. Cremers e L. J. Radziemski, Handbook of Laser-Induced Breakdown Spectroscopy, John Wiley and Sons, Ltd., 2006.

[3] W. Miziolek, V. Palleschi e I. Schechter, Laser-induced breakdown spectroscopy (LIBS): Fundamentals and applications, Cambridge : Cambridge University Press, 2006.

[4] S. C. Jantzi, V. Motto-Ros, F. Trichard, Y. Markushin, N. Melikechi e A. De Giacomo, «Sample treatment and preparation for laser-induced breakdown spectroscopy,» *Spectrochimica Acta Part B: Atomic Spectroscopy,* vol. 115, pp. 52-63, 2016.

[5] A. De Giacomo, R. Gaudiuso, C. Koral, M. Dell'Aglio e O. De Pascale, «Nanoparticle Enhanced Laser Induced Breakdown Spectroscopy: Effect of nanoparticles deposited on sample surface on laser ablation and plasma emission,» *Spectrochimica Acta Part B: Atomic Spectroscopy,* vol. 98, pp. 19-27, 2014.

[6] A. De Giacomo, R. Gaudiuso, C. Koral, Dell'Aglio e O. De Pascale, «Nanoparticle-Enhanced Laser-Induced Breakdown Spectroscopy of Metallic Samples,» *Analytical Chemistry,* vol. 85, pp. 10180-10187, 2013.

[7] A. De Giacomo, R. Gaudiuso, C. Koral, M. Dell'Aglio e G. Valenza, «Perspective on the use of nanoparticles to improve LIBS analytical performance: nanoparticle enhanced laser induced breakdown spectroscopy (NELIBS),» *Journal of Analytical Atomic Spectrometry,* vol. 31, pp. 1566-1573, 2016.

[8] A. De Giacomo, R. Gaudiuso, C. Koral, M. Dell'Aglio e G. Valenza, «Nanoparticle Enhanced Laser-Induced Breakdown Spectroscopy for Microdrop Analysis at subppm Level,» *Analytical Chemistry,* vol. 88, n. 10, pp. 5251-5257, 2016.

[9] M. Dell'Aglio, R. Alrifai e A. De Giacomo, «Nanoparticle Enhanced Laser Induced Breakdown Spectroscopy (NELIBS), a first review,» *Spectrochimica Acta Part B: Atomic Spectroscopy,* vol. 148, pp. 105-112, 2018.

[10] Z. Salajkova, V. Gardette, J. Kaizer, M. Dell'Aglio e A. De Giacomo, «Effect of spherical gold nanoparticles size on nanoparticle enhanced laser induced breakdown spectroscopy,» *Spectrochimica Acta Part B: Atomic Spectroscopy,* vol. 179, p. 106105, 2021.

[11] A. De Giacomo, R. Alrifai, V. Gardette, Z. Salajkova e M. Dell'Aglio, «Nanoparticle enhanced laser ablation and consequent effects on laser induced plasma optical emission,» *Spectrochimica Acta Part B: Atomic Spectroscopy,* vol. 166, p. 105794, 2020.

[12] C. Koral, M. Dell'Aglio, R. Gaudiuso, R. Alrifai, M. Torelli e A. De Giacomo, «Nanoparticle-Enhanced Laser Induced Breakdown Spectroscopy for the noninvasive analysis of transparent samples and gemstones,» *Talanta,* vol. 182, pp. 253-258, 2018.

[13] C. Koral, A. De Giacomo, X. Mao, V. Zorba e R. E. Russo, «Nanoparticle Enhanced Laser Induced Breakdown Spectroscopy for improving the detection of molecular bands,» *Spectrochimica Acta Part B: Atomic Spectroscopy,* vol. 125, pp. 11-17, 2016.

[14] A. Bertolini, G. Carelli, F. Francesconi, M. Francesconi, L. Marchesini, P. Marsili, F. Sorrentino, G. Cristoforetti, S. Legnaioli, V. Palleschi, L. Pardini, V. Palleschi e A. Salvetti, «Modi: a new mobile instrument for in situ double-pulse LIBS analysis,» *Analytical and Bioanalytical Chemistry,* vol. 385, p. 240–247, 2006.

[15] V. Dhand, L. Soumya, S. Bharadwaj, S. Chakra, D. Bhatt e B. Sreedhar, «Green synthesis of silver nanoparticles using Coffea Arabica seed extract and its antibacterial activity,» *Materials Science and Engineering C,* vol. 58, pp. 36-43, 2016.

[16] D. Paramelle, A. Sadovoy, S. Gorelik, P. Free, J. Hobley e D. G. Fernig, «A rapid method to estimate the concentration of citrate capped silver nanoparticles from UV-visible light spectra,» *Analyst,* vol. 139, pp. 4855-4861, 2014.

Chapter 3:

Pulsed Laser Ablation in Liquids (PLAL) System Setup

Chapter 3 - Index

3 – Pulsed Laser Ablation in Liquids (PLAL) System Setup

One of the main criticalities for NELIBS is the quality and availability of noble metal nanoparticles (NPs) that are suitable for the analysis. In Chapter 2 it was demonstrated how Green-synthesized NPs can be used successfully for NELIBS, although the results did not reach the optimal signal enhancement values reported in literature. In order to improve the results obtainable with NELIBS it was decided investigate a methodology that would allow for a faster synthesis of NPs, as well as improving their quality.

In this Chapter, the Pulsed Laser Ablation in Liquid (PLAL) technique will be presented, as it was chosen for the preparation of NPs. Moreover, an overview of the steps that were necessary to adapt the available LIBS system for the PLAL technique will be given, as well as the optimization procedure that was conducted to reliably obtain AgNPs that are suitable for NELIBS and other analytical applications.

3.1 – Introduction to the PLAL technique

Due to the growing interest in metallic nanostructures (and especially nanoparticles) for catalysis, biomedical application, nano-electronics and nano-optics, many methods have been proposed for their synthesis. Among these, PLAL holds several advantages, such as environmental friendliness, simple instrumental setup, purity and stability of the produced NPs [1]. Several studies have been focused on increasing the yield of the NPs, as well as to refine their size distribution during the preparation [2] [3]. A thorough discussion on PLAL has been the subject of a number of publications [4] [5] and is out of the scope of this work. Nevertheless, it is worth to mention briefly some of the processes that are involved during PLAL.

The general procedure for the synthesis of nanoparticles using PLAL is fairly straightforward. In brief, a target of the required material (generally a metal or an alloy) is immersed in a liquid, either pure or containing a stabilizing and capping agent like a salt or a polymer. A pulsed laser is then used to ablate the target inside the liquid to generate the nanoparticles. A schematic representation of a PLAL setup can be observed in Figure 1.

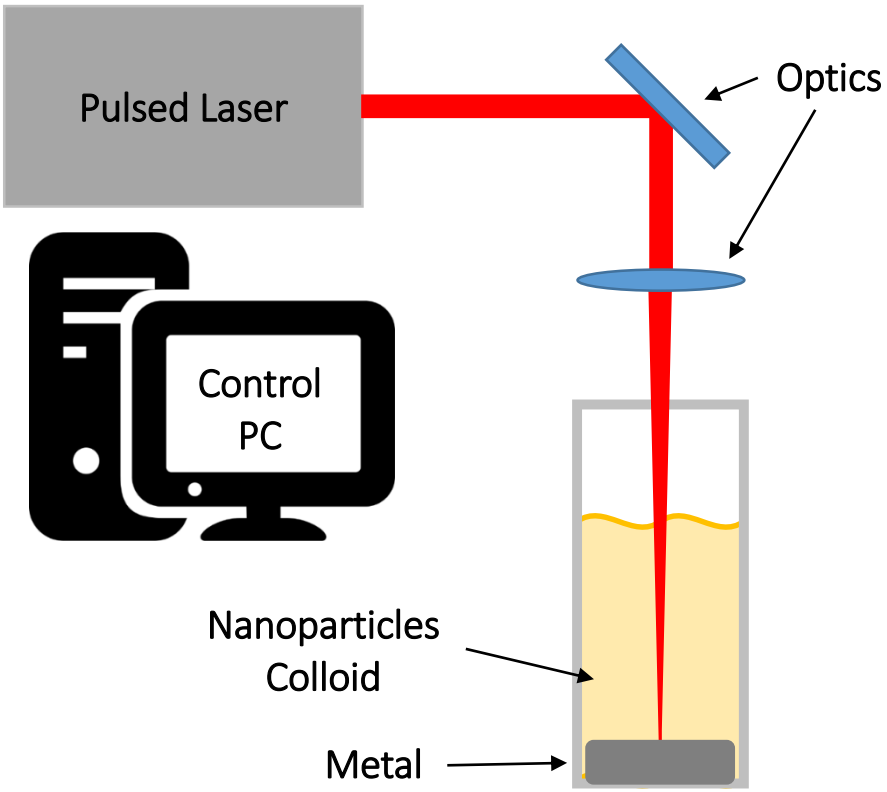

Figure 1 - Schematic representation of a PLAL setup

During the laser irradiation of the target, seed electrons are ejected and, by inverse Bremsstrahlung, the ablated particles give rise to a hot plasma. Due to the incompressibility of the liquid, the plasma is confined and maintains a high degree of ionization and a high density. The plasma then cools down gradually, with a process where most of the ablated mass undergoes phenomena that lead to the formation of NPs. Since the cooling happens under constant thermodynamic conditions, the nanoparticles are generated with similar sizes and shapes, dependent on the experimental conditions [6], by both condensation/evaporation and electrostatic mechanisms [7]. The production of the nanoparticles occurs very rapidly, due to the high thermal capacity of the liquid itself [8] [9], even if immediately after the laser pulse, the plasma conditions do not allow for the formation of the NPs.

While most PLAL applications are based on a batch process (i.e. the metal target is immersed in a fixed volume of liquid) [10] [11] [12] [13], a number of studies have explored the possibility of using a continuous method to increase the volumes of NPs that can be produced without the need to manipulate the instrumentation [14] [15]. Similarly, the use of multiple laser pulses (i.e. Double Pulse laser ablation, see Chapter 1) for PLAL has been investigated [16] [17].

3.2 – PLAL methodology and instrumental configuration

As illustrated in the previous section, the PLAL method of nanoparticle synthesis can be implemented using either a batch or a continuous approach. In this study, the continuous approach

was briefly considered but ultimately not chosen. In fact, the added complexity required for the instrumental setup (i.e. a pumping and solvent circulating apparatus, as well as a continuous-flow chamber where the ablation would take place) does not offer any significant advantage for the selected NELIBS applications. Indeed, a continuous-flow system would allow for the production of larger volumes of AgNP solutions, but only a few hundred µL are generally required for a NELIBS measurement session. A batch PLAL apparatus is also much faster to set up, and it generally requires only the preparation of the sample cuvette and the re-adjustment of the laser focus.

The configuration of the LIBS setup at the beginning of this study is illustrated in Figure 2.

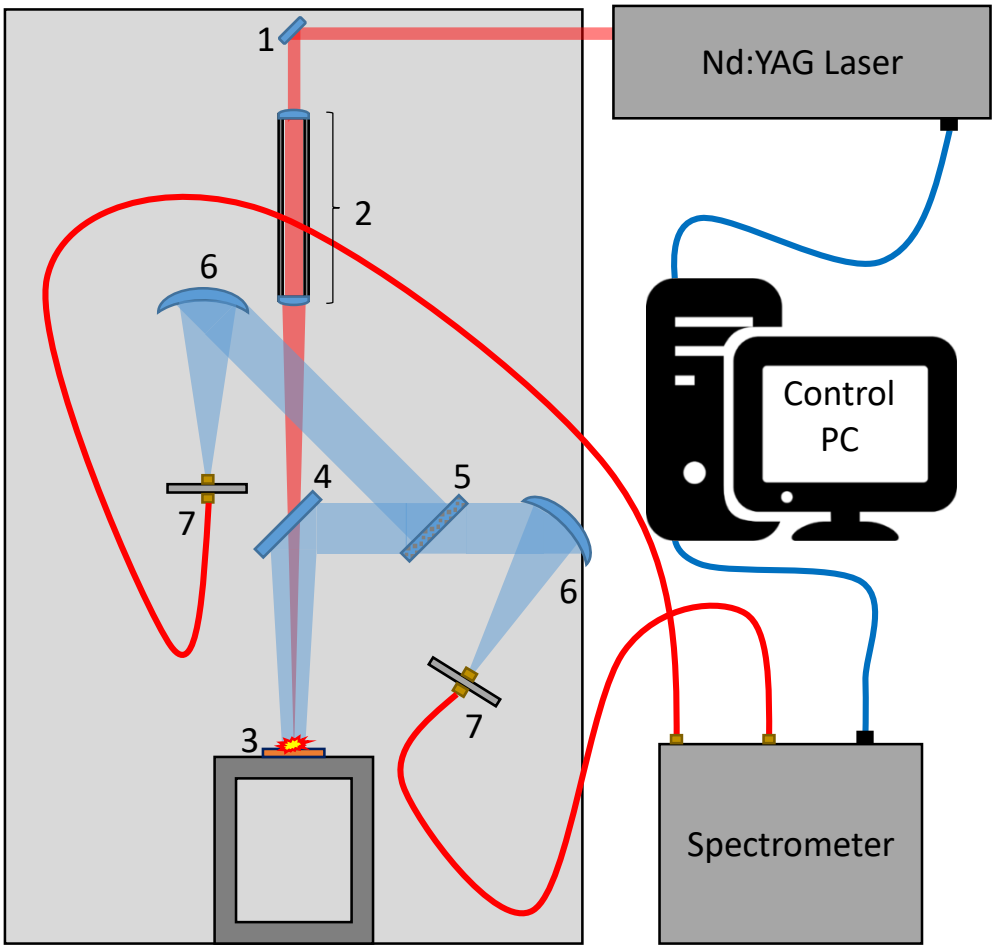

Figure 2 - Initial configuration of the LIBS system

The system used a solid state, double pulse Nd:YAG laser (LS-2134D, Lotis) operating at the fundamental wavelength of 1064 nm, and a two-channel Czerny-Turner spectrometer (AvaSpec LS2048CL-2-EVO, Avantes). The fairly complex arrangement of optics and mirrors was composed of:

1- Primary mirror for redirecting the laser beam
2- 300 mm beam expander
3- Fixed sample holder at the focal point of the beam expander output lens (f= 600 mm)

4- Primary light collection mirror. This mirror was axially mounted to the optical path of the laser and is custom-made with a central hole to allow passage of the LIBS pulse
5- “Polka Dot” splitter mirror. This custom-made mirror can split the plasma light, redirecting part of it (30%/70%) towards one of the collection points
6- Parabolic mirrors
7- Optical fiber holders and fiber heads

Initially, the system was designed ad-hoc as a prototype for the on-line analysis of coal and ash samples inside of a coal-fired power station. As such, it was built to satisfy a certain set of requirements, namely sturdiness, safety, ease of use and an all-in-one configuration. In particular, the optical setup was given a long focal plane, as it was designed to allow for the analysis of samples of variable geometry without the need for focus adjustment. Similarly, the light collection geometry aimed at maximizing the area from which the plasma emission was collected.

From an initial set of tests, it was found that this configuration was not ideal for this study. The focal length of the system made it difficult to properly position small samples, as was the case with NELIBS measurements and for PLAL applications. The complex arrangement of mirrors and lenses, while ideal for the original scope, was suboptimal for research purposes, and required fine tuning and thorough cleaning to maintain the required level of performance. Finally, the spectrometer was found to be lacking in both the spectral and temporal resolution that was required for subsequent studies. As such, part of the research work was dedicated to the reconfiguration and optimization of this instrumentation.

The first step was the simplification of the entire LIBS system, converting it from its prototype configuration into a more conventional laboratory setup. As such, the beam expander section was removed and a plano-convex lens with a focal length of 100 mm was installed. The configuration of the sample holder was also changed to accommodate support blocks of various dimensions, which can be easily swapped according to the analyzed sample. Each block is marked and their installation is guided by a rail system to guarantee maximum reproducibility of each measurement. To compensate for the variable sample position, the focusing lens was mounted on variable height support, which allows for the fine adjustment of the laser focus. Finally, three different configurations for the light collection system were tested, schematized in Figures 3-5.

The first configuration utilized the same parabolic mirrors that were included in the original system, re-configured for the new sample and laser positions. Ideally, this configuration would allow for the collection of the entire image of the plasma plume, compensating for any variation in the plasma morphology between different measurements.

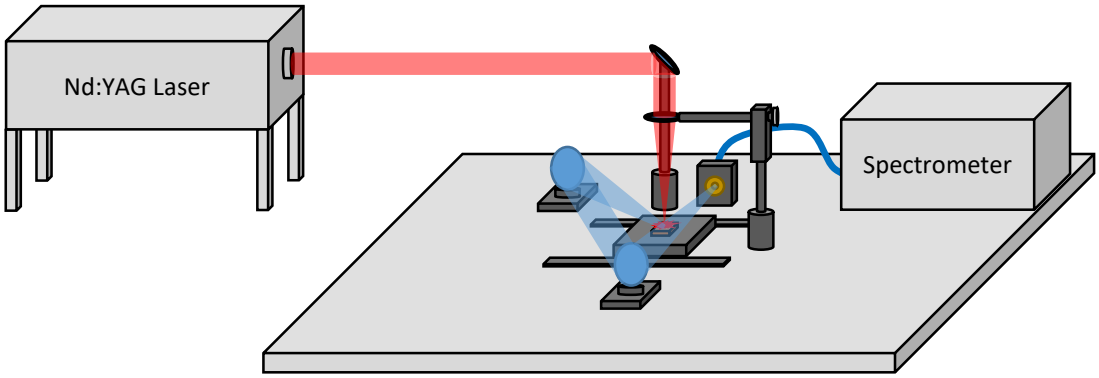

Figure 3 - LIBS configuration using two parabolic mirrors

In practice, it was found that this configuration was the most problematic, although the spectra registered from preliminary tests were satisfactory. To obtain the optimal alignment of the parabolic mirrors, they had to be placed at a distance from the sample and from each other (approximately 350 cm) that greatly affected the repeatability of the measurements. In fact, even small discrepancies in the laser beam path or in the position of the sample had serious effects on the amount of plasma emission that was collected by the mirrors. Moreover, the large area occupied by the setup and the complex optical path of the plasma emission rendered the manipulation and preparation of the samples much more difficult than anticipated.

The second setup that was tested used two plano-convex lenses, arranged in a telescope configuration placed at 45° relative to the incident laser beam. The telescope arrangement was mounted on two translational stages, which allowed for the fine tuning of its X-Y position. The height was fixed, according to the focal length of the lenses. The light collection lens had a focal length of 45 mm, and the focusing lens had a focal length of 30 mm. The fiber head holder is mounted on the telescope tube, fixed in place at the appropriate distance from the focusing lens. The 45° inclination of the optical arrangement was chosen over a more conventional 90° orientation (i.e. when the light collection axis is perpendicular to the incident laser beam) to allow for the collection of the entire plasma emission. While this slightly increased the complexity of the system, it compensated for changes in the morphology of the plasma plume, which could cause unwanted variations in the registered spectra for an orthogonal configuration.

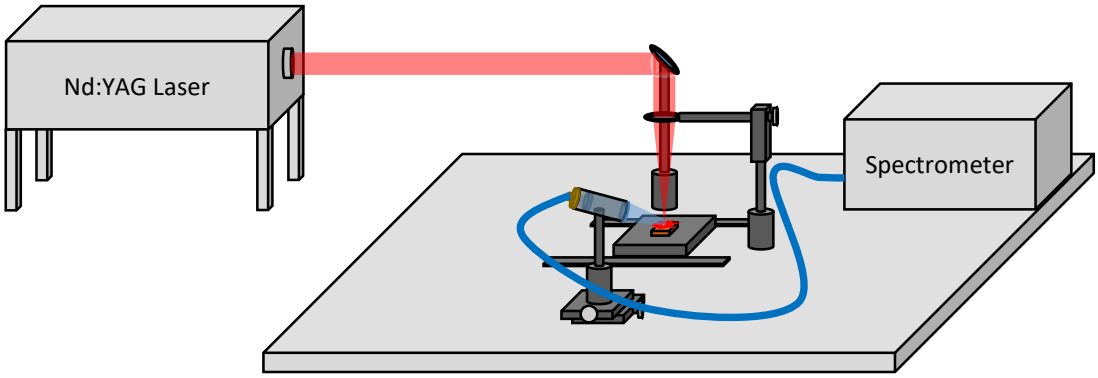

Figure 4 - LIBS configuration using a telescope system

The results obtained with this configuration were significantly improved over the ones observed using the first setup. Both the absolute intensity and signal to noise ratio of the registered spectra were increased, and the time required for the focusing operation was greatly reduced. Indeed, when using samples of different geometries, only slight adjustments of the telescope's position were required, and the space required by this configuration was extremely compact.

Lastly, a far simpler solution for the optical arrangement was tested. In this configuration, the light is collected directly by the head of an optical fiber and transferred to the spectrometer. The fiber head was placed at an angle of 45° with respect to the incident laser beam and at a distance of approximately 2 cm from the sample. The distance was chosen so that the entire image of the plasma plume was gathered by the optical fiber, according to the acceptance angle of the fiber itself. The fiber holder was again mounted on two translational stages, and its height was adjusted manually.

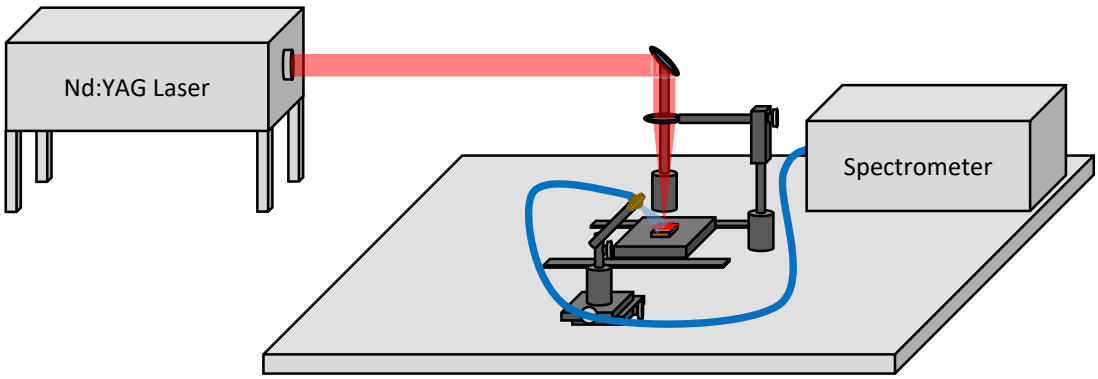

Figure 5 - LIBS configuration using the fiber head as a direct light collection system

A set of preliminary measurements showed that this approach, like in the case of the telescope arrangement, allowed for the obtainment of good LIBS spectra. Indeed, the use of an unfocused acquisition of the plasma light caused these spectra to have a slightly lower signal to noise ratio, but the loss in spectral quality was deemed acceptable in light of the advantages this configuration provided. This configuration was found to be the most compact and easy to set up, and the

alignment procedure required a very short time (i.e. about 10 minutes, compared to about 1 hour for the telescope arrangement). Moreover, the fiber could be quickly removed, for calibrating the spectrometer or to manipulate the sample and sample holders, and reinstalled without the need for further re-alignment.

Subsequent studies were all performed using the fiber optic head as the light collection system, as it was proven to be the easiest and quickest method for collecting the plasma emission, without compromising the spectral quality.

To further increase the performances of the LIBS system, the original spectrometer was removed and an Echelle spectrometer was coupled to the system. The new spectrometer is an Aryelle 200 (LTB Lasertechnick Berlin) Echelle spectrograph, with a spectral range of 590 nm (200 nm to 790 nm). It is coupled with an air-cooled ICCD (iStar DH334T-18F03, Andor), which gives the setup a resolving power of 9000. The spectrometer was calibrated before each measurement session using a Deuterium-Hg lamp (Ocean Optics).

Finally, the re-configured LIBS system was used for the production of metallic nanoparticles using PLAL, and its performances were evaluated. A scheme of the PLAL setup used in this work is reported in Figure 6.

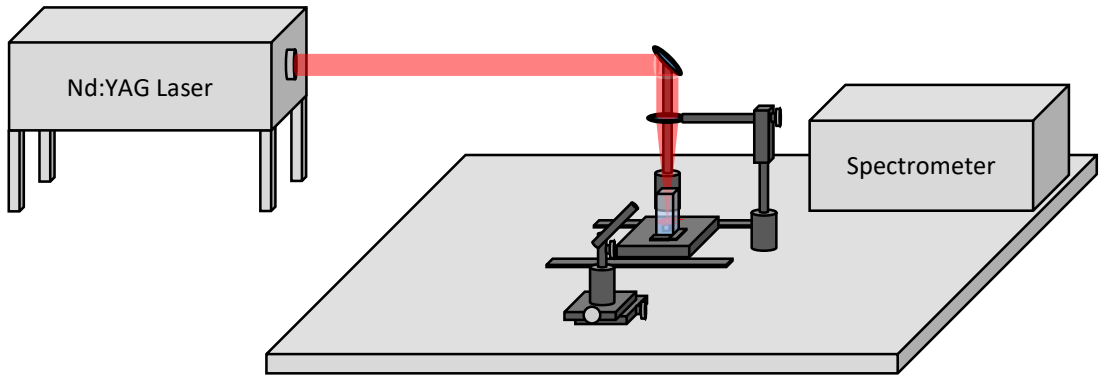

Figure 6 – PLAL system configuration

Briefly, the sample holder was removed and replaced with a holder for a UV-Vis PET cuvette (3 mL volume). The fiber optic was also removed, to prevent damage and possible contamination during the nanoparticle production process. The laser focusing lens was adjusted to compensate for the shift in the focal point due to the presence of the liquid medium.

Using the described PLAL setup, Silver nanoparticles (AgNPs) were produced throughout the study, thanks to the ready availability of high-purity Ag (Silver foil, 2,0 mm thickness, 99,9% trace metal basis, Sigma-Aldrich), as well as to their stability and NELIBS effectiveness. Au and Cu NPs were also prepared for a comparison but the results were not satisfactory. In particular, CuNPs were observed to be fairly unstable, giving rise to a precipitate and large aggregates minutes after their

preparation. Moreover, as most NELIBS samples used in these studies are copper-based, the use of CuNPs would interfere with the analytical results. The AuNPs, on the other hand, were very stable, but the purity of the gold PLAL target was not sufficient to ensure the monometallic nature of the nanoparticles (i.e. the obtained NPs were not pure gold but an alloy of uncertain composition).

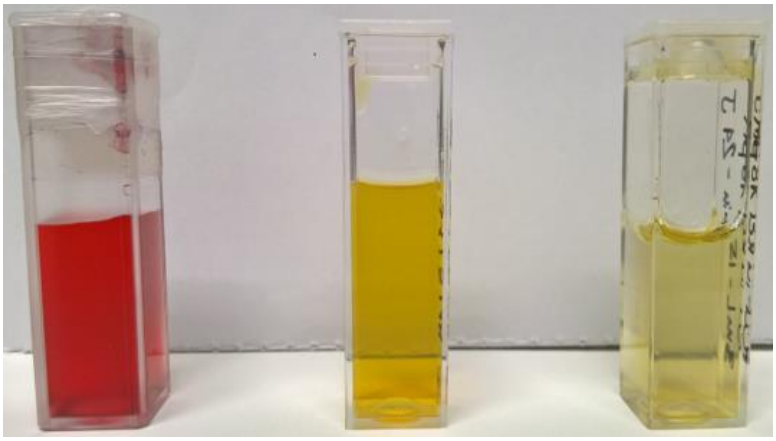

Figure 7 - From the left: Au nanoparticles, Ag nanoparticles and Cu nanoparticles

Various tests were conducted using the fundamental laser wavelength of 1064 nm or the first harmonic of the Nd:YAG laser at 532 nm to determine whether the best nanoparticles were obtained, in terms of stability of the solution and homogeneity in the dimensions [18]. No significant difference was found between the NP batches, both in their average dimensions or stability. The implementation of the second harmonic generator required a fairly extensive modification of the laser apparatus, namely the installation of a non-linear crystal in the laser beam path, the substitution of the lenses and mirrors and the re-focalization and collimation of the system. Moreover, doubling the frequency of the laser light also implies a significant loss in overall energy, putting additional strain on the system. Because of this, it was chosen to use the fundamental wavelength for the production of subsequent batches of AgNPs.

The laser beam was focused just below the surface of the metal target, after compensating for any focal shift due to the presence of the solvent. Subsequently, the pulse energy was increased until a reliable and repeatable plasma was formed on the target surface. This value was found to be about 100 mJ. While higher energy values could lead to a faster production of the AgNPs, two main issues can be encountered. Firstly, highly energetic laser pulses increase the dimensions of the cavitation bubble generated alongside the plasma. As the larger bubble collapses, the liquid violently rebounds, spraying droplets out of the cuvette and towards the focusing lenses. Secondly, if the laser pulse is too energetic, a laser-supported detonation regime can be reached, and a fraction of the metal target can be ejected into the liquid as large, irregular fragments. While some

of these could be ablated by the subsequent laser pulses, they inevitably lead to a lower quality and stability of the AgNP dispersion.

In this study, the average diameter and the concentration of the nanoparticles was estimated using the procedure and the data provided in the work by Paramelle and co-workers [19]. In brief, the absorbance of a suitably diluted aliquot of the AgNP dispersion was measured using an UV-Vis spectrometer, and the concentration was estimated using the Lambert-Beer relation and the molar extinction coefficients reported in literature. Similarly, the average dimension of the nanoparticles was estimated from the λ corresponding to maximum absorbance value.

The two stabilizing and capping agents most common in the PLAL preparation of silver nanoparticles are Potassium Chloride (KCl) and Sodium Citrate. Each one of these agents has its own advantages and limitations. For example, Citrate-capped AgNPs exhibit exceptional stability, provided they are stored in the dark and at low temperature (around 4°C). Similarly, KCl-capped AgNPs are also fairly stable but generally do not require special storing conditions. As it can be seen from Figure 8, a quick test using a 2 mM Sodium Citrate solution as a stabilizing agent [12] allowed for the preparation of a good AgNP batch. The metal target was ablated for approximately 4 minutes and the AgNPs were estimated to have a diameter of 11 nm and a concentration of 0,01 mg/mL.

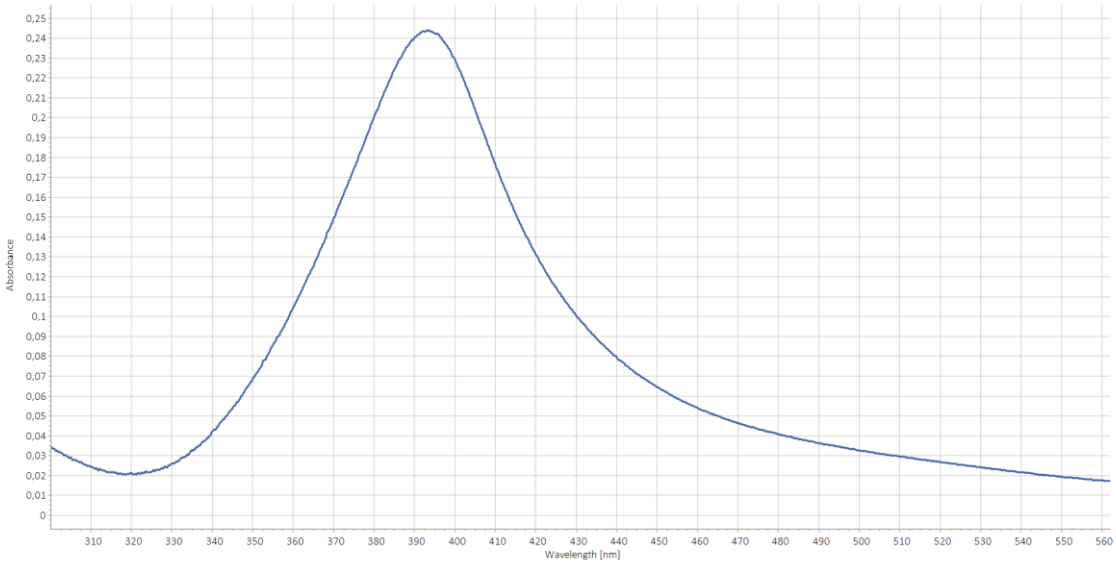

Figure 8 - UV-Vis spectra of Citrate Capped AgNPs

One of the issues that Citrate can cause in LIBS and NELIBS is due to its organic nature. The presence of an organic coating on the AgNPs can negatively affect the plasmon resonance phenomena that occur during NELIBS. It should also be noted that a fraction of the energy of the laser pulse would be expended for the atomization and vaporization of the organic matter, lowering the energy that interacts with the sample and the nanoparticles. Moreover, KCl is much easier to obtain with the

degree of purity required by the analysis of trace metals. Based on these considerations, it was chosen to use KCl as a stabilizing agent.

In Table 1 are reported the results of various batches of AgNPs prepared with different concentrations of KCl. Each dispersion was prepared by a 4 min ablation of the Ag target immersed in 2 mL of the corresponding KCl solution.

KCl Concentration (mM)	AgNP Diameter (nm)	AgNP Concentration (mg/mL)
2	11	0,014
10	11	0,016
50	>50	0,001
100	>90	0,003

Table 1 - Results for the AgNP dispersions prepared with different KCl concentrations

It was observed that, with increasing concentration of KCl, the laser pulse did not reach the metal target, or produced an irregular plasma spark. No correction on the focusing lens position allowed for the correction of this behavior. Nevertheless, high concentration of the stabilizing agent should be avoided whenever possible. Even if the emission lines arising from the added K onto the samples do not compromise the quality of the spectra, any contamination (when present) would be significantly enhanced by the NELIBS effects. As such, a KCl concentration of 2 mM was chosen for the preparation of the AgNPs.

While different stabilizing agents can influence the size (and in a limited way, the shape) of the produced nanoparticles, the ablation time is mainly correlated to the AgNP concentration of the dispersions. Indeed, this parameter can be adjusted depending on the requirements of the study, and there is generally not an optimal ablation time. Nevertheless, it was found that if the PLAL process is allowed to continue for longer periods of time, the sizes of the nanoparticles tend to converge to their average value [18], as the larger structure can be further ablated by the incident laser pulse. On the other hand, once a sufficiently high concentration of AgNPs is reached, the laser light is absorbed and scattered up to the point where each pulse reaches the metallic target with increasing difficulty. In Figure 9, the concentration of different batches of AgNPs are reported as a function of the PLAL ablation time, as well as the average diameter estimated for the nanoparticles.

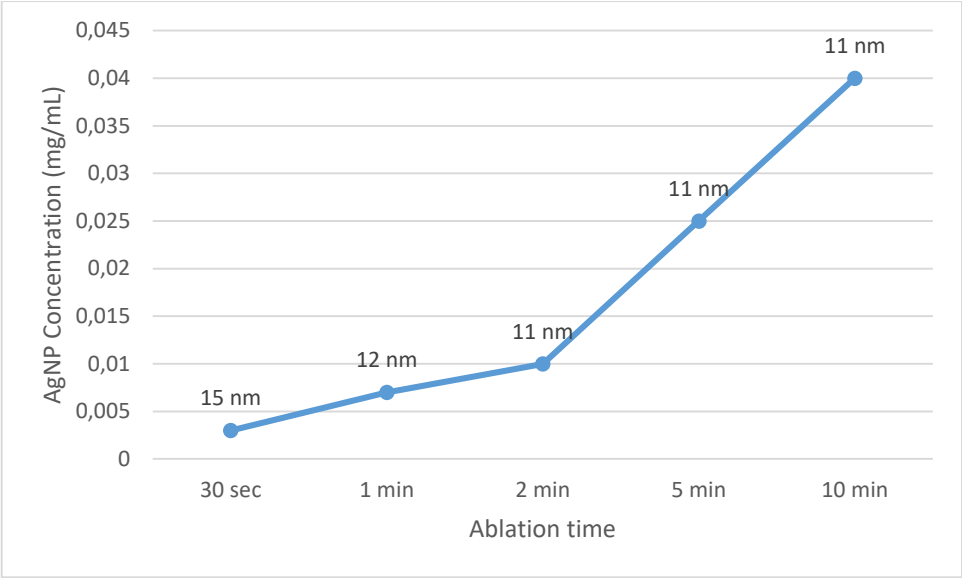

Figure 9 - AgNP concentration as a function of the ablation time. The average AgNP diameter is also reported

For this study, an ablation time of 5 minutes was chosen, which corresponds to a AgNP concentration of approximately 0,02 mg/mL. This concentration, which is comparable to that of commercially available AgNP dispersions, was found to be ideal for NELIBS applications, and no further dilution was necessary. Moreover, it was found that the prepared AgNPs with this concentration remain stable for long periods of time (i.e. over a month) without the need of carefully controlled storage conditions. Table 2 shows the data for the same batch of AgNPs, measured when they were prepared and after 2 months of storage in a glass vial wrapped in aluminum foil, at room temperature (≈21°C).

Date	AgNP Diameter (nm)	AgNP Concentration (mg/mL)
May	11	0,03
July	12	0,027

Table 2 – Data of AgNP dispersions after 2 months of storage

Additionally, in the last part of this research work, this setup was successfully used (with minimal adjustments) for the preparation of Graphene nanosheets (GNS) using the laser ablation of an aqueous graphite dispersion. The detailed procedure and results are discussed in Chapter 5 of this manuscript.

3.3 – PLAL-produced AgNPs for SERS applications

In addition to their use for all subsequent NELIBS tests, the silver nanoparticles prepared using the PLAL methodology developed and optimized in this study were successfully used for Surface Enhanced Raman Spectroscopy (SERS) applications. In this work [20], AgNPs prepared by PLAL were employed for the detection of anthraquinone dyes in textiles.

A comparison of the Raman spectra of the PLAL AgNPs and a more conventional Ag colloid prepared using sodium citrate as a reductant for $AgNO_3$ (Lee-Meisel method, see Ref. [21]), showed that a cleaner spectrum in the case of the PLAL colloid, as reported in Figure 10.

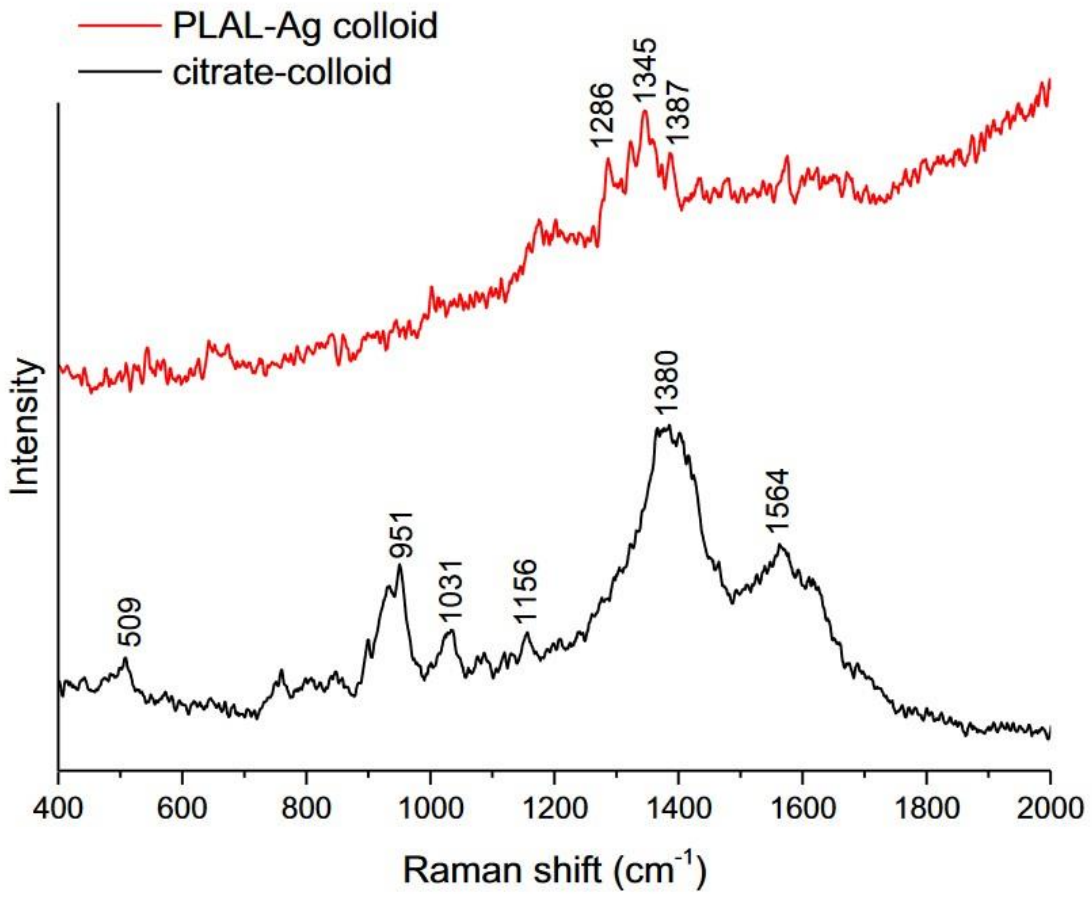

Figure 10 – Normalized SERS spectra of Ag films obtained from citrate colloid (black) and concentrated PLAL-Ag colloid (red). Figure from [20]

The PLAL nanoparticles also show a higher stability than the citrate-reduced ones, as mentioned in the previous sections, since they can be stored at room temperature and are relatively resilient towards light-induced degradation. Moreover, a comparison of SERS signals obtained from the deposition of 10^{-4} M alizarin on citrate and PLAL AgNPs, showed that the spectra are perfectly comparable both in terms of position of the peaks and the signal-to-noise ratio, as reported in Figure 11.

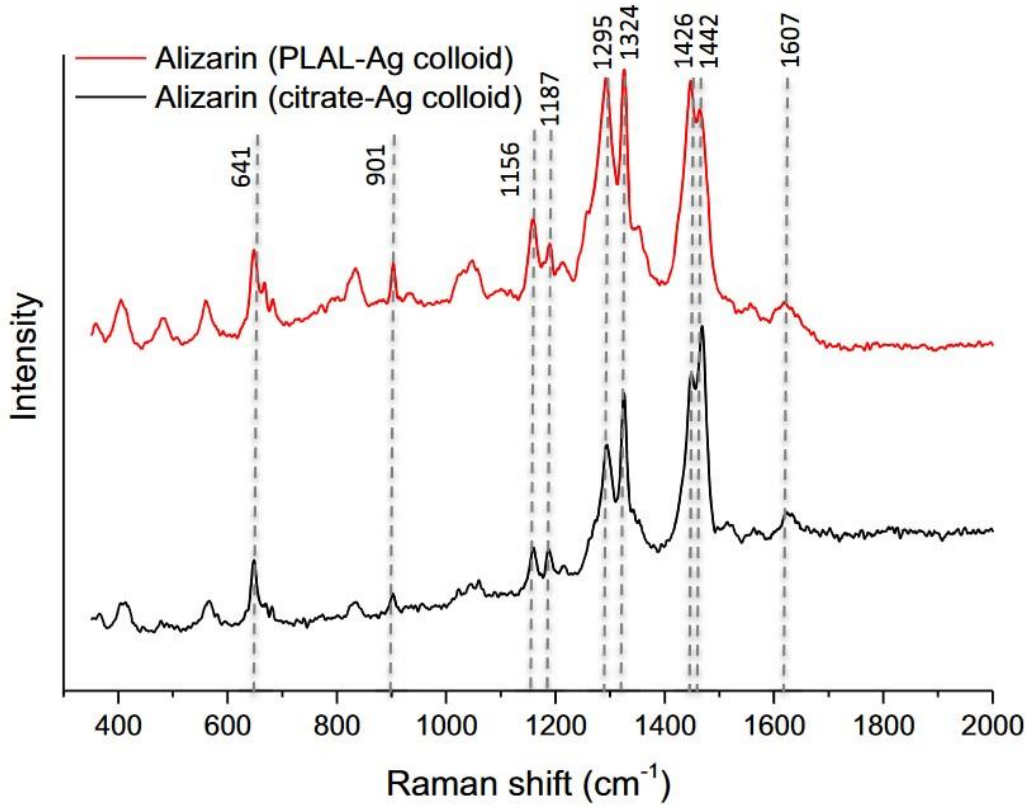

Figure 11 - Comparison of normalized SERS spectra of alizarin obtained with concentrated PLAL-Ag colloid (red) and citrate colloid (black). Figure from [20]

For the SERS measurements, 5 µL of the colloidal Ag solution were deposited on a microscope glass slide with a micropipette and dried using a jet of hot air. This process was repeated six times in order to obtain a highly concentrated deposition of nanoparticles. The fiber sample was then fixed to the glass side with adhesive tape and gently rubbed with the dried PLAL-Ag colloid. The method proved its efficiency in the analysis of anthraquinone dyed fibers having different nature, thanks to the suppression of the Raman fluorescence and the obtainment of clear peaks from the various samples, as shown in Figure 12.

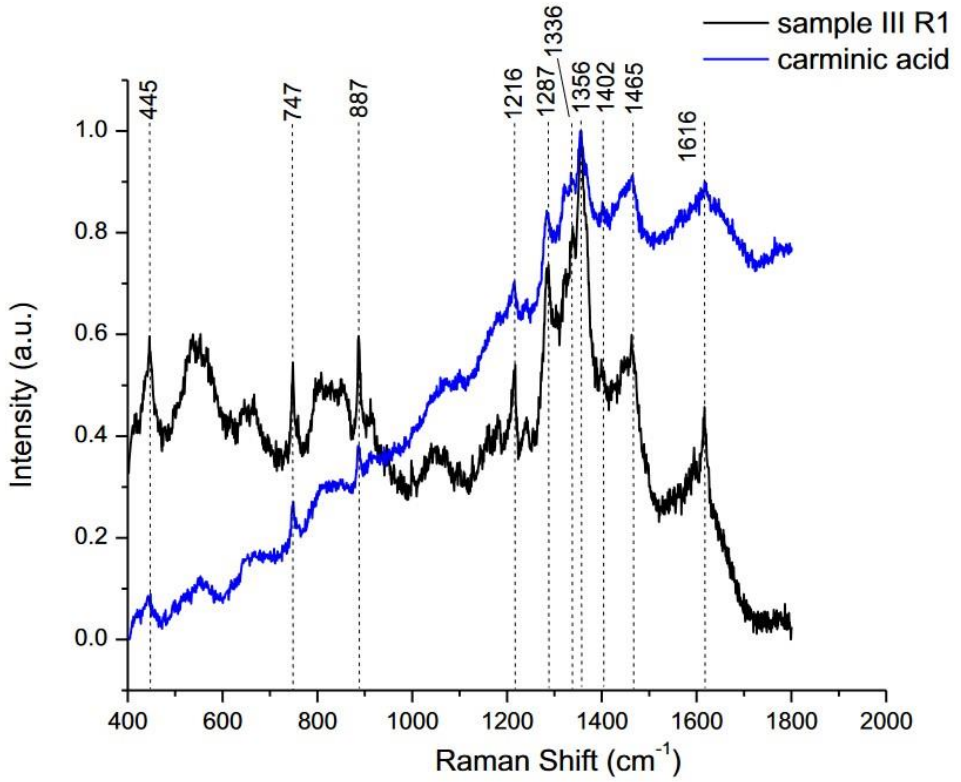

Figure 12 - SERS spectrum recorded with concentrated PLAL-Ag colloid, obtained from a silk sample dyed with cochineal (Reprinted from [20])

Bibliography

[1] V. Amendola e M. Menghetti, «What controls the composition and the structure of nanomaterials generated by laser ablation in liquid solution?,» *Physical Chemistry Chemical Physics ,* vol. 9, n. 15, pp. 3027-3046, 2013.

[2] F. Mafuné, J. Kohno, Y. Takeda, T. Kondow e H. Sawabe, «Formation and Size Control of Silver Nanoparticles by Laser Ablation in Aqueous Solution,» *The Journal of Physical Chemistry B,* vol. 104, n. 39, pp. 9111-9117, 2000.

[3] V. Amendola e M. Menghetti, «Laser ablation synthesis in solution and size manipulation of noble metal nanoparticles,» *Physical Chemistry Chemical Physics,* vol. 11, n. 20, p. 2009, 3805-3821.

[4] S. Barcikowski, F. Devesa e K. Moldenhauer, «Impact and structure of literature on nanoparticle generation by laser ablation in liquids,» *Journal of Nanoparticle Research,* vol. 11, pp. 1883-1893, 2009.

[5] S. Barcikowski e G. Compagnini, «Advanced nanoparticle generation and excitation by lasers in liquids,» *Physical Chemistry Chemical Physics,* vol. 15, pp. 3022-3026, 2013.

[6] C. Rehbock, J. Jakobi, L. Gamrad, S. van der Meer, D. Tiedemann, U. Taylor, W. Kues, D. Rath e S. Barcikowski, «Current state of laser synthesis of metal and alloy nanoparticles as ligand free reference materials for nano-toxicological assays,» *Beilstein Journal of Nanotechnology,* vol. 5, pp. 1523-1541, 2014.

[7] M. Dell'Aglio, V. Motto-Ros, F. Pelascini, I. B. Gornushkin e A. De Giacomo, «Investigation on the material in the plasma phase by high temporally and spectrally resolved emission imaging during pulsed laser ablation in liquid (PLAL) for NPs production and consequent consideration on NPs formation,» *Plasma Sources Science and Technology,* vol. 28, p. 085017, 2019.

[8] M. Dell'Aglio, R. Gaudiuso, O. De Pascale e A. De Giacomo, «Mechanisms and processes of pulsed laser ablation in liquids during nanoparticle production,» *Applied Surface Science,* vol. 348, pp. 4-9, 2015.

[9] F. Taccogna, M. Dell'Aglio, M. Rutigliano, G. Valenza e A. De Giacomo, «On the growth mechanism of nanoparticles in plasma during pulsed laser ablation in liquids,» *Plasma Sources Science and Technology,* vol. 26, p. 045002, 2017.

[10] G. Palazzo, G. Valenza, M. Dell'Aglio e A. De Giacomo, «On the stability of gold nanoparticle synthetized by laser ablation in liquids,» *Journal of Colloid and Interface Science,* vol. 489, pp. 47-56, 2017.

[11] M. C. Sportelli, M. Clemente, M. Izzi, A. Volpe, A. Ancona, R. A. Picca, G. Palazzo e N. Cioffi, «Exceptionally stable silver nanoparticle synthetized by laser ablation in alcoholic organic solvent,» *Colloids and Surfaces A,* vol. 559, pp. 148-158, 2018.

[12] M. Dell'Aglio, V. Mangini, G. Valenza, O. De Pascale, A. De Stradis, G. Natile, F. Arnesano e A. De Giacomo, «Silver and gold nanoparticles produced by pulsed laser ablation in liquid to

investigate their interaction with Ubiquitin,» *Applied Surface Science,* vol. 374, p. 297–304, 2016.

[13] H. Qayyum, R. Ali, Z. U. Rehman, S. Ullah, B. Shafique, A. H. Dogar, A. Shah e A. Qayyum, «Synthesis of silver and gold nanoparticles by pulsed laser ablation for nanoparticle enhanced laser-induced breakdown spectroscopy,» *Journal of Laser Applications,* vol. 31, p. 022014, 2019.

[14] S. Kohsakowski, A. Santagata, M. Dell'Aglio, A. De Giacomo, S. Barcikowski, P. Wagener e B. Gökce, «High productive and continuous nanoparticle fabrication by laser ablation of a wire-target in a liquid jet,» *Applied Surface Science,* vol. 403, pp. 487-499, 2017.

[15] S. Kohsakowski, A. Santagata, M. Dell'Aglio, A. De Giacomo, S. Barcikowski e P. Wagener, «Pulsed laser ablation of wire-shaped target in a thin water jet: Effects of plasma features and bubble dynamics on the PLAL process».

[16] V. S. Burakov, N. V. Tarasenko, A. V. Butsen, V. A. Rozantsev e M. I. Nedel'ko, «Formation pf nanoparticles during double-pulse laser ablation of metals in liquids,» *The European Physical Journal: Applied Physics,* vol. 30, pp. 107-112, 2005.

[17] M. Dell'Aglio, R. Gaudiuso, R. El Rashedy, O. De Pascale, G. Palazzo e A. De Giacomo, «Collinear double pulse laser ablation in water for the production of silver nanoparticles,» *Physical Chemistry Chemical Physics,* vol. 15, pp. 20868-20875, 2013.

[18] T. Tsuji, K. Iryo, N. Watanabe e M. Tsuji, «Preparation of silver nanoparticles by laser ablation in solution: influence of laser wavelength on particle size,» *Applied Surface Science,* vol. 202, pp. 80-85, 2002.

[19] D. Paramelle, A. Sadovoy, S. Gorelik, P. Free, J. Hobley e D. G. Fernig, «A rapid method to estimate the concentration of citrate capped silver nanoparticles from UV-visible light spectra,» *Analyst,* vol. 139, pp. 4855-4861, 2014.

[20] A. Botto, B. Campanella, I. Degano, S. Legnaioli, G. Lorenzetti, S. Pagnotta, F. Poggialini e V. Palleschi, «Direct analysis of anthraquinone dyed textiles by Surface Enhanced Raman Spectroscopy and Ag nanoparticles obtained by pulsed laser ablation,» *The European Phyisical Journal Plus,* vol. 134, p. 414, 2019.

[21] P. C. Lee e D. Meisel, «Adsorption and surface-enhanced Raman of dyes on silver and gold sols,» *Journal of Physical Chemistry,* vol. 86, n. 17, pp. 3391-3395, 1982.

Chapter 4:

Investigating Double Pulse Nanoparticle Enhanced Laser Induced Breakdown Spectroscopy

Chapter 4 - Index

4 - Investigating Double Pulse Nanoparticle Enhanced Laser Induced Breakdown Spectroscopy

4.1 – Introduction

As mentioned in the previous sections of this work, among the major drawbacks of LIBS is the low sensitivity when compared to other conventional elementary spectroscopy techniques, such as ICP-OES. An overview of several methods that have been proposed to enhance the performances of the technique is given in Chapter 1, consisting in either improving the instrumental setup or by treating the analyzed samples.

For example, plasma confinement has been explored for the enhancement of the LIBS signal, either by the use of a cavity [1] where the plasma radiation and shockwave are reflected and compressed, or by the application of a magnetic field [2] where the plasma parameters such as temperature, electron density and morphology can be modified by varying the local magnetic field. One issue arising with this kind of approach is the realization and optimization of a more complex instrumental setup. For example, in the case of a spatially confined plasma, the dimensions and position of the cavity are crucial for the obtainment of a good enhancement and, in general, they limit the size and nature of the sample that can be analyzed. A similar consideration can be made for the application of a localized and fine-tuned magnetic field that must be kept stable throughout the analysis.

Many approaches use multiple, consecutive laser pulses. The most common one being the employment of two laser pulses in the DP-LIBS configuration. The advantages and characteristics of DP-LIBS have been already presented in Chapter 1 and are discussed thoroughly in literature [3] [4] [5] [6]. Briefly, in the conventional DP-LIBS configuration, two collinear laser pulses are delivered onto the same spot on the sample surface, with a suitable interpulse delay. The first pulse generates a plasma as well as a shockwave expanding in the ambient gas that leaves behind a rarefied environment surrounding the measurement spot. The second laser pulse interacts within such a rarefied environment and, due to a lowered shielding and plasma confinement during the initial stages of expansion, yields an enhanced LIBS signal. These mechanisms have been verified in a number of subsequent studies [7] [8] using variable atmospheric pressures, as well as with the use of an Orthogonal DP-LIBS configuration. In recent years, the introduction of commercially available lasers capable of delivering two consecutive pulses with short interpulse delays, has made DP-LIBS very attractive due to its versatility and enhancement capabilities.

Among the methodologies that propose an additional sample treatment to enhance the LIBS performances, the recently proposed Nanoparticle Enhanced LIBS (NELIBS) by De Giacomo et al [9]

is of particular interest for its fast and relatively easy implementation. The mechanisms and the procedures involved in NELIBS have been discussed in Chapter 1. In brief, the technique allows for the improvement of the LIBS technique capabilities and analytical response by using a dispersion of noble metal nanoparticles (NPs) that are deposited on the sample surface. The interaction of the laser electromagnetic field with the surface conduction electrons of the NPs induces a polarization and strong oscillation of the electrons and, in turn, a charge accumulation on the NPs borders. The generated dipole produces a large electromagnetic enhancement confined to the NPs surface and the adjacent regions. This phenomenon effectively increases the intensity of the electromagnetic field induced by the laser on the sample surface, the number of emitted electrons, the ablated mass and the plasma emission intensity.

It should be stressed out that, even though NELIBS requires minimal sample preparation, this step is crucial for obtaining a consistent and significant enhancement [10]. It has been demonstrated how the ratio between the NPs dimensions and the inter-particle distance influences the signal enhancement. A similar connection is observed for the NPs concentration and homogeneous deposition on the sample surface. The instrumental setup is also critical, as it has been demonstrated how the optimal NELIBS effects are obtained within a certain range of laser irradiance.

A number of papers have been published, exploring various applications of NELIBS. In addition to the first application to metallic samples [9], the technique has been tested for the detection of molecular bands [11] and, as a substrate, for the analysis of liquid samples [12] [13] and a work by Yang et al [14] proposes the application of Double Pulse (DP) with a NELIBS (DP-NELIBS) approach for the analysis of crystal SiO_2 using a collinear pulse configuration.

It has been proved how, generally, the NPs are removed from the ablation spot after the laser pulse [9] meaning that, in the case of collinear DP-NELIBS, only the first laser pulse would interact with the NPs. A solution could be the usage of two slightly offset laser pulses, such as the advantages from DP and NELIBS are maintained. While the first pulse would create a low-density environment, the second pulse would interact with an undisturbed NPs deposition inside this environment and, theoretically, give rise to a much more intense LIBS signal than the one obtained from NELIBS alone. At the time this work was performed, there were only two published papers that investigated the application of spatially offset (SO) laser pulses for LIBS analysis [15] [16], showing the potential of this approach.

In this work the feasibility of SO-DP-NELIBS is discussed, presenting the results of the investigation of instrumental parameters such as laser pulse energy and beam offset distance. The results

obtained from SO-DP-NELIBS are then compared with those obtained from conventional single pulse NELIBS, as well as LIBS and DP-LIBS.

4.2 – Materials and Methods

4.2.1 – Materials

Commercially available silver nanoparticles (AgNPs) (Silver dispersion, aqueous buffer, sodium citrate stabilizer from Sigma-Aldrich, 0.02 mg/ml) with a diameter of 10 nm were used during the optimization phase. The certified concentration and dimensions of commercially available nanoparticles allow the obtainment of a benchmark for further optimization of the NELIBS methodology. It was found that, in fact, the presence of the citrate stabilizing agent in the dispersion had a dampening effect on both the signal enhancement and the plasma generation, as well as a lower homogeneity of the dried NP droplets. For these reasons, AgNPs prepared by Pulsed Laser Ablation in Liquid (PLAL) were used for SO-DP-NELIBS and the correlated experiments.

Silver foil (2 mm thickness, 99,9% trace metal basis from Sigma-Aldrich) and a 2 mM KCl (powder, Sigma-Aldrich) aqueous solution were used for PLAL synthesis of AgNPs. The procedure for the preparation of AgNPs is described in detail in Chapter 3, as well as in a recent work by Botto et al [17]. In brief, a pulsed laser, operating at the fundamental wavelength of 1064 nm, with a repetition rate of 10 Hz and a pulse energy of approximately 100 mJ, was focused on a silver target immersed in a KCl solution. The ablation time was 5 minutes. The produced AgNP dispersion was characterized by UV-Vis spectroscopy (Perkin Elmer Lambda 25 double beam spectrophotometer, scans from 300 nm to 600 nm, scan rate 240 nm/min, 1 nm slits). The values of maximum absorbance and the corresponding wavelength in the spectrum were used to estimate the size and concentration of the NPs solution using Lambert-Beer's law and the data indicated in literature [18]. The synthesized nanoparticles were found to have an average diameter of 13 nm and a concentration of 0,024 mg/mL.

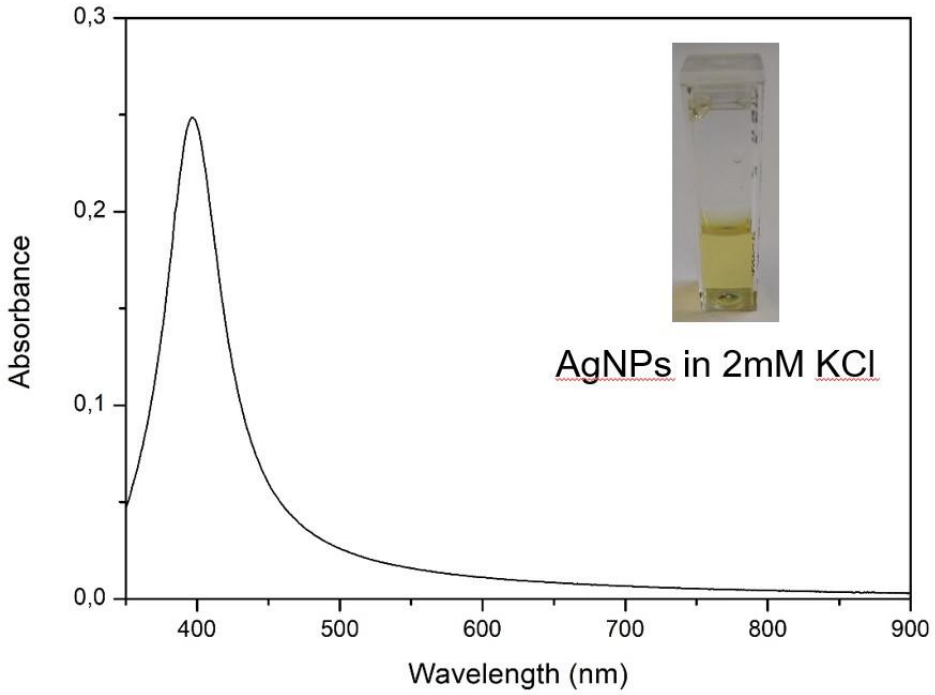

Figure 1 - UV-Vis spectrum of the synthetized AgNPs (shown in the inset)

A series of preliminary single-pulse NELIBS measurements were performed in order to determine the optimal AgNP concentration for the selected instrumental setup. During these tests, a laser pulse energy of approximately 95 mJ and copper sheet samples were used throughout. Opportune volumes of the mother solution were added to 2mM KCl solutions to obtain progressively more diluted dispersion for testing.

The AgNP concentration that allowed for the maximum signal enhancement was found to be 0,014 mg/mL, and this solution was used for SO-DP-NELIBS analyses. The AgNPs were deposited onto the sample surface by drop-casting 5 µL of the suspension and promptly dried with hot air. Generally, the dried droplets had a diameter of approximately 4 mm, corresponding to a surface concentration of approximately $6 \cdot 10^{-4}$ mg/cm^2.

Commercially available copper sheets, ideal NELIBS substrates due to their metallic and highly conductive nature, were used as samples throughout the study. Preliminary analyses with a portable XRF instrument (Elio PXRF, XGLab) showed a >99% Cu composition. The copper sheets were cut into small pieces, thoroughly cleaned and treated with a solution of HCl (ACS reagent, 37% from Merck) in order to remove the surface oxidation layer before the analysis. In addition, in order to remove any deposited contamination and surface imperfection, two preliminary cleaning laser pulses were performed on the measurement spot.

Deionized water was obtained from an Elga Purelab Option DV 35 (Veolia Environment, France) water filtration system, and used throughout the study.

4.2.2 – Instrumentation

The instrumental setup for LIBS and NELIBS analysis, schematized in Figure XX, utilized a double pulse Nd:YAG laser (LS-2134D, Lotis) operating at the fundamental wavelength of 1064 nm. The laser delivered 2 pulses of up to 200 mJ each in 20 ns, with an interpulse delay, optimized by the manufacturer, of 1 µs. The diameter of the measurement spot of each laser beam was set to be approximately 1 mm. In the Spatially Offset configuration, both laser pulses were focused inside the larger dried AgNP droplet.

The laser was focused on the sample with a plano-convex lens (f=100 mm) and the light was collected by a fiber optic placed at 45° with respect to the incident laser beam and at a distance of about 2 cm from the plasma plume generated by laser pulse. In this configuration, the fiber's acceptance angle allowed for the collection of the whole plasma light. In the SO-DP configuration, the second laser pulse was shifted from the original measurement spot while the first pulse remained stationary. The fiber optic head was then translated and re-aligned in order to collect the light emitted by the plasma generated by the second laser pulse. A scheme of the setup used in this study is reported in Chapter 3 (see Chapter 3: Figure 5)

The spectra are obtained through the use of an Aryelle 200 Echelle spectrograph (200 nm to 790 nm, LTB Lasertechnick Berlin) coupled with an air-cooled ICCD (iStar DH334T-18F03, Andor), with a resolving power of 9000. The acquisition delay was set to 500 ns after the second laser pulse and the integration time was 10 µs, in accordance with routine LIBS analyses. The spectrometer was calibrated using a Deuterium-Halogen lamp (Ocean Optics DH-2000).

4.3 – Results and Discussion

4.3.1 – Spatially Offset DP-LIBS

It was shown [8] how the intensity of the LIBS signal in the case of an offset DP configuration is comparable to the case of a collinear DP configuration, in typical LIBS experimental conditions. In addition, a distinct increase in crater depth and ablated volume was registered in the case of offset DP, due to the absence of particulate and atomized species in the optical path of the second laser pulse, which could lead to a lower ablation efficiency in the case of collinear DP. However, these phenomena do not cause any direct signal enhancement.

At inter-pulse delay times of 1 µs, the induced plasma and the shockwave created by the first laser pulse have already expanded through the air around and above the spot where the second laser pulse is focused, provided the separation of the two beams is not excessive. In these conditions,

the second laser pulse interacts with a rarefied environment, as it is the case of a collinear DP configuration.

In order to determine the feasibility of a SO-DP configuration with the available instrumental setup, a series of preliminary measurements were carried out with approximately 95 mJ of energy per each pulse, a commonly used laser output power for routine analyses. In particular, the aim was to verify that there was no significant decrease in the spectra quality and intensity when fully separating the two laser beams, indicating that the second beam was still inside the low-density environment created by the first pulse.

Spectra were first obtained using a conventional collinear DP configuration. Then, the internal laser mirrors regulating the optical path of the second laser beam were suitably adjusted to shift the beam's position onto the sample surface, obtaining two laser spots separated by approximately 0,5 mm (Figure 2).

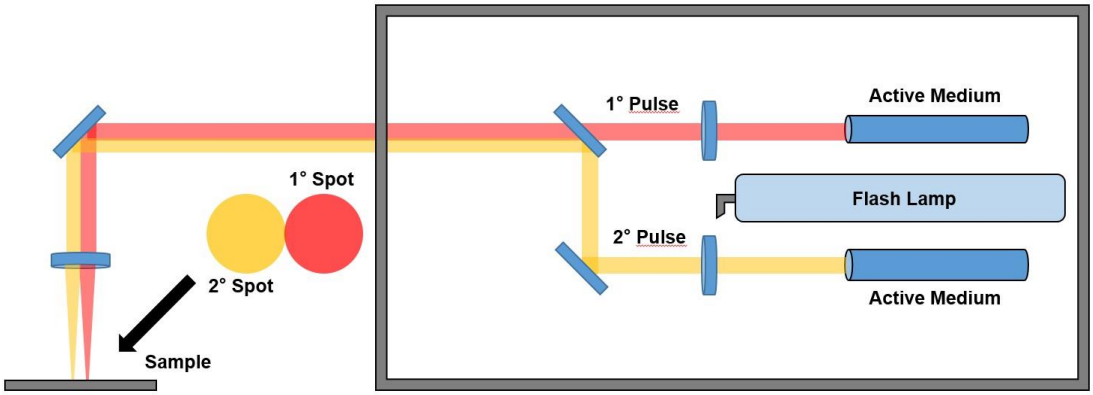

Figure 2 - Schematic representation of the SO-LIBS configuration

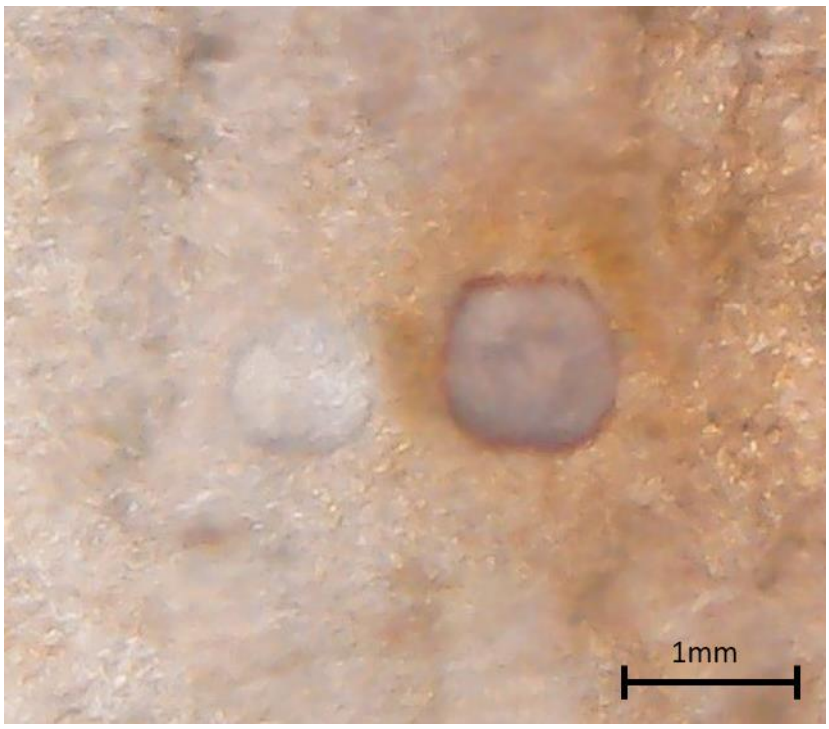

Figure 3 - Offset laser-induced craters on copper sheet sample

The focusing optics and mirrors were adjusted accordingly and the spectra for SO-DP were registered. The results are reported in Figure 4.

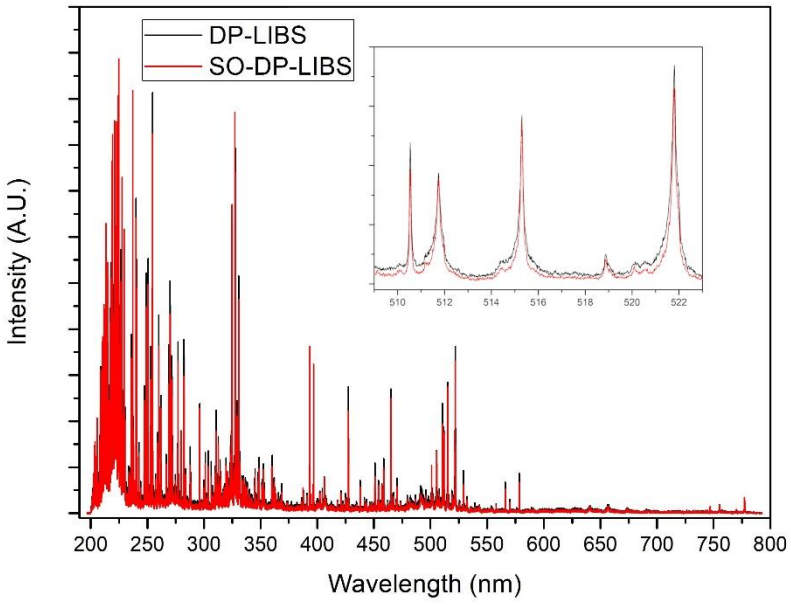

Figure 4 - LIBS spectra for the conventional and the spatially offset configurations. The inset shows the Cu I emission lines

The obtained spectra showed how the overall spectral intensity was comparable for both configurations, also indicating that no significant adjustment of the light collection system was required.

4.3.2 – AgNPs persistence in SO-DP-NELIBS

The removal of the AgNPs from the sample surface during the NELIBS analysis [9] was easily demonstrated by registering a second spectrum after the laser pulse and in the same position, and comparing the Ag emission lines.

In this case, the two spectra were registered in the collinear DP configuration, both after the first and the second laser pulse, using a 5 µL deposition of the Sigma-Aldrich nanoparticles.

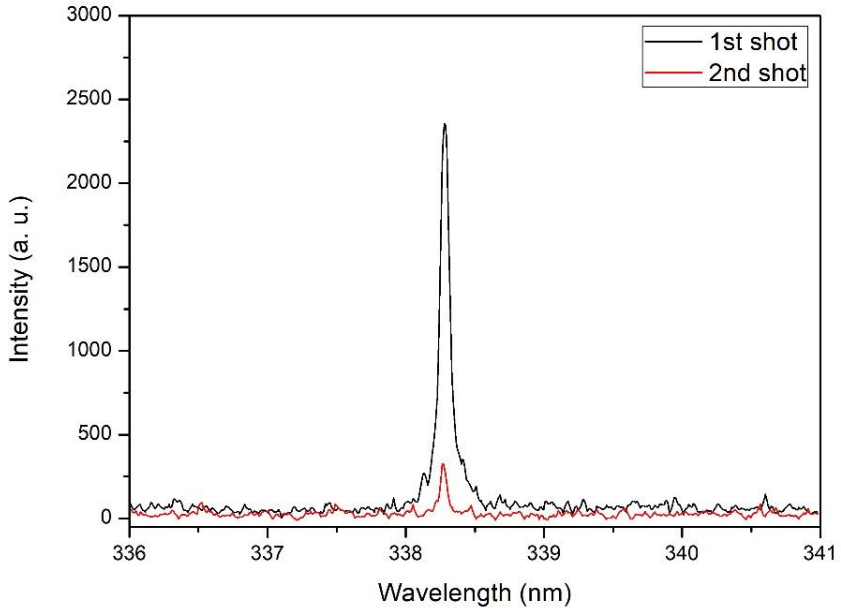

Figure 5 - Spectral window showing the Ag I emission line for the collinear DP configuration

As it can be seen from Figure 5, the Ag emission line in the red spectrum (relative to the 2nd laser shot) is much weaker than the first one, indicating that the silver content inside the measurement spot was almost completely depleted after the first laser pulse.

This suggests that, in the case of DP-NELIBS, all of the NPs would be removed after the first laser pulse and the enhancement effect, if present, would be much lower. To confirm this hypothesis, a conventional DP-LIBS analysis on a Cu target, using the collinear DP configuration, was performed on a Sigma-Aldrich NP deposition.

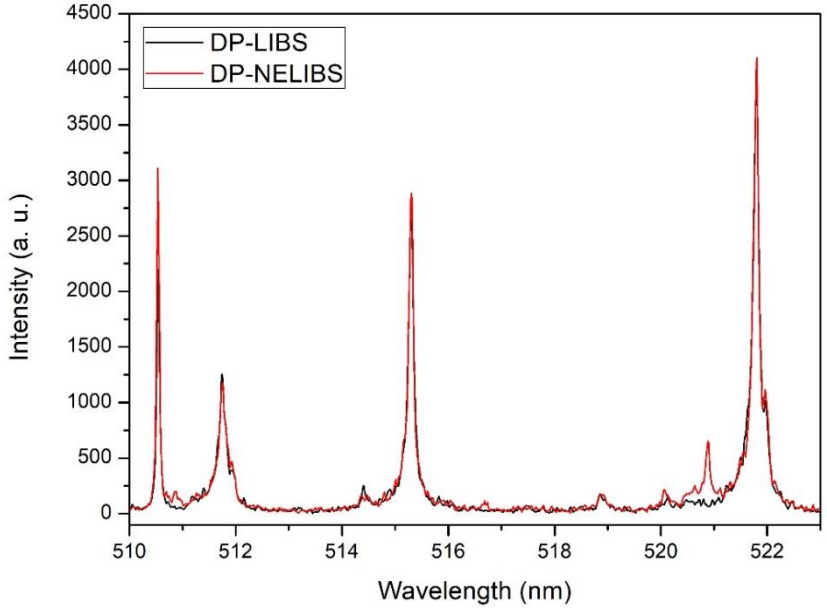

Figure 6 - Spectra comparison for DP-LIBS on a sample with (red) and without (black) the AgNP deposition, showing Cu emission lines

The resulting spectra (Figure 6) show how the line intensity for Cu is comparable in the case of DP-LIBS and DP-NELIBS, and how no appreciable enhancement is observed.

However, when the two pulses were spatially offset, as in the case of the proposed SO-DP-NELIBS experiments, the results were much different.

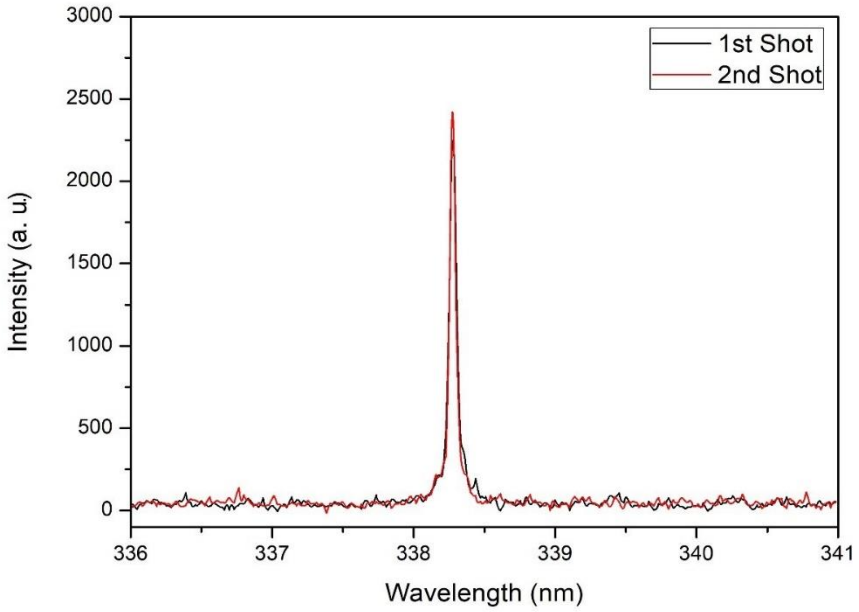

Figure 7 - Spectral window showing the Ag I emission line for the collinear SO-DP configuration

As it can be observed from Figure 7, the Ag emission line in the red spectrum is comparable with that from the black spectrum, indicating that both the laser pulses interacted with an unperturbed NPs deposition and, in theory, could give rise to NELIBS enhancement each time.

All the spectra were registered using a laser pulse energy of approximately 95 mJ.

4.3.3 – Spatially Offset Double-Pulse NELIBS

A series of measurements were conducted in order to test the feasibility of the proposed SO-DP-NELIBS approach, using the Sigma-Aldrich AgNPs. It was deemed necessary to the identification of the pulse energy that would produce the highest signal enhancement. The Enhancement Factor (EF) was calculated for all the experiments as the ratio between the integrated NELIBS and LIBS intensities for the Cu I emission line at 521,8 nm, while maintaining the same laser parameters. Each measurement was repeated 5 times with the same experimental conditions and the resulting spectra were averaged.

For this purpose, the laser was operated in single pulse (SP) mode and the energy was varied from approximately 40 mJ, the minimum value that allowed for a measurable plasma for this experimental set-up, to 200 mJ, the maximum operational limit for the laser.

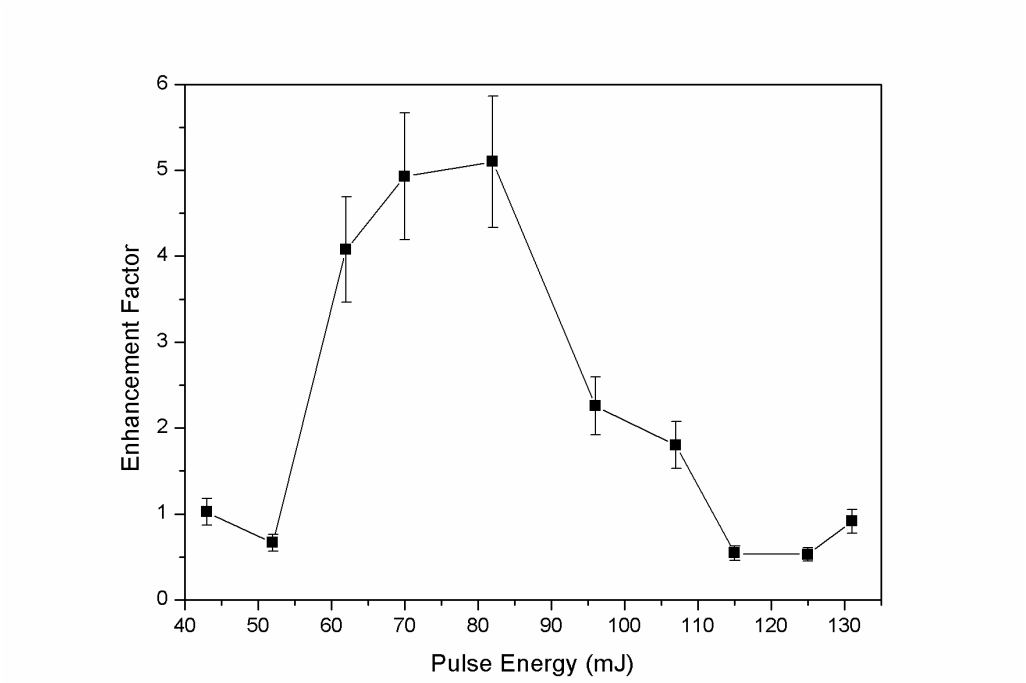

Figure 8 - Enhancement Factor dependence on pulse energy for SP-NELIBS. Error bars are estimated on the repeatability of the results

As reported in Figure 8, it was found that the highest EF for SP-NELIBS was observed for a pulse energy of about 85 mJ, which equals to a laser irradiance of 0,55 GW/cm^2. No signal enhancement was observed for energies over 130 mJ.

Then, another set of measurements was performed using the SO-DP configuration with the Sigma-Aldrich AgNP dispersion. The trend of the EF, reported as a function of the total pulse energy (1st Pulse + 2nd Pulse) is shown in Figure 9.

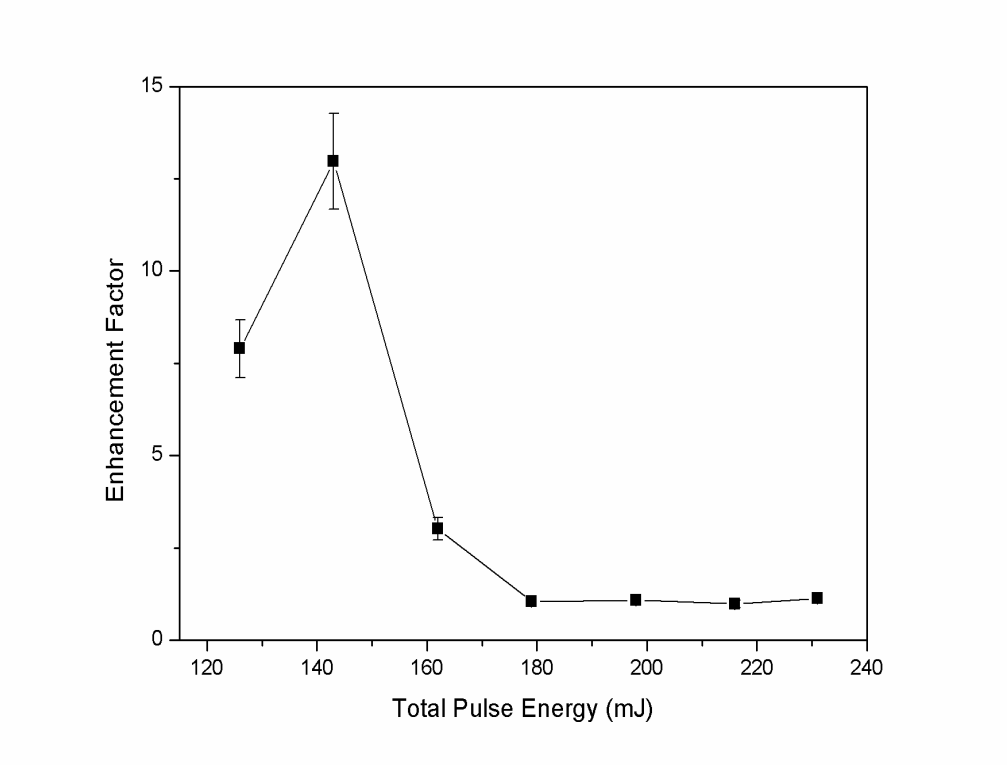

Figure 9 - Enhancement Factor dependence on the cumulative pulse energy for SO-DP-NELIBS. Error bars are estimated on the repeatability of the results

It can be seen how, even though the total pulse energy delivered on the sample surface is higher than in SP-NELIBS, the highest EF is registered for a single pulse energy that is slightly lower, at approximately 75 mJ per pulse. Moreover, a rapid decrease of EF was observed for higher pulse energy values.

Another important result to observe is the magnitude of the EF registered in the SO-DP-NELIBS, with the integrated line intensity for NELIBS reaching as high as 12 times the one for LIBS. Being twice the EF registered for SP-NELIBS, this shows the potential for this approach, and even more so when considering the already much higher intensity and quality of the DP-LIBS spectra.

4.3.4 – Offset distance and EF

To estimate the offset distance effect on the EF, a series of analyses were performed with the two laser spots in specific conditions: separated by approximately 0,5 mm, adjacent, partially overlapping and completely overlapped (collinear DP configuration). The laser pulse energy was set to 75mJ per pulse and 5 µL of the AgNP PLAL solution were used for the NELIBS measurements.

The results are presented in Figure 10 as the average of 5 repetitions performed using the same experimental conditions.

Due to the constraints of the experimental setup, it was not possible to register spectra for SO configuration where the spot separation was greater than 1 mm. Even in the case of 1 mm separation, it was found that the laser beams for the two pulses were reflected almost off the edges of the primary mirror, and then passing through the focusing lens close to its edges. In these conditions, it was found that the quality of the laser-induced plasma, as well as that of the spectrum, were unsatisfactory. Moreover, increasing spot separation brought the two measurement spots closer to the edge of the AgNPs dried deposition, where a coffee-ring effect was present and the deposition was less homogeneous, thus hindering the NELIBS measurements. For these reasons it was decided not to investigate offset configurations greater than 0,5 mm in this work.

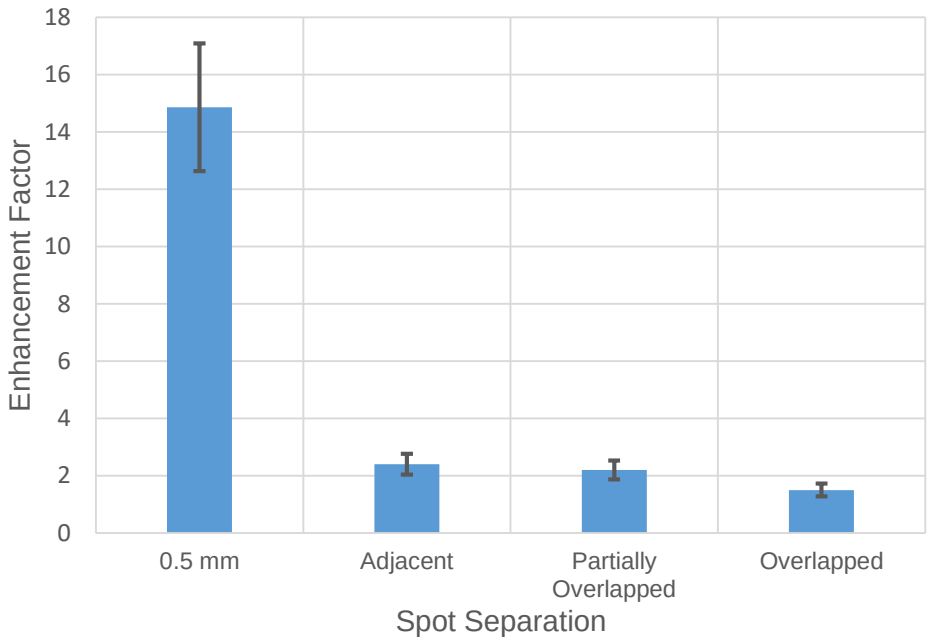

Figure 10 - Observed EF for the different positions of the measurement spots. Error bars are estimated on the repeatability of the results

The obtained results confirmed the expected EF trend. The highest EF was observed in the case of 0,5 mm separated measurement spots, while a decreasing enhancement magnitude was observed in the case of adjacent spots. This suggests that, as long as the two laser spots are separated enough, the NP deposition is not altered, and can be exploited during both laser pulses, while in the case of adjacent spots a part of the deposition is removed, thus reducing the signal enhancement.

In the case of partially overlapped spots, the results are comparable to those obtained for collinear DP-NELIBS, with almost no observable signal enhancement. This suggests that, after the first pulse, the NP deposition is compromised enough that the second pulse does not benefit from NELIBS effects.

4.3.5 – Considerations on SO-DP-NELIBS

One critical observation that must be addressed is the overall magnitude of EF observed during this study, both in the case of SP-NELIBS and DP-NELIBS. When compared to the works published in literature that can reach EF of up to 100 or more, the values obtained in this work are much lower.

This is most likely due to both the experimental conditions and the nature of NELIBS itself. For example, NELIBS technique is heavily influenced by the sample preparation and the NP deposition nature, in particular, by the distance between the deposited NPs in relation with their dimension. A non-homogenous NP deposition can lead to a lower registered EF and a lower reproducibility in the results.

In this work, the NP deposition was realized so that both of the measurement spots would be positioned in the middle of the NP drop. Even though this reduces the effects of a possible inhomogeneity, and removes the issues coming from the formation of a coffee ring, in an ideal NELIBS experiment, the whole NP drop should be contained in the measurement spot.

Due to the optical and laser setup, it was not possible to further enlarge the measurement spot, even though the laser's power output would in theory allow it, while maintaining the same irradiance values. If the spot is enlarged, the two beams would need to be shifted further to maintain the optimal separation but such adjustment meant that the beams were directed too close to the edges of the mirrors and focusing lenses, leading to a severe degradation of the beam quality.

Nonetheless, the presence of an appreciable improvement of the emission line intensities for both SP-NELIBS and DP-NELIBS, showed that the instrumental setup and experimental procedure could yield a signal enhancement and that the proposed SO-DP-NELIBS approach is promising.

An interesting comparison is reported in Figure 11.

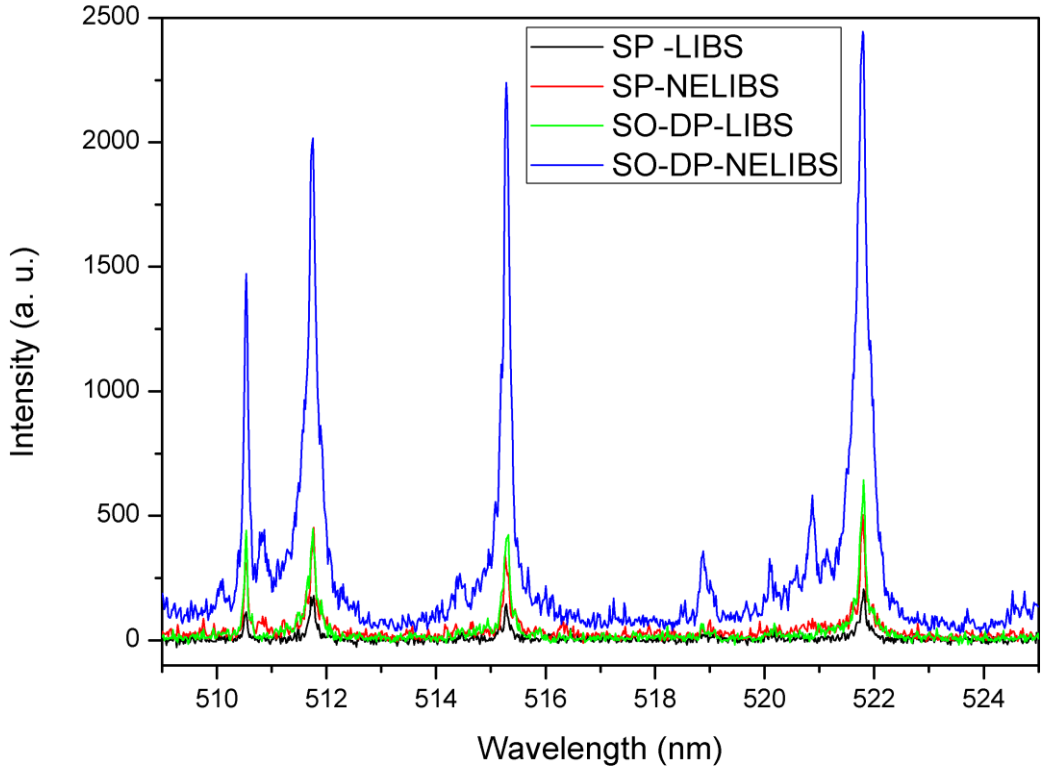

Figure 11 - Spectra comparison between SP-LIBS, SP-NELIBS, SO-DP-LIBS and SO-DP-NELIBS, showing the Cu I emission lines

Here, a comparison between the spectra for SP-LIBS, SP-NELIBS, SO-DP-LIBS and SO-DP-NELIBS is shown. Both the LIBS and NELIBS spectra were registered using the same experimental conditions. These were the parameters that allowed for the highest EF and that were also comparable to the optimal ones that are usually employed for routine LIBS analyses.

As it can be seen, the spectrum with the lowest intensity is the one relative to SP-LIBS, as it was expected. Interestingly, it was observed that with these experimental conditions the spectra for SP-NELIBS and SO-DP-LIBS appear to have comparable intensities. The most intense spectrum is, as expected, the one relative to SO-DP-NELIBS, several times more intense than SP-NELIBS and SO-DP-LIBS.

It should be noted that, generally, the SP-LIBS and DP-LIBS spectra could be enhanced by using higher laser pulse energies. Within certain limits, the spectra intensity proportionally increases until it starts to encounter strong self-absorption phenomena and saturation of the signal. If these higher-energy spectra were to be compared to the strongest NELIBS spectra registered in this study, which are quite lower than the ones reported in literature, a decrease in the EF would most likely be observed.

This is due to the fact that the NELIBS approach is intrinsically tied to a certain optimal pulse energy range, as well as NP deposition characteristics and sample nature, and it might not be suitable for all the possible applications of LIBS research. Indeed, the main criticality that was encountered in this study was the limited dimension of the laser beam spot, which should be large enough to ablate the entire NP deposition for an optimal NELIBS measurement [12]. For a SO-DP-NELIBS this would not only complicate the deposition process (i.e. two separate NP deposition would be required), but the increased spot size would also require a larger beam separation. While this could be achieved using an *ad-hoc* optical setup, the efficiency of the DP configuration would be greatly reduced due to the increased beam separation and spot size.

Nonetheless, the results obtained for the SO-DP-NELIBS approach are very promising, showing that a further improvement of NELIBS is possible and that the technique is adaptable to more diverse instrumental setups.

4.4 – Conclusions

In this work a novel approach to the NELIBS technique for the signal enhancement of LIBS spectra was proposed.

In particular, the application of a SO-DP-LIBS configuration was investigated for the coupling of NELIBS and DP advantages in order to further increase the signal enhancement. To do so, a DP-LIBS instrumental setup was modified so that each laser pulse interacted with different spots on the sample surface, while maintaining the low density environment typical of DP-LIBS.

The feasibility of the SO-DP-NELIBS approach was successfully demonstrated, obtaining an even higher EF than the one registered during SP-NELIBS analyses with comparable experimental configuration. Moreover, it was shown how the EF decreased with a decreasing laser beam offset distance.

The results obtained in this work are very promising and, once more, show the potential of NELIBS as well as its versatility.

Indeed, the extent of the interaction of the enhancing effects of DP and NELIBS is worthy of further investigation, with a particular focus on the laser-induced plasma dynamics and evolution in the case of SO-DP-NELIBS.

Bibliography

[1] A. M. Popov, F. Colao e R. Fantoni, «Enhancement of LIBS signal by spatially confining the laser-induced plasma,» *Journal of Analytical Atomic Spectrometry,* vol. 24, n. 5, pp. 602-604, 2009.

[2] P. Liu, R. Hai, D. Wu, Q. Xiao, L. Sun e H. Ding, «The Enhancement effect of optical emission from laser induced breakdown spectroscopy of an Al-Li alloy in the presence of magnetic field confinement,» *Plasma Science Technologies,* vol. 17, n. 8, pp. 687-692, 2015.

[3] S. Musazzi e U. Perini, Laser Induced Breakdown Spectroscopy: Theory and Application, Hiedelberg: Springer, 2014.

[4] D. A. Cremers e L. J. Radziemski, Handbook of Laser-Induced Breakdown Spectroscopy, John Wiley and Sons, Ltd., 2006.

[5] W. Miziolek, V. Palleschi e I. Schechter, Laser-induced breakdown spectroscopy (LIBS): fundamentals and applications, Cambridge: Cambridge University Press, 2006.

[6] E. Tognoni e G. Cristoforetti, «Basic mechanisms of signal enhancement in ns double-pulse laser-induced breakdown spectroscopy in a gas environment,» *Journal of Analytical Atomic Spectrometry,* vol. 29, pp. 1318-1338, 2014.

[7] G. Cristoforetti, S. Legnaioli, V. Palleschi, A. Salvetti e E. Tognoni, «Influence of ambient gas pressure on laser-induced breakdown spectroscopy technique in the parallel double-pulse configuration,» *Spectrochimica Acta Part B: Atomic Spectroscopy,* vol. 52, n. 12, pp. 1907-1917, 2004.

[8] G. Cristoforetti, S. Legnaioli, L. Pardini, V. Palleschi, A. Salvetti e E. Tognoni, «Spectroscopic and shadowgraphic analysis of laser induced plasmas in the orthogonal double pulse pre-ablation configuration,» *Spectrochimica Acta Part B: Atomic Spectroscopy,* vol. 61, n. 31, pp. 340-350, 2006.

[9] A. De Giacomo, R. Gaudiuso, C. Koral, M. Dell'Aglio e O. De Pascale, «Nanoparticle-enhanced laser-induced breakdown spectroscopy of metallic samples,» *Spectrochimica Acta Part B: Atomic Spectroscopy,* vol. 85, n. 21, pp. 10180-10187, 2013.

[10] M. Dell'Aglio, R. Alrifai e A. De Giacomo, «Nanoparticle Enhanced Laser Induced Breakdown Spectroscopy (NELIBS), a first review,» *Spectrochimica Acta Part B: Atomic Spectroscopy,* vol. 148, pp. 105-112, 2018.

[11] C. Koral, A. De Giacomo, X. Mao, V. Zorba e R. E. Russo, «Nanoparticle Enhanced Laser Induced Breakdown Spectroscopy for improving the detection of molecular bands,» *Spectrochimica Acta Part B: Atomic Spectroscopy,* vol. 125, pp. 11-17, 2016.

[12] A. De Giacomo, C. Koral, G. Valenza, R. Gaudiuso e M. Dell'Aglio, «Nanoparticle enhanced laser-induced breakdown spectroscopy for microdrop analysis at subppm level,» *Analytical Chemistry,* vol. 88, p. 5251−5257, 2016.

[13] W. Xu, Q. Lin, G. Niu, S. Qi e Y. Duan, «Emission enhancement of laser-induced breakdown spectroscopy for aqueous sample analysis based on Au nanoparticles and solid-phase substrate,» *Applied Optics,* vol. 55, n. 24, p. 6706–6712, 2016.

[14] F. Yang, L. Jiang, S. Wang, Z. Cao, L. Liu, M. Wang e Y. Lu, «Emission enhancement of femtosecond laser-induced breakdown spectroscopy by combining nanoparticle and dual-pulse on crystal SiO2,» *Optical Laser Technilogy,* vol. 93, p. 194–200, 2017.

[15] D. Nishijima, E. M. Hollmann e R. P. Doerner, «Spatially-offset double-pulse laser-induced breakdown spectroscopy: A novel technique for analysis of thin deposited layers,» *Spectrochimica Acta Part B: Atomic Spectroscopy,* vol. 124, pp. 82-86, 2016.

[16] G. Cristoforetti, S. Legnaioli, V. Palleschi, E. Tognoni e A. Benedetti, «Crater drilling enhancement obtained in parallel non-collinear double-pulse laser ablation,» *Applied Physics A,* vol. 98, p. 219, 2009.

[17] A. Botto, Campanella B, I. Degano, S. Legnaioli, G. Lorenzetti, S. Pangotta, F. Poggialini e V. Palleschi, «Direct analysis of anthraquinone dyed textiles by Surface Enhanced Raman Spectroscopy and Ag nanoparticles obtained by pulsed laser ablation,» *European Physical Journal Plus,* vol. 134, p. 414, 2019.

[18] D. Paramelle, A. Sadovoy, S. Gorelik, P. Free, J. Hobley e D. G. Fernig, «A rapid method to estimate the concentration of citrate capped silver nanoparticles from UV-visible light spectra,» *Analyst,* vol. 139, p. 4855–4861, 2014.

Chapter 5:

Combining Nanoparticle Enhanced Laser Induced Breakdown Spectroscopy with Graphene-based microextraction for real-time metal trace analysis in liquids

Chapter 5 – Index

5 – Combining Nanoparticle Enhanced Laser Induced Breakdown Spectroscopy with Graphene-based microextraction for real-time metal trace analysis in liquids

5.1 – Introduction

In recent years the demand for fast and reliable analytical methods has grown significantly. In particular, for those techniques that can produce (almost) real time results and that are also capable of in-situ measurements. Laser Induced Breakdown Spectroscopy (LIBS) has many characteristics that make it one of the ideal candidates to fill this role [1] [2], as previously mentioned in Chapter 1. LIBS is able to analyze almost any kind of sample directly, in a wide range of ambient conditions. The instrumentation can also be scaled down to be sufficiently portable, and robust enough for remote or in-situ measurements. For these reasons, many applications of LIBS can be found in the monitoring of industrial processes, quality control of pharmaceutical and food production, but also in the archeology and cultural heritage fields as well as in space exploration.

Nevertheless, one of the major drawbacks of LIBS is the low performance for the analysis of liquid samples. When compared to conventional analytical techniques such as Flame Atomic Absorption (FAAS), Inductively Coupled Plasma Optical Emission (ICP-OES) or Mass (ICP-MS) spectroscopies, the LODs that can be reached with LIBS are much higher, in the order of tens or hundreds of mg/L. Over the years, several methods have been proposed to enhance the performances of the technique for the analysis of liquid samples, either by improving the instrumental setup or by treating the analyzed samples [3] [4]. For example, some works propose to perform the LIBS measurement directly on the surface of the liquid sample, to generate an aerosol or a liquid jet to increase the performances of the technique [2]. On the other hand, some authors propose to convert the liquid matrix into a solid in order to eliminate many of the issues [5] [6] [7] [8].

Surface Enhanced LIBS (SENLIBS) can also be used for improving the capabilities of LIBS in the analysis of liquid samples. This approach consists in the deposition and drying of a liquid sample on a suitable substrate (i.e. a conductive material like a metal sheet or a silicon wafer), onto which the LIBS measurement is performed. The conductive nature of the substrate can greatly aid in the generation of the laser plasma, as well as to increase the plasma temperature and emission from the analyte species. Indeed, Ma and co-workers investigated SENLIBS for the detection of heavy metals in aqueous solutions using different substrates [9], allowing for the detection of less than 0,01 mg/mL of Pb and Cr. Nevertheless, SENLIBS does not allow for the pre-concentration of analytes, as the sample solution is deposited on the substrate as-is. This could hinder the

detection of analytes when their concentration is too low to obtain a homogeneous deposition on the SENLIBS substrate (e.g. drying multiple droplets on the same spot can produce coffee ring effects).

An alternative route to improve the LODs for metals in solution is the use of Solid Phase Extraction (SPE) techniques and, in particular, of Solid Phase Microextraction (SPME). SPME uses a small amount of a sorbent material (a few μg) to extract and concentrate the analytes in a solution and therefore minimizes the amount of sorbent needed, while allowing for very fast extraction times.

Wang et al [10] were the first to combine SPME and LIBS for the determination of metals in aqueous solutions. In their work, they used a Dispersive SPME (D-SPME) methodology based on graphite nanoparticles, combined with a preemptive chelation of the metals in solution. The analysis of the dried solid phase allowed for the determination of Cr, Mn and Ag at concentrations of 17 μg/L and lower. Subsequently, Ruiz et al [11] proposed an improvement of the D-SPME method by using Graphene Oxide (GO) as an adsorbent. They were able to eliminate the metal chelation step during sample preparation and still obtain LODs lower than 50 μg/L.

While D-SPME can be relatively easy to couple with LIBS, there is still the issue of recovering the extractant from the liquid sample, drying it and treating it to produce a suitable matrix for LIBS. Thin Film Microextraction (TFME) uses a solid substrate coated with a thin layer of sorbent material. This allows for an easier recovery of the sorbent phase as it remains adhered to the rigid substrate during the extraction. While a desorption phase is generally required, this step is not necessary if LIBS is used for the measurement. Ripoll et al [12] demonstrated the effectiveness of a combined TFME-LIBS approach for the extraction of heavy metals from aqueous solution. Using GO as an adsorbent, the authors prepared TFME supports by mold deposition and obtained LODs in the order of 50 μg/L. Ripoll and co-workers also recently investigated an improved methodology for the preparation of TFME supports, based on electrospray deposition (ESD) of GO [13]. In this work the authors obtained even lower LODs, in the order of 15 μg/L, demonstrating the increased performances of the ESD supports over other deposition methods.

Another methodology proposed to enhance the LIBS performances is Nanoparticle Enhanced LIBS (NELIBS), proposed by De Giacomo et al [14] and illustrated in Chapter 1. This technique is of particular interest for its fast and relatively easy implementation, and a recently published review by Dell'Aglio et al [15] thoroughly describes the phenomena and the mechanisms correlated to NELIBS, while highlighting the criticalities of the approach. NELIBS was successfully used to enhance the performances of LIBS towards the detection of metals in liquids by depositing

droplets of the analyte solution on a layer of dried NPs, in a similar fashion to the SENLIBS approach [16].

In a work by Wen et al, a substrate prepared using AuNPs and porous electrospun ultrafine fibers was tested successfully for the detection of µg/mL heavy metals in aqueous samples [17]. The authors showed how the structure of such substrate, coupled with the AuNPs can greatly improve the detection of the extracted analytes, thanks to the large surface area of the fibers. Nevertheless, the preparation of the fibers requires dedicated instrumentation and knowledge on how to operate it to obtain an optimal product.

This work, performed in part in the laboratories of the University of Alicante (Spain), explores the feasibility of a combined approach of TFME and NELIBS. To the best of our knowledge, this is the first time such an approach has ever been proposed and tested for the determination and LOD estimation of heavy metals extracted from aqueous solutions. Moreover, both the AgNPs and the GNS were prepared using the same PLAL setup, significantly reducing complexity, costs and the time required for the experiments.

In addition, it was possible to develop and test a functionalization step of the glass substrates, in order to increase the retention of the GNS film. This would, in theory, increase the resistance of the TFME supports to the immersion in solutions, as well as facilitate the creation of larger and more homogeneous depositions.

5.2 – Materials and Methods

5.2.1 – Materials

Graphene nano-sheets (GNS) were prepared starting from pure graphite (Graphite flakes, Sigma-Aldrich).

Glass microscope slides (Plain microscope slides, J. Melvin Freed Brand, USA) were cut to approximately 1x1.5 cm pieces and used as substrates for the preparation of TFME supports. Chemical etching of the glass slides was performed using a commercially available glass etching paste (Idea VETRO etching paste, Maimeri, Italy).

Silver nanoparticles (AgNPs) were prepared by Pulsed Laser Ablation in Liquid (PLAL). Silver foil (2 mm thickness, 99,9% trace metal basis from Sigma-Aldrich) and a 2 mM KCl (powder, Sigma-Aldrich) aqueous solution were used for PLAL synthesis of AgNPs. The procedure for the preparation of AgNPs is described in detail in a recent work by Botto et al. [18]. In brief, a pulsed laser, operating at the fundamental wavelength of 1064 nm, with a repetition rate of 10 Hz and a pulse energy of 100 mJ, was focused on a silver target immersed in the KCl solution. After an ablation time of 5 minutes, the AgNP dispersion was characterized by UV-Vis spectroscopy (Jasco

V-750 double beam spectrophotometer, scans from 300 nm to 600 nm, scan rate 300 nm/min). The values of maximum absorbance at the corresponding wavelength in the spectrum can be used to readily estimate the size and concentration of the NPs solution using Lambert-Beer's law and the data indicated in literature [19]. The synthesized nanoparticles were found to have an average diameter of 11 nm and a concentration of 0,02 mg/mL.

Standard aqueous solutions containing Cu, Cr, Ni and Pb were prepared by appropriate dilution of 1000 mg/L mono-element stock solutions (High-Purity mono-element standard solutions, Charleston, UK).

APTES (3-(Aminopropyl)triethoxysilane, 99%, Sigma-Aldrich) was purchased from Merck. Graphene oxide powder was purchased from GrapheneA (Spain). NaOH (pellets, Honeywell/Fluka), Ethanol (Absolute for HPLC, PanReac AppliChem) and Acetone (Chromasolv for HPLC, Honeywell/Riedel-de Hoen) were used for the functionalization of glass substrates.

Deionized water was obtained from an Elga Purelab Option DV 35 (Veolia Environment, France) water filtration system, and used throughout the study.

5.2.2 – Instrumentation

This work was performed using the LIBS instrumentations provided by the ICCOM-CNR in Pisa (Italy) and the University of Alicante (Spain). The former was used during the GNS and AgNPs preparation as well as the investigation of the optimal parameters for support preparation, extraction and NELIBS, while the latter was used for building calibration curves and for NELIBS experiments.

At CNR, LIBS analyses were performed using the Modì portable LIBS instrument [20]. Modì is equipped with a Nd:YAG laser (LS2134-D, Lotis Lasers) operating at the fundamental wavelength (1064 nm) and delivering two laser pulses of up to 110 mJ per pulse in 15 ns FWHM. In this work, the system was operated on Single-Pulse mode. The maximum pulse repetition rate is 10 Hz. The laser beam is focused into an experimental chamber and the plasma emission is collected by an optical fiber placed at a distance of 1 cm from the sample and at an angle of 45° with respect to the laser beam. The ablation spot is about 300 µm. The system was coupled with an Aryelle 200 Echelle spectrograph (200 nm to 790 nm, LTB Lasertechnick Berlin) coupled with an air-cooled ICCD (iStar DH334T-18F03, Andor), with a resolving power of 9000. The acquisition delay was set to 500 ns after the second laser pulse and the integration time was 10 µs, in accordance with routine LIBS analyses. The spectrometer was calibrated with a Deuterium-Halogen lamp (Ocean Optics DH-2000).

At the University of Alicante, the LIBS instrument used a Nd:YAG laser (Handy-YAG model HYL 101, Q-switched, Quanta System S.P.A., Varese, Italy), operating at the fundamental wavelength with a nominal pulse width of 6 ns FWHM, and a compact time-integrated spectrometer (five channel spectrometer, model AvaSpec-2048-SPU, Avantes, Eerbeek, The Netherlands). The laser is focused on the sample by a 60 mm focal length biconvex lens. The sample is placed on a manually-operated x/y translation stage. Plasma emission is collected and sent to the entrance slit of the five-channel spectrometer by a five-furcated optical fibre (5 ×400 µm fibre optic cable, model FC5-UV400-2, Avantes, Eerbeek, Netherlands), which is positioned at 60° with respect to the incident laser beam and at approximately 2 cm from the sample surface. The ablation spot was estimated at approximately 170 µm. Each measurement is externally controlled by manually triggering the laser firing sequence (i.e. external triggers are sent to the laser flash-lamp and Q-switch) with two pulse generators (Digital delay/pulse generator, model DG 535, Stanford Research Systems, Inc. and 1 MHz–50 MHz pulse/ function generator, model 8116A, Hewlett Packard/Agilent Technologies, Santa Clara, USA). The laser pulse and the spectrometer are further synchronized with the aid of the spectrometer software (AvaSoft©, v8.5.0.0, Avantes, Eerbeek, Netherlands). Each laser pulse had an energy of approximately 180 mJ. LIBS spectra were collected 1.5 µs after the plasma generation, with a 1 ms integration time (set by the manufacturer).

All the LIBS spectra were analyzed using the in-house developed LIBS++ software.

The PLAL setup for the preparation of both the GNS and NPs schematized in Figure 1. The system uses a double pulse Nd:YAG laser (LS-2134D, Lotis) operating at the fundamental wavelength of 1064 nm. The laser was operated in single pulse mode, with a pulse energy around 130 mJ in 25 ns.

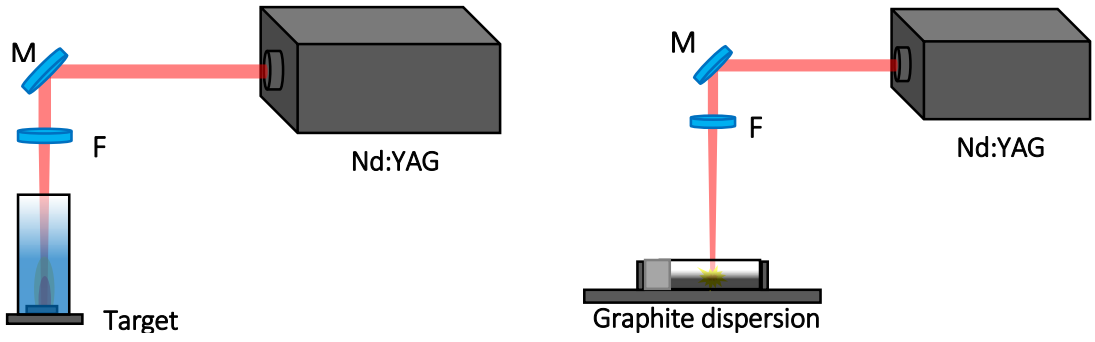

Figure 1 - PLAL instrumental setup for AgNPs synthesis (left) and GNS synthesis (right)

5.2.3 – GNS preparation

The procedure for the preparation of the GNS dispersion was adapted from the work of Pramanik et al [21].

A dispersion of graphite flakes was prepared, having a concentration of 10 mg/mL, using MilliQ water. The dispersion was sonicated until the graphite was fully dispersed (2x30 min sessions). 2 mL of this dispersion were placed in a clear glass vial sealed with plastic screw-caps for headspace analysis. The vial was placed sideways under the path of the laser beam (see Figure 1).

The laser was operated in repetition mode with a shot frequency of 10 Hz, while the pulse was focused inside the liquid. The irradiation time was 5 min and the shock from each laser pulse was sufficient for stirring the dispersion inside the vial. After the irradiation, the vial was removed and allowed to cool down. Built up pressure was vented by inserting a syringe needle into the vial through the cap septum. The irradiation process was repeated three times, for a cumulative irradiation time of 15 min. The dispersion was then sonicated for 30 min (2x15 min sessions with 5min of cooling time in between) at room temperature.

At the end of the preparation procedure, a homogeneous black dispersion was obtained, with no discernible flakes at the naked eye. The dispersions were deposited on a glass slide and analyzed using a Renishaw RM 2000 Raman instrument, coupled with an optical Leica DLML microscope, equipped with a 50x NPLAN objective. The laser source was a He-Ne laser with a wavelength of 633 nm and a laser power output on the sample of about 0.07 mW. Several spectra were registered on different depositions, obtaining perfectly reproducible results. The spectra were compared to those reported in literature [21] [22] [23].

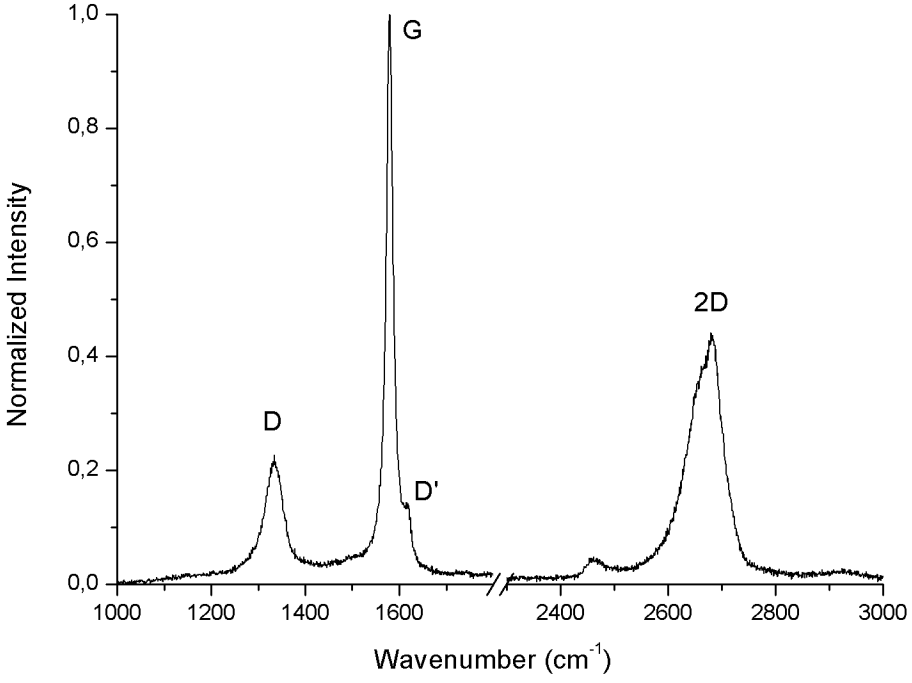

Figure 2 – Normalized Raman spectrum of the prepared GNS deposition

The Raman spectra show the presence of strong G (≈1580 cm^{-1}) and 2D (≈2685 cm^{-1}) bands. The relatively broad, but symmetrical, 2D band confirms the presence of a multilayer structure of graphene, coherent with the deposition methods. Moreover, the presence of the D' (≈1615 cm^{-1}) and of the D (≈1350 cm^{-1}) bands, suggests the introduction of defects in the graphene structure during the PLAL process, such as oxygen- and hydroxyl-containing groups. This is not unwelcome for this work, as it can increase the extraction power of the GNS thanks to the formation of stronger electrostatic bonds with the metal ions in the sample solutions, similar to the behavior observed in the case of graphene oxide [24] [25].

5.3 – Results and Discussion

5.3.1 – Glass substrates and TFME supports optimization

The method chosen for the preparation of the TFME supports was the drop casting of the GNS dispersion on the glass substrates, followed by thermal drying. Other methods of preparation were considered, but ultimately discarded for this work.

A custom dip-coating apparatus was devised and built, with the help of Prof. Hidalgo, in order to test this coating method for the preparation of the TFME supports. The system is composed of an aluminum support structure where 3D printed components are attached. The substrate holder piece is designed to accept multiple substrates in different positions, if necessary. The graphene dispersion in held in a glass vial under constant agitation, in line with the substrate holder. A stepper motor and pulley system, controlled using an Arduino Uno board, is used to accurately raise and lower the glass substrates into the graphene dispersion. The immersion and drying times, as well as the motor speed, are adjusted using a custom Arduino script. Figure 3 shows a picture of the assembled system.

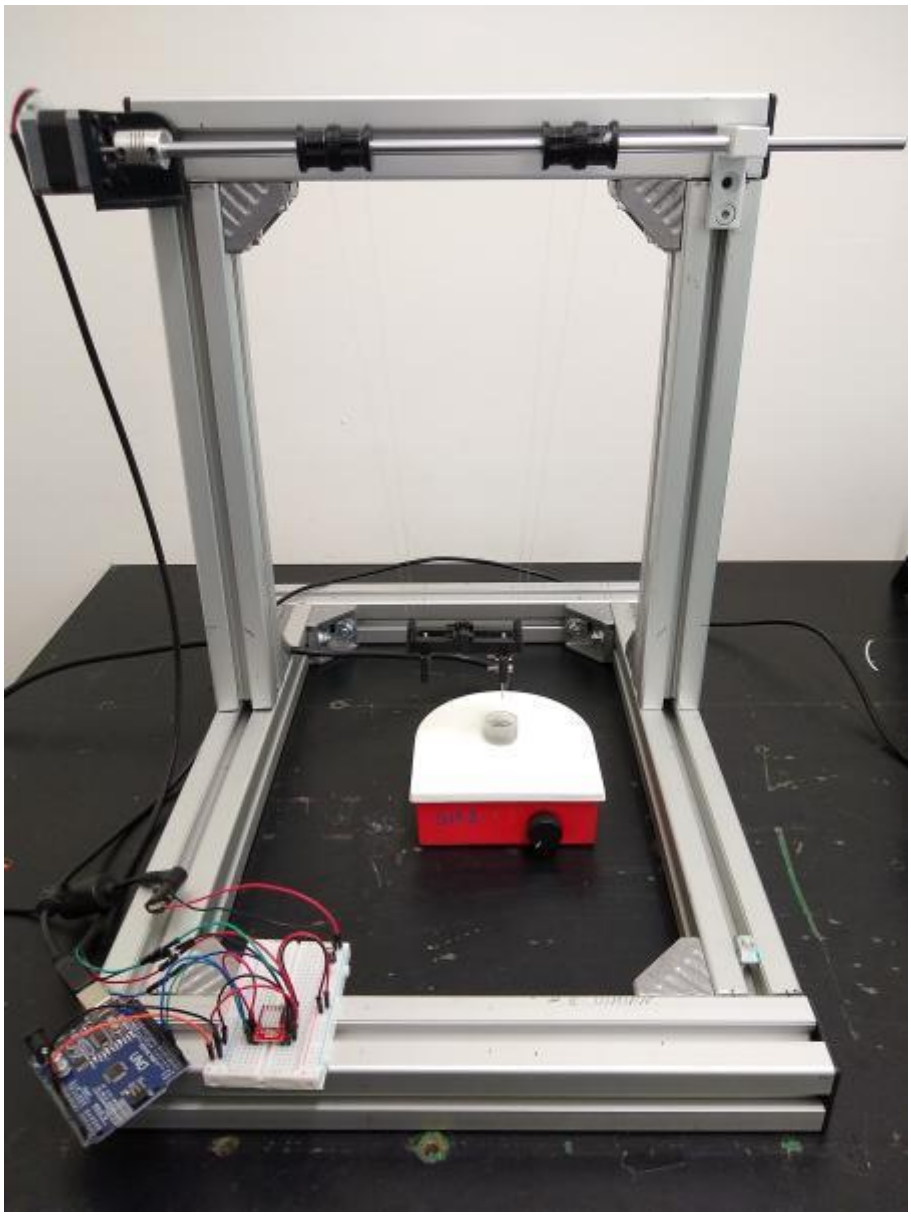

Figure 3 - Home-built dip coating apparatus

Preliminary coating tests conducted using this apparatus showed that the time spent for the preparation of the number of supports required for this study was too inefficient, requiring several hours and several cycles of immersion and drying to obtain just two supports. Moreover, this approach added the disadvantage of a much higher complexity of the preparation procedure.

A similar conclusion was drawn from the consideration of an electrospray (ES) deposition approach for the preparation of the TFME supports, which would have also required a more complex system dedicated to the ES technique. Additionally, spin coating was not employed due to the high volumes of GNS solution required for a homogeneous coating of the substrates.

A preliminary investigation was conducted to identify the ideal type of substrate for preparing TFME supports. Untreated microscope glass slides (suitably cut) were tested alongside mechanically and chemically etched slides.

Mechanical etching was performed using a high-speed rotary tool with an abrasive tip. One face of each substrate was grinded as homogeneously as possible, then washed thoroughly with tap water, deionized water and dried on a hot plate.

Chemical etching was conducted by following the specifications of the manufacturer of the etching paste. In brief, the paste was applied to one side of the glass slides and left to react for 15-20 minutes. Once the etching reaction occurred, the slides were cut to the required dimension, washed and dried.

An example of the etched glasses is reported in Figure 4.

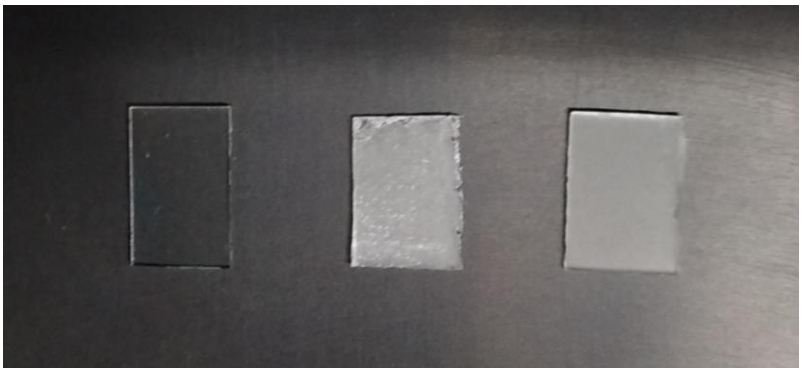

Figure 4 - Different types of glass substrates. Plain glass (left), mechanically etched (center) and chemically etched (right)

To identify the optimal procedure for drying the GNS onto the glass substrates, various methods were tested on both the mechanically and chemically etched substrates. Plain glass slides were used as a benchmark by drop casting 10 µL of GNS on their surface.

Initially it was considered to let the TFME supports dry in open air at room temperature, but this method was soon discarded as the time required was in the order of several hours. Drying using a flow of hot air (using a heat gun or a blow dryer) was tested with some success. The time required to completely dry up the supports was reduced significantly (from hours to tens of seconds). However, it was noticed that the droplets were not drying homogeneously, showing visible “coffee rings” and halos. Moreover, the air flow caused some droplets to deform and occasionally spill out of the substrates.

More promising results were observed while drying the supports on a hot plate. The temperature was set around 90°C to avoid boiling of the liquid. When the supports were placed in direct contact with the plate, however, it was noticed that the drying process was often not

homogeneous. In several tests, the GNS layer cracked and failed to adhere properly to the glass. This was remedied by placing a double layer of paper towel between the substrates and the hot plate surface. This had the effect of slowing down the drying process (which can take up to a minute), making it more homogeneous and less violent. The result was a nearly perfect circular layer of GNS deposited on the glass surface.

This procedure was followed to prepare TFME supports with plain and etched glass slides, and the results are reported in Figure 5. A deposition of 10 µL of graphite on plain glass was added for a visual comparison.

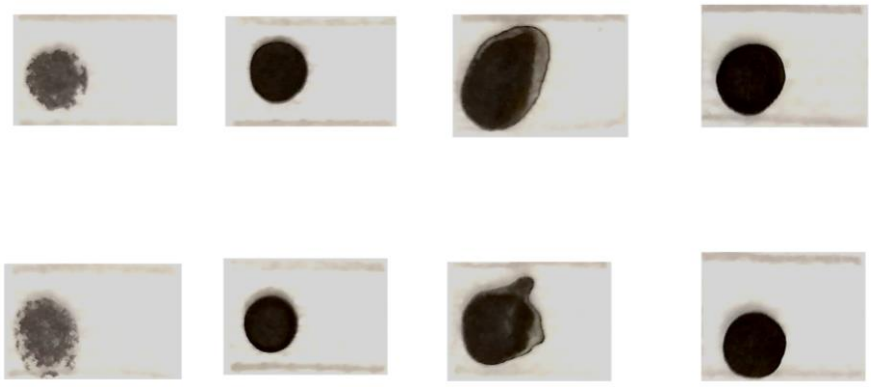

Figure 5 - TFME supports prepared with different glass substrates. From left to right: graphite on plain glass, GNS on plain glass, GNS on mechanically etched glass, GNS on chemically etched glass

As it can be seen, the best results are obtained using plain glass and chemically etched glass. When the GNS are deposited on mechanically etched glass substrates, the droplets do not conserve their shape and tend to dry in a disordered fashion, which can severely hinder the reproducibility of the extraction procedure and LIBS measurement.

To test the stability of the different supports against immersion in a liquid, three of each type were inserted in a plastic vial containing 1,5 mL of H_2O.

It was rapidly observed how the plain glass supports are extremely fragile and unsuitable for TFME, as the GNS layer detached immediately on contact with the water, remaining afloat on the surface (while maintaining the circular structure). Attempts to recover it were unsuccessful. The mechanically etched supports showed a higher tolerance to immersion and manipulation. Nevertheless, this etching procedure cannot produce homogeneous and reproducible patterns, and some supports crumbled and broke off the glass shortly after immersion or upon removal from the vial. The best results were obtained with chemically etched supports. As well as being the most homogeneous, they showed a surprisingly high resilience to manipulation and immersion, remaining intact even after 24h of continued immersion.

As a result, the TFME supports used throughout the study were prepared using chemically etched glass substrates, with drop casting of GNS dispersion, and dried on a hot plate with paper towel partial insulation.

5.3.2 – TFME conditions optimization

To determine the optimal extraction procedure, supports were prepared using 10 µL of GNS. The supports were then immersed on aqueous solutions containing 20 mg/L of Cr (pH ≈ 7) for an increasing amount of time, namely 5, 10, 15, 30 and 60 minutes. After the extraction process, each support was removed from the solution and dried on a hot plate with paper towel insulation for approximately 15 minutes, to ensure complete evaporation of the liquid. Each extraction test was repeated three times and the obtained LIBS spectra were averaged. The results are reported on Figure 6.

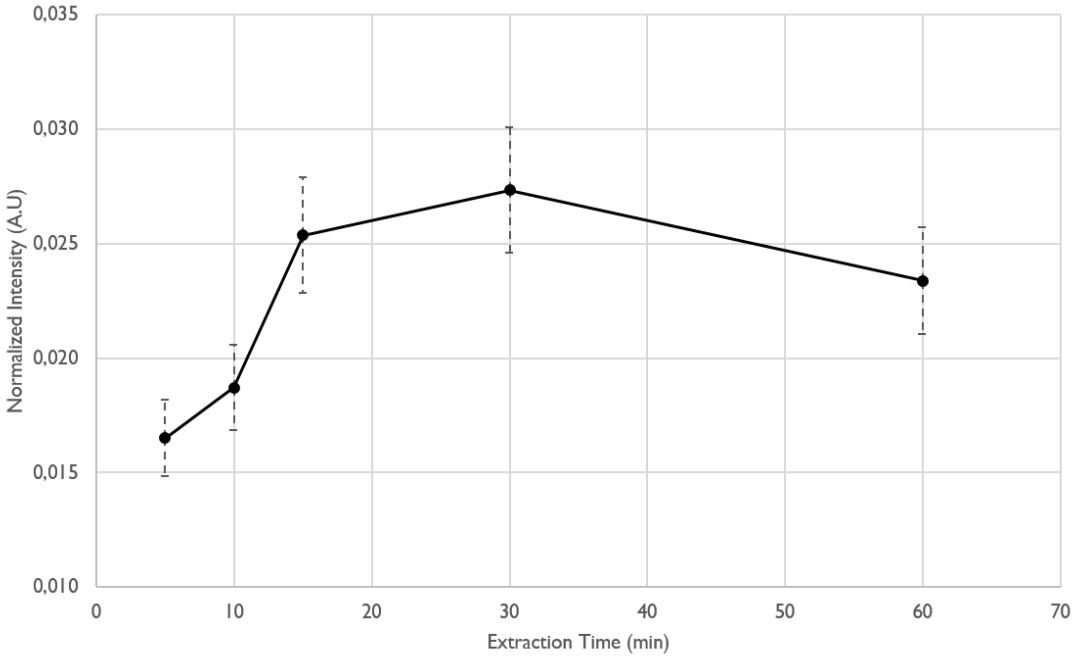

Figure 6 - Normalized intensity of Cr (360,5 nm) depending on the extraction time

The Y-axis in Figure 6 represents the integrated intensity of the Cr I emission line at 360,5 nm, normalized on the total integrated intensity of the spectrum.

It can be observed how there is a pronounced growth of the Cr intensity in the first few minutes of the extraction process. After 15 minutes of immersion, the signal appears to stabilize, with a shallow decline towards 60 minutes of immersion. This can be ascribed to both the saturation of the free sites on the support, where the metal ions can be adsorbed, as well as to the microscopic degradation of the GNS layer due to the prolonged exposure to the aqueous environment.

For this study, an extraction time of 15 minutes was optimal, as it guaranteed a high signal from the analyte, while keeping the extraction time relatively short. The small increase in signal intensity at 30 minutes of extraction was not deemed strong enough to justify doubling the extraction time.

To find the optimal volume of GNS for the preparation of the supports, various drop castings were realized, increasing the deposited volume of GNS in 10 µL aliquots. In theory, a higher volume of adsorbent is always preferable, as it increases the number of binding sites for the analytes, as well as increasing the efficiency of the extraction [26]. In this work however, it was quickly observed that preparing supports with large amounts of GNS was not feasible. 20 µL depositions (2x10 µL aliquots) allowed for the preparation of homogeneous and robust supports, which easily handled the extraction and subsequent manipulations. Increasing the deposition volume to 30 µL (3x10 µL aliquots) caused the formation of disordered flakes and non-homogeneous layers of GNS. Such layers had the tendency of breaking off during the extraction of cracking during the drying process, hindering the LIBS measurement greatly. It was then decided to limit the GNS volume to 20 µL for this study.

New TFME supports were used for building calibration curves from the extraction of Cr aqueous solutions. Five standard solutions with Cr concentration in the range 0,05 mg/L – 1 mg/L were prepared by dilution of a 1000 mg/L chromium stock solution. The extraction procedure was repeated five times for each concentration and the resulting spectra were averaged. The results are shown in Figure 7.

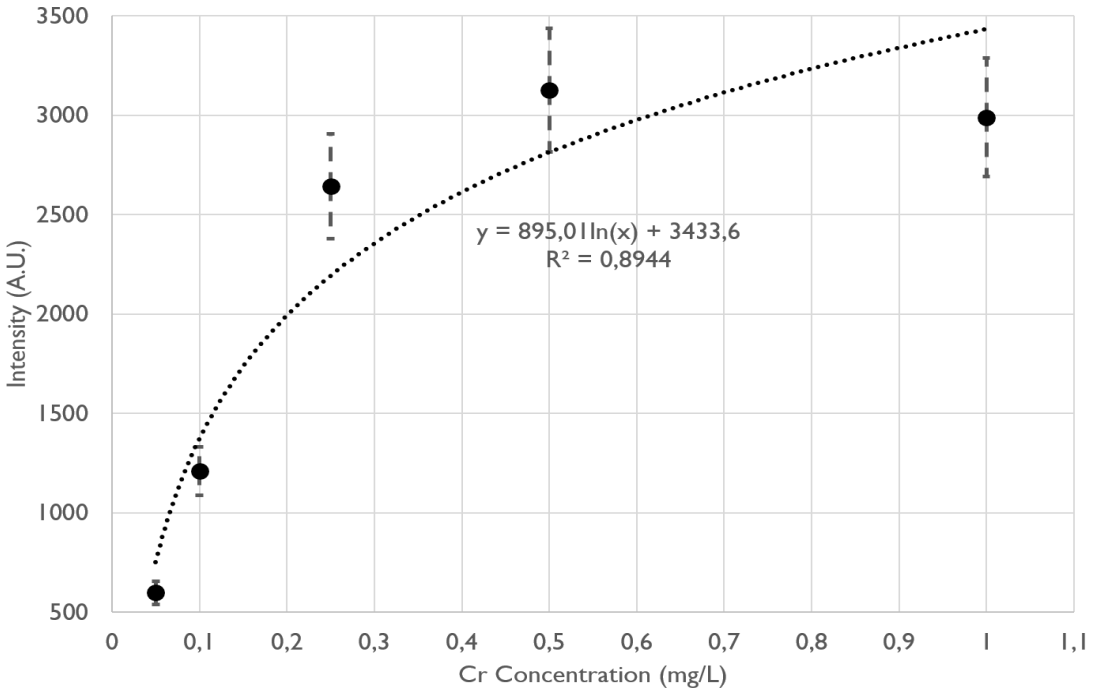

Figure 7 - Calibration curve for Cr

It can be seen how the curve has a logarithmic trend, sharply growing for the first three concentrations and then reaching a plateau for higher concentrations. This can be ascribed to the relatively low volume of GNS that is used to produce the supports. The free sites are rapidly and readily occupied by the metal ions and higher concentrations can saturate the supports during the extraction time. In fact, a similar trend was observed in previous experiments using higher concentrations of Cr (not reported in this manuscript), and the plateau was observed around the same value of concentrations reported here. Nevertheless, the logarithmic curve still shows a value of R^2 = 0,8944.

If the two points relative to the higher concentrations are removed (i.e. 1 mg/L and 0,5 mg/L), the calibration curve becomes linear and reaches a value of R^2 = 0,9971. The LOD for Cr was estimated from the linear calibration curve using the formula $LOD = \frac{3\sigma}{Slope}$ and it was found to be 0,055 mg/L.

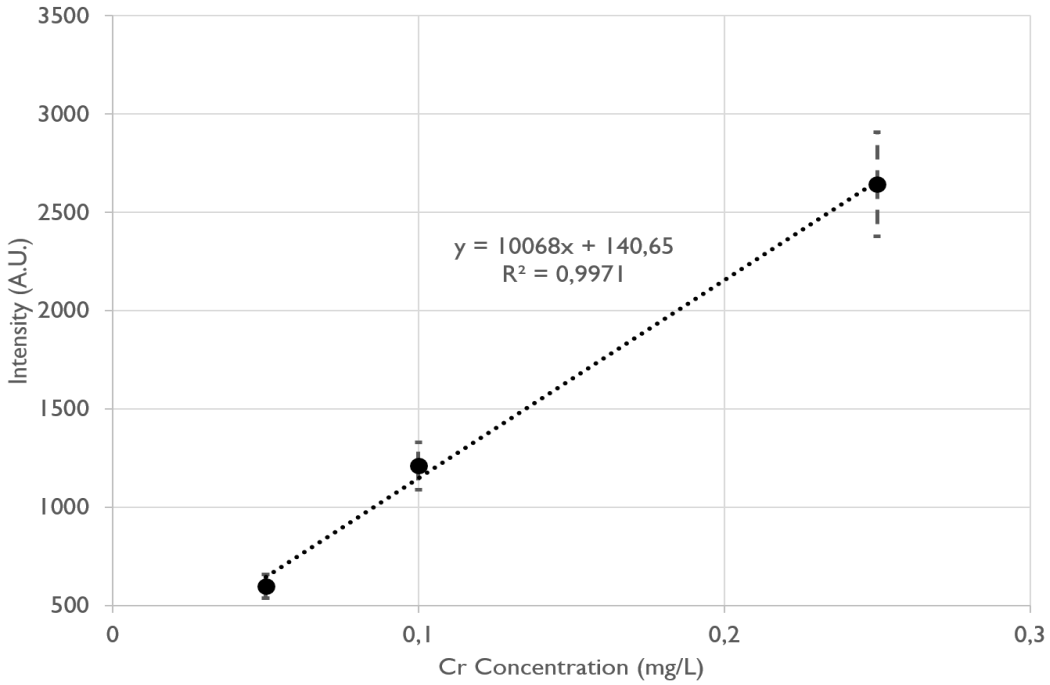

Figure 8 - Calibration curve for Cr (high concentration points removed)

A new batch of supports was used to test their performances towards the extraction of a multielemental aqueous solution. Five multielemental standard solutions containing Cr Ni, Pb and Cu in a concentration range 0,01 mg/L – 0,25 mg/L were prepared by dilution of 1000 mg/L mono-element stock solutions. The extraction procedure was repeated five times for each concentration and the resulting spectra were averaged. The monitored emission lines are reported on Table 1.

Element	Wavelength
Cr I	360,5 nm
Pb I	368,4 nm
Cu I	327,5 nm
Ni I	341,6 nm

Table 1 - Monitored emission lines

Due to the almost complete non-specificity of GNS, it was expected that all analytes would adsorb onto the supports, driven by their mobility, size and electrostatic affinity to the GNS sites. The results are reported in Figure 9. It should be noted that the Ni emission lines were not observed after the extraction, and so are not reported in this Figure.

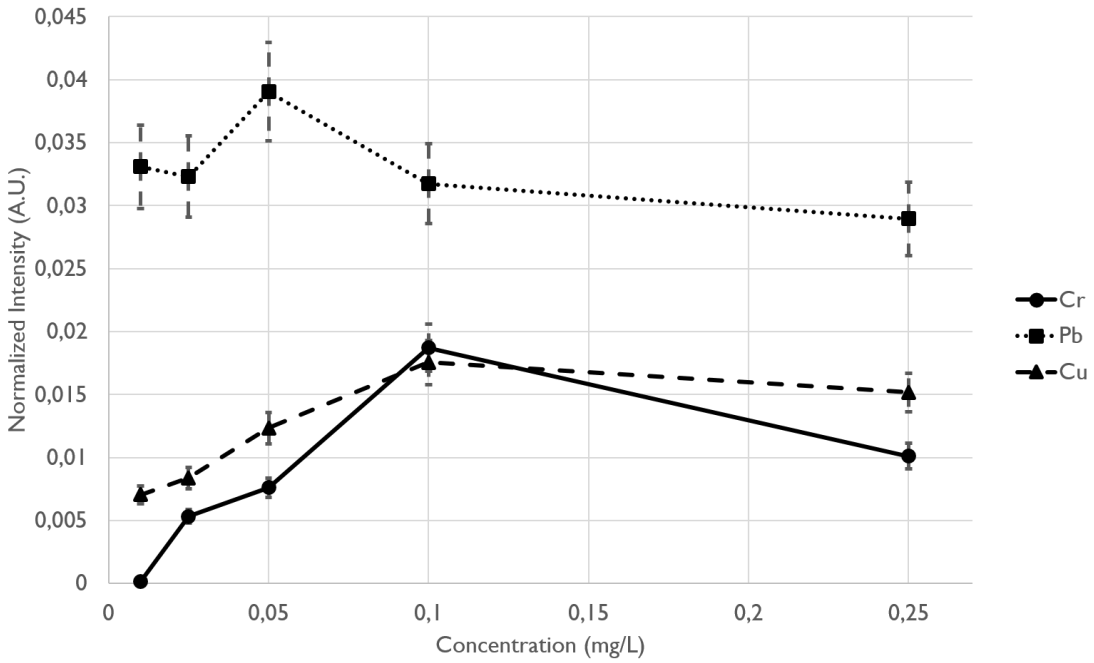

Figure 9 – Normalized line intensity trend for the monitored analytes (see Table XX)

The Y-axis in Figure 9 represents the integrated intensity of the emission lines, normalized on the total integrated intensity of each spectrum.

As it can be seen from the graph, not all analytes follow the same trend with increasing concentration. While Cu and Cr intensities grow from 0,01 mg/L to 0,1 mg/L and then reach a plateau, the intensity of Pb appears to remain more or less constant throughout the experiment. It is likely that the presence of more than one analyte gives rise to competition phenomena for the occupation of GNS sites. In fact, Pb appears to be more prevalent than Cr and Cu, and its constant emission intensity suggests that it is adsorbed faster than the other analytes.

While using larger volumes of GNS for the preparation of TFME supports might help to mitigate this behavior (i.e. by increasing the amount of available sites for the extraction of the analytes), it still does not solve the universal character of GNS as a sorbent. The use of functionalized GNS would allow for the preparation of supports that can be specifically tuned for the extraction of a single analyte, although this method would significantly increase the difficulty of the support preparation procedure.

5.3.3 – NELIBS and TFME coupling

To investigate the possibility of combining the NELIBS approach with the obtained TFME supports, three different methods for the integration of the AgNPs with the GNS.

The first method (Top Deposition, TD) follows the typical procedure of NELIBS, with a deposition of 10 µL AgNP dispersion on top of the GNS support, which is then dried.

In the second method (Bottom Deposition, BD) 10 µL of AgNPs were deposited on a chemically etched glass substrate, dried and the GNS were deposited on top of the nanoparticles. This approach is similar to the SENLIBS technique, described in the work of De Giacomo et al [16].

The last method (Composite, C) that was investigated was the preparation of a composite dispersion of AgNPs and GNS. To prepare the composite a given volume of GNS dispersion was centrifuged to separate the graphene from the solvent, which was removed. The graphene was then dispersed in the same volume of the AgNPs solution, sonicated and then used to prepare the TFME supports by using, as in the previous methods, 10µL of GNS-AgNPs dispersion. The method was tested using various AgNPs concentrations. The results reported in this work refer to the supports that gave the best results, which corresponded to an AgNP concentration of 0,02 mg/mL.

Each type of support was used for the extraction of a 0,2 mg/L Cr solution and the Cr I (360,5 nm) emission line was monitored. The tests were repeated five times and the resulting spectra were averaged. The Enhancement Factor (EF) for NELIBS was obtained as the ratio of the emission intensity of the Cr line between plain GNS supports and the various AgNPs treated supports. The results are reported in Figure 10.

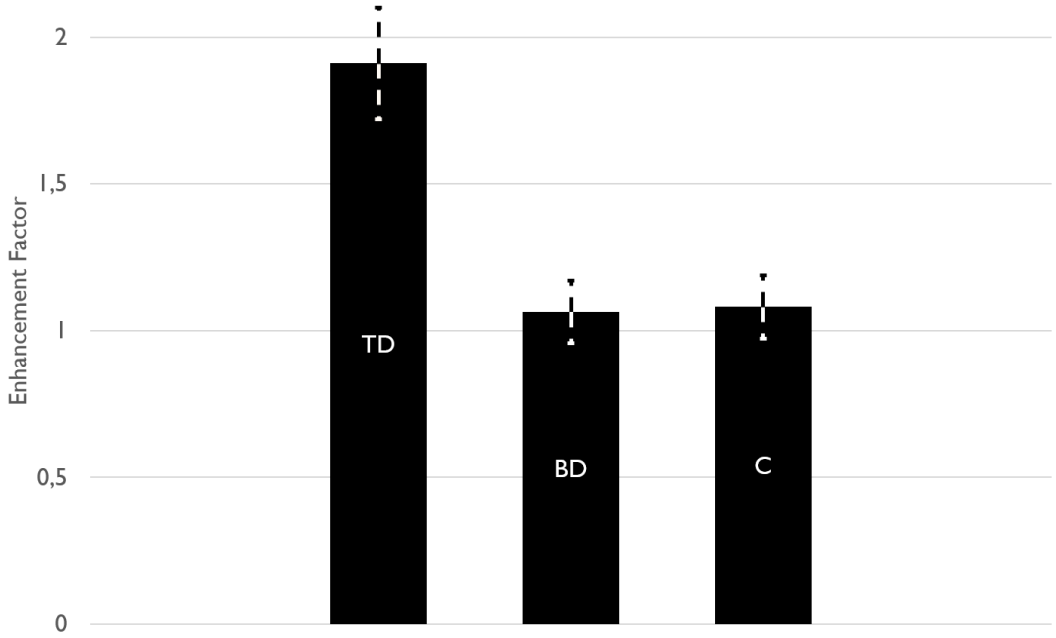

Figure 10 - Signal enhancement for different TFME support types

As reported in the graph, the EF values for both BD and C supports are close to 1, meaning that almost no discernible signal enhancement was observed. In the case of BD, this can be attributed to the complete absorption of the laser pulse by the GNS layer. This effectively prevents the interaction of the laser with the underlying AgNPs, rendering them ineffective. On the other hand, the presence of AgNPs in direct contact with the GNS during the preparation of the C supports can contribute to a partial saturation of the free sites in the graphene by the adsorption of the metal nanoparticles, which would then hinder the extraction of the analytes from the sample solutions.

The highest observed values for EF were obtained for the conventional NELIBS sample preparation method, that is the deposition of AgNPs directly on the GNS films. As such, this method was chosen for the subsequent experiments.

To determine the optimal amount of AgNPs that should be used on the GNS supports, various tests were conducted while increasing the amount of AgNPs (in 10 µL increments) deposited. Each test was repeated five times and the resulting spectra were averaged. A 0,2 mg/L Cr solution was used for the extraction and the Cr I (360,5 nm) emission line was monitored. In Figure 11 are reported the observed values of EF.

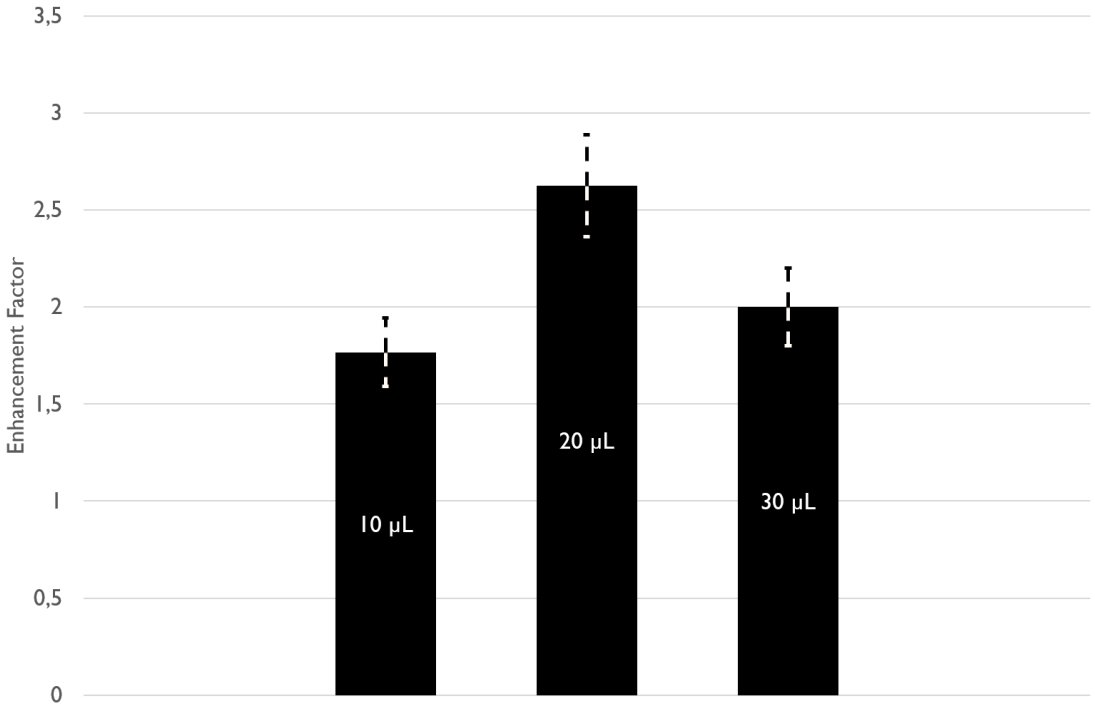

Figure 11 - Signal enhancement for increasing amounts of AgNPs deposited

The highest EF values observed were obtained for an AgNPs deposition of 20 µL (2x10 µL) on the GNS supports. It should be noted that 30 µL (3x10 µL) was chosen as the upper limit because adding more AgNPs to the GNS supports severely compromised their integrity, causing cracks and breaking up the layers.

Using the experimental parameters obtained in the previous tests, the GNS supports combined with a AgNPs deposition were used to build a calibration curve for a Cr. As in the previous section, five Cr standard solutions in the concentration range 0,05 mg/L – 1 mg/L were prepared. The extraction procedure was repeated five times for each concentration and the resulting spectra were averaged. The results are shown in Figure 12, where the calibration curve obtained using plain GNS supports is also reported for comparison.

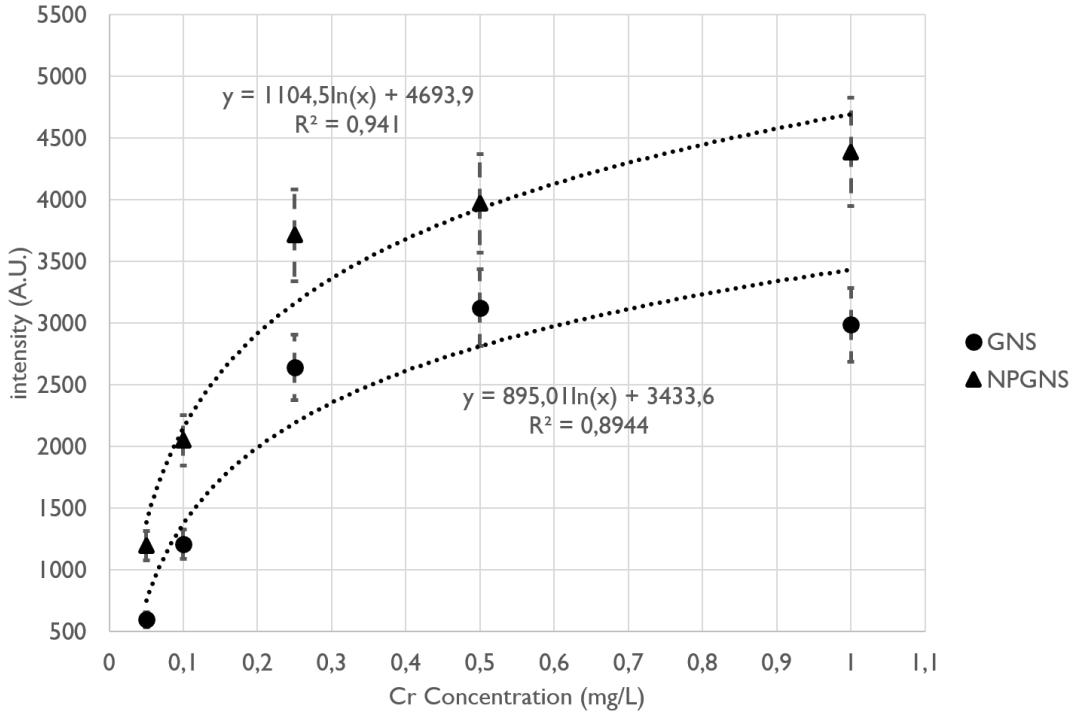

Figure 12 - Calibration curves for Cr of GNS and NPGNS

It can be seen that the calibration curve for Nanoparticle/GNS supports (NPGNS) also has a logarithmic trend, reaching a plateau between 0,3 and 0,5 mg/L of Cr. However, it should be noted that the NPGNS logarithmic curve has a higher R^2 value than the GNS curve, the value being $R^2 = 0,941$.

By removing the two points relative to the higher Cr concentrations, as it was done for the GNS curve, we obtain a linear calibration curve with a value of $R^2 = 0,9905$. The increase in signal enhancement due to the application of the AgNPs also allows for a slightly lower LOD than the one obtained from the GNS calibration. The NPGNS LOD was estimated to be 0,032 mg/L.

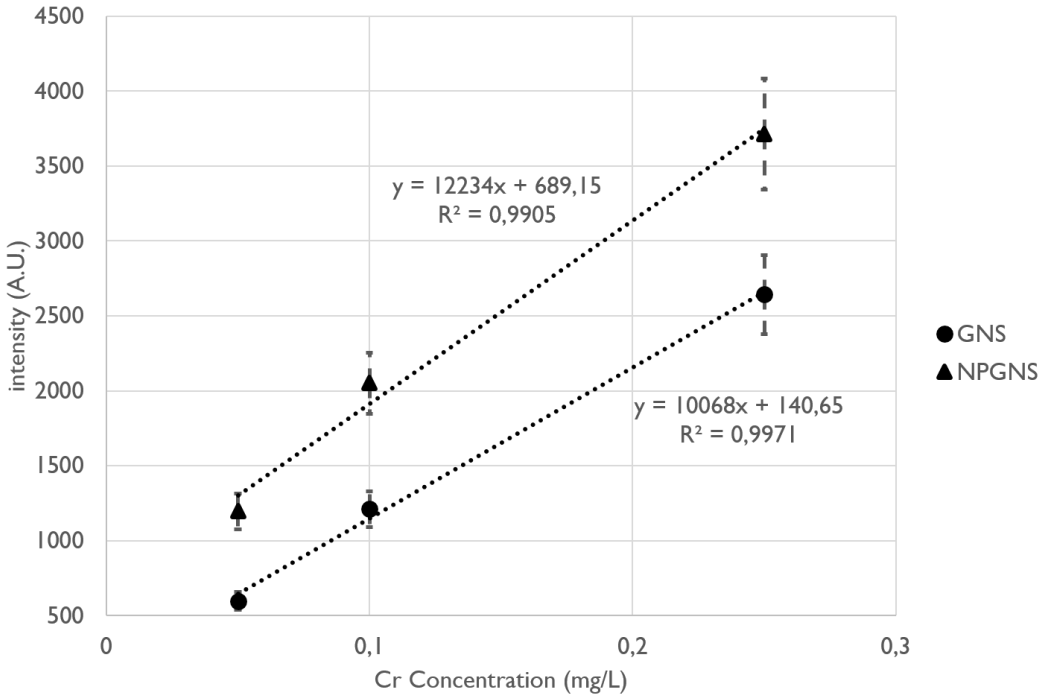

Figure 13 - Calibration curves for Cr (high concentration points removed)

5.3.4 – Enlargement of the measurement spot

One of the considerations that should be taken into account when working with NELIBS is that the laser spot size can greatly influence the magnitude of the signal enhancement that is observed. Indeed, in the works by De Giacomo et al, the laser spot size is large enough so that the entire NP deposition is ablated during the measurement (in the order of mm). Nevertheless, the laser fluence on the sample surface must be kept at a value that is sufficient for the NELIBS effects to take place. This generally requires a laser with a power output that is not common.

In this work, thanks to the higher power output of the laser installed in the LIBS system at the University of Alicante, it was possible to gradually increase the laser spot size on the analyzed samples in order to verify the presence of a further increase in NELIBS performances.

Following the TFME procedure described in the previous sections, several supports were prepared and analyzed using the NELIBS approach. The solutions used for the extraction contained 0,2 mg/L of Cr, and the Cr I (360,5 nm) emission line was monitored. Each measurement was repeated 5 times and the resulting spectra were averaged. The results are reported in Figure 14.

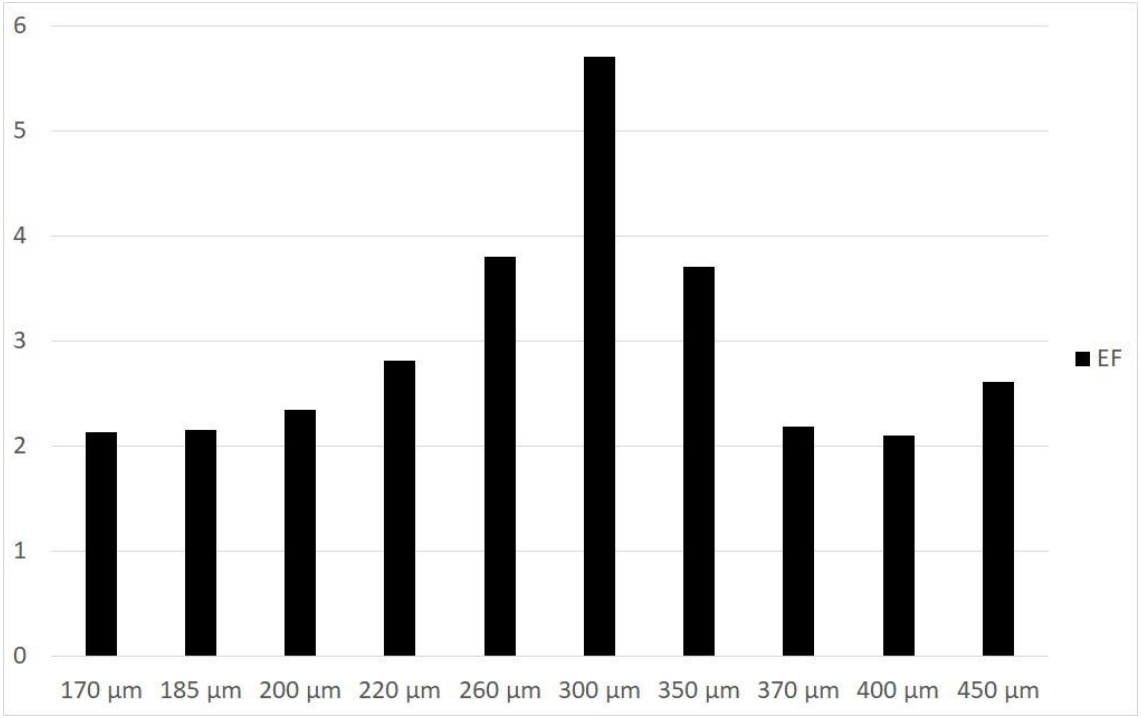

Figure 14 - EF trend as a function of the laser spot size. The laser pulse energy is kept constant throughout

It can be seen how an increase of the laser spot size is followed by an increase in the registered value of EF. Indeed, upon reaching 300 µm, the observed EF reaches almost the value of 6. Further increases of the laser spot size cause a reduction of the registered EF, as well as of the overall spectral intensity. This could be explained by both a decrease of the NELIBS enhancement due to the decreasing laser fluence, and to the decrease of the plasma energy and emission intensity.

5.3.5 – Glass substrate functionalization with APTES

The last section of this work was dedicated to investigating the functionalization of the glass substrates to increase the GNS adhesion and stability during immersion.

The compound that was chosen for this process is APTES (3-Aminopropyl)triethoxysilane). This substance is widely used in literature for the functionalization of both glass and graphene, using similar procedures [27] [28] [29] [30] [31] [32] [33]. Indeed, in some works, it is used for the synthesis of glass fiber/graphene compounds for extraction processes.

Based on the literature, a new procedure for the functionalization of the glass substrates was developed and tested. The same procedure was used to functionalize both plain glass substrates and chemically etched glass substrates.

All the glass substrates were thoroughly cleaned before the procedure using an ultrasound bath. The substrates were sonicated for 5 minutes in acetone, and then for 5 minutes in deionized water. A 3-minute sonication step using a 0,1 M NaOH solution was used to activate the OH

groups on the surface of the substrates. This step was followed by an additional ultrasonic cleaning session of 15 minutes (3 x 5 minutes) in water. The substrates were then allowed to dry under a glass petri dish.

A 1% solution of APTES in ethanol was prepared and heated to 60°C. The substrates were immersed in this solution for 1 hour.

Figure 15 - APTES treatment of glass substrates

Subsequently, the substrates were removed and placed in an oven at 100°C for a 1-hour curing period.

Once ready, the substrates are cut into suitable pieces and treated using both GNS and graphene oxide (GO). The deposition methods that were chosen for this test consists of the drop casting method, already used in this work, and a “passive coating” method, which consists in the immersion of the substrates in a GO or GNS 0,1 mg/mL dispersion, under agitation, for 2 hours. The results are reported in Figure 16.

Figure 16 - Passive coating using GNS (left) and GO (right)

It was observed how the GNS gave rise to a thin film on the glass substrates, even though the low concentration of the solutions did not allow for the formation of a uniform and prominent coating. In the case of GO, instead, a coagulation phenomenon was observed after a few minutes of immersion of the glass substrate, significantly limiting the amount of material that adhered to the glass itself. It was speculated that the cause is an interaction of the amino groups introduced during the functionalization step that, reacting with the functional groups of GO, that induces the aggregation and flocculation. A possible solution to this issue could be the use of a dip-coating procedure, which limits the prolonged exposure of the GO solution to the functionalized glass.

For the drop casting method, many of the expected results were confirmed, also based on observation from previous tests. GNS was able to form homogeneous and resilient films, while GO was unable to adhere to the glass (both plain and etched). Moreover, it was observed how the GNS could adhere perfectly to the functionalized, but not etched, glass.

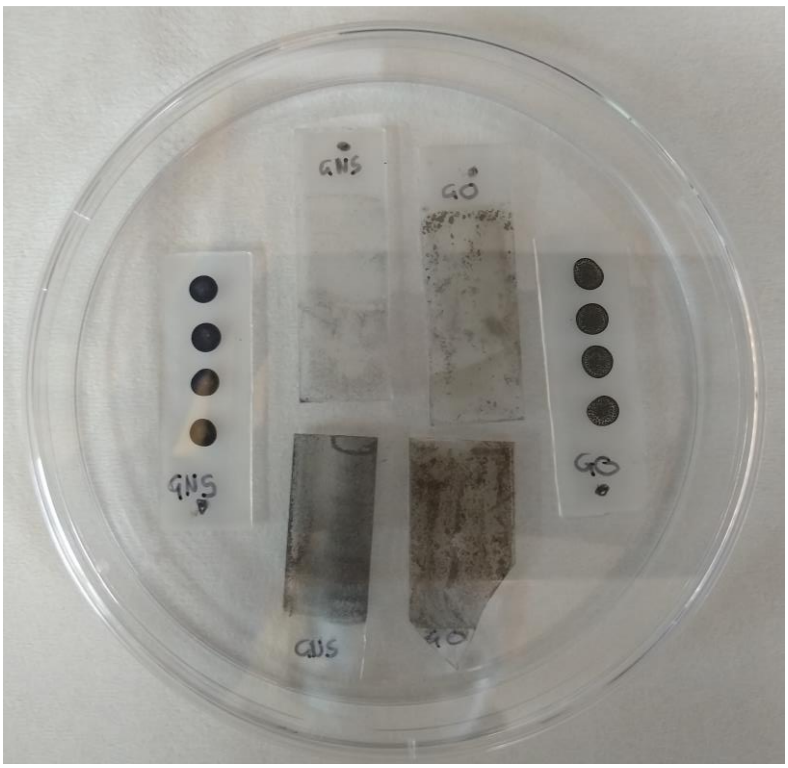

Figure 17 - The coated substrates before the immersion test

To evaluate the stability of these substrates, they were immersed in deionized water for up to 24 hours, and the results are reported in Figure 18.

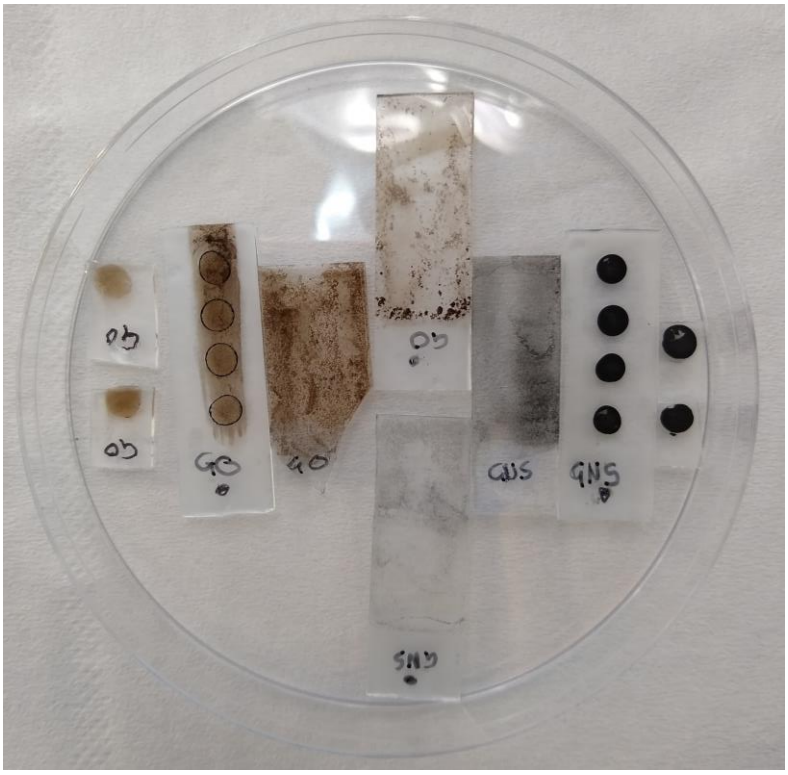

Figure 18 - The coated substrates after the immersion test

It can be seen how the GO supports do not have the stability required to withstand immersion. Indeed, most of the observed damage to the supports occurred during the first few seconds of the immersion in water.

5.4 – Conclusions

A novel approach to the NELIBS technique for the signal enhancement of LIBS was proposed in this work, combining the enhancing effects of the AgNPs with the TFME methodology.

Graphene nanosheets were successfully prepared using a pulsed laser and used for the preparation of TFME supports. Various kinds of glass substrates were tested and the procedure for the preparation of the TFME supports was optimized. This allowed for the LIBS analysis of metals in liquid samples, obtaining sub-ppm LODs. Moreover, it was demonstrated that NELIBS can be coupled with TFME to allow for the obtainment of even lower LODs.

Nevertheless, further studies should be carried out to further optimize the methodology, investigating different deposition methods for both the GNS and the AgNPs. In particular, the preparation of a ready-to-use AgNP/GNS composite would further simplify the procedure, enabling the use of this technique for in-situ and online measurements. In addition, the use of functionalized GNS and graphene is also worthy of investigation, for the preparation of ad-hoc TFME supports for pre-determined analytes.

Furthermore, it was demonstrated that the registered EF increased when increasing the dimensions of the laser measurement spot. The use of a more powerful laser would, in theory, allow for the obtainment of even higher EF values, and should also be investigated.

Finally, a procedure for the functionalization of the glass substrates was proposed and tested. The APTES treatment allowed for a much higher stability of the GNS TFME supports, while no observable improvement was found for GO TFME supports. Also in this case, it could be worth investigating different deposition strategies, particularly dip coating. This could allow for the preparation of much more homogeneous and large substrates, which could boost the TFME performances greatly. Indeed, a thorough optimization of this technique would be necessary, to improve the preparation times and simplify the preparation processes.

Bibliography

[1] A. Miziolek, V. Palleschi and I. Schechter, Laser Induced Breakdown Spectroscopy (LIBS): Fundamentals and Applications, Cambridge: Cambridge University Press, 2006.

[2] S. Musazzi and U. Perini, Laser-Induced Breakdown Spectroscopy: Theory and Applications, Springer, 2014.

[3] Y. Li, D. Tian, Y. Ding, G. Yang, K. Liu, C. Wang and X. Han, "A review of laser-induced breakdown spectroscopy signal enhancement," *Applied Spectroscopy Reviews,* vol. 53, no. 1, pp. 1-35, 2018.

[4] D. A. Cremers and J. L. Radziemski, Handbook of Laser Induced Breakdown Spectroscopy, West Sussex: John Wiley & Sons, 2006.

[5] N. Aras and S. Yalcin, "Development and validation of a laser-induced breakdown spectroscopic method for ultra-trace determination of Cu, Mn, Cd and Pb metals in aqueous droplets after drying," *Talanta,* vol. 149, pp. 53-61, 2016.

[6] S. Niu, L. Zheng, A. Q. Khan, G. Feng and H. Zeng, "Laser indced breakdown spectroscopic detection of trace level heavy metal in solution on a laser pretreated metallic target," *Talanta,* vol. 179, pp. 312-317, 2018.

[7] L. Fang, N. Zhao, M. Ma, D. Meng, Y. Jia, X. Huang, W. Liu and J. Liu, "Detection of heavy metals in water samples by laser induced breakdown spectroscopy combined with annular groove graphite flakes," *Plasma Science and Technology,* vol. 21, 2018.

[8] L. Ripoll and M. Hidalgo, "Electrospray deposition followed by laser induced breakdown spectroscopy (EDS-LIBS): a new method for trace elemental analysis of aqueous samples," *Journal of Analytical Atomic Spectrometry,* vol. 34, pp. 2016-2026, 2019.

[9] S. Ma, Y. Tang, Y. Ma, Y. Chu, F. Chen, Z. Hu, Z. Zhu, L. Guo, X. Zeng and Y. Lu, "Determination of trace heavy metal elements in aqueous solution using surface-enhanced laser-induced breakdown spectroscopy," *Optics Express,* vol. 27, no. 10, pp. 15091-15099, 2019.

[10] X. Wang, L. Shi, Q. Lin, X. Zhu and Y. Duan, "Simultaneous and sensitive analysis of Ag(I)m Mn(II) and Cr(III) in aqueous solutions by LIBS combined with dispersive solid phase micro-extraction using nano-graphite as an adsorbent," *Journal of Analytical Atomic Spectrometry,* vol. 29, pp. 1098-1104, 2014.

[11] F. J. Ruiz, L. Ripoll, M. Hidalgo and A. Canals, "Dispersive micro solid-phase extratction (DμSPE) with graphene oxide as adsorbent for sensitive elemental analysis of aqueous samples by laser induced breakdow spectroscopy (LIBS)," *Talanta,* vol. 191, pp. 162-170, 2019.

[12] L. Ripoll, J. Navarro-Gonzalez, S. Legnaioli, V. Palleschi and M. Hidalgo, "Evaluation of thin film microextraction for trace elemental analysis of liquid samples using LIBS detection," *Talanta,* vol. 223, 2021.

[13] L. Ripoll, S. Legnaioli, V. Palleschi and M. Hidalgo, "Evaluation of electrosprayed graphene oxide coatings for elemental analysis by thin film microextraction followed by laser induced breakdown spectroscopy detection," *Spectrochimica Acta Part B: Atomic Spectroscopy,* vol. 183, 2021.

[14] A. De Giacomo, R. Gaudiuso, C. Koral, M. Dell'Aglio and O. De Pascale, "Nanoparticle-enhanced laser-induced breakdown spectroscopy of metallic samples," *Spectrochimica Acta Part B: Atomic Spectroscopy,* vol. 85, no. 21, pp. 10180-10187, 2013.

[15] M. Dell'Aglio, R. Alrifai and A. De Giacomo, "Nanoparticle Enhanced Laser Induced Breakdown Spectroscopy (NELIBS), a first review," *Sepctrochimica Acta Part B: Atomic Spectroscopy,* vol. 148, pp. 105-112, 2018.

[16] A. De Giacomo, C. Koral, G. Valenza, R. Gaudiuso and M. Dell'Aglio , "Nanoparticle Enhanced Laser-Induced Breakdown Spectroscopy for Microdrop Analysis at subppm Level," *Analytical Chemistry,* vol. 88, no. 10, p. 5251–5257, 2016.

[17] X. Wen, Q. Lin, G. Liu, Q. Shi and X. Duan, "Emission enhancement of laser-induced breakdown spectroscopy for aqueous sample analysis based on Au nanoparticles and solid-phase substrate," *Applied Optics,* vol. 55, no. 24, pp. 6706-6712, 2016.

[18] A. Botto, B. Campanella, I. Degano, S. Legnaioli, G. Lorenzetti, S. Pagnotta, F. Poggialini and V. Palleschi, "Direct analysis of anthraquinone dyed textiles by Surface Enhanced Raman Spectroscopy and Ag nanoparticles obtained by pulsed laser ablation," *European Physics Journal Plus,* vol. 134, p. 414, 2019.

[19] D. Paramelle, A. Sadovoy, S. Gorelik, P. Free, J. Hobley and D. G. Fernig, "A rapid method to estimate the concentration of citrate capped silver nanoparticles from UV-visible light spectra," *Analyst,* vol. 139, pp. 4855-4861, 2014.

[20] A. Bertolini, G. Carelli, F. Francesconi, M. Francesconi, L. Marchesini, P. Marsili, F. Sorrentino, G. Cristoforetti, S. Legnaioli, V. Palleschi, L. Pardini and A. Salvetti, "Modi: a new mobile instrument for in situ double-pulse LIBS analysis," *Analytical and Bioanalytical Chemistry,* vol. 385, pp. 240-247, 2006.

[21] A. Pramanik, S. Karmakar, P. Kumbhakar, S. Biswas, R. Sarkar and P. Kumbhakar, "Synthesis of bilayer graphene nanosheets by pulsed laser ablation in liquid and observation of its tunable nonlinearity," *Applied Surface Science,* vol. 449, 2020.

[22] V. N. Popov, "2D Raman band of single-layer and bilayer graphene," *Journal of Physics: Conference Series,* vol. 682, 2016.

[23] L. M. Malard, M. A. Pimenta, G. Dresselhaus and M. S. Dresselhaus, "Raman spectroscopy in graphene," *Physics Reports,* vol. 473, pp. 51-87, 2009.

[24] I. Duru, D. Ege and A. R. Kamali, "Graphene oxides for removal of heavy and precious metals from wastewater," *Journal of Material Science,* vol. 51, no. 13, pp. 6097-6116, 2016.

[25] F. Perreault, A. F. De Faria and M. Elimelech, "Environmental applications of graphene-based nanomaterials," *Chemical Society Reviews,* vol. 44, no. 16, pp. 5861-5896, 2015.

[26] J. Pawliszyn, Handbook of Solid Phase Microextraction, Elsevier, 2012.

[27] S. Ferraris, A. Nommeots-Nomm, S. Spriano, E. Vernè and J. Massera, "Surface reactivity and silanization ability of borosilicate and Mg-Sr-based bioactive glasses," *Applied Surface Science,* vol. 475, pp. 43-55, 2019.

[28] S. Dowlatshah, A. Ghiasvand, A. Barkhordari and V. Jalili, "Layer-by-Layer Coating of Graphene Oxide on Fused Silica Fibers for Headspace Sampling of Nicotine in Hair Samples," *Analytical and Bioanalytical Chemistry,* vol. 8, no. 1, pp. 15-25, 2020.

[29] E. Vernè, S. Ferraris, C. Vitale-Brovarone, S. Spriano, C. L. Bianchi, A. Naldoni, M. Morra and C. Cassinelli, "Alkaline phosphatase grafting on bioactive glasses and glass ceramics," *Acta Biomaterialia,* vol. 6, pp. 229-240, 2010.

[30] E. Verné, C. Vitale-Brovarone, E. Bui, C. L. Bianchi and A. R. Boccaccini, "Surface functionalization of bioactive glasses," *Wiley Periodicals,* 24 July 2008.

[31] J. Arreola, M. Matzkow, M. Palomar Duràn, A. Greeff, M. Kausgen and M. J. Schoning, "Optimization of the immobilization of bacterial spores on glass substrates with organosilanes," *Physica Status Solidi A,* vol. 213, no. 6, pp. 1463-1470, 2016.

[32] S. Li, Z. Wang, J. Jia, C. Hou, X. hao and H. Zhang, "Preparation of Hydroxyl and (3-aminopropyl) Triethoxysilane Functionalized Multiwall Carbon Nanotubes for Use as Conductive Fillers in the Polyurethane Composite," *Polymer Composites,* pp. 1212-1222, 2018.

[33] X. Yin and J. Bao, "Glass fiber coated with graphene constructed through electrostatic self-assembly and its application in poly(lactic acid) composite," *Journal of Applied Polymer Science,* p. 43296, 2015.

Chapter 6:

Time-Independent Extended C-Sigma (TIECS) for the determination of spectroscopic parameters from LIBS measurements

Chapter 6 – Index

6 – Time-Independent Extended C-Sigma (TIECS) for the determination of spectroscopic parameters from LIBS measurements

6.1 – Introduction

The central part of a LIBS analysis is the characterization and study of the laser-induced plasma (LIP). Naturally, this kind of study tends to be simpler if only optically thin spectral lines are encountered. This is usually not the case in most LIBS analysis, where self-absorption phenomena are encountered. This is especially true in the case of very intense LIBS signals, which are generally caused by high plasma temperature or by plasma rich in optically active species. This phenomenon can make studying the plasma and spectral parameters a much more difficult process.

Indeed, in the works presented in the previous chapters, the monitored emission lines that were chosen in each study had to keep the presence of self-absorption into account. This is particularly true when studying, for example, copper samples. The strongest emission lines for Cu, located at 324,7 nm and 327,4 nm, are also the ones that are more affected by self-absorption. This precludes their use for analytical purposes in most cases, as their intensity cannot be readily correlated to the concentration of the analyte in the analyzed samples.

Having access to a method that could determine the extent of self-absorption phenomena on a LIBS emission line, starting from the experimental data, would greatly help in the extraction of analytical (as well as spectroscopic) information from the registered LIBS spectra.

In this chapter, the work performed in collaboration with the ALS-Lab research group of ICCOM-CNR will be presented. We developed a new method, based on the previously established Extended C-Sigma method [1], called Time-Independent Extended C-Sigma. This method allows for the construction of a model that interprets experimental parameters (e.g. plasma temperature, electron density, line intensity) and calculates the extent of the effects of self-absorption on the experimentally measured linewidth of spectral lines in LIBS spectra.

6.1.1 – Principles of the C-Sigma method

The spectroscopic analysis of laser-induced plasmas can provide useful information about some fundamental plasma parameters, such as transition probabilities [2] [3] [4] [5] and Stark broadening coefficients [6] [7] [8]. The procedure seems to be straightforward since, in the approximation of optically thin [9], homogeneous plasma in Local Thermal Equilibrium [10], the transition probability of a line emitted by a given element may be obtained by simply comparing

the measured line intensity with that of an emission line of the same species, whose transition probability is known:

$$A_{ki} = \frac{I}{I^{ref}} \frac{g_k^{ref}}{g_k} A_{ki}^{ref} e^{-\frac{E_k^{ref} - E_k}{k_B T}} \qquad \text{Equation 6.1}$$

where E_k is the energy of the upper level of the transition, E_k^{ref} is the intensity of the reference line, g_k and g_k^{ref} are the degeneracies of the upper level, k_B is the Boltzmann constant and T is the plasma electron temperature, which has to be determined independently. When more than one reference line is available, the determination of the unknown A_{ki} can be obtained from the Boltzmann plot as the value that brings the corresponding point in the plot on top of the best fit line of the other experimental points, as a function of the energy of the upper level of the transition. In this case, the logarithm of the line intensity is involved.

The determination of the Stark broadening coefficient [11] ω_S seems to be even simpler, since the measurement involves the determination of the emission line width that, under proper conditions, can be expressed as:

$$\Delta\lambda = \omega_S n_e \qquad \text{Equation 6.2}$$

where n_e is the electron number density, which must be determined independently (typically, by measuring the Stark broadening of another line whose ω_S coefficient is known):

$$\omega_S = \omega_S^{ref} \frac{\Delta\lambda^{ref}}{\Delta\lambda} \qquad \text{Equation 6.3}$$

or using the broadening of the Hydrogen Balmer alpha line [12].

It should be noted that the calculation of the electron number density from the Stark broadening of emission lines does not rely on the existence of Local Thermal Equilibrium conditions in the plasma. Nevertheless, the conditions of an optically thin, homogeneous plasma must be fulfilled, in order to be able to determine the A_{ki}coefficients using Eq. (6.1) or the Boltzmann plot.

Generally, during LIBS measurements, reasonably homogeneous plasmas in conditions close to Local Thermal Equilibrium are obtained. However, the issues related to self-absorption are not easily resolved, since these effects are intrinsic in the physics of plasma. Moreover, the optimal conditions for achieving Local Thermal Equilibrium are not optimal for minimizing the self-absorption effects, and vice-versa.

Starting from these considerations, several authors have recently proposed methods which take into account the presence of self-absorption in the laser plasmas [1]. Safi et al have proposed an extension of the C-Sigma method introduced by Aguilera and Aragon [13], which can be applied

also in case of very strong self-absorption and guarantees the linearity of the C-Sigma plot for all the values of the self-absorption parameter. The formulation of the Extended C-Sigma approach can be summarized briefly as follows.

The spectral line intensity can be associated to the plasma temperature using the equation:

$$I = \beta N g_k A_{ki} \frac{e^{-\frac{E_k}{k_B T}}}{U(T)} \qquad \text{Equation 6.4}$$

where β is a factor taking into account the efficiency of the spectral detector, N is the number density of the emitting species and $U(T)$ is the partition function for the species at the temperature T.

6.4 is the optically thin plasma approximation of a more general expression, called a Curve of Growth (COG), describing the propagation of radiation in a homogeneous plasma column of length l:

$$I = \beta B(\lambda_0) \int_{LINE} \left(1 - e^{-k(\lambda) l}\right) d\lambda \qquad \text{Equation 6.5}$$

where $B(\lambda_0)$ is the black-body emission at the center of the line λ_0 and $k(\lambda)$ is given by:

$$k(\lambda) = \frac{\pi e^2 \lambda_0^2}{mc^2} f N g_i \frac{e^{-\frac{E_i}{k_B T}}}{U(T)} \mathcal{L}(\lambda) \qquad \text{Equation 6.6}$$

In Eq. (6.6), m and e are the electron mass and charge, c is the speed of light, f is the oscillator strength of the transition, g_i and E_i are the degeneracy and the energy of the lower level of the transition and $\mathcal{L}(\lambda)$ is the normalized lineshape, which in LIBS conditions can be typically approximated with a Lorentzian curve.

In their work, Aguilera and Aragòn [13] modeled the plasma inhomogeneity using two different distributions (one for ions and one for neutral atoms) having two different temperatures. The generalized COG found by the authors is:

$$\frac{I}{B(\lambda_0)} \frac{l}{\Delta\lambda_0} = f(C\sigma_l, \Delta\lambda_0) \approx f(C\sigma_l) \qquad \text{Equation 6.7}$$

The term σ_l is the absorption cross section (i.e. absorption coefficient per atom/ion). It is a parameter that approximates the absorption of radiation in the plasma by the sample atoms as a series of “opaque” discs, defined as:

$$\sigma_l = \frac{k_l}{N_a} = \frac{\tau_l}{10^{-2} C N l} \qquad \text{Equation 6.8}$$

Where k_l is the effective absorption coefficient and τ_l the effective optical depth. C is the species concentration, N is the species density and l is the LOS optical length. This method has the

advantage of being widely applicable while having almost no restrictions. It is, however, a fairly complicated approach, as the model contains an integral part that has to be solved by recursive analysis of the experimental data in order to obtain the C-Sigma plot.

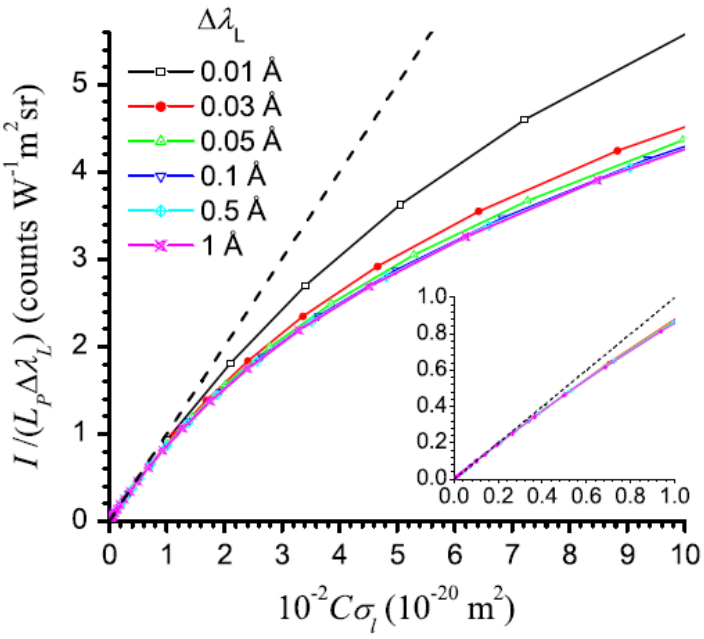

Figure 1 - Example of a C-Sigma plot. Reprinted from [13]

The method by Cristoforetti and Tognoni [14] introduces a new parameter called columnar density. Moreover, the optical depth, τ_l, is calculated from experimental data. The authors were able to build a linear Columnar Density Saha-Boltzmann, instead of the non-linear C-Sigma plot. Indeed, the proposed method allows for a much simpler calculations and fit of the experimental data but it can only be applied to optically thick spectral lines.

Using these considerations and making explicit the integral over the line in Eq. (6.5), Safi et al [1] were able to propose a simplification of the generalized COG model using the experimental line width. It was demonstrated that:

$$\frac{I}{B(\lambda_0)}\frac{\overline{\Delta\lambda}}{(\Delta\lambda_0)^2} = \beta\tau_i = 10^{-2}\beta C_S\sigma_l Nl \qquad \text{Equation 6.9}$$

where Nl is the columnar density [14] of the element, C_S is the concentration of the species considered and σ_l is the absorption cross-section averaged along the line profile.

Therefore, an Extended C-Sigma plot can be obtained by plotting on the y-axis the quantity on the left side of Eq. (6.9). both the line intensities I and the linewidths $\overline{\Delta\lambda}$ can be experimentally determined. The dependence of the left term is linear on $C_S\sigma_l$. This makes the fit of the experimental data fast and accurate, allowing an easier calculation of the plasma parameters with respect to the original formulation of the method.

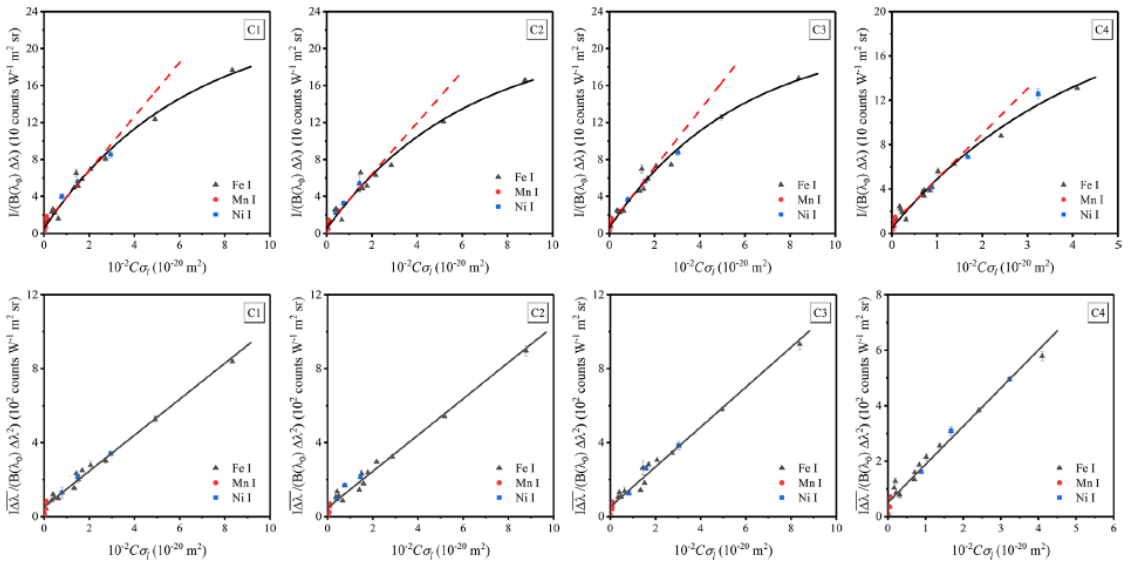

Figure 2 - C-Sigma (top) and Extended C-Sigma (bottom) plots, showing the linearity of the ECS model. Reprinted from [1]

However, the knowledge of the optically thin linewidths $\Delta\lambda_0$ is still required for the calculation of the C-Sigma ordinate. This means that the Stark broadening coefficients of the emission lines must be known for determining $\Delta\lambda_0$.

This work demonstrates how it would be possible, by acquiring LIBS spectra at different times after the onset of the plasma, to obtain the Stark coefficients of emission lines whose transition probabilities are known. Vice versa, a similar procedure can be used for the determination of the transition probabilities of emission lines whose Stark coefficients are known.

6.1.2 – Principles of the Time Independent Extended C-Sigma method

From Eq. (6.9) it can be deduced that the slope of the Extended C-Sigma plot is proportional to the columnar density Nl of the studied element. The element number density N remains constant in time, but the size of the plasma increases due to its expansion. As a result, it would be impossible to plot on the same curve the data obtained at different delay times, without knowing the value of the corresponding plasma size $l(t)$ at different times. Nevertheless, literature shows [15] that a plasma formed in air, after an initial fast expansion in the first hundreds of nanoseconds, can be considered stationary at longer time delays. Cristoforetti et al. [16] demonstrated that in conditions similar to the ones used in this work, the diameter of a laser-induced plasma in air stabilizes at a value around 2 mm about 500 ns after the laser pulse. Therefore, it would be safe to assume that in similar conditions $l(t) \cong l_{MAX}$ for $t \cong 500\ ns$, and that this value would remain almost constant at longer times.

Another point to consider is that the concentration of the neutral and ionic species varies with time according to the Saha-Eggert [17] relation, and can be expressed as:

$$C_S = \frac{1}{1 + \frac{C_S^{II}}{C_S^I}} \quad neutral\ species$$

$$C_S = \frac{C_S^{II}}{C_S^I(1 + C_S^{II}/C_S^I)} \quad ionic\ species$$

Equation 6.10

From these considerations, all the experimental data acquired at different delays can be placed on a single TIECS plot. The points corresponding to a few optically thin lines can be used as reference, from which it is possible to calculate the plasma temperature and the electron number density at the different time delays. After this curve is defined, the ordinates of the optically-thick lines can be calculated to have their corresponding points lie on the previously determined curve, having as the only free parameter the Stark broadening value. This parameter should be considered independent of the temperature, inside of the range considered. Each emission line would be plot n times, with n equal to the number of different delays considered. This means that acquiring the spectra at many different delays would improve the precision in the final estimation of the Stark coefficients. In addition, the comparison of the different values of the Stark coefficient would allow for easier spotting of anomalies that could be caused by the failure of some of the assumptions (i.e. homogeneous and stationary plasma in LTE).

Additionally, it should be noted that the TIECS method could also be used for the determination of the composition of an unknown sample, provided all the spectral parameters are already known (i.e. when well-known spectral lines are monitored). The mathematical procedure is similar to that used for the determination of the Stark coefficients. Once the general TIECS plot has been built using a sample of known concentration and lines with known spectral parameters, a series of measurements could be performed on an unknown sample. Then, instead of using the w_s parameter as a free variable (or the A_{ki}), the concentration of the species in the plasma can be adjusted until the value that brings the experimental points on the TIECS curve is found. This would allow for quantitative analyses with LIBS when strong self-absorption phenomena are observed. Nevertheless, this method assumes a stoichiometric composition of the plasma (i.e. the concentration of the species in the plasma is equivalent to those in the sample) and the possibility of performing measurements with different time delays of the same sample.

6.2 – Materials and Methods

6.2.1 – Instrumentation

LIBS measurements were performed using the system schematized in Figure 3. The system was equipped with a Nd:YAG laser having a pulse energy of up to 100 mJ in 20 ns. The laser pulse was

focused on the sample by a plano-convex lens with a focal length of 100 mm lens. The measurement spot on the target surface had a diameter of about 1 mm. The plasma emission was collected by a telescope system and sent through an optical fiber to the entrance slit of an Echelle spectrometer (Aryelle 200, LTB Lasertechnik Berlin, Germany). The spectrometer was coupled with an Andor iStar iCCD, which allows for a temporal resolution lower than 2 ns and a relative spectral resolution of 9000 (which corresponds to an instrumental broadening of 28 pm at a wavelength of 250 nm). The spectrometer was calibrated before each measurement session using a Deuterium-Hg lamp (Ocean Optics DH-2000) before the analysis. For LIBS analyses, 10 spectra were accumulated at each delay (ranging from 200 ns to 1,4 µs, at 400 ns steps, with a 400 ns gate) after 3 preliminary cleaning shots.

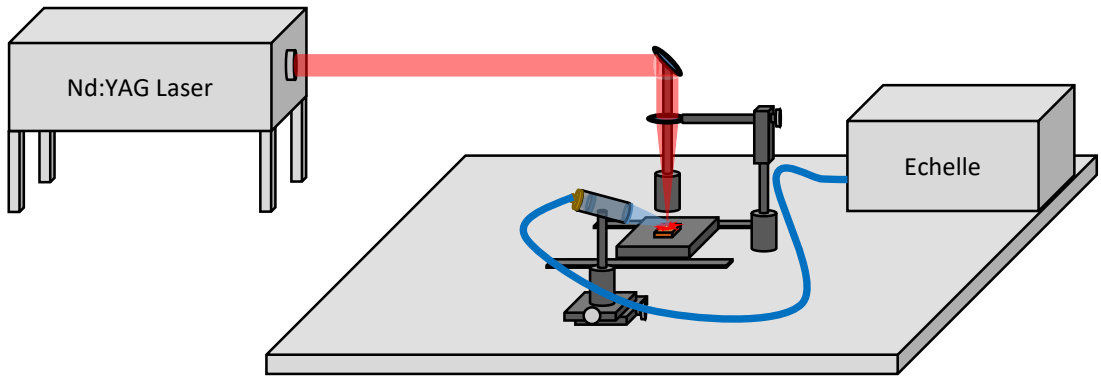

Figure 3 - Scheme of the LIBS system used in this work

6.2.2 – Materials

Tantalum is a transition metal, mainly obtained from Columbite-Tantalite (Coltan) mineral, which has many uses in the industry of electronic devices [18]. Studies on tantalum by LIBS are quite limited and many fundamental parameters required for quantitative analysis are not precisely known. For example, no information is available in the literature about the Stark broadening coefficients of Tantalum lines.

In this work, LIBS measurements were performed on the surface of a tantalum foil (250 µm thick, 99.9% purity, Sigma-Aldrich). The foil was moved after each series of 3 + 10 laser shots, to avoid effects related to the laser-induced crater. The temporal evolution of the line intensity and FWHM of 26 Ta lines (6 neutral and 20 ionic lines) were studied. The relevant spectral parameters are reported in Table 1.

$\Delta\lambda_0$ (nm)	A_{ki} (s^{-1})	Ion. St.	E_i (cm^{-1})	g_i	E_k (cm^{-1})	g_k
214,6877	$5{,}17 \times 10^8$	II	1031,36	5	47595,98	3
218,2723	$2{,}24 \times 10^8$	II	1031,36	5	46831,35	7
219,6056	$5{,}20 \times 10^8$	II	4415,79	8	49937,74	9

221,0042	4,99 x 10^8	II	0	3	45223,91	3
221,5600 *	2,08 x 10^8	II	4415,79	9	49536,24	7
224,8495 *	2,73 x 10^8	II	9746,28	9	54206,69	9
224,9791	6,75 x 10^8	II	0	3	44434,79	1
225,0769	4,68 x 10^8	II	1031,36	5	45446,85	5
226,2302	5,13 x 10^8	II	2642,26	7	46831,35	7
227,1847	2,93 x 10^8	II	2642,26	7	46645,7	9
227,2600	5,57 x 10^8	II	3180,04	5	47168,9	7
243,1055	1,11 x 10^8	II	1031,36	5	42153,29	5
243,3586	3,11 x 10^8	II	3180,04	5	44259,2	5
247,0898	1,21 x 10^8	II	6186,81	11	46645,7	9
248,8707	8,52 x 10^8	II	4415,79	9	44585,17	11
253,2125	5,28 x 10^8	II	2642,26	7	42122,91	9
255,462	3,76 x 10^8	II	2642,26	7	41775,29	9
263,5583	6,871 x 10^8	II	1031,36	5	38962,32	7
265,3272	2,559 x 10^8	I	2010,10	6	39668,2	6
267,590	7,67 x 10^8	II	4415,79	9	41775,29	9
285,0978	1,60 x 10^8	I	5621,04	10	40686,42	10
321,3906 *	8,22 x 10^7	II	5657,90	5	36763,7	7
331,1135	2,48 x 10^7	I	5621,04	10	35813,47	12
331,8847	1,07 x 10^7	I	2010,10	6	32132,38	8
360,7405 *	5,58 x 10^6	I	2010,10	6	29722,95	8
362,661 *	7,67 x 10^6	I	3963,92	8	31530,02	10

*Table 1 – Spectral parameters of the Ta emission lines used in this study. The lines marked with * are the ones used for calculating the plasma temperature and electron number density*

The Kurucz [19] and NIST [20] databases were used as references for the spectroscopic parameters needed in this work.

6.3 – Results and Discussion

The first step for the construction of the TIECS plot was the measurement of the plasma temperature and electron number density of the Ta plasma at different delays. The tantalum spectrum is particularly complex, as shown in Figure 4, and the high-resolution spectrometer used unavoidably introduces several ghost lines, due to the cross-talk between the orders of the Echelle spectrometer. This effect produces additional difficulties in the correct interpretation of the spectral lines.

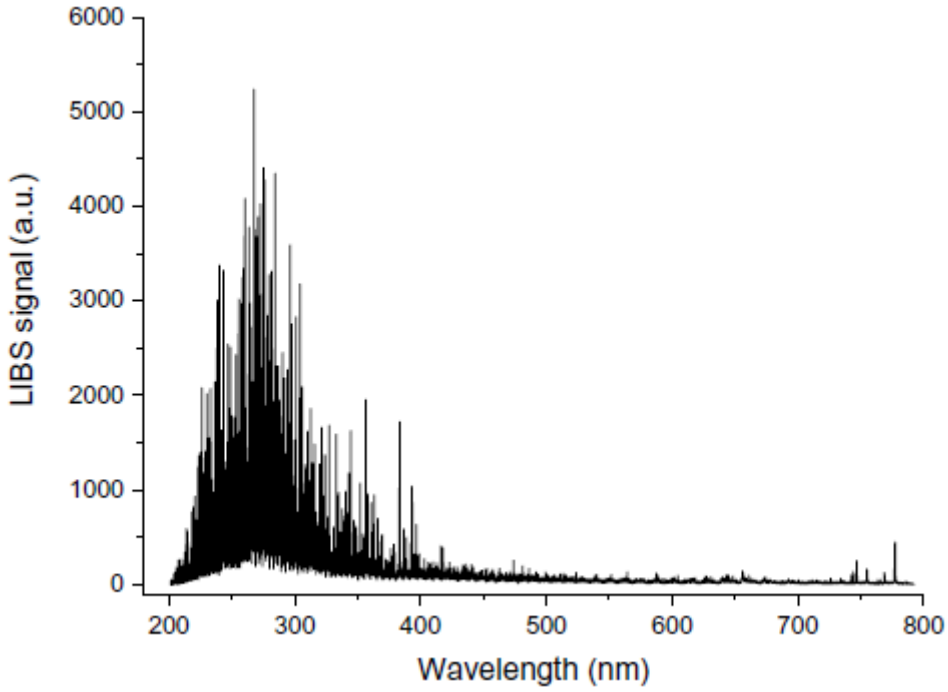

Figure 4 - LIBS spectrum of the Ta sample

The electron number density was obtained from the determination of the Stark linewidth of the Hydrogen Balmer alpha line at 656,3 nm. While keeping in mind the effects of self-absorption, a group of low intensity, non-resonant lines were selected for measuring the electron temperature using the Saha-Boltzmann method [21]. These lines are marked with an asterisk in Table 1. The Saha-Boltzmann plot corresponding to 1 µs delay is shown in Figure 5.

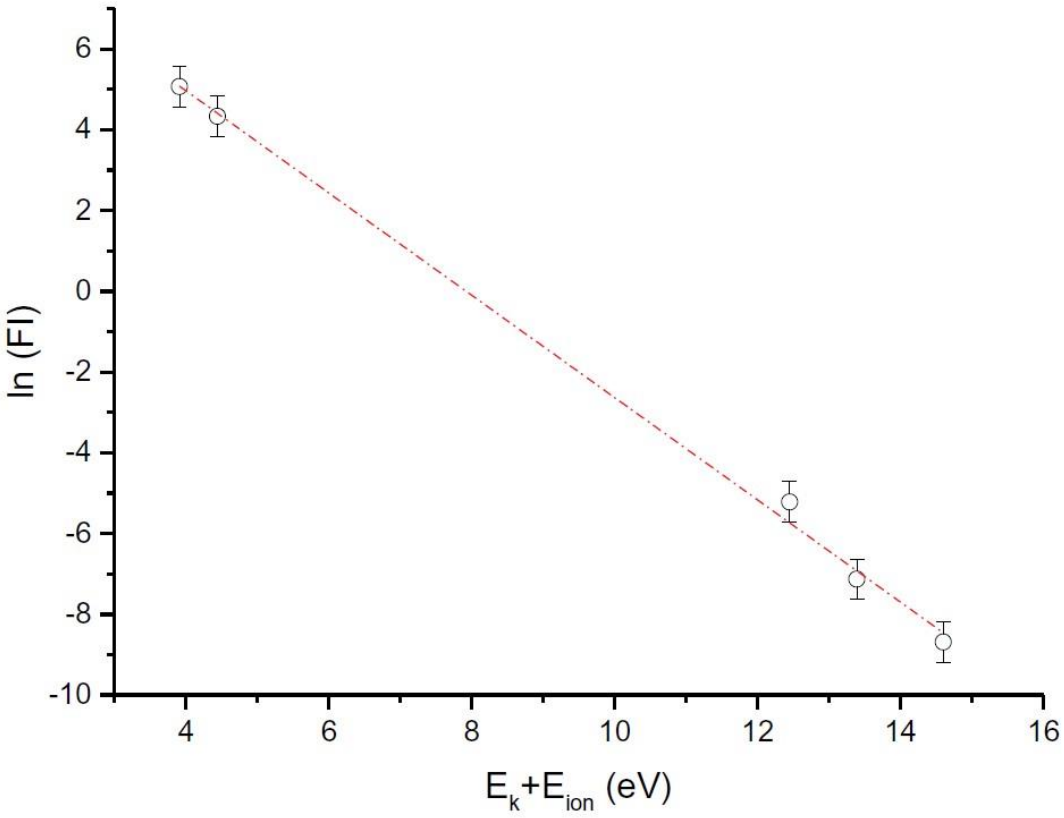

Figure 5 - Saha-Boltzmann plot for Ta, 1000 ns delay

No appreciable differences were found between the values of plasma temperature estimated using independently neutral lines or ionic lines, at all of the delays considered. Therefore, a model of homogeneous plasma is used, described by a single temperature for neutral and ionic species. The plasma parameters at the different time delays are reported in Table 2.

Delay (ns)	Plasma Temperature (eV)	Electron Number Density $cm^{-3} \times 10^{-17}$
200	1,1	6,14
600	0,89	3,28
1000	0,80	1,79
1400	0,81	1,40

Table 2 - Plasma parameters at various time delays

It should be noted that at 200 ns the plasma is still expanding quickly, therefore the LTE approximation is likely not fulfilled [20]. Therefore, the estimated plasma temperature at that delay should not be considered as reliable and the corresponding spectrum was not considered in the subsequent calculations.

The time-independent Extended C-sigma plot for the Ta lines in Table 1 is shown in Figure 6. It should be noted that the effects of self-absorption, for the moment, are not considered. The plot contains 78 points in total (26 lines x 3 delays).

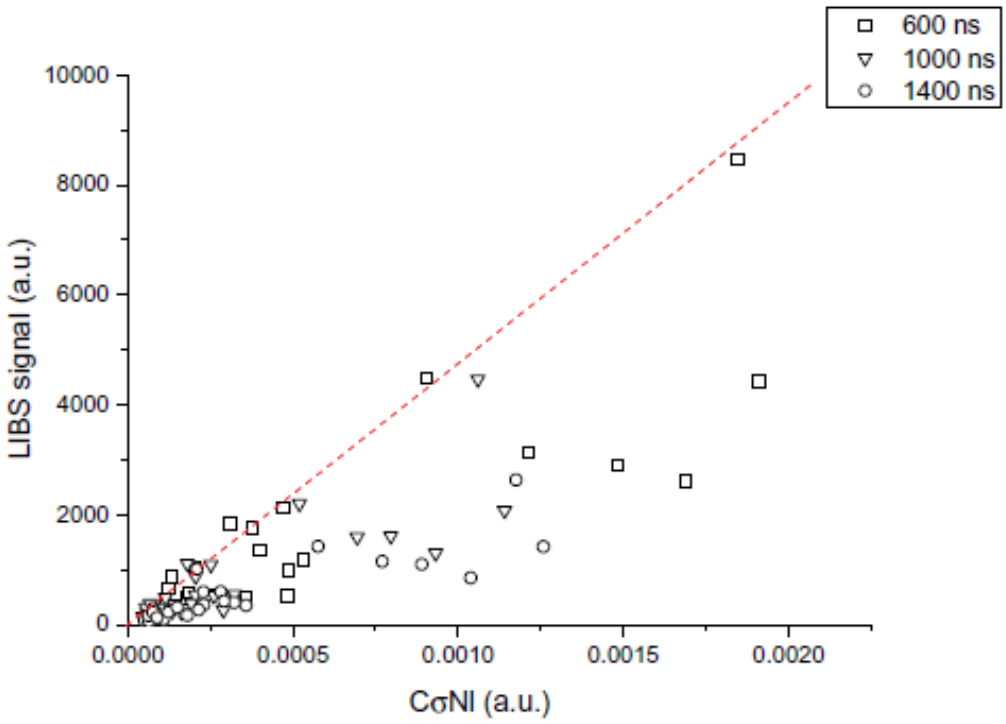

Figure 6 - C-Sigma plot, not considering self-absorption. The dashed line represents the reference TIECS curve which takes into accounts self-absorption.

As noted in [13], Figure 6 can be assimilated to what would have been obtained using a multi-elemental Boltzmann plot approach, assuming an optically thin plasma $\left(i.e.\ \frac{\overline{\Delta\lambda}}{\Delta\lambda_0} = 1\right)$ for the corresponding lines.

The red dashed line in Figure 6 represents the reference line on top of which all the points corresponding to the (possibly optically thick) emission lines will be placed, by adjusting the relevant Stark broadening coefficients for obtaining the right $\frac{\overline{\Delta\lambda}}{\Delta\lambda_0}$ values from the knowledge of the experimental linewidths ($\overline{\Delta\lambda}$) and of the electron number densities at the different delays considered.

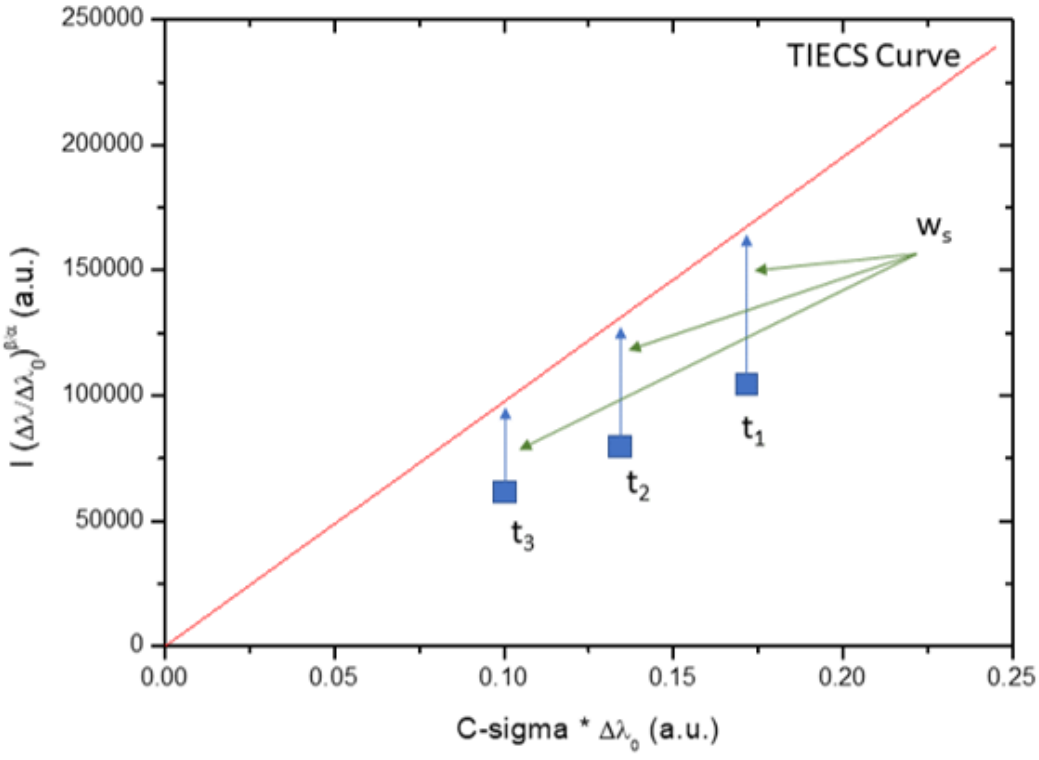

Figure 7 - Schematic representation of the procedure for the determination of the w_s coefficients

In Table 3, the results of the calculations are reported. It should be noted that some coefficients could not be calculated because the measured linewidth is comparable with the instrumental broadening, which must be subtracted beforehand from the experimental linewidth to obtain the Lorentzian component of the Voigt profile, corresponding to the Stark broadening of the line. The uncertainty is evaluated as the standard deviation of the different estimates at the three time delays considered.

Species	Wavelength (nm)	Stark coefficient $nm/cm^3 \times 10^{17}$	Standard deviation $nm/cm^3 \times 10^{17}$
Ta I	265,3272	0,006	0,003
Ta I	285,0978	0,0021	2×10^{-4}
Ta I	331,1135	0,008	0,006
Ta I	331,8847	0,009	0,005
Ta I	360,7405	-	-
Ta I	362,661	-	-
Ta II	214,6877	0,006	0,004
Ta II	218,2723	0,008	0,003
Ta II	219,6056	0,010	0,002

Ta II	221,0042	0,006	0,003
Ta II	221,5600	0,016	0,003
Ta II	224,8495	0,009	0,002
Ta II	224,9791	0,008	0,004
Ta II	225,0769	0,0125	0,002
Ta II	226,2302	0,008	0,002
Ta II	227,1847	0,0027	9×10^{-4}
Ta II	227,2600	0,0054	6×10^{-4}
Ta II	243,1055	-	-
Ta II	243,3586	0,0018	7×10^{-4}
Ta II	247,0898	0,0055	0,001
Ta II	248,8707	0,0037	8×10^{-4}
Ta II	253,2125	0,009	0,002
Ta II	255,462	0,019	0,003
Ta II	263,5583	0,0065	0,001
Ta II	267,590	0,0170	0,006
Ta II	321,3906	0,031	0,01

Table 3 - Stark broadening coefficients of the studied lines

6.4 – Conclusions

This work presented a new method for building a Time-Independent Extended C-Sigma curve, that can be used for evaluating the extent of the effects of self-absorption on the experimentally measured linewidth of spectral lines in LIBS spectra.

Based on reasonable assumptions (i.e. homogeneous and stationary plasma, in Local Thermal Equilibrium) it was possible to determine the Stark broadening parameters of 23 Ta lines (4 neutral and 19 ionic) with reasonable precision (around 30% on average). Indeed, the knowledge of these parameters could be useful for further spectroscopic studies of Ta samples, as well as being a method that could be implemented for the determination of unknown spectral parameters of other elements.

Indeed, TIECS was applied in a more recent work [22] for the determination of the spectroscopic parameters of Ag I and Ag II emission lines. In this work, the full potential of TIECS was used, and it was possible to determine not only the Stark coefficient, but also the transition probabilities of the studied lines.

Bibliography

[1] A. Safi, S. H. Tavassloli, G. Cristoforetti, E. Tognoni, B. Campanella, S. Legnaioli, S. Pagnotta, F. Poggialini e V. Palleschi, «Exploiting Self-Absorption for Plasma Characterization in Laser-Induced Breakdown Spectroscopy Experiments: A Comparison of Two Recent Approaches,» *Analytical Chemistry,* vol. 91, pp. 8595-8601, 2019.

[2] J. Manrique, J. A. Aguilera e C. Aragòn, «Determination of transition probabilities by laser-induced breakdown spectroscopy with curve-of-growth measurements,» *Journal of Quantitative Spectroscopy and Radiative Transfer,* vol. 112, n. 1, pp. 85-91, 2011.

[3] J. A. Aguilera, J. Manrique e C. Aragòn, «Stark width measurements of Fe II lines with wavelengths in the range 230–260 nm,» *Journal of Physics B: Atomic, Molecular and Optical Physics,* vol. 44, p. 245701, 2011.

[4] E. A. Den Hartog, A. J. Palmer e J. E. Lawler, «Radiative lifetimes and transition probabilities of neutral lanthanum,» *Journal of Physics B: Atomic, Molecular and Optical Physics,* vol. 48, p. 155001, 2015.

[5] M. Ortiz, J. Campos, R. Mayo, K. Blagoev e G. Malcheva, «Possibility of LIBS for transition probabilities determination,» in *Proceedings Volume 5830, 13th International School on Quantum Electronics: Laser Physics and Applications*, Bourgas, 2005.

[6] F. Bredice, F. O. Borges, H. Sobral, M. Villagran-Muniz, H. O. Di Rocco, G. Cristoforetti, S. Legnaioli, V. Palleschi, A. Salvetti e E. Tognoni, «Measurement of Stark broadening of Mn I and Mn II spectral lines in plasmas used for Laser-Induced Breakdown Spectroscopy,» *Spectrochimica Acta Part B: Atomic Spectroscopy,* vol. 62, n. 11, pp. 1237-1245, 2007.

[7] C. Aragòn, J. A. Aguilera e J. Manrique, «Measurement of Stark broadening parameters of Fe II and Ni II spectral lines by laser induced breakdown spectroscopy using fused glass samples,» *Journal of Quantitative Spectroscopy and Radiative Transfer,* vol. 134, pp. 39-45, 2014.

[8] A. M. El Sherbini, T. El Sherbini, H. Hegazy, G. Cristoforetti, S. Legnaioli, L. Pardini, V. Palleschi, A. Salvetti e E. Tognoni, «Measurement of the Stark Broadening of Atomic Emission Lines in Non–Optically Thin Plasmas by Laser-Induced Breakdown Spectroscopy,» *Spectroscopy Letters,* vol. 40, n. 4, pp. 643-658, 2007.

[9] R. D. Cowan e G. H. Dieke, «Self-Absorption of Spectrum Lines,» *Reviews of Modern Physics,* vol. 20, n. 2, p. 418, 1948.

[10] G. Cristoforetti, A. De Giacomo, M. Dell'Aglio, S. Legnaioli, E. Tognoni, V. Palleschi e N. Omenetto, «Local Thermodynamic Equilibrium in Laser-Induced Breakdown Spectroscopy: Beyond the McWhirter criterion,» *Spectrochimica Acta Part B: Atomic Spectroscopy,* vol. 65, n. 1, pp. 86-95, 2010.

[11] H. R. Griem, «Stark Broadening,» *Advances in Atomic and Molecular Physics,* vol. 11, pp. 331-359, 1976.

[12] L. Pardini, S. Legnaioli, G. Lorenzetti, V. Palleschi, R. Gaudiuso, A. De Giacomo, D. M. Diaz Pace, F. Anabitarte Garcia, G. de Holanda Cavalcanti e C. Parigger, «On the determination of plasma electron number density from Stark broadened hydrogen Balmer series lines in Laser-Induced Breakdown Spectroscopy experiments,» *Spectrochimica Acta Part B: Atomic Spectroscopy,* vol. 99, pp. 98-103, 2013.

[13] C. Aragòn e J. A. Aguilera, «CSigma graphs: A new approach for plasma characterization in laser-induced breakdown spectroscopy,» *Journal of Quantitative Spectroscopy and Radiative Transfer,* vol. 149, pp. 90-102, 2014.

[14] G. Cristoforetti e E. Tognoni, «Calculation of elemental columnar density from self-absorbed lines in laser-induced breakdown spectroscopy: A resource for quantitative analysis,» *Spectrochimica Acta Part B: Atomic Spectroscopy,* Vol. %1 di %279-80, pp. 63-71, 2013.

[15] N. Farid, S. S. Harilal, H. Ding e A. Hassanein, «Emission features and expansion dynamics of nanosecond laser ablation plumes at different ambient pressures,» *Journal of Applied Physics,* vol. 115, 2014.

[16] G. Cristoforetti, S. Legnaioli, L. Pardini, V. Palleschi, A. Salvetti e E. Tognoni, «Spectroscopic and shadowgraphic analysis of laser induced plasmas in the orthogonal double pulse pre-ablation configuration,» *Spectrochimica Acta Part B: Atomic Spectroscopy,* vol. 61, n. 3, pp. 340-350, 2006.

[17] A. R. Choudhuri, «How the Saha Ionization Equation Was Discovered,» 2018. [Online]. Available: https://arxiv.org/ftp/arxiv/papers/1810/1810.10898.pdf. [Consultato il giorno 10 02 2022].

[18] «Niobium and tantalum,» [Online]. Available: https://pubs.er.usgs.gov/publication/pp1802M. [Consultato il giorno 10 02 2022].

[19] P. L. Smith, C. Heise, J. R. Esmond e R. L. Kurucz, «Atomic spectral line database from CD-ROM 23 of R. L. Kurucz.,» [Online]. Available: https://lweb.cfa.harvard.edu/amp/ampdata/kurucz23/sekur.html. [Consultato il giorno 10 02 2022].

[20] «NIST: Atomic Spectra Database Lines Form,» [Online]. Available: https://physics.nist.gov/PhysRefData/ASD/lines_form.html. [Consultato il giorno 10 02 2022].

[21] S. Yalcin, D. R. Crosley, G. P. Smith e G. W. Faris, «Spectroscopic Characterization of Laser-Produced Plasmas for In Situ Toxic Metal Monitoring,» *Hazardous Waste and Hazardous Materials,* vol. 13, n. 1, 2009.

[22] A. Safi, S. M. Aberkane, A. Botto, B. Campanella, S. Legnaioli, F. Poggialini, S. Raneri, F. Rezaei e V. Palleschi, «Determination of Spectroscopic Parameters of Ag(I) and Ag(II) Emission Lines Using Time-Independent Extended C-Sigma Method,» *Applied Spectroscopy,* vol. 75, n. 6, pp. 654-660, 2021.

Chapter 7:

General Conclusions

7 – General Conclusions

Over the course of this PhD research, novel LIBS methodologies and procedures, based on the use of noble metal nanoparticles (NELIBS) have been developed. NELIBS allowed for the increase of LIBS analytical performances, and lowered the detection limits for the studied analytes to less than 1 ppm in the case of solid samples and a few µg/L in the case of analytes extracted from a liquid matrix. Moreover, it was demonstrated how the NELIBS approach can be used with portable LIBS instruments and how it can be combined with the double pulse approach or with TFME to further increase the performances of these two methodologies.

Chapter 2 proved how metal nanoparticles synthetized with "green" methodologies can be used for NELIBS applications. An optimal procedure for the synthesis of Silver nanoparticles (AgNPs) from silver nitrate solutions and coffee extract was developed, and the AgNPs were tested for the analysis of Copper standard reference materials (SRMs). The sample preparation procedure was optimized and the results showed the effectiveness of the "green" NPs. By constructing LIBS and NELIBS calibration curves, it was demonstrated how the limits of detection of Cr and Zn in a solid copper matrix could be lowered significantly. Additionally, the analyses were performed using a portable instrument, the first time for NELIBS, which suggests the possibility for future in-situ applications.

The available LIBS system was re-configured for the production of high-quality, pure and reproducible metal nanoparticles in relatively large quantities, using the Pulsed Laser Ablation in Liquid technique. The procedure allowed for the extremely reproducible production of NP dispersion with tunable concentration and dimensions, with the addition of different surfactants, depending on the analytical requirements. The nanoparticles produced by PLAL during this phase of the research work, described in Chapter 3, were successfully used for NELIBS, but also for Surface-Enhanced Raman (SERS) applications. The same LIBS/PLAL system was also used successfully for the production of graphene-based nanosheets that were used for micro-extraction applications.

The possibility of combining the advantages of DP-LIBS and NELIBS was demonstrated in Chapter 4. The main problematic that was observed in DP-NELIBS was the almost complete removal of the NPs after a single laser pulse, which would prevent the second pulse from interacting with the NP deposition. To solve this problem, a LIBS setup that used two parallel and non-collinear laser pulses was chosen. This ensured the activation of NPs during both pulses, while maintaining the low-density environment typical of DP-LIBS. Several tests on copper targets have been performed to determine the best set-up for the maximum magnitude of the signal enhancement by adjusting different parameters such as pulse energies and offset distances. Commercially

available silver NPs and NPs prepared by PLAL have been tested and their performances compared with standard DP-LIBS. In the end, a novel approach, called Spatially-Offset Double-Pulse LIBS (SO-DP-LIBS) was proposed. The feasibility of this approach was successfully demonstrated, obtaining an even higher enhancement factor (EF) than the one registered during SP-NELIBS analyses with a comparable experimental configuration. Moreover, it was shown how the EF decreased with a decreasing laser beam offset distance. The results obtained were very promising and showed the potential of NELIBS as well as its versatility. Nevertheless, the extent of the interaction of the enhancing effects of DP and NELIBS is worthy of further investigation, with a particular focus on the laser-induced plasma dynamics and evolution in the case of SO-DP-NELIBS.

In Chapter 5, a novel strategy for the analysis of liquid samples based on the combination of TFME and NELIBS, was proposed and tested. The research activity was focused on improving the capabilities of graphene and graphene oxide thin film micro-extraction (TFME) substrates for LIBS analysis by the application of noble metal NPs. Graphene nanosheets (GNS) were successfully prepared using a pulsed laser and used for the preparation of TFME supports. Various kinds of glass substrates were tested and the procedure for the preparation of the TFME supports was optimized. This allowed for the LIBS analysis of metals in liquid samples, obtaining sub-ppm LODs. Moreover, it was demonstrated that NELIBS can be coupled with TFME to allow for the obtainment of even lower LODs. Nevertheless, studies should be carried out to further optimize the methodology. In particular, the preparation of a ready-to-use AgNP/GNS composite would further simplify the procedure, enabling the use of this technique for in-situ and online measurements. In addition, the use of functionalized GNS and graphene is also worthy of investigation, for the preparation of ad-hoc TFME supports for pre-determined analytes. Lastly, a procedure for the functionalization of the glass substrates was proposed and tested. The treatment of glass substrates with APTES allowed for a much higher stability of the GNS TFME supports. Also in this case, it could be worth investigating different deposition strategies, particularly dip coating. This could allow for the preparation of much more homogeneous and large substrates, which could boost the TFME performances greatly. Indeed, a thorough optimization of this technique would be necessary, to improve the preparation times and simplify the preparation processes.

In Chapter 6, the development of a novel approach for spectral analysis and treatment, called Time-Independent Extended C-Sigma (TIECS) was described. Indeed, a method that allows for the determination of the extent of the effects of self-absorption on the spectral lines monitored in LIBS, using directly the experimental data obtained from a LIBS spectrum, is a valuable tool for both quantitative analysis and spectral studies of LIBS plasmas. The method developed in this

research work exploits the spectral information extracted from LIBS spectra acquired at different delay times after the laser pulse for building a time-independent Extended C-Sigma curve, and intrinsically includes in the calculation the effects of self-absorption. It was possible to determine the Stark broadening parameters of 23 Ta lines (4 neutral and 19 ionic) with reasonable precision (around 30% on average). Indeed, the knowledge of these parameters could be useful for further spectroscopic studies for the determination of unknown spectral parameters of other elements. For instance, TIECS was applied in a more recent work for the determination of the spectroscopic parameters of Ag I and Ag II emission lines. In this work, the full potential of TIECS was used, and it was possible to determine not only the Stark coefficient, but also the transition probabilities of the studied lines.